NASA Tech Briefs

National
Aeronautics and
Space
Administration

The fully-automatic AutoMicrobic System [AMS] detects harmful micro-organisms and measures their susceptibility to agents such as antibodies. A sample is automatically fed nutrients or antibodies, and an optical scanner and a computer monitor growth.

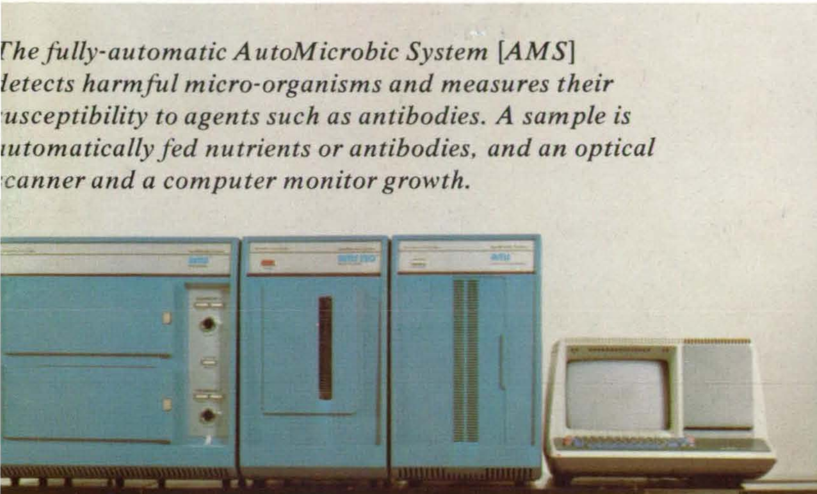

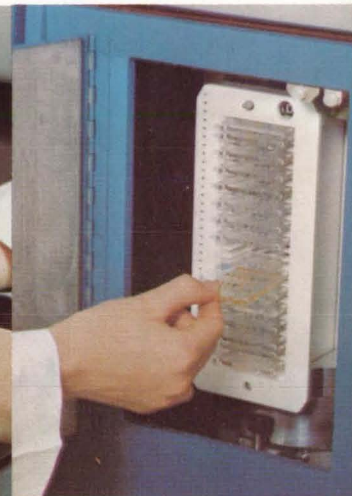

An economical separator for NiZn batteries, developed at Lewis Research Center, increases energy-to-weight ratios, extends battery life, and reduces costs. In cooperation with the U.S. Postal Service, NASA is testing the new batteries for powering electric delivery vans.

Vol. 2, No. 1

SPRING 1977

About the NASA Technology Utilization Program

The National Aeronautics and Space Act of 1958, which established NASA and the United States civilian space program, requires that "The Administration shall provide for the widest practicable and appropriate dissemination of information concerning its activities and the results thereof."

To help carry out this objective the NASA Technology Utilization (TU) Program was established in 1962. It offers a variety of valuable services to facilitate the transfer of aerospace technology to nonaerospace applications, thus assuring American taxpayers maximum return on their investment in space research; thousands of spinoffs of NASA research have already occurred in virtually every area of our economy.

The TU Program has worked for engineers, scientists, technicians, and businessmen. And it can work for you.

NASA Tech Briefs

Tech Briefs is published quarterly and is free to any U.S. citizen or organization. It is both a current-awareness medium and a problem-solving tool. Potential products ... industrial processes ... basic and applied research ... shop and lab techniques ... computer software ... new sources of technical data ... concepts ... you will find them all in NASA Tech Briefs. The first section highlights a few of the potential new products contained in Tech Briefs. The remainder of the volume is organized by technical category to help you quickly review new developments in your areas of interest. Finally, a subject index makes each issue a convenient permanent reference file.

Further Information on Innovations

Although many articles are complete in themselves, others are backed up by Technical Support Packages (TSP's). TSP's are available without charge and may be ordered by simply completing the enclosed TSP Request Card. Further information on some innovations is available for a nominal fee from other sources, as indicated at the ends of the articles. In addition, Technology Utilization Officers at NASA Field Centers will assist you directly when necessary. (See page A4.)

Patent Licenses

Many of the inventions described are under consideration for patents or have been patented by NASA. Unless NASA has decided not to apply for a patent, the patent status is described at the end of each article. For further information about the Patent Program see page A8.

Other Technology Utilization Services

To assist engineers, industrial researchers, business executives, city officials, and other potential users in applying space technology to their problems, NASA sponsors six Industrial Applications Centers. Their services are described on page A6. In addition, an extensive library of computer programs is available through COSMIC, the Technology Utilization Program's outlet for NASA-developed software. (See page A5.)

Applications Program

To help solve public-sector problems in such areas as safety, health, transportation, and environmental protection, NASA TU Applications Teams, staffed by professionals from a variety of disciplines, work with Federal agencies, local governments, and health organizations to identify critical problems amenable to technical solutions. Among their many significant contributions are a rechargeable heart pacemaker, a lightweight fireman's breathing apparatus, aids for the handicapped, and safer highways.

Reader Feedback

We hope you find the information in NASA Tech Briefs useful. A reader feedback card has been included because we want your comments and suggestions on how we can further help you apply NASA innovations and technology to your needs. Please use it, or if you need more space, write us a letter.

NASA Tech Briefs

National
Aeronautics and
Space
Administration

SPRING 1977

Volume 2, Number 1

COVERS: The photographs on the front and back covers illustrate recent developments by NASA and its contractors that have resulted in commercial and nonaerospace spinoffs. The battery used in the utility van is described on pages 4 and 5 of this issue; for information about the AutoMicrobic System, circle 104 on the Reader Service Card. The padding illustrated on the back cover is described in NASA Tech Briefs, Vol. 1, No. 4, p. 582 [also circle 105 on the Reader Service Card in this issue].

About This NASA Publication

NASA Tech Briefs, a quarterly publication, is distributed free to U.S. citizens to encourage commercial application of U.S. space technology. For information on publications and services available through the NASA Technology Utilization Program, write to the Director, Technology Utilization Office, P. O. Box 8756, Baltimore/Washington International Airport, Maryland 21240.

"The Administrator of National Aeronautics and Space Administration has determined that the publication of this periodical is necessary in the transaction of the public business required by law of this Agency. Use of funds for printing this periodical has been approved by the Director of the Office of Management and Budget through August 31, 1977."

Change of Address

Change of Address: If you wish to have NASA Tech Briefs forwarded to your new address, use one of the Subscriptions cards enclosed in the back of this volume of NASA Tech Briefs. Be sure to check the appropriate box indicating change of address.

Communication Concerning Editorial Matter

For editorial comments or general communications about NASA Tech Briefs, you may use the self-addressed Feedback card in the back of NASA Tech Briefs, or write to: The Publications Manager, Technology Utilization Office (Code KT), NASA Headquarters, Washington, DC 20546. Technical questions concening specific articles should be directed to the Technology Utilization Officer of the sponsoring NASA Center (addresses listed on page A4.)

NASA
TU SERVICES

THE NASA TECHNOLOGY UTILIZATION OFFICERS

They will help you apply the innovations described in Tech Briefs.

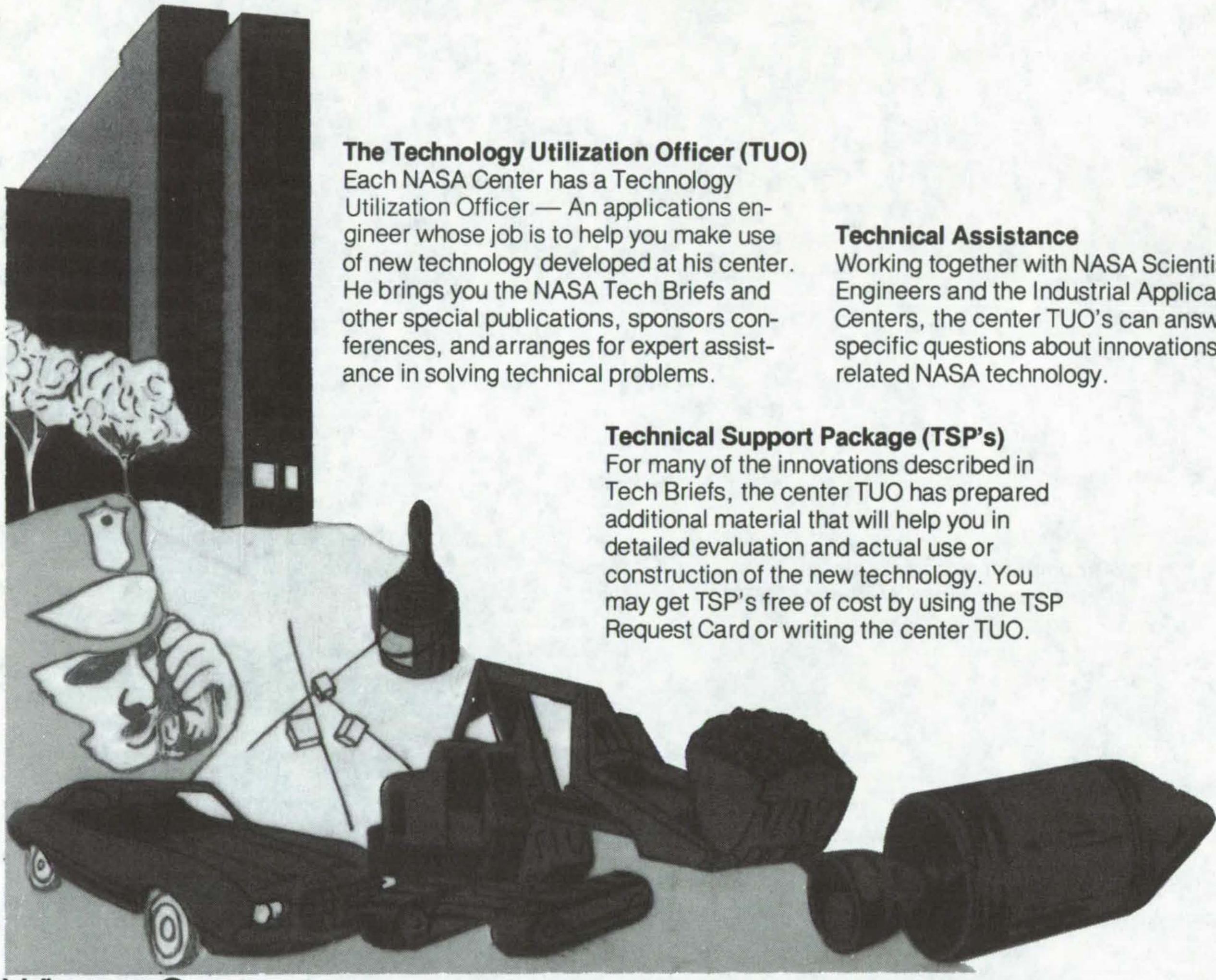

The Technology Utilization Officer (TUO)
Each NASA Center has a Technology Utilization Officer — An applications engineer whose job is to help you make use of new technology developed at his center. He brings you the NASA Tech Briefs and other special publications, sponsors conferences, and arranges for expert assistance in solving technical problems.

Technical Assistance
Working together with NASA Scientists and Engineers and the Industrial Applications Centers, the center TUO's can answer specific questions about innovations and related NASA technology.

Technical Support Package (TSP's)
For many of the innovations described in Tech Briefs, the center TUO has prepared additional material that will help you in detailed evaluation and actual use or construction of the new technology. You may get TSP's free of cost by using the TSP Request Card or writing the center TUO.

Who to Contact.

Of course, many technical questions about Tech Briefs are answered in the TSP's, but when no TSP is available, or you have further questions, write the Technology Utilization Officer at the center that sponsored the research at the address listed below.

Charles K. Kubokawa
Ames Research Center
Code AU: 230-2
Moffett Field, CA 94035
(415) 965-5554

Clinton T. Johnson
Hugh L. Dryden Flight Research Center
P. O. Box 273
Edwards, CA 93523
(805) 258-3311, Ext. 568

Donald S. Friedman
Goddard Space Flight Center
Code 704.1
Greenbelt, MD 20771
(301) 982-6242

John T. Wheeler
Johnson Space Center
Code AT3
Houston, TX 77058
(713) 483-3809

Raymond J. Cerrato
John F. Kennedy Space Center
Code SA-RTP
Kennedy Space Center, FL 32899
(305) 867-2780

John Samos
Langley Research Center
Mail Stop 139A
Hampton, VA 23665
(804) 827-3281

Paul Foster
Lewis Research Center
21000 Brookpark Rd.
Cleveland, OH 44135
(216) 433-4000, Ext. 6832

Aubrey D. Smith
Marshall Space Flight Center
Code AT01
Marshall Space Flight Center, AL 35812
(205) 453-2224

John C. Drane
NASA Resident Legal Office-JPL
4800 Oak Grove Drive
Pasadena, CA 91103
(213) 354-6420

Gilmore H. Trafford
Wallops Flight Center
Wallops Island, VA 23337
(804) 824-3411, Ext 201

Louis Mogavero, Director
Technology Utilization Office
Code KT
NASA Headquarters
Washington, DC 20546
(202) 755-3103

COSMIC

(Computer Software Management & Information Center)

AN ECONOMICAL SOURCE OF COMPUTER PROGRAMS DEVELOPED BY THE GOVERNMENT.

COSMIC is sponsored by NASA to give you access to over 1400 computer programs developed by NASA and the Department of Defense, and selected programs from other government agencies. It is one of the Nation's largest software libraries.

COSMIC charges very reasonable fees for programs to help cover part of their expenses—and NASA pays for the remainder. Programs generally cost from \$500 to \$1000, but a few are more expensive and many are less. Documentation is available separately and very inexpensively.

COSMIC collects and stores software packages, insures that they are complete, prepares special announcements (such as Tech Briefs), publishes an indexed software catalog, and reproduces programs for distribution. COSMIC helps customers to identify their software needs, follows up to determine the successes and problems, and provides updates and error corrections. In some cases, NASA engineers can offer guidance to users in installing or running a program.

COSMIC programs range from management (pert scheduling) to information science (retrieval systems) and computer operations (hardware and software). Hundreds of engineering programs perform such tasks as structural analysis, electronic circuit design, chemical analysis, and design of fluid systems. Others determine building energy requirements, optimize mineral exploration, and draw maps of water-covered areas using NASA satellite data. In fact, the chances are, if you use a computer, you can use COSMIC.

COSMIC is eager to help you get the programs you need. For more information about services or software available from COSMIC, fill out and mail the COSMIC Request Card in this issue.

COSMIC: Computer Software Management and Information Center

Suite 112, Barrow Hall, Athens, Georgia 30602 Phone: (404) 542-3265

WHERE IS THE WORLD'S LARGEST BANK OF TECHNICAL DATA

?

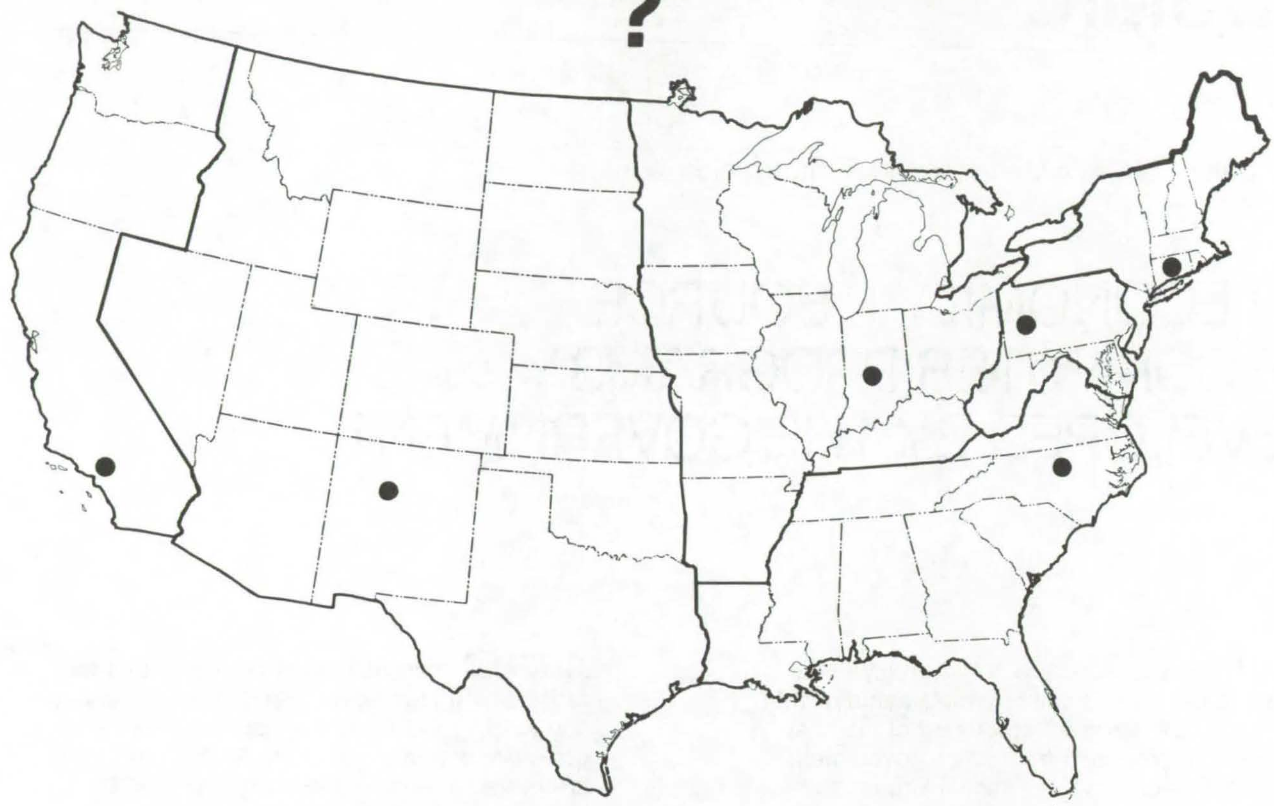

It's in Bloomington and Pittsburgh, it's in Storrs, Connecticut and Research Triangle Park, North Carolina; and it's in Albuquerque and Los Angeles.

NASA IAC's — INDUSTRIAL

You can get more information and more data on more technical subjects through NASA's network of IAC's than anywhere else in the world. About 8,000,000 documents and growing at the rate of 50,000 more each month!

Major sources include:

- 750,000 NASA Technical Reports
- Selected Water Resources Abstracts
- NASA Scientific and Technical Aerospace Reports
- Air Pollution Technical Information Center
- NASA International Aerospace Abstracts
- Chem Abstracts Condensates
- Engineering Index
- Nuclear Science Abstracts
- NASA Tech Briefs
- Government Reports Announcements

and many other specialized files on food technology, textile technology, metallurgy, medicine, business, economics, social sciences, and physical science.

The IAC's are one of the most economical ways of staying competitive in today's world of exploding technology. The help available from the network ranges from literature searches through expert technical assistance.

Literature Searches
Help in designing your search, typically from 30 to 300 abstracts in as narrow or broad an area as you need, and complete reports when you need them. The most complete "search before research" available!

Current Awareness
Consult with our applications engineers to design your personal program — selected monthly or quarterly abstracts on new developments in your speciality. It's like having your own journal!

Technical Assistance
Our applications engineers will help you evaluate and apply your literature-search results. They can help find answers to your technical problems and put you in touch with scientists and engineers at NASA Field Centers.

To obtain more information about how NASA's IAC's can help you —
Check the IAC box on the TSP Request Card in this issue,
Or write or call the IAC nearest you.

APPLICATIONS CENTERS

How to get reports and other documents discussed in this issue of Tech Briefs

Many of the innovations in Tech Briefs are described in detail in reports available at a reasonable cost through one or more of the IAC's. To order a report, call or write the IAC referenced at the end of the Tech Brief article at the address below. Be sure to list the titles and accession numbers (N76-..., N75-..., etc.) of those you wish to purchase.

Aerospace Research Application Center (ARAC)
Indiana University-Purdue University at Indianapolis
1201 E. 38th St.
Indianapolis, IN 46205
E. Guy Buck, Director
(317) 264-4644

Knowledge Availability Systems Center (KASC)
University of Pittsburgh
Pittsburgh, PA 15260
Edmond Howie, Director
(412) 624-5211

New England Research Application Center (NERAC)
Mansfield Professional Park
Storrs, CT 06268
Dr. Daniel U. Wilde, Director
(203) 486-4533

North Carolina Science & Technology Research Center (NC/STRC)
P. O. Box 12235
Research Triangle Park, NC 27709
Peter J. Chenery, Director
(919) 549-0671

Technology Application Center (TAC)
University of New Mexico
Albuquerque, NM 87131
Stanley A. Morain, Director
(505) 277-4000

Western Research Application Center (WESRAC)
University of Southern California
University Park
Los Angeles, CA 90007
Radford King, Director
(213) 746-6132

NASA INVENTIONS AVAILABLE FOR LICENSING

Over 3,500 NASA inventions are available for licensing in the United States - both exclusive and nonexclusive.

Nonexclusive Licenses

Nonexclusive licenses for commercial use are encouraged to promote competition and to achieve the widest use of inventions. They must be used by a negotiated target date but are usually royalty free.

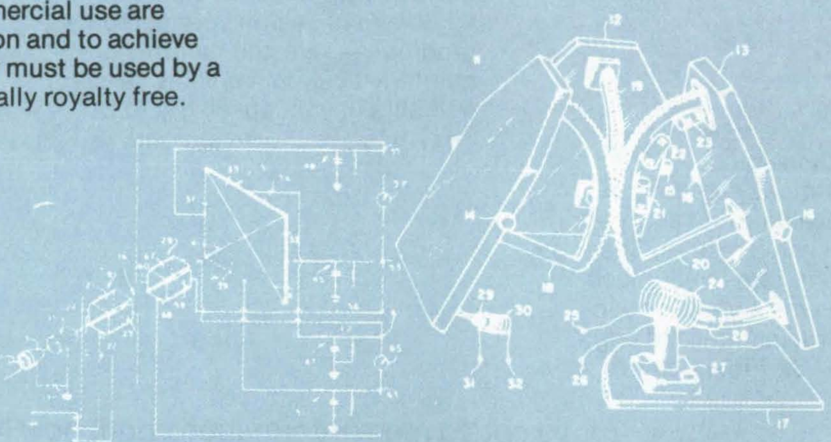

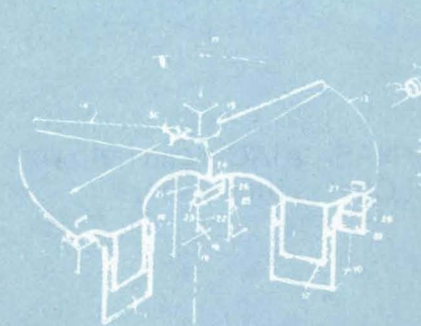

Exclusive Licenses

An exclusive license may be granted to encourage early commercial development of NASA inventions, especially when considerable private investment is required. These are generally for 5 to 10 years and usually require royalties based on sales or use.

The NASA patent licensing program also provides for licensing of NASA-owned foreign patents. In addition to inventions described in Tech Briefs, "NASA Patent Abstract Bibliography," containing abstracts of all NASA inventions, can be purchased from: National Technical Information Service, Springfield, Va., 22161. This document is updated semi-annually.

Patent Licenses and the NASA Tech Brief

Many of the inventions reported in Tech Briefs are patented or are under consideration for a patent at the time they are published. When this is the case, the current patent status is described at the end of the article; otherwise, there is no statement about patents. **If you want to know more about the patent program or are interested in license for a particular invention, write the Patent Counsel at the NASA Field Center** that sponsored the research. Be sure to refer to the NASA reference number in parenthesis at the end of the Tech Brief.

Robert F. Kempf
NASA Headquarters, Code GP
400 Maryland Ave., S.W.
Washington, DC 20546
(202) 755-3932

Darrell G. Brekke
Ames Research Center
Mail Code: 200-11A
Moffett Field, CA 94035
(415) 965-5104

John O. Tresansky
Goddard Space Flight Center
Mail Code: 204
Greenbelt, MD 20771
(301) 982-2351

Marvin F. Matthews
Lyndon B. Johnson Space Center
Mail Code: AM
Houston, TX 77058
(713) 483-4871

James O. Harrell
John F. Kennedy Space Center
Mail Code: SA-PAT
Kennedy Space Center, FL 32899
(305) 867-2544

Howard J. Osborn
Langley Research Center
Mail Code: 313
Hampton, VA 23665
(804) 827-3725

Norman T. Musial
Lewis Research Center
Mail Code: 500-113
21000 Brookpark Road
Cleveland, OH 44135
(216) 433-4000

Leon D. Wofford, Jr.
Marshall Space Flight Center
Mail Code: CC01
Marshall Space Flight Center, AL 35812
(205) 453-0020

Monte F. Mott
NASA Resident Legal Office-JPL
4800 Oak Grove Drive
Pasadena, CA 91103
(213) 354-2700

NEW PRODUCT IDEAS

NEW PRODUCT IDEAS are just a few of the many innovations described in this issue of NASA Tech Briefs and having promising commercial applications. Each is discussed further on the referenced page in the appropriate section in this issue. If you are interested in developing a product from these or other NASA innovations, you can receive further technical information by requesting the TSP referenced at the end of the full-length article or by writing the Technology Utilization Office of the sponsoring NASA center (see page A4). NASA's patent-licensing program to encourage commercial development is described on page A8.

Wetting Agent for Stud Welding

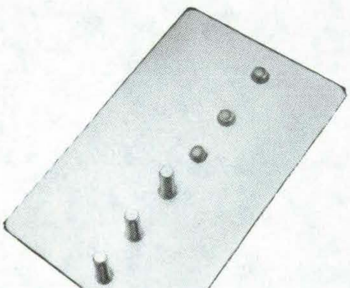

An easily-formulated detergent solution lowers the cost and increases the quality of aluminum stud welds made by capacitor-discharge welding. The detergent, an aromatic polyglycol ether used to clean glassware, is mixed with water and brushed over the weld area. Despite its simplicity, this procedure has remarkable payoffs: no bonding of excess metal around the stud; higher welding voltages can be used; the arc initiates at a lower voltage; tensile strength and reliability are improved, and final appearance is improved and controlled. The wetting agent is easy to use (the formula is sufficiently viscous for applying to vertical and overhead welds), results in improvements that suggest less expensive and more portable welding equipment, produces a better appearance that can make the process useful for many commercial products, and allows less-experienced welders to work on a wider range of projects.
(See page 141.)

Longer-Lasting Solar Collector Coating

A new electroplated black-nickel coating withstands heat and humidity without sacrificing optical properties. This improved humidity resistance is achieved by increasing the concentration of metal hydroxide in the coating. Such a coating was prepared by increasing the pH and the plating-current density. After 14 days at 95 percent relative humidity and 38° C, the optical properties of the coating were essentially unchanged. The solar absorption of the conventional formula degraded from 0.96 to 0.72 under the same conditions.
(See page 87.)

Solar Radiation Shadow Detector

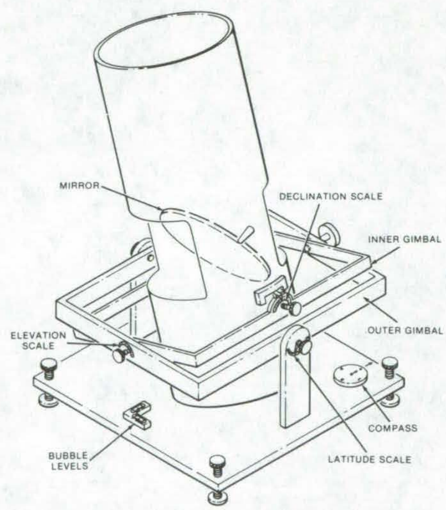

A portable shadow-surveying instrument can be quickly and easily used to select the site for a solar collector. It requires little operator skill and provides immediate and accurate shadow determination. After setting up the unit, the operator looks into the mirror in the sight tube and scans the sky from east to west horizons. Any object sighted through the tube will cast a shadow at the location of the instrument. The time and day when the shadow will appear are determined from the elevation and declination angle settings. In this way a site can be chosen to have the maximum Sunlight throughout the year or during a particular period, such as the winter.
(See page 45.)

High-Performance Flat-Plate Solar Collector

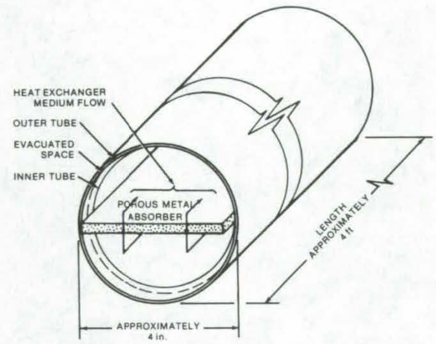

A proposed efficient high-temperature solar collector combines a vaccum to reduce convection losses, a selective coating, and a porous absorber. The tube-shaped collector has a concentric glass-tube envelope with an antireflection coating; it surrounds a flat-plate absorber having a spectrally selective coating. The heat-transfer medium is a gas, such as air, that circulates along a hairpin path. The envelope is evacuated to reduce heat losses, and a thin selective coating on the absorber improves the absorbance-to-emittance ratio. These features combine to form a particularly efficient collector that could be made relatively inexpensively.
(See page 43.)

Inexpensive Mass Flowmeter

The mass flow of fluids, such as water, oil, gasoline, and kerosine, can be measured directly with a simple flowmeter. Most of the parts

for the flowmeter are available off-the-shelf, and the only unusual components required are a "sensor/target" and a combination lever arm and diaphragm. The flowmeter, as illustrated, is constructed from pipe fittings, strain gages, and the special target. Furthermore, a given target will be useful with many types of fluids and flow rates. The target, which is placed in the flow stream, is a body with a known drag coefficient. The drag force on the target is measured by strain gages joined to a beam connected to the target. The strain-gage reading can then be used to determine the flow rate.
(See page 115.)

New Separator Increases Battery Life and Capacity

A new rechargeable NiZn battery holds three times the charge of NiCd or lead acid batteries of the same weight. The use of an inexpensive new separator makes the battery cost equivalent to that of a lead acid battery and extends the battery life. The batteries have been tested in an electrical utility van and are expected to contribute significantly to the development of electric urban vehicles. The new separator responsible to the improvements is made from sheets of an economical porous substate such as groundwood web (newsprint). It is coated with a polymer and fillers and is rolled in sheets for handling. The separator is flexible and strong, thus preventing damage due to electrode warpage and dendrite growth.
(See pages 4 and 5.)

Collectors for Vacuum-Cleaning Lines

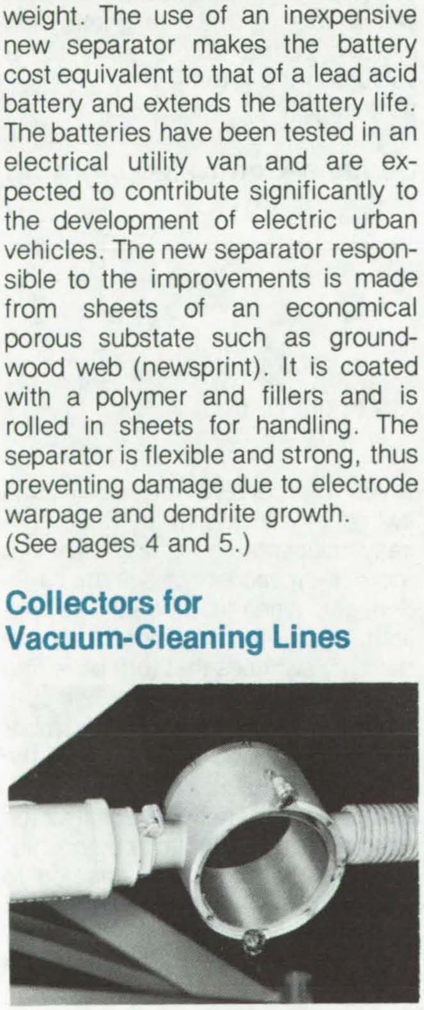

An inexpensive clear plastic filter traps screws, washers, and other small parts swept up by vacuum cleaners. The collector was designed for branch lines of central vacuum systems used to clean up shops where it was desired to save many of the small parts that had fallen to the floor. The filter is a screen that allows dust and small particles to pass through, but retains larger debris. A friction-held cover opens easily for the removal of collected objects.
(See page 154.)

Optical Sensor for NC Tooling

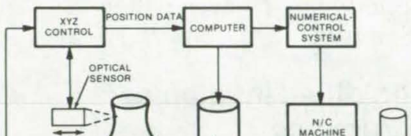

An optical profile-measuring system has been proposed as the basis for a numerical-control tooling technique. It could be used with soft or delicate models such as art objects. The shape and dimensions of a model could be stored in an NC file without actual contact with the model. This technique would allow industrial parts (such as automobile fenders) to be modeled in a manageable medium, such as clay, and then tooled in metal without preparation of an intermediate hard model.
(See page 152.)

Lower Fiber-Composite Costs

Fiber-reinforced polyimide composites could be made less expensively, using a mixture of amines that lowers the melting point. The fabrication of parts with a commercially available polyimide, which normally requires around 600° F and 1,000 psi, can be carried out at about 200° F and 200 psi. In addition to the lower temperature and pressure required to fabricate parts, the melting-point depression via an isometric mixture of methylene dianilines produces a polymer that can be thermoformed at elevated temperatures after an initial consolidation at lower temperatures.
(See page 88.)

Angle-Indicating Digital Servo

An angle-indicating servo determines the position of a capacitive pickup relative to a gravity-stabilized inductive element, without mechanical links, gear trains, or motors. Developed as a readout device for wind-tunnel testing, the digital servo uses two fixed-resistor networks to null the output of a detector consisting of the pendulum-mounted inductive element about which the capacitive pickup rotates. As the capacitive pickup rotates relative to the gravity-stabilized pendulum, signals are picked up, amplified, filtered, and fed to a phase detector. The phase detector senses the phasor difference between the pickup signal and the phase of a reference-winding voltage. An up/down counter outputs a new code in response to the detector output and also sources the readout circuits and displays.
(See page 28.)

Tube-Bending Scale/Protractor

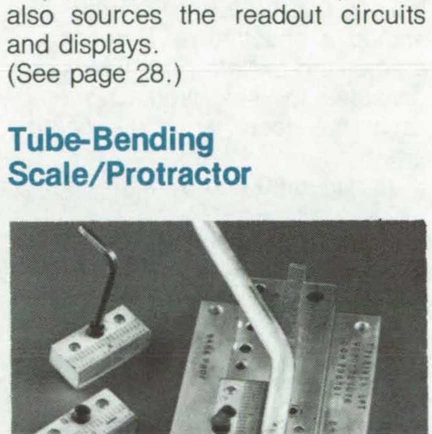

A new combination protractor and scale for measuring tube bends has a novel pivot that allows the tube to remain in contact with the scale arms for all bend angles. It permits rapid and accurate scribing and measurement of mockup fluid lines to obtain production data. Time is
(continued on next page)

saved because it is not necessary to "sight" onto fixed scales, as with other instruments of this type. The tool can be made to accommodate tubes with reverse bends by removing portions of the sectioned precision scale as necessary. With the present design, tubes with diameters of up to 1-1/4 in. and bend parameter lengths of up to 6 in. may be measured, and similar instruments may be made for larger tubing.
(See page 155.)

Improved Intumescent Coating

A new intumescent coating, with an endothermic filler, protects surfaces from extreme heat or fire. These coatings react at high temperatures to produce an insulative char. The new formulation is based on 4,4′ dinitrosulfanilide and begins to swell around 200° C. It adheres well and can be applied by spraying or brushing on wood, plastic, cardboard, and metals. The insulative properties of this and other intumescent coatings using nitroaromatic amines can be further improved by adding an endothermic filler such as ammonium oxalate. The filler compensates for heat-producing reactions that occur when the coating swells.
(See pages 80 and 81.)

Cable Connector for Circuit Boards

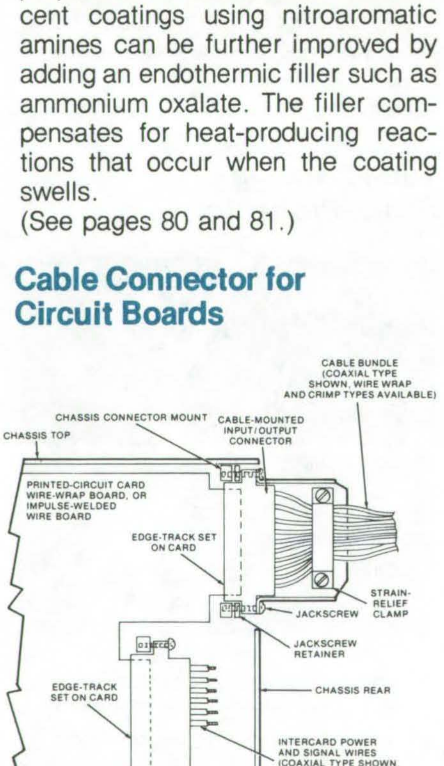

A connector adapted from readily available components simplifies electronic packaging and interconnection wiring in assemblies that consist of several identical printed-wiring boards. External cables are directly mated to the edge tracks of each board, without additional connector-to-connector wiring and input/output connectors. Jackscrews hold the connector to chassis-mounted captive nuts, and a clamp provides external cable strain relief. Intercard connections utilize a portion of the board edge track. An I/O cable-mounted card-edge connetor was used in the prototypes, but a set of three connectors could be designed and manufactured to perform the job even better.
(See page 18.)

Rigidified Inflatable Structures

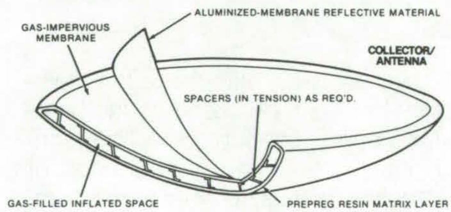

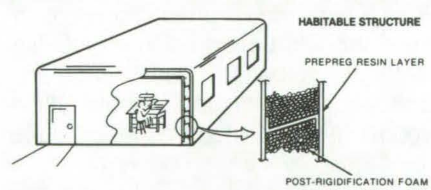

A suggested alternative to conventional inflated structures combines the light weight and convenience of inflatables with the security and permanence of rigid structures. A pretreated resin/matrix material is formed to produce the desired shape when blown up, and the material would become rigid upon exposure to Sunlight or heat. This approach could be used with many current inflatables, such as "bubble" buildings and lifeboats, or could be used to construct equipment that has heretofore been thought unsuitable for inflatables. For further strength, the inflatable could be made with double walls that could be filled with foam after they are put up.
(See page 149.)

Electrical Generator Uses Ocean Waves

A new electrical generator is powered by the up-and-down motion of any body or equipment to which it is attached. It can be used to produce electrical power through the movement of ocean waves, vehicles moving over land or water, or balloons. The only requirement is that the generator be moved up and down by some external force. The generator consists of a permanent magnet stator, a rotor, and two helical coil springs mounted in a canister. The canister rides on the surface of the water; as the water moves the canister up, the stator moves with it, but the rotor lags behind because of its inertia. This causes the bottom spring to compress and the upper spring to elongate. These motions in turn cause the springs to rotate the rotor, which, moving in the magnetic field created by the stator, generates a voltage in the rotor.
(See page 7.)

Demand-Controlled Lighting

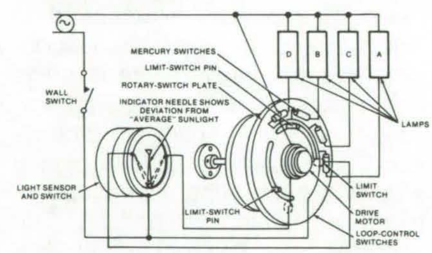

An inexpensive photocell and switch saves energy by automatically adjusting the lighting level in a room in response to variations in Sunlight. When there is little natural light, an electric motor throws mercury switches that turn on wiring loops. Each loop is connected to a particular set of lights. The number of lights turned on increases until the illumination reaches a desired level. The cell and switch are constructed from readily available components. Switch systems can be selected to allow from two to several light levels. They would be particularly useful with fluorescent lights, which cannot be easily controlled with dimmers.
(See page 27.)

Electronic Components and Circuits

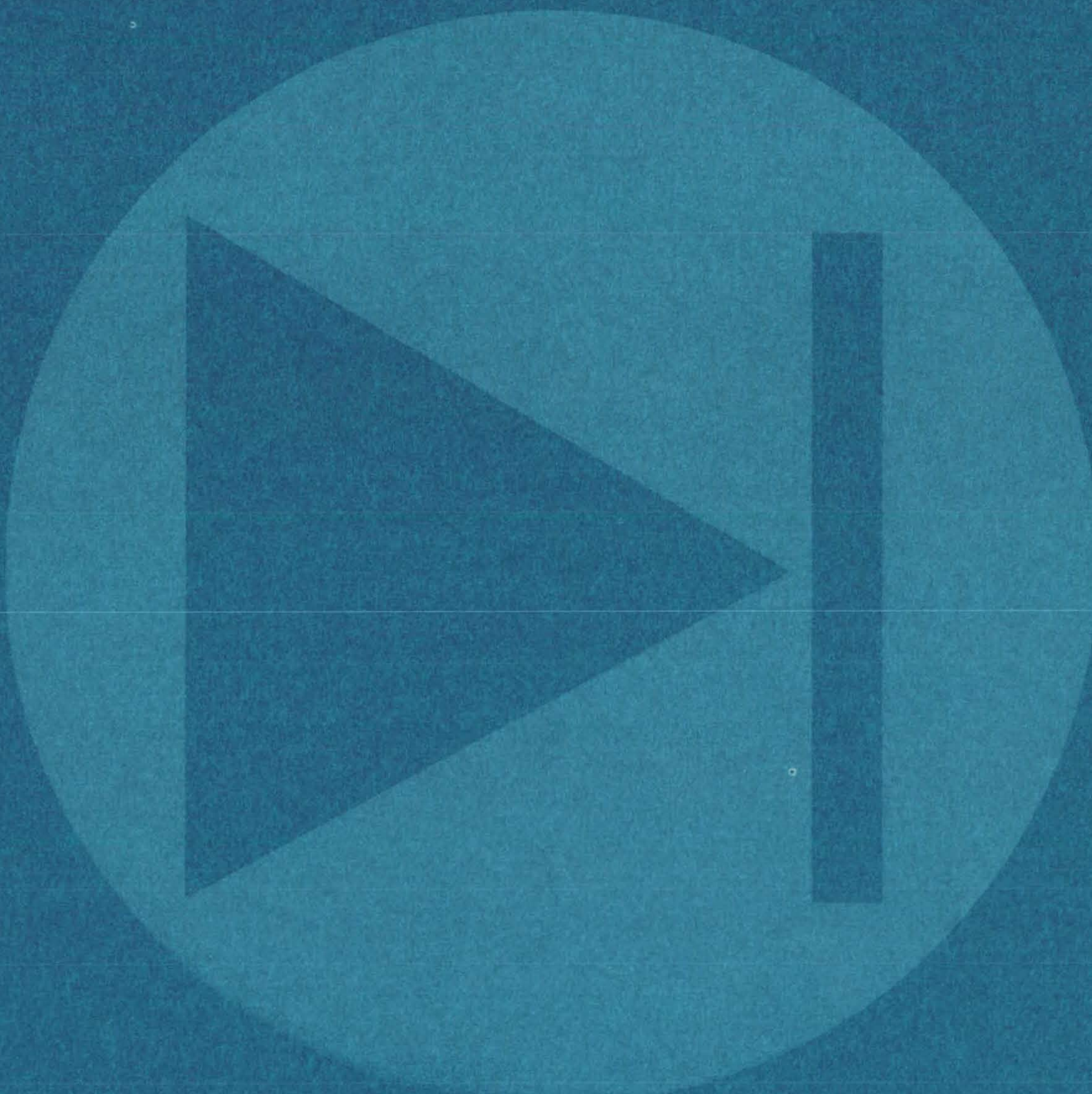

Hardware, Techniques, and Processes

Battery Peak-Charge Voltage Monitor

Self-contained device for telemetry systems employs standard integrated circuits to measure maximum voltage during battery charge.

Langley Research Center, Hampton, Virginia

A low-power battery peak-charge voltage monitor has been designed, built, and tested for use on the Dual Air Density Satellite (DADS). It is self-contained and derives its internal power from the input source. The device utilizes standard integrated-circuit components, a thin-film resistor network, plus several passive components.

The performance and life of a satellite depend heavily on its battery, and battery life depends to a major extent on the maximum voltage reached by the battery while it is being charged. This measurement cannot be made during periods of data transmission, but must be made between interrogations while the battery is charging. A device was developed that can monitor the battery between interrogations, measure the peak-charge voltage, and hold the measurement for subsequent transmission. Since the holding time could be as long as 40 minutes for interrogations in darkness, something more sophisticated than a simple holding capacitor was required.

The monitor is basically a parallel feedback analog-to-digital converter with an up-counter in the feedback loop. It is connected directly across the monitored battery, which also serves as the power source for the monitor. It is powered continuously with quiescent input current of 3 mA and a worst case current during counting of 4 mA. The device occupies only 40 cm^2 of a printed circuit board within a larger electronic package.

The control logic, with output characteristics similar to those of a switch, employs an eight-stage binary counter. With the reference voltage from the voltage regulator

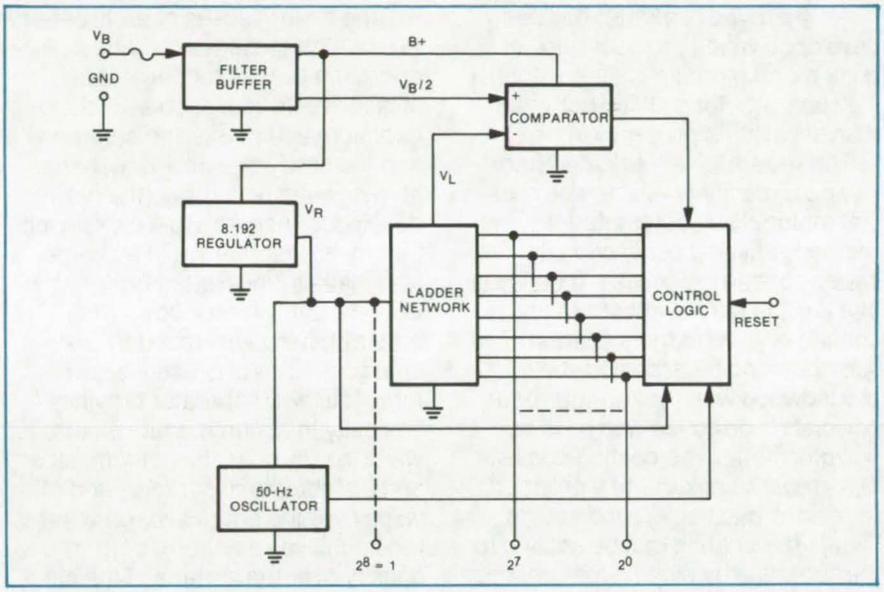

The **Peak-Charge Voltage Monitor** for rechargeable batteries measures the peak-charge voltage of the battery and holds this data for transmission at a later time.

used as the logic supply, the counter outputs serve as ladder switches. The ladder is a thin-film resistor network designed to keep the variation of the ladder-switch impedance negligible and to minimize power dissipation. All the resistors are ratio matched and, being in the same package, track well under temperature variations.

The comparator output is a "1" or "0", which is used to control the counter. The binary count at the ladder inputs represents the maximum voltage attained by the input. The monitor output reading is available as eight parallel logic lines, the ninth being an implied "1". To obtain a new reading, the count is reset and the measuring process is repeated. On the DADS, the monitor is reset at the end of each interrogation by the main-bus off command.

The battery monitor has undergone complete preflight qualification and flight level testing. Tests were conducted at the design input voltage range of 11 to 16 V at temperatures of 60°, 25°, and -30° C. Six units were built, and all performed satisfactorily through subsystem, spacecraft qualification, and preflight tests and during DADS integration and environmental checkout. This battery peak-charge voltage monitor is readily adaptable for use in other systems.

This work was done by Thomas A. Shull of **Langley Research Center.** *Further information may be found in NASA TM X-72669 [N75-30512], "Battery Peak Charge Voltage Monitor for Dual Air Density Satellite," a copy of which may be obtained at cost from the North Carolina Science & Technology Research Center [see page A7].*
LAR-11978

Flexible Separator for Alkaline Batteries

Flexible low-cost long-lived separator extends battery life.

Lewis Research Center, Cleveland, Ohio

An improved separator has been developed which provides a lower cost, much more flexible, and longer life separator for alkaline batteries than separators presently in use.

The separator is fabricated from low-cost readily-available commercial materials by automated methods utilizing conventional paper-coating processes. It consists of a flexible porous substrate and a coating applied to the substrate. The substrate can be asbestos sheet, groundwood web (newsprint), or a polyolefin nonwoven web such as polypropylene. The coating consists of a prepared mixture of a polymer or resin, a plasticizer, and several fillers. The coating can be applied to the substrate by dipping, saturation, or the various methods of knife or roller coating. After being dried, the separator material is collected in rolls for shipping, storage, and use in the manufacture of batteries. The utilization of low-cost materials and automated fabrication, flexibility, and roll packaging all contribute to the low cost of producing and using this separator.

The flexibility of this new battery separator prevents cracking and disintegration caused by electrode warpage and dendrite growth, which are the major causes of early battery failure with present separators. The operating lives of rechargeable alkaline batteries, such as nickel-cadmium and silver-zinc batteries, and the newly-developed rechargeable nickel-zinc battery (the newly-developed rechargeable nickel-zinc battery is described in "Rechargeable Nickel-Zinc Batteries," LEW-12784, which follows this article) have been limited by the characteristics of present separators. This new separator provides flexibility to accommodate electrode warpage. Further, the uniform size and distribution of particles and voids over the entire separator surface achieves a uniform current density over the surface of the electrodes, which reduces dendrite and nodule growth. Thus the utilization of this new separator in combination with ample electrolyte and proper choice of absorber material on the nickel electrode will significantly extend battery life.

The development of this low-cost, flexible, longer life separator, together with the development of the rechargeable nickel-zinc battery, contributes substantially toward the realization of practical urban electric automobiles.

This work was done by Dean W. Sheibley of **Lewis Research Center.** *Further information may be found in:*

NASA TM-X-3465 [N77-14585], "New Separators for Nickel-Zinc Batteries,"
NASA TM-X-3357 [N76-17645], "Functioning of Inorganic/Organic Battery Separators in Silver-Zinc Cells,"
NASA TM-X-3199 [N75-17807], "Factors Influencing Flexibility, Resistivity, and Zinc Dendrite Penetration Rate of Inorganic Separators for Alkaline Batteries," and
NASA TM-X-3080 [N74-27535], "Structure and Function of an Inorganic-Organic Separator for Electrochemical Cells — Preliminary Study."

Copies of these reports may be obtained at cost from the New England Research Application Center *[see page A7]*.

This invention is owned by NASA, and a patent application has been filed. Inquiries concerning nonexclusive or exclusive license for its commercial development should be addressed to the Patent Counsel, Lewis Research Center *[see page A8]*. *Refer to LEW-12649.*

Rechargeable Nickel-Zinc Batteries

Up to three times the capacity of a NiCd battery at the cost of a lead-acid battery

Lewis Research Center, Cleveland, Ohio

Rechargeable nickel-zinc batteries have been developed through the utilization of advanced battery-separator technology. Compared to the widely-used lead-acid batteries, nickel-zinc batteries have three times the energy content for the same weight and can be produced at a comparable cost. Compared to the popular nickel-cadmium batteries, nickel-zinc batteries have two and one-half to three times the energy content for the same weight and can be produced at much lower cost. Nickel-zinc batteries have great potential for powering utility vehicles and automobiles for many purposes.

Prototype nickel-zinc batteries tested in a commercial electric utility van improved the acceleration rate and nearly doubled the driving range between rechargings. An experimental nickel-zinc battery, using advanced separator technology (The new flexible inorganic-organic separator developed for alkaline batteries is described in the preceding article, "Flexible Separator for Alkaline Batteries," LEW-12649) and assembled from

cells fabricated by two commercial battery manufacturers under NASA contracts, was installed in the battery compartment of an Otis P-500 utility van. Standard operating tests on a test track showed that the nickel-zinc battery delivered 190 stop-and-go driving cycles per charge, compared to 99 cycles with the same weight lead-acid battery. At a constant speed of 20 miles/hr (32 km/hr), the nickel-zinc battery drove the vehicle 54.9 miles (88.3 km) between charges, compared to 29.4 miles (47.3 km) with the lead-acid battery.

Laboratory tests of the nickel-zinc cells have established their rechargeability. Over 800 charge-discharge cycles at 50-percent depth of discharge have been achieved.

As described in the preceding article, the rechargeability of nickel-zinc batteries has been achieved through the use of a new flexible inorganic-organic separator developed for alkaline batteries. Heretofore, secondary (rechargeable) nickel-zinc batteries have not been commercially developed because of shape-change problems with the zinc electrode. Using standard separators, zinc dendrite growth or slumping occurs during battery use. In slumping, battery cycle life is reduced when particles of zinc drift from the upper corners of the cell downward to the center. Dendrite growth shortens battery life because the zinc dendrites eventually penetrate the battery separator and cause shorting of the nickel and zinc electrodes. The new separator has been found to eliminate or greatly reduce zinc-electrode shape change. Consequently, experimental nickel-zinc batteries capable of performing in high discharge rate, multiple-cycle applications (e.g., powering electric vehicles) have been developed.

This work was done by Daniel G. Soltis of **Lewis Research Center.** *For further information, Circle 1 on the TSP Request Card.*
LEW-12784

Strong Lightweight Battery Housing

Aluminum honeycomb and high-strength plastic reduce housing weight 50 percent.

Marshall Space Flight Center, Alabama

The battery housing shown in the figure holds 15 battery cells weighing 2.8 pounds (1.3 kg) each, withstands 10 g vibration continuously, can be pressurized to 25 psig (175×10^3 N/m^2), and can withstand the corrosive effects of KOH. At the same time, it weighs 62 percent less than similar cast-aluminum or cast-magnesium housings. As a bonus, it offers the potential for low-cost fabrication and increased accessibility to the enclosed battery cells.

Other uses for housings of similar construction would be to protect expensive portable instruments, as to hold vital equipment for soldiers and to carry supplies and tools in rescue/survival situations. Use in airprops is considered feasible.

The base of the battery housing illustrated was machined from aluminum 0.062 in. (0.157 cm)

(continued on next page)

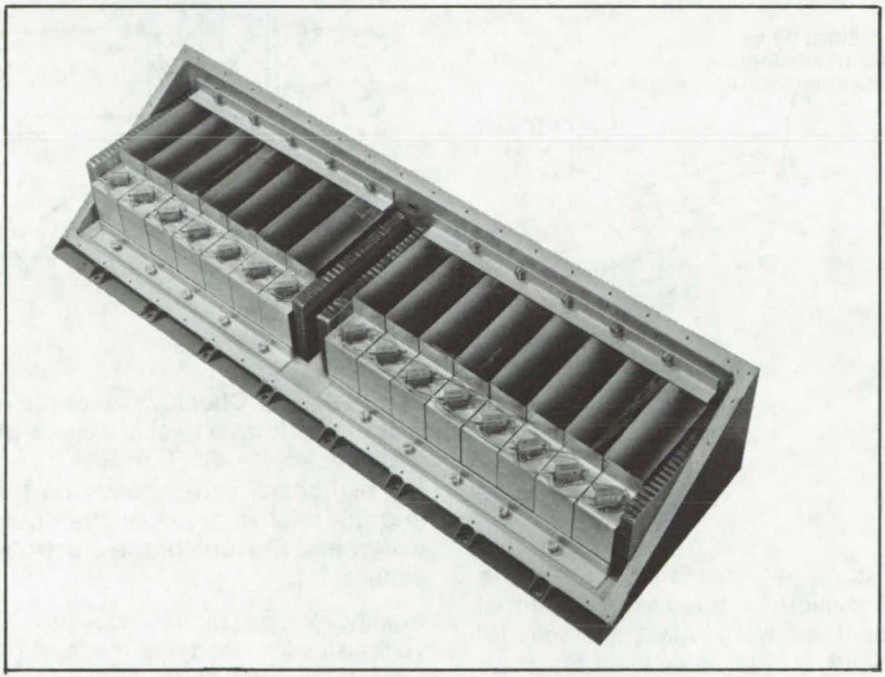

Lightweight Battery Housing consists of an aluminum base, aluminum honeycomb side panels, and a laminated plastic cover.

thick. The walls were made with a high-density honeycomb core. The cells were made of 0.125-in. (0.317-cm) honeycomb (5052-H39 aluminum alloy) with a wall thickness of 0.003 in. (0.007 cm). The panels had a density of about 12 lb/ft^3 (192 kg/m^3). Facesheets were made from 2024-T81 aluminum alloy 0.020 in. (0.05 cm) thick. The honeycomb sandwich was bonded with an adhesive film specifically developed for that purpose. For corrosion inhibition, a protective film of a modified phenolic primer was included in the adhesive system.

The reinforced plastic laminate used for the cover was made from a roll of organic fiber cloth 38 in. (96.5 cm) wide and 4 mils (0.010 cm) thick. The stiffness-to-density ratio was about 3 times that of most metals. Approximately 2 yd (1.8 m) of material were used to fabricate the 4-layer laminated cover in a wet-layup process, using thermosetting epoxy resin.

This work was done by William T. Perreault of Martin Marietta Corp. for **Marshall Space Flight Center.** *For further information, Circle 2 on the TSP Request Card.*
MFS-23079

Single-Fill-Point Battery Reservoir

Snap-on reservoir for multicell storage batteries allows unattended operation for extended periods.

Marshall Space Flight Center, Alabama

A proposed detachable snap-on reservoir automatically restores the electrolytic solution in all cells of a storage battery. The reservoir is a clear-plastic manifold, which is filled with a pint of distilled water from a single point and then is sealed with a plastic cap. When snapped onto an existing storage battery, the reservoir provides a steady source of water for uniform distribution to all cells. At the inlet of each individual cell a floating-ball check valve allows the cell to fill to a prescribed level and prevents contamination between cells. The concept is easily adaptable to various types of existing batteries.

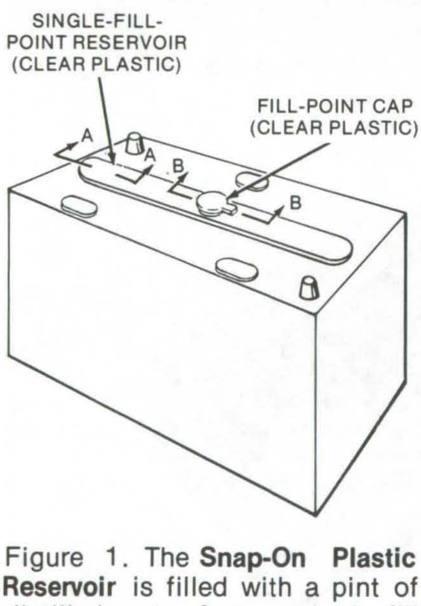

Figure 1. The **Snap-On Plastic Reservoir** is filled with a pint of distilled water from a single fill point and is sealed with a clear plastic cap. Figure 2 shows the fit of the reservoir over a single battery cell.

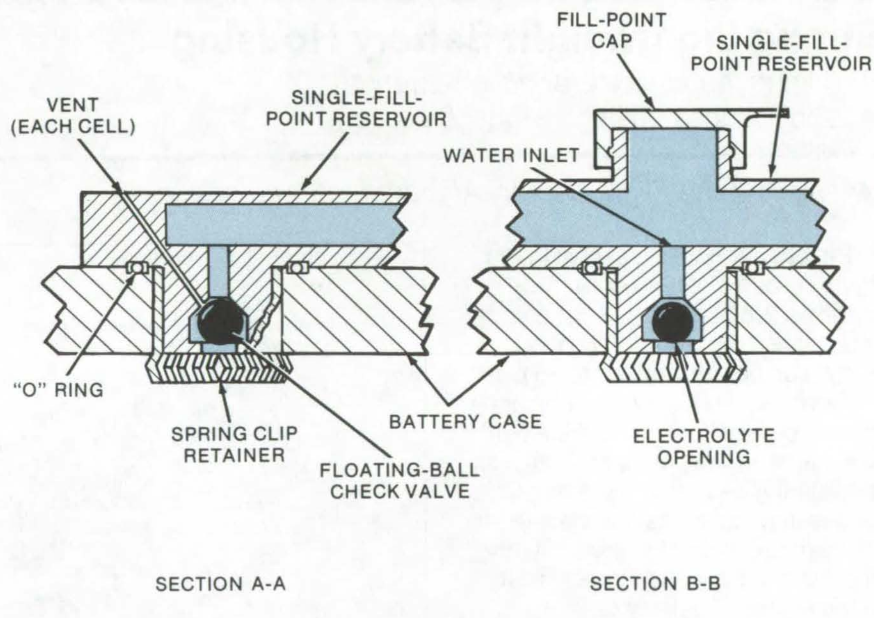

Figure 2. The **Check Valve** at the inlet of the cell contains a soft plastic ball that acts as a gasket seal to prevent contamination of the reservoir with electrolyte. Section B-B (from Figure 1) illustrates the operation of the ball check valve, based on the relative water/electrolyte densities and the relative areas of the openings. The electrolyte is heavier than water, and the area of the electrolyte opening is three times that of the water inlet.

Among the major advantages of this single-fill-point reservoir are long service intervals between refillings, reduced contamination (only a single cap per battery), and constant visibility of the reservoir water level for easier monitoring.

This work was done by Robert Manoli and Bertram R. Ulrich of Rockwell International Corp. for **Marshall Space Flight Center.** *No further documentation is available.*
MFS-16801

Electrical Generator Uses Ocean Waves

The up-and-down motion of ocean waves is converted to electrical energy by a "plunging generator."

Langley Research Center, Hampton, Virginia

Providing power for devices such as lighted ocean buoys and remote data-gathering stations has always been a difficult problem. Batteries have limited lives unless regularly recharged. The problem then, assuming batteries are otherwise suitable, is one of finding a compatible recharging scheme.

A new electrical generator that is powered by the up-and-down motion of any body or equipment to which it is attached can be used to produce electrical power through the movement of ocean waves. The concept is not limited to water waves, however; it can be used with vehicles moving over land or water or even with balloons. The only requirement is that the generator be moved up and down by some external force.

As shown in Figure 1, the generator consists of a permanent magnet stator, a rotor, and two helical coil springs mounted in a canister. The canister rides on the surface of the water and moves up and down with the waves. As the water moves the canister up, the stator moves with it, but the rotor lags behind because of its inertia. This causes the bottom spring to compress and the upper spring to elongate. These motions in turn cause the springs to rotate the rotor, which, moving in the magnetic field created by the stator, generates a voltage in the rotor.

As long as wave motion continues, the rotor will be constantly moving up and down and rotating, first in one direction and then in the other. The resulting ac voltage is then rectified (Figure 2) and is used to maintain the charge on a battery. Note that the oscillating generator could be made quite large to generate substantial amounts of power.

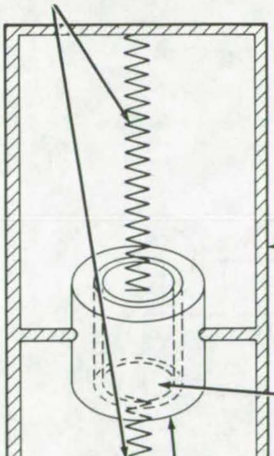

Figure 1. **Plunging Generator** uses two helical springs to convert up-and-down motion of the canister into up, down, and angular motions of the rotor. Thus an ac voltage of variable frequency and magnitude is produced through the interaction of the motions of the rotor and the magnetic field of the stator.

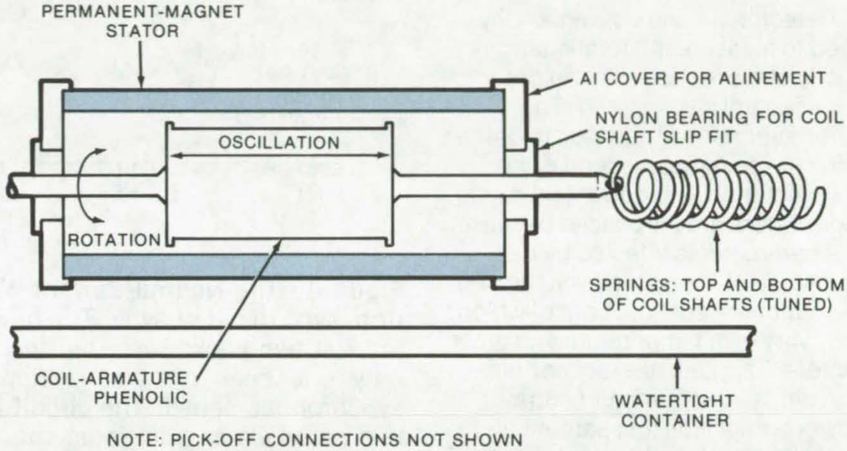

Figure 2. The **Rotor** is free to move longitudinally in response to inertial forces and to rotate in response to spring forces.

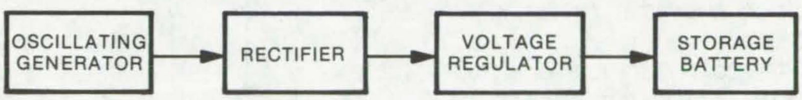

Figure 3. **A Complete Power System** for a remote station consists of a plunging generator, a rectifier, a voltage regulator, and a storage battery.

This work was done by David C. Grana and Richard T. Wilem of **Langley Research Center.** *No further documentation is available.*

Inquiries concerning rights for the commercial use of this invention should be addressed to the Patent Counsel, Langley Research Center [see page A8]. Refer to LAR-11551.

A Spin-Motor Rotation Detector

A simple circuit for detecting rotation speed can be used with two-phase motors.

Goddard Space Flight Center, Greenbelt, Maryland

Detector circuits conventionally used to measure the rotational speed of gyroscope spin motors have several weaknesses. The parameter normally sensed to determine the spin-motor speed is the spin-motor neutral-current amplitude. Errors are introduced because this parameter is affected by the amplitude of the applied voltage and the motor impedance, both of which may vary with temperature and other factors. This lack of exact correlation between spin-motor neutral-current amplitude and percent of synchronous speed severely limits the accuracy of any spin-motor rotation detector that senses only current amplitude, regardless of the precision involved in measuring this amplitude.

A new spin-motor rotation detector (SMRD) for square-wave driven motors detects a sharp characteristic change in the shape of the spin-motor neutral waveform that occurs as the motor slips into synchronization with the rotating field it tries to follow. This SMRD, in fact, is practically insensitive to spin-motor neutral-current amplitude.

The shape changes that occur in the neutral-current waveforms when synchronization occurs and how the sync detector waveforms look for each condition are shown in Figure 1. The transition between the two waveforms is very abrupt and thus offers a means of detection when the spin motor is within a few percent of synchronous speed. The small low-frequency variations in spin-motor velocity, commonly called "spin-motor hunt," are apparent in the synchronous-speed neutral-current waveform as a low-frequency variation in the relative amplitudes of the two peaks. Thus, a circuit capable of measuring the relative amplitude of these peaks (wave shape) offers a very sensitive indication of the spin-motor instantaneous velocity.

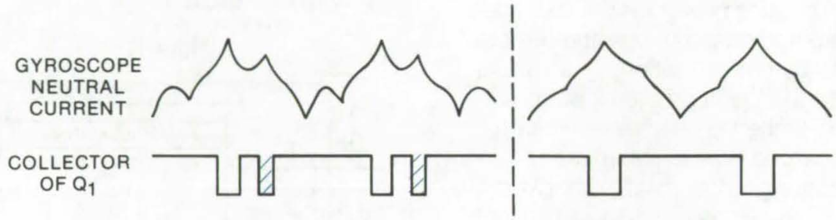

Figure 1. The **Neutral-Current Waveform** changes shape when passing from sync to out of sync. The fundamental difference is the existence of at least two peaks every half period when the motor is in sync and of only one peak per half period when the motor is running below synchronous speed. The circuit in Figure 2 distinguishes between the two cases via an additional saturation pulse on the collector of Q_1 for the in-sync condition. Waveforms are for square wave driven motors.

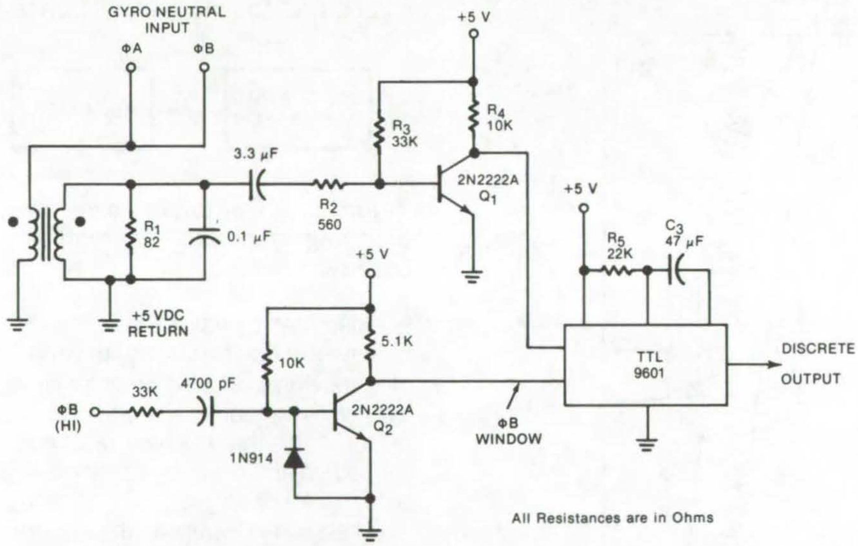

Figure 2. The **Spin-Motor Rotation Detector** uses a self-biasing threshold circuit and missing-pulse detector to convert motor neutral-current peaks to pulses and to look for either one or two pulses per drive cycle. This results in an indication of nonsynchronous or synchronous motor operation.

Circuitry that is sensitive to the spin-motor neutral-current wave shape is shown in Figure 2. The spin-motor neutral current is transformer coupled to drive transistor Q_1 through capacitor C_2. The base of Q_1 conducts current only during the positive excursions of the spin-motor current waveform. A small current flows in the opposite direction when the spin-motor neutral-current waveform is negative going, producing, a negative voltage bias on the base of Q_1 which is approximately proportional to the ratio of resistor R_3 to R_2. Q_1 saturates each time there is a positive excursion of the spin-motor current waveform above the bias level.

Since the spin-motor neutral-current waveform has two positive excursions per cycle when the spin

motor is in sync but only one positive excursion per cycle when not in sync, the shaded pulse on the collector of Q_1 (Figure 1) is present only when the spin motor is in sync. The one-shot is a missing-pulse detector gated by the falling edge of the ΦB drive signal. If the pulse is present (spin motor in sync), the one-shot is triggered continuously and never completes its timing cycle ("times out"). If the pulse is not present (spin motor not in sync), the one-shot "times out" and provides a discrete indication of this condition.

Breadboard tests of the SMRD indicate a very low sensitivity to spin-motor current amplitude (spin supply voltage was varied 20 percent without loss of function) and to ambient temperature variation. This sync detector should, therefore, require no calibration. Resistor R_2 can be selected to detect the variations in spin-motor instantaneous velocity. An optimum compromise between sensitivity and reliability occurred for $R_2 = 560$ ohms, giving a shaded pulse width of about 50 μs.

This work was done by John E. Kuslich of Honeywell Inc. for **Goddard Space Flight Center.** *For further information, Circle 3 on the TSP Request Card.*
GSC-11953

Very Low-Power Power Supplies

Logic and energy storage techniques yield power processing efficiencies of 1,000:1 over conventional designs.

Langley Research Center, Hampton, Virginia

Some conventional dc-to-dc power supplies normally operate at approximately 50 percent efficiency; i.e., half of the power transformed is dissipated internally. The central element in most power converters is the transformer, which provides the desired voltage transformation. In a conventional system, power is dissipated even when the transformer output current is zero, because a certain minimum level of power is required to magnetize the transformer core. This energy waste is significant in low-power battery-powered systems where available energy is limited and at a premium.

In one commercially available low-level power converter, for example, an output of 1,000 V is produced at an output power level of 1 W. At 50 percent efficiency, nearly 1 W of power is being dissipated internally, even at zero output. This loss may be acceptable in some cases, but it is totally unacceptable where the required output power is on the order of 1 mW. In such a case, a continuous 1-W power drain could not be tolerated.

A recent NASA requirement defined a need for a spacecraft experiment bias voltage supply operating continuously at voltages up to 1,000 V with a power load requirement at or below 1 mW for a 5- to 6-month mission duration from a self-contained battery system. For this application, a new, low-dissipation power processor was necessary to minimize battery weight.

One approach to obtaining high efficiency is to use logic circuitry and energy storage techniques that allow the power supply to remain dormant during a significant portion of its duty cycle. Energy is stored in an ultra-low-leakage capacitor which supplies the steady-state output power requirements. In this design, ultra-low-power analog and digital integrated circuits disconnect the conventional power supply from both the source voltage and the output circuitry. The system remains in this state until the capacitor reaches a predetermined level of drain or charge, at which point the logic circuitry reconnects the power supply.

The above system operated satisfactorily for over 2,500 hours, supplying 900 to 1,000 V continuously. The net power drain was at the milliwatt level, yielding an increase in efficiency by a factor of 1,000 over a conventional supply operating at approximately 50 percent efficiency at a 1-W power-drain level.

A second version of the very low-power power supply replaces the commercial converter with a logic-controlled timed-recharge subsystem. Coulometers are used to measure average voltage and total charge flow into the load. This simplified design, with fewer parts and current drainage paths, has a power consumption of approximately 500 μW.

Both of the approaches described provide outstandingly low power consumption. In addition to numerous spacecraft applications, these very low-power supplies can be used in other systems requiring milliwatt power for bias voltage functions and can be used as a control mechanism for large electric power systems.

This work was done by Neal L. Roy and David K. Hoffmaster of TRW, Inc., for **Langley Research Center.** *For further information, Circle 4 on the TSP Request Card.*

Inquiries concerning rights for the commercial use of this invention should be addressed to the Patent Counsel, Langley Research Center [see page A8]. Refer to LAR-12117.

Bridge/Amplifier Configuration for Switched Arrays

Zero power is drawn during standby, in this concatenated circuit organized as a 2-node element.

Langley Research Center, Hampton, Virginia

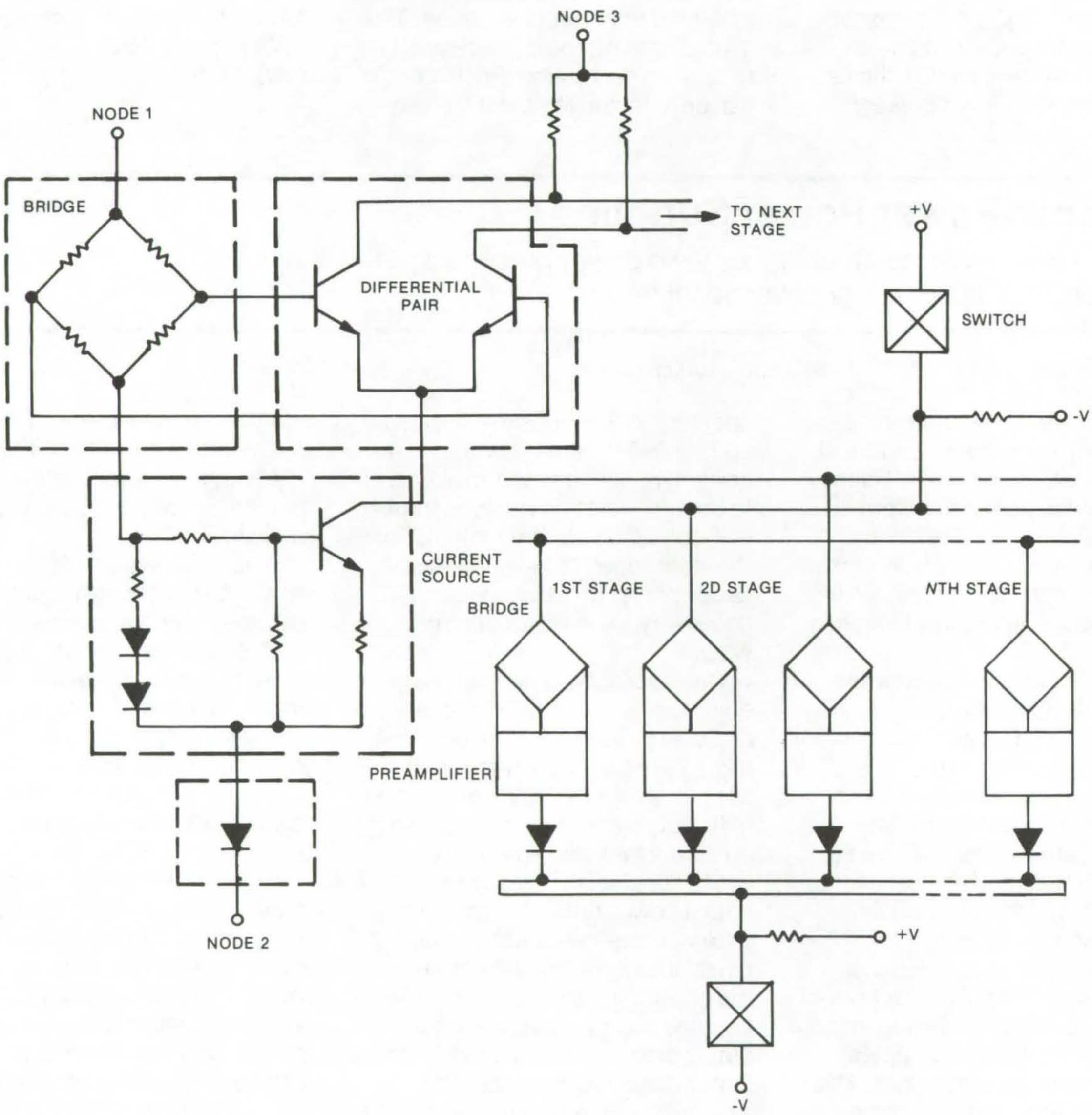

The **Bridge/Amplifier Circuit** shown on the left consists of a four-port bridge, a differential transistor pair, a current source and a diode. Node 2 must be more negative than node 1 for current to flow. In an array of the circuits, as shown on the right, a bridge-and-amplifier unit can be turned on selectively, making the circuit useful for applications such as with bubble-domain memories. A single circuit or group of circuits is actuated by switching the node-1 line positive, once node 2 is negative.

A circuit may be arrayed with other similar circuits and configured so that it can be either selectively activated or activated in a group, using a minimum number of control lines. One such circuit is a bridge network connected to a differential amplifier and used with bubble-domain memories. It draws no power during standby and can be arrayed with other bridge amplifiers of like design.

As illustrated, the circuit is organized such that node 2 must be more negative than node 1 for current to flow. Therefore, in an array of like circuits all current flow stops when the node-2 common line is switched positive. Any one circuit or a selected group of circuits may be activated by switching the node-1 line positive once node 2 is negative.

This 2-node arrangement greatly simplifies conventional configura-

tions where more than two nodes are involved to achieve complete current shutoff. The collectors of the differential amplifier pair (node 3) must be connected to a positive supply equal to or greater than node 1. However, node 3 need not be switched to activate/deactivate the circuit.

This work was done by Oliver D. Bohning of Rockwell International Corp. for **Langley Research Center.** *For further information, Circle 5 on the TSP Request Card.*

Title to this invention has been waived under the provisions of the National Aeronautics and Space Act[42 U.S.C. 2457 (f)], to the Rockwell International Corp., Electronics Group, 3370 Miraloma Ave., Anaheim, California 92803. LAR-11652

Constant-Power Source for Resistive Load

Feedback control is used to supply constant power to variable-resistance load.

Marshall Space Flight Center, Alabama

In specialized low-power instrumentation applications, the illustrated electronic feedback circuit can deliver constant power, adjustable between 0.1 and 1.0 W, to a load resistance varying between 60 and 600 ohms. The circuit consists of a series of operational amplifiers, an output power amplifier, and associated components. Overall stability is 5 percent.

In contrast to power sources that supply either a constant voltage or a constant current, the maintenance of constant-power dissipation in a resistive load is based on signals that are proportional to the load voltage (V_L) and the load current (I_L). These signals are multiplied together to obtain the product P_L ($V_L I_L$), which is equal to the load power. The difference between some reference power (P_R) and P_L is the error, which must be added to the reference power to form the corrected control signal ($2P_R - P_L$).

If the device controlling the load power is voltage activated, the control signal is divided by I_L to generate a control voltage

$$V_D = \frac{2P_R - P_L}{I_L} = \frac{2P_R}{I_L} - V_L$$

For a current-activated device, the control signal is divided by V_L to obtain the control current

$$I_C = \frac{2P_R}{V_L} - I_L$$

In either case, control is accomplished through the use of one divider and one subtractor.

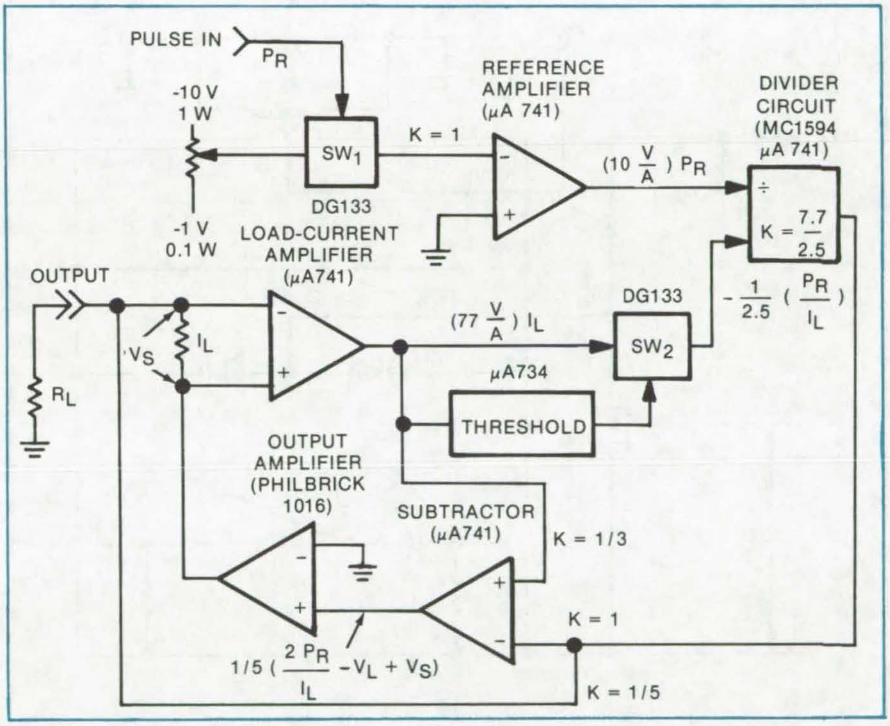

The **Constant-Power Source** uses operational amplifiers, a divider, a subtractor, a pulsed reference amplifier, and associated integrated-circuit components to deliver continuously-adjustable constant power to a variable-resistance load. The diagram applies to a voltage-activated device.

As is indicated in the functional block diagram of the constant-power source, in addition to the divider circuit and subtractor, additional amplifiers are used to sense the load current, to generate the reference signal, and to provide adequate output power. Except for the output amplifier, the design is implemented with integrated circuits.

The threshold stage and switch (SW_2) at the input of the divider circuit insure linear operation of the power source. For example, with the load switched off, the load current I_L would be zero and the quotient P_R/I_L would become infinite. To avoid saturation of the amplifiers and the divider in this case, the trigger level of the threshold stage is set to the lowest current value the system is expected to deliver. For values of I_L lower than the minimum, the threshold stage triggers

(continued on next page)

and switches the input of the divider to the minimum-current signal. The system stays in the linear range until I_L again exceeds the minimum value.

Pulsed operation of the output is provided by a switch (SW_1) at the input of the reference amplifier.

This work was done by E. M. Nagle of RCA Corp. for **Marshall Space Flight Center.** *For further information, Circle 6 on the TSP Request Card.*

Title to this invention has been waived under the provisions of the National Aeronautics and Space Act [42 U.S.C. 2457(f)], to RCA Corp., 201 Washington Rd., Princeton, New Jersey 08540.
MFS-23171

FM Oscillator Has Improved Deviation Linearity

Frequency of VCO is linearized with an FET
and total deviation is varactor controlled.

Marshall Space Flight Center, Alabama

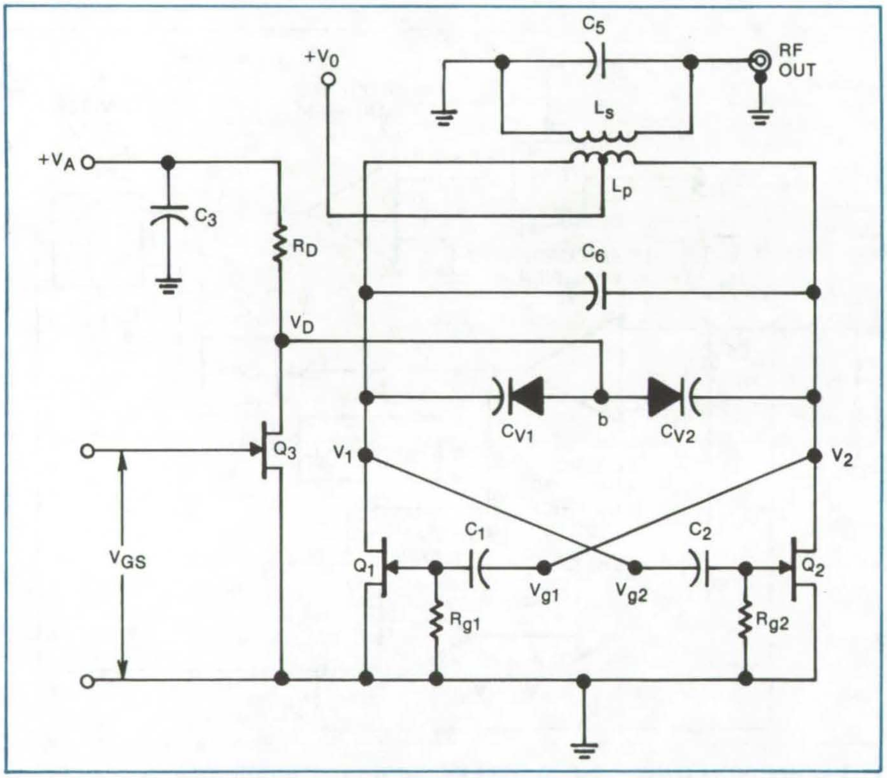

Figure 1. **Deviation Linearity** of voltage-controlled FM oscillator is determined by voltage V_{GS}. Frequency deviator is controlled by the reverse voltage on the varactor diodes.

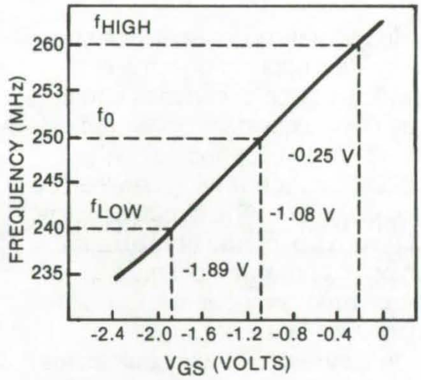

Figure 2. **Output Frequency** versus V_{GS} for an oscillator designed for a center frequency of 250 MHz, deviation of ±10 MHz, and nonlinearity of less than ±1 percent. Design is based on computer program written in BASIC.

A voltage-controlled FM oscillator having high deviation linearity can be obtained by driving the basic circuit through a nonlinear FET input stage. The basic oscillator circuit, shown in Figure 1, uses two varactor diodes, CV_1 and CV_2, to vary the frequency of the tank circuit, which includes C_6 and L_p.

The reverse voltage (V_D) on the varactors controls the capacitance of these diodes, and thus the tank frequency. The capacitance of the varactors is not a linear function of V_D, however, but is given by

$$C = C_{ph} + C_0(1 + V_R/V_T)^{-n}$$

where C_{ph} is the capacitance of the varactor package, V_R is the reverse voltage, V_T is a constant (0.7 V for silicon), and n is a characteristic of the varactor; n ranges from about 0.4 to 0.6 for the varactors used in the design. The voltage V_D, at the drain terminal of the FET, is a function of V_0, V_A, and the drain current of the FET. Drain current of the FET follows the equation

$$I_D = I_{DSS}(1 - V_{GS}/V_p)^m$$

where V_{GS} is the gate voltage, and I_{DSS}, V_p, and m are constants. Thus I_D is a nonlinear function of V_{GS}. An analysis of the circuit, based on the above relationships, and carried out with the aid of a computer, revealed that the frequency-versus-voltage characteristic of a varactor-modulated VHF oscillator was linearized by utilizing the nonlinear characteristic of a field-effect transistor amplifier to predistort the modulating signal. Values of m between 1.5 and 1.6 produced optimum linearity in the 250-MHz oscillator.

It also was determined that the total frequency deviation for a given change in input-signal amplitude is a function of the varactor junction exponent and of the difference between the oscillator and amplifier supply voltage. This voltage difference, which determines the varactor operating point, also affects the frequency-deviation linearity.

Deviation linearity measurements made on a 130-MHz experimental oscillator agree with 1 percent with computed results from the mathematical model of the oscillator. The computerized model was also used to determine the effect of pertinent parameters on the linearity of frequency deviation as a function of input-signal voltage amplitude. The 130-MHz experimental oscillator constructed exhibited a linearity of better than ± 1 percent for a total frequency deviation of ± 10 MHz.

This work was done by M. A. Honnell of Auburn University for **Marshall Space Flight Center.** *For further information, Circle 7 on the TSP Request Card.*
MFS-23562

Production of Large "Violet" Solar Cells

Laboratory process is successfully transferred to pilot-plant operation.

Marshall Space Flight Center, Alabama

Violet solar cells respond better to ultraviolet radiation than conventional cells, and, in fact, respond better over the whole visible spectrum. Their conversion efficiency is thus higher, especially in space, where ultraviolet radiation from the Sun is not attenuated by the atmosphere.

Violet cells obtain their good response because of a very shallow (0.1 μm) highly doped n^+ layer diffused into p silicon. This shallow pn junction leads to high open-circuit voltage along with good response to all visible wavelengths. But the production of such cells requires much tighter control of all manufacturing steps than the production of conventional cells.

The contact metal structure, for example, must not form an opposing voltage barrier at the back contact, and it must not penetrate the shallow junction. Front-contact resistance is reduced by the use of 10 to 35 metal lines per cm across the surface. An antireflection coating must then be applied. This coating must transmit short wavelengths well. The coating used with the violet cells requires that an additional cover be used for maximum response. The cover must also transmit short wavelength light.

PARAMETER	RANGE
I_{SC} (short-circuit current)	306 to 323 mA
V_{OC} (open-circuit voltage)	581 to 592 mV
I_{475} (current at 475 nm)	290 to 303 mA
CFF (curve-fill factor)	0.74 to 0.78

Properties of Typical Violet Cells are shown for pilot-plant production runs after analysis and refinement of fabrication techniques. The current and voltage characteristics are tested for 2 by 4 cm violet cells at 28° C, having an antireflection coating and a 0.35-micrometer cut-on wavelength filter.

All the problems associated with violet cells were solved first for 2 by 2-cm units and then for 2 by 4-cm units. But the larger slices of silicon, whether cut parallel to or across the growth axis, have a wider variation in resistivity and other properties than the smaller slices. Further differences in properties only showed up after very close control of the pilot line had been achieved.

The pilot-plant operation produced upwards of 300 violet cells having the general characteristics shown in the table.

This work was done by Peter Iles of Globe Union, Inc. for **Marshall Space Flight Center.** *For further information, Circle 8 on the TSP Request Card.*
MFS-23549

Hybrid Optical/Digital Detector

A hybrid optical/digital Fourier-transform detector for automatic diffraction-pattern recognition uses a fiber-optic array. Light passes through the film-image and a lens to produce the Fourier transform of the image. The transform is converted to digital data for computerized pattern recognition.
(See page 72.)

Optical Integrated-Circuit Tester

Inspecting integrated circuits for defects can be done accurately and quickly by a computerized optical system. The system examines IC's for defects that can cause catastrophic failure. It also can compare IC's with photolithographic masks at various stages of processing.
(See page 112.)

Use of Miniature, Single-Wire, Sheathed Thermocouples

In very-small thermocouples with protective metal sheaths, high-temperature electrical shunting and diffusion lead to drift and failure. Single-wire sheathed thermocouples increase the interelement insulation by a factor of 2-1/2 with the same sheath outside diameters.
(See page 119.)

High-Voltage Capacitor-Coupling Circuit

An inexpensive coupling scheme for photomultipliers reduces capacitor-generated noise susceptibility.

Lyndon B. Johnson Space Center, Houston, Texas

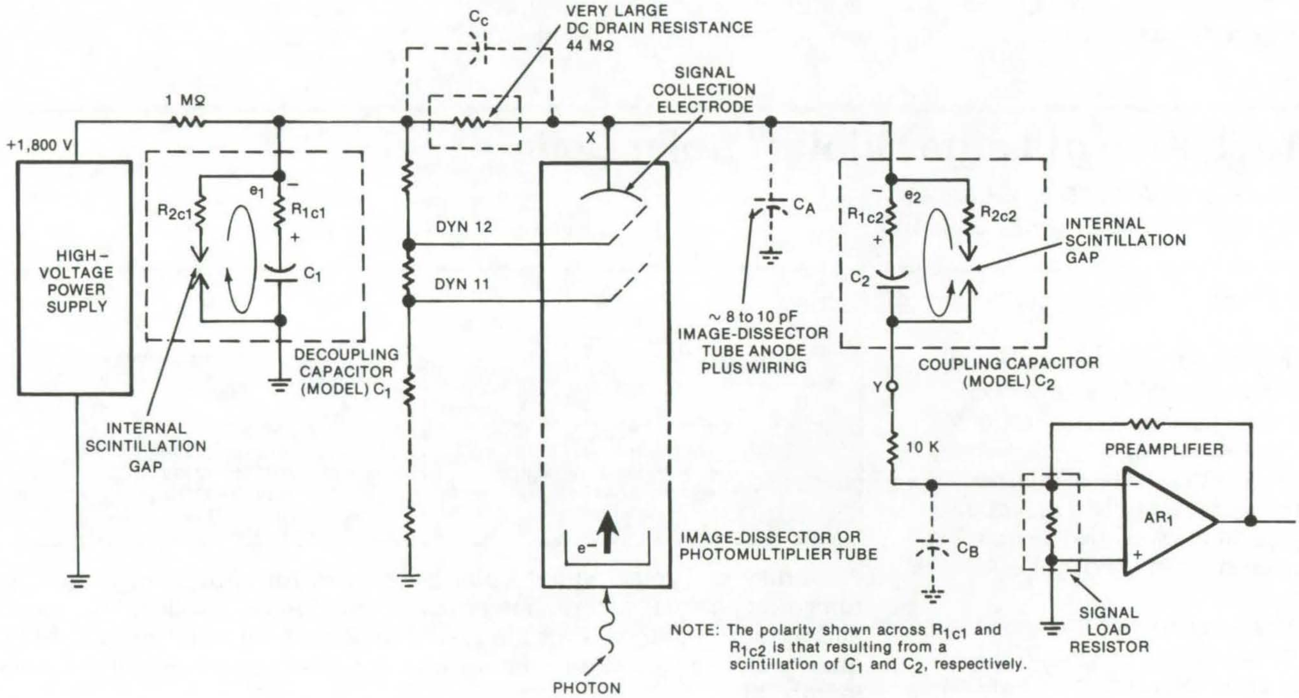

The Preamplifier Input Circuit uses inexpensive ceramic capacitors. Yet the effects of capacitor noise are considerably reduced. Test data results give a counting rate (scintillation rate for the capacitor) of 0.1/hour after 78 hours of testing. The capacitor operated at a rated voltage with a threshold of 1.5×10^{-9} amperes.

In utilizing capacitive coupling between the anode of a photomultiplier or an image-dissector tube and the video preamplifier, false "events" may be generated by a corona discharge inside the coupling capacitor. The problem is particularly troublesome in applications where the event rate is low. Unlike thermal noise, this noise is characterized by single events or scintillations with long periods of inactivity in between.

By a simple rearrangement of circuit components the susceptibility to capacitor noise in such high-voltage high-impedance circuits can be markedly reduced. As can be seen in the schematic of the new circuit, the high-voltage power supply must be coupled to the anode. Thus there will be a dc path from the photocathode to the high-voltage supply. By making this dc path very high impedance, advantage is taken of the already high-impedance signal source. The effect is that any coupling-capacitor noise pulses, generated by corona discharge, are minimized by limiting the current the discharge can force into the signal-load resistor and the preamplifier input. The arrangement thus realizes a high degree of immunity to such capacitor scintillations.

The circuit is implemented by placing the signal-load resistor on the preamplifier side of the coupling capacitor and a very large dc drain resistance from the power supply to the anode of the photomultiplier. This results in the model for capacitor noise shown in the figure.

A scintillation in C_2 results in an impulse voltage e_2 generated across R_{1c2}. This transient is a positive-going pulse at terminal Y.

This impulse is of the opposite polarity from that of a photoevent which would result in an electron current into the X port and hence a negative-going pulse at Y. Note that C_A plays an important role here in that it ac-grounds port X under this transient condition and greatly increases the magnitude of the input current, as compared to the situation when the current is limited by the 44-MΩ resistor (as in the case when C_2 recharges after a scintillation). The recharge current is also seen as a positive current at Y, again the opposite polarity from a photoevent signal.

When a step-function change e_1

(see figure) occurs as a result of a scintillation in decoupling capacitor C_1, it is sensed at the Y terminal via two mechanisms: (1) the capacitor voltage divider consisting of the feed-ahead capacitor C_C and the anode shunt capacitor C_A and (2) the steady-state effect which is negligible compared to (1) above. The transient condition (1) is discriminated against by the video-amplifier bandwidth and the filter that follows the amplifier. Such a scintillation of the decoupling capacitor C_1 is seen at the Y terminal as a negative-going pulse and hence is the same polarity as that of a photon signal.

This work was done by Wayne W. Frame of Ball Brothers Research Corp. for **Johnson Space Center.** *For further information, Circle 9 on the TSP Request Card.*
MSC-16034

Low-Cost Polycrystalline Process for Solar Cells

Economical batch fabrication includes resolidification step to improve conversion efficiency.

Goddard Space Flight Center, Greenbelt, Maryland

A new fabrication process could help to bring the cost of producing solar cells down to a level at which solar energy can compete economically with other energy sources. Batches of pn-junction silicon solar cells are fabricated by depositing silicon and dopants on a substrate of metallurgical-grade silicon, graphite, or steel. The process may be useful for making solar cells from other materials as well, such as cadmium sulfide/copper sulfide.

The deposited silicon is polycrystalline, and therefore the cells convert light to electricity less efficiently than single-crystal cells, such as those used in the space program. But the new process includes a melting-resolidification step that enlarges the polycrystals and thereby quadruples conversion efficiency. Although the efficiency is still nowhere near that of single-crystal devices, the cost of solar power should be much less for the polycrystalline cells, perhaps on the order of one-tenth the cost (per peak watt) of high-quality single-crystal cells.

The first step in the process, for a graphite substrate, is the deposition of an initial layer of silicon. Any of the usual commercial techniques for depositing polycrystalline silicon can be used; for example, thermal decomposition of silane. Diborane gas is decomposed simultaneously to make the layer low-resistivity p-type.

To improve conversion efficiency, the layer is melted and allowed to resolidify. (To provide enough surface tension to prevent the thin layer of molten silicon from forming a bubble, the surface of the substrate should be roughened; for example, by sand blasting.) For this step, zone melting can be used, or, more promisingly for economical mass production, all the silicon can be melted at once and allowed to resolidify from one end to the other. This unidirectional solidification prevents the bulge that would result if the silicon were allowed to solidify from the outside inward.

(continued on next page)

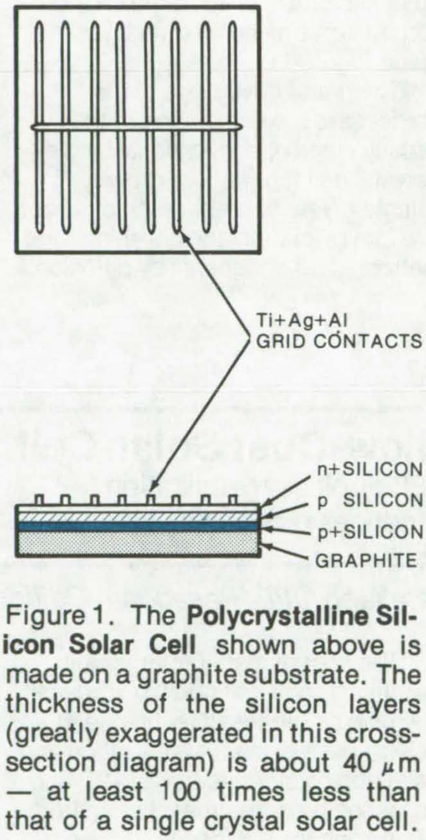

Figure 1. The **Polycrystalline Silicon Solar Cell** shown above is made on a graphite substrate. The thickness of the silicon layers (greatly exaggerated in this cross-section diagram) is about 40 μm — at least 100 times less than that of a single crystal solar cell.

Resolidification is controlled by adjusting the spacings of the RF heating coil to give a unidirectional temperature gradient. The result is large crystallites in the polycrystalline silicon; as large as 2 cm in length and several millimeters in width.

Next, two more layers of silicon are deposited — a high-resistivity p-type layer and an n-type layer — to form a pn-junction. As for the first layer, any vapor-deposition technique can be used. Phosphine gas furnishes the phosphorus dopant for the n-layer. These layers grow epitaxially and thus assume the large crystallite dimensions of the resolidified layer.

To complete the solar cell, a metallic grid is evaporated on the top to serve as an electrical contact (see Figure 1).

The major advantage of the process is the elimination of the costly steps of conventional single-crystal cell fabrication: growth of single crystals, preparation of silicon wafers by cutting and polishing, and introduction of dopants by diffusion.

Polycrystalline cells with polycrystalline silicon substrates can be made by much the same method described for graphite sub-

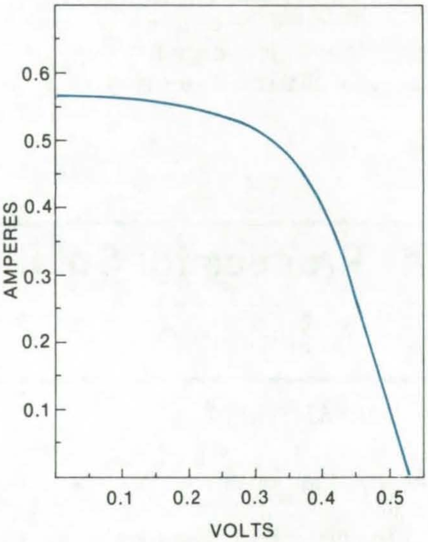

Figure 2. The **Current-Voltage Characteristic** is shown for a typical polycrystalline device illuminated by simulated Sunlight. The cell efficiency is 5 percent; its area is about 30 cm^2.

strates. In fact, electrical performance proved to be superior for the silicon substrates. Steel substrates can also be used, but present special problems. The steel must be coated with some material that prevents iron from diffusing into the silicon, and the coating material must be chosen to help match the widely different thermal expansion coefficients of steel and silicon.

Experimental devices made by the process vary in conversion efficiency from 1.4 to more than 6 percent. Figure 2 is a representative current-voltage characteristic for a graphite-substrate unit.

This work was done by Ting L. Chu of Southern Methodist University for The National Science Foundation and **Goddard Space Flight Center.** *For further information, Circle 10 on the TSP Request Card.*

This invention has been patented by NASA [U.S. Patent No. 3,961,997]. Inquiries concerning nonexclusive or exclusive license for its commercial development should be addressed to the Patent Counsel, Goddard Space Flight Center [see page A8]. Refer to GSC-12022

Low-Cost Solar-Cell Fabrication

Electroless metalization reduces processing steps.

Caltech/JPL, Pasadena, California

The cost of manufacturing a rectifier/solar cell could be reduced by using a proposed technique of electroless plating. Metalization and one doping step are combined, and only one heat treatment is required. This concept is a modification to a method of fabricating solar cells by diffusing different dopants into opposite sides of a silicon wafer.

An n material, such as phosphorus, arsenic, or antimony, is diffused on one side; and a p dopant, such as boron, aluminum, or gallium, is diffused on the other. It has been known that both diffusions can be made to occur simultaneously, if a suitable dopant source is present on each side. The new process further improves this efficient approach by combining the deposition of one of the dopants with the metalization of that side.

The process is illustrated in the figure. A Pd/HF sensitizing solution is applied to one face of a silicon wafer by a suitable method such as roller coating. The wafer is then immersed in an electroless-deposition medium, selected to codeposit the desired dopant. Examples are hypophosphite nickel (as used for power transistors) and a boron/nickel bath (as used in certain types of thyristors). The other surface is coated with a dopant of the opposite type; this could be done with a spin-on, a spray-on, or a roller-coat technique.

The wafer is then heated to form a diffusion region and a junction on one side, while a metal/silicide/ohmic contact is formed on the other side. The wafer can then be immersed a second time in an electroless nickel bath to deposit an adherent solderable nickel coating over the nickel silicide layer.

The junction surface may be metalized with nickel during this operation (by using a mask), or it may be metalized with some other suitable metal such as aluminum. Conventional techniques can be

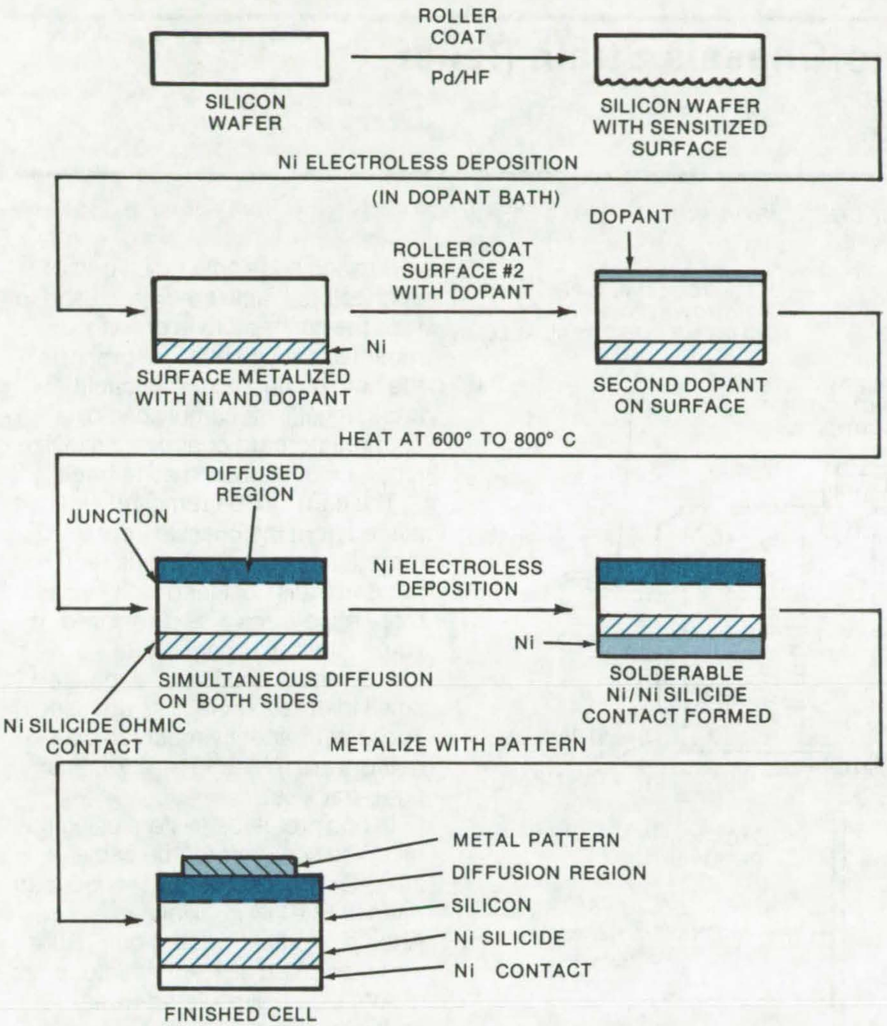

The **Rectifier/Solar-Cell Fabrication** proceeds by a series of metalization steps as outlined above. The Ni electroless deposition serves both as a metalization and a source of one of the dopants. If an n/p cell is desired, the electroless deposition is done with a boron/nickel bath; boron is the p dopant, and an n material (e.g., phosphorus) is used as the other dopant. If a p/n cell is desired, hypophosphite nickel is used for the electroless plating, and a p dopant such as boron is used for the other side.

used.

It may also be desired to coat one surface of the silicon wafer with the dopant source and to heat it modestly to cure the source prior to sensitizing with palladium. This will reduce any unwanted deposition of the electroless metal on the front surface, at the expense of a second moderate heat treatment. Alternatively, one surface of the silicon can be protected with a suitable masking material such as black wax as the first step in the coating sensitization procedure.

This work was done by James A. Amick and Brown F. Williams of RCA Corp. for **Caltech/JPL.** *No further documentation is available.* *NPO-13992*

Electrically-Controlled Variable-Color Optical Filters

Spectral transmission characteristics of optical filters may be changed electrically, using birefringent elements. A ceramic plate with a high index of refraction and a high dielectric constant retards certain wavelengths when a given voltage is applied. In addition, fixed birefringent elements retard specific wavelengths.
(See page 59.)

Printing Circuits Without a Mask

High-resolution fine-line patterns are plated by a constant-flow stream of plating solution directed from a high-pressure nozzle toward the substrate. The plating solution serves as a positive electrode that can be electronically modulated to create the desired pattern on the negative substrate.
(See page 143.)

Differential Multi-MOSFET Nuclear Radiation Sensor

A proposed circuit could increase the effectiveness of a MOSFET as a nuclear radiation detector. With the new arrangement, it should be possible to measure radiation doses as low as 10^{-3} rad. Other advantages are minimization of thermal-drift errors, low power consumption, and operation over a wide dynamic range.
(See page 70.)

Connector With Cable-to-Chassis Strain Relief

For direct interface between interrack cables and a printed-wiring card edge

Goddard Space Flight Center, Greenbelt, Maryland

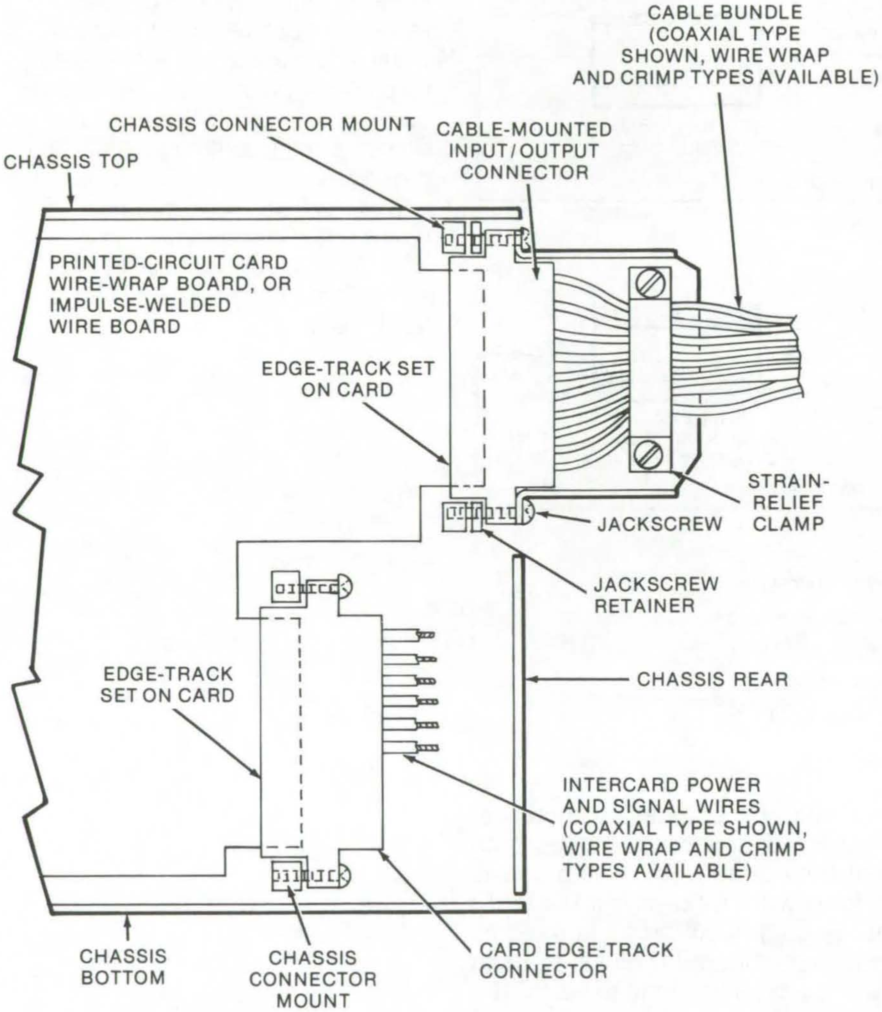

The **Connector** mates external cables directly to a printed-wiring board edge track. The connector is held via jackscrews to chassis-mounted captive nuts integral with the card guides. Additional connector-to-connector wiring is eliminated, as are chassis-mounted input/output connectors required by conventional packaging methods.

An electronic connector adapted from readily available components simplifies electronic packaging and interconnection wiring in assemblies that consist of several identical printed-wiring boards. As illustrated, the connector directly mates external cables to the edge tracks of each board. Thus it does away with additional connector-to-connector wiring and additional input/output connectors. Jackscrews are used to hold the connector via chassis-mounted captive nuts integral with the card guides. External cable strain relief is accomplished by a clamp. Intercard connections utilize a portion of the board edge track.

The card can be removed and replaced from the chassis front. If more than one connector is required per card, it is designed with two or more edge-track sets as needed. If some intercard connectors, such as for power distribution, are required, small internal connectors are used. These permanently mounted connectors are mated to an additional edge-track set.

In one prototype system using the modified connectors, the cable interfaces consisted of 15-conductor pairs of RG-174 coaxial cable. Another multiple twisted-pair cable was fabricated of 15-conductor pairs of AWG20-size insulated wire. Following these wire-size guidelines, a technician can fabricate a multiple connector containing up to 30 single conductors of AWG20 or smaller.

The cable-mounted card-edge connector described here was used because it was readily available, but it is not ideal for the purpose. A new type of connector could be manufactured specifically for this purpose.

This work was done by Kenneth W. Tuskind of RCA Corp. for **Goddard Space Flight Center.** *For further information, Circle 11 on the TSP Request Card.*
GSC-12164

Electro-optically-Indexed Microwave Switch

An optoelectronic control improves switch-detent accuracy and lengthens lifespan.

Caltech/JPL, Pasadena, California

The problems of wear and reduced lifespan of mechanical components in microwave waveguide switches are overcome by a four-position microwave switch. The mechanical parts used in conventional switches to index the stepper motor that drives the switch elements are replaced by an optoelectronic indexing device that directly controls a magnetic-detent motor. This eliminates a major source of wear and maintains detent accuracy for a longer period of time. The switch also incorporates an improved rotor with optimized slot dimensions and simplified fluid cooling for high-power applications.

Photo of **Electro-optically-Indexed Microwave Switch,** with cover removed, illustrates the optoelectronic elements of the indexing system and the connections to the magnetic-detent motor.

A solid-state optical system, consisting of a light-emitting diode and a phototransistor, electrically interrupts the stepping-motor pulses to index the microwave switch rotor. The diode light source is mounted in the shutter cover plate, coaxially alined with a bore through the shutter. The phototransistor is located in the flanged body opposite the shutter-plate bore and is coaxial with it. When the switch is properly indexed with the light beam from the diode light source, the transistor energizes a solid-state switch that interrupts the stepping pulses to the detent motor. The motor, through magnetic detenting, indexes at the proper position of the 200 steps in its arc of rotation within $\pm 0.06°$.

For ultra-high-power applications, liquid coolant needs to be introduced at only one end of the rotor since excess heating is less than in conventionally designed switches. Elimination of the usual maze of coolant passages precludes coolant leakage into the waveguide.

The overall design of the microwave switch achieves a reduction of insertion loss, crosstalk, and waveguide reflections when receiving and transmitting. Insertion loss of the straight-through ports is 0.009 dB; through the curved ports it is 0.012 dB. Isolation of the microwave switch channels is greater than 70 dB in the operating range from 7 to 10 GHz.

This work was done by Dudley E. Neff, David L. Nixon, and Harry F. Reilly of **Caltech/JPL.** *For further information, Circle 12 on the TSP Request Card.*
NPO-11851

Collapsible Corrugated Horn Antenna

A high collapse ratio, plus a configuration that, when extended, is similar to that of a rigid antenna.

Langley Research Center, Hampton, Virginia

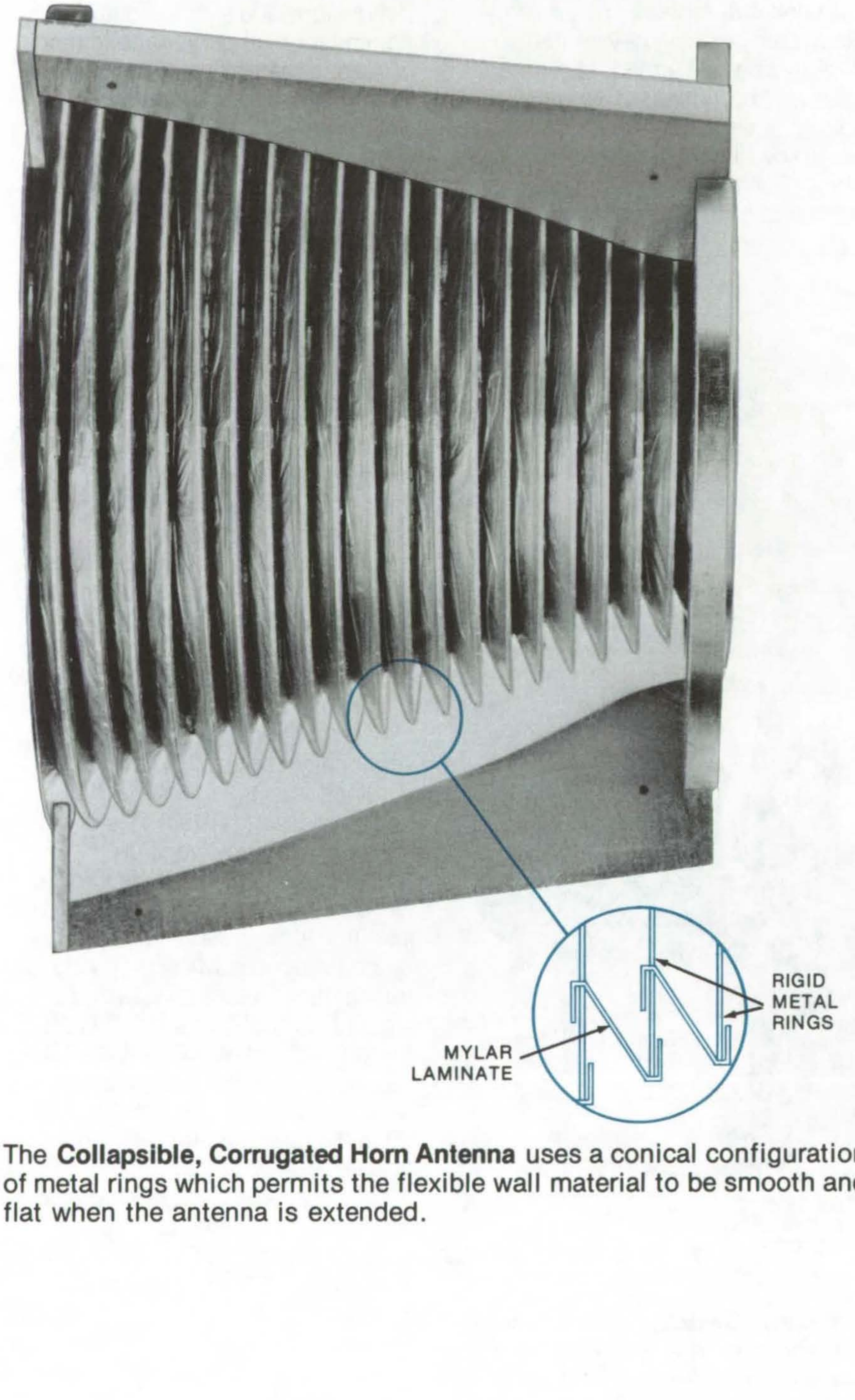

The **Collapsible, Corrugated Horn Antenna** uses a conical configuration of metal rings which permits the flexible wall material to be smooth and flat when the antenna is extended.

A lightweight readily-collapsible horn antenna with a high collapse ratio (extended length vs. collapsed length) utilizes a configuration which, when extended, is similar to that of a rigid laboratory antenna fabricated from a solid piece of aluminum.

The collapsible antenna consists of a series of flat annular metal rings. The number of rings and their relative diameters are not critical and can vary, depending on the performance requirements imposed on the antenna. The rings are connected to one another via a sheet of very thin, flexible, metalized material. In one implementation an aluminum Mylar laminate is used (see the figure).

The antenna is assembled by cutting circular segments of the metalized laminate of the proper inside and outside diameters. These flat rings are then clipped, starting with the largest ring visible. As rings are added, material is folded around the inside and outside circumferences of two adjacent metal rings, as shown in the enlarged sectional view. Once the assembly is completed, the rings and laminate form an unbroken conductive surface extending from the first ring to the last.

This work was done by Donald E. Barthlome of **Langley Research Center.** *No further documentation is available.*

Inquiries concerning rights for the commercial use of this invention should be addressed to the Patent Counsel, Langley Research Center [see page A8]. Refer to LAR-11745.

Lightning-Activated Electrical Ground for Cable Shields

A cable-shield ground, normally open, is activated by the high voltage of a lightning discharge.

Lyndon B. Johnson Space Center, Houston, Texas

When shielded wire or cable is used to connect circuits that are physically separated, different voltages can exist in the ground circuit (structure) between the two circuit locations. The wire or cable shield is therefore usually grounded at only one end. This is generally the case because, if the signal cable shield is permanently grounded at both ends, a "shield loop" current flows, producing a voltage gradient along the cable shield. This both-ends-grounded configuration allows electrical interference (noise) to be capacitively coupled into the cable wiring by the resulting electrostatic field produced within the shield.

However, if only one shield ground is used (for noise immunity) and the cable is subjected to a magnetic field generated by lightning, high voltage will be induced in the cable shield. Since there is, however, no complete electrical path from both ends of the shield to ground (so that the induced voltages can drive the current in the shield through a completed ground path), the lightning will induce unwanted voltages into the shielded wiring and the shield is ineffective. A completed electrical path from the shield to ground at both ends of the cable would, however, allow current to flow through the shield, setting up a counter magnetic flux within the shielded cable that will tend to cancel the lightning-current magnetic flux and protect the shielded signal wires.

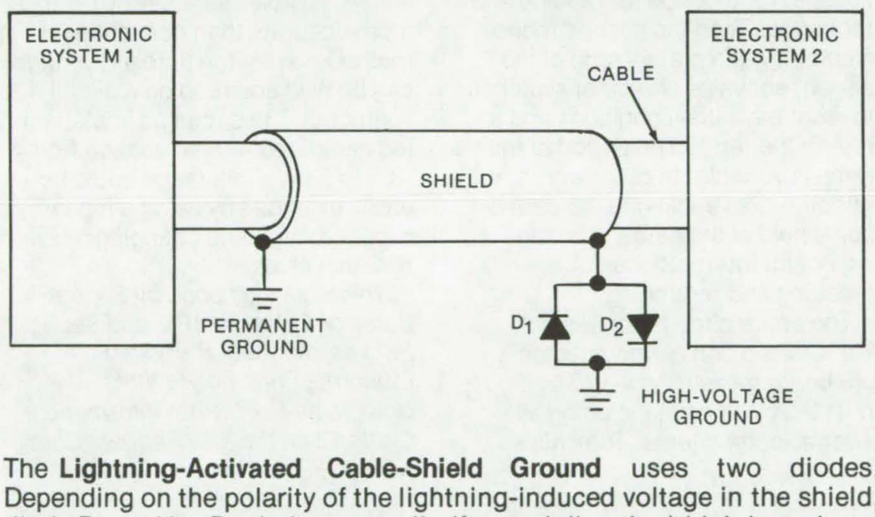

The **Lightning-Activated Cable-Shield Ground** uses two diodes. Depending on the polarity of the lightning-induced voltage in the shield, diode D_1 and/or D_2, being normally (forward direction) high impedance (open), will now conduct (short), thus completing the electrical ground path for the lightning-induced shield current. After the lightning-induced voltage in the shield disappears, the diode high impedance (open) will be reestablished, and again the ground at only one end of the cable-shield circuit is established for signal-wiring electrical-interference (noise) immunity.

To provide protection from both lightning-induced high voltage and cable-induced electrical interference (noise), a cable with two separate shields insulated from each other has been used in the past. The outer shield was grounded at both ends for lightning-induced high-voltage protection, and the inner shield was grounded at one end for electrostatic protection.

The lightning-activated electrical cable shield has two opposite, parallel diodes connected on one end; the other end is connected directly to ground (see figure). The diodes are normally in the forward high-impedance region of their operating characteristics (before forward diode conduction begins). The circuit is open, and there is no shield current loop (noise). When lightning strikes, the diode forward breakdown voltage (approximately 0.5 to 0.8 volt for silicon diodes) is exceeded, and the diode operates in its forward-biased, low-impedance region. This will complete the shield ground circuit and allow shield currents (due to the lightning) to flow in the shield, thus protecting the shielded cable wiring from induced high voltages; the circuit returns to a high-impedance open configuration after the lightning-induced shield voltage is dissipated.

This work was done by Kent D. Castle of ***Johnson Space Center.*** *No further documentation is available.*
MSC-12745

Fast Measurement of MOS Capacitors

The flatband voltage of MOS capacitors is measured quickly and accurately with a simple circuit.

Caltech/JPL, Pasadena, California

The usual method for measuring the capacitance-voltage curve of a MOS capacitor is with a ramp generator, a capacitance bridge, and an X-Y plotter. When the capacitance is to be studied during a thermal annealing operation or in other situations, continuous measurement of the flatband voltage is desired, but without continuously retracing the C-V curve.

The figure outlines a method for measuring capacitance rapidly and precisely while the capacitor is being subjected to the desired conditions. The analog output voltage of a capacitance meter, which is directly proportional to the capacitance being measured, is compared with a dialed-in voltage proportional to the calculated flatband capacitance C_{FB} by means of a comparator circuit. The bias to the MOS capacitor, supplied through the capacitance meter, is provided by a ramp voltage. When the ramp voltage reaches a certain dc level, the high-frequency capacitance of the MOS capacitor, as measured by the 1-MHz signal of the capacitance meter, becomes C_{FB}. At that instant, the comparator switches and triggers a series of two monostable multivibrators in succession.

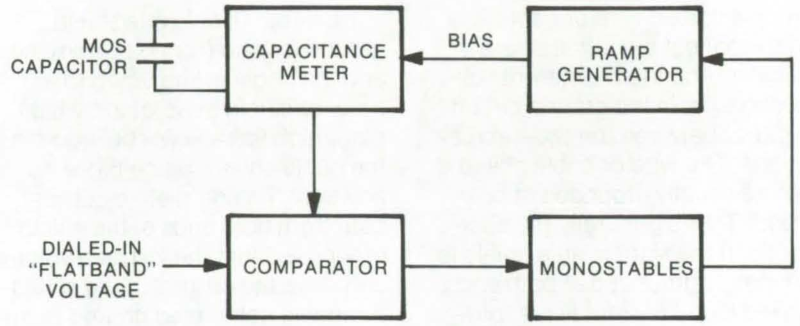

Flatband Voltage Measurements of thin-film MOS capacitors can be made quickly and precisely by comparing the output of a capacitance meter with a voltage proportional to the Flatband capacitance.

The first monostable activates a switch to hold the ramp voltage, which is then taken as the flatband voltage, for a period for reading and recording. Then the second monostable, triggered at the end of the period, activates two other switches to reset the initial conditions and to restart the ramp. The period of the ramp is variable. In other words, the effective bias applied to the capacitor is held at the flatband voltage, except for interruptions during resetting and reramping.

The entire circuit requires only five IC's and can be mounted on a DIP board measuring 4-1/2 by 5-1/2 in. (11.5 by 14 cm), including all external components. The entire circuit, shielded in a metal box, was tested in actual measurement of MOS capacitors and was found to be stable, reliable, time saving, and more accurate than conventional methods, since the flatband voltage can be held and read on a digital voltmeter. The circuit as implemented generated a ramp voltage from -8.5 to 9.0 V. This range could be easily extended by using a higher supply voltage and changing a few resistor values.

This work was done by Eugene T. Bates of **Caltech/JPL** *and Seung P. Li and Michael P. Ryan of California State Polytechnic University. For further information, Circle 13 on the TSP Request Card.* *NPO-13892*

Logic-State-Change Indicator and Frequency Doubler

Low-power TTL circuit produces an output pulse whenever the logic level at its input terminal changes.

Goddard Space Flight Center, Greenbelt, Maryland

A circuit consisting of a one-shot multivibrator IC, a pair of diodes, and some resistors and capacitors delivers an output pulse when the logic state at its input terminal changes — either from high to low or from low to high. Thus this circuit can serve as a state-change indicator or as a frequency doubler for a square-wave input.

Any monostable can be used; the arrangement in the figure achieves low power dissipation (80 milliwatts) by using half of a Fairchild 96L02 transistor-transistor-logic dual multivibrator. As the truth table shows, the 96L02 is triggered when pins 3 and 5 are high and pin 4 changes state from low to high. It also triggers if pin 3 is high, pin 4 is low, and pin 5 changes from high to low.

The circuit shown here allows these conditions to be satisfied with a single input terminal, plus the fixed

Triggering Conditions for 96L02

Pin 5	Pin 4	Pin 3
H→L	L	H
H	L→H	H

bias on pin 3; the arrangement of resistors, capacitors, and diodes automatically biases pin 5 high when transmitting a rising transition to pin 4 and biases pin 4 low when applying a falling transition to pin 5.

For example, if the input terminal has been low and then goes high, C_1 charges through a forward-biased diode that shunts its 100-ohm resistor; therefore pin 5 goes high immediately. C_2 charges through 100 ohms, however, because its diode is back biased, so the rising level is not applied to pin 4 until 5 is already high. Therefore the conditions for triggering an output pulse are satisfied.

The output pulse duration, t, is set by the value of time constant R_XC_X.

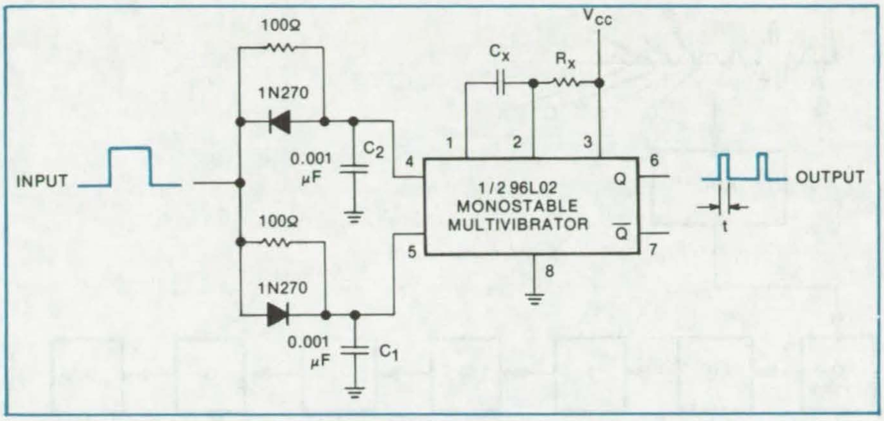

An output **Pulse Indicates Logic Change** at the input terminal of this TTL circuit. Thus, as the waveforms indicate, the circuit can also be used for doubling a square-wave frequency. The duration of the output pulse depends on the R_XC_X time constant.

This work was done by John I. Hudgins of **Goddard Space Flight Center.** *No further documentation is available.*
GSC-12169

Digital Filter for Voiceband Noise

Filter eliminates noise from communications signals by statistical techniques.

Marshall Space Flight Center, Alabama

General-purpose digital computers have been used for years to filter voice signals for spectral analysis. But efforts to adapt digital filtering techniques to special-purpose circuits for communications equipment have been hindered by the lack of suitable electronic components. Since high-speed, low-power analog-to-digital and digital-to-analog converters and shift registers have become available, digital filtering (for radios in aircraft, for example) has become much more practical.

A filter that uses such components is shown in the illustration. The filter operates over a 300- to 3,000-Hz range, and contains 10-bit, 10-kHz converters and equally fast registers. Briefly, the circuit samples a signal and filters it by adding together balanced pairs of the sample values and then multiplying each pair by a selected filter constant. The products obtained in this way are summed to form a filtered version of the original signal. In statistical terms, the procedure is equivalent to filtering N points of data with an nth order polynomial by regression calculation.

In the filter, an analog-to-digital converter changes samples of the input audio signal into digitally coded values. These values are shifted in sequence through a chain of shift registers. The chain thus contains, at any given instant, a series of digital representations of the signal sample. Although the samples are actually spaced in time, the register chain makes them all available for processing simultaneously.

It is important that there be an odd number of registers in order to establish an unambiguous center value. The illustration shows seven registers, and this number has been found to produce excellent filtering. However, for a wider frequency range, more registers (and more signal samples) would be necessary.

Next, the samples are weighted and averaged. The first and last samples, in time, in registers A and G are added and sent to digital multiplier 0. The second and next to last samples, in time, in registers B and F are added and sent to multiplier 1. This process continues until, finally, the center sample from register D is applied to digital multiplier 3.

Each of the digital multipliers is fed a filter constant — C_0, C_1, C_2, and C_3, respectively. The values are selected from published tables to yield the passband required of the filter.

The weighted outputs of the multipliers are added together and sent to the digital-to-analog converter, which changes the digital data into

(continued on next page)

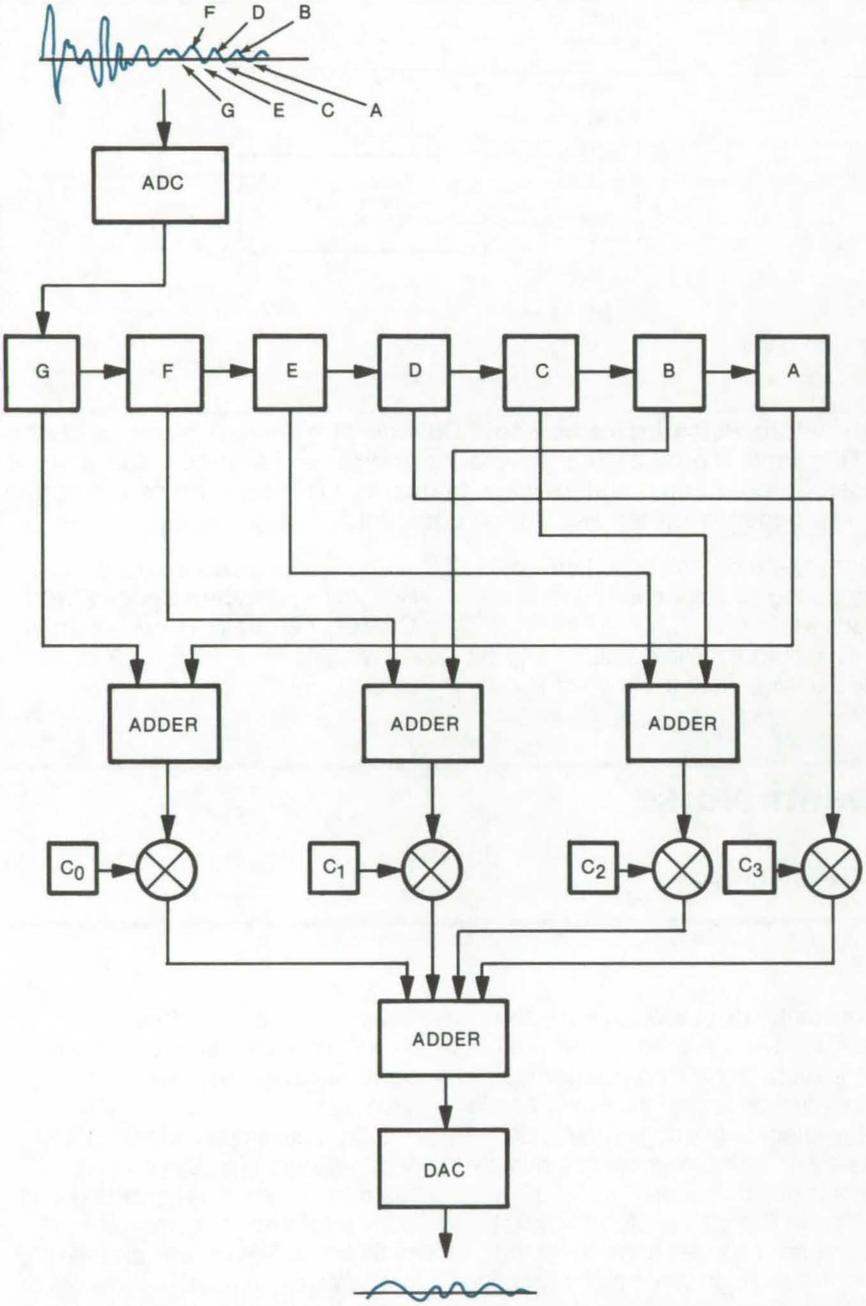

The **Digital Filter for Communications** combines and weights digital samples of an analog signal and reconstructs the signal with the noise above 3,000 Hz eliminated. Weighting factors are $C_0 = 7$, $C_1 = 6$, $C_2 = 3$, and $C_3 = -2$. For a higher frequency low-pass filter, or for a high-pass filter, different weighting factors and different numbers of registers would be used. The clock rate of the register should be above the audio range of the speakers, earphones, or other receiving device to avoid a hum.

analog form. The output is a replica of the input to the filter, but with a substantial amount of the noise (that above 3,000 Hz) eliminated. The output is delayed in time, with respect to the input, by a factor of (N-2)/2R, where N is the number of shift registers and R is the clock rate of the registers. A modified version of Efroymson's stepwise multiple-linear-regression model-making logic will be available in the near future in a machine-independent FORTRAN program. This algorithm incorporates coefficient selection based upon the highest partial correlation coefficient with statistical acceptance or rejection at each step according to a user-specified confidence level.

This work was done by Thomas R. Edwards and Hugh W. Zeanah of **Marshall Space Flight Center.** *For further information, Circle 14 on the TSP Request Card.*

This invention has been patented by NASA [U.S. Patent No. 3,949,206]. Inquiries concerning nonexclusive or exclusive license for its commercial development should be addressed to the Patent Counsel, Marshall Space Flight Center [see page A8]. Refer to MFS-23699.

Electronic Systems

Hardware, Techniques, and Processes

Books and Reports

Demand-Controlled Lighting

Indoor lighting is switched off and on as needed to supplement Sunlight.

John F. Kennedy Space Center, Florida

Many rooms, especially in office buildings, receive a substantial amount of Sunlight during the day. Yet lighting is designed to provide the intensity necessary when there is no other illumination source. Obviously, energy costs could be reduced by continuously adjusting the lighting level; but to be effective, the adjustment should be automatic and should be responsive to illumination variations in the same room.

An inexpensive photocell and switch can meet this need when used as part of a loop-wiring plan. During periods of low illumination, the cell drives an electric motor that controls a number of mercury switches. The approximately 1-rpm motor is slow enough to prevent overshooting and responding to brief changes of light level such as lightning. The switches activate wiring loops, each of which is connected to a particular set of lights. The number of loops activated, and thus the number of lights turned on, will increase until the illumination, as measured by the photocell, becomes sufficient. When the illumination intensity is too high, the reverse is true.

The cell and switch are illustrated in the figure as used to control the lights in a room. The mercury switches are mounted on a rotating plate that is controlled by a conventional wall switch and by the photocell. As the plate is rotated, groups of lights are turned on or off in sequence. In the example illustrated, the first loop energized turns on one of the sets of the lights furthest from the window. Additional loops will be activated when the photocell indicates less Sunlight and the need for more artificial light.

In the switch circuit, the mercury switches are connected between a power source and the lights, and the lights are connected to the power source to complete the circuit. The light sensor activates a drive motor that rotates the mercury switches.

A limit switch prevents the rotary plate from turning 360° and causing the lights to switch on and off continuously, as could happen with very low or very high illumination. A pair of switch pins protrude through a slot on the plate; when the last mercury switch in a sequence is engaged, the plate depresses a switch pin to turn off the drive motor. The pin position may be set so that all or only some of the mercury switches can be activated.

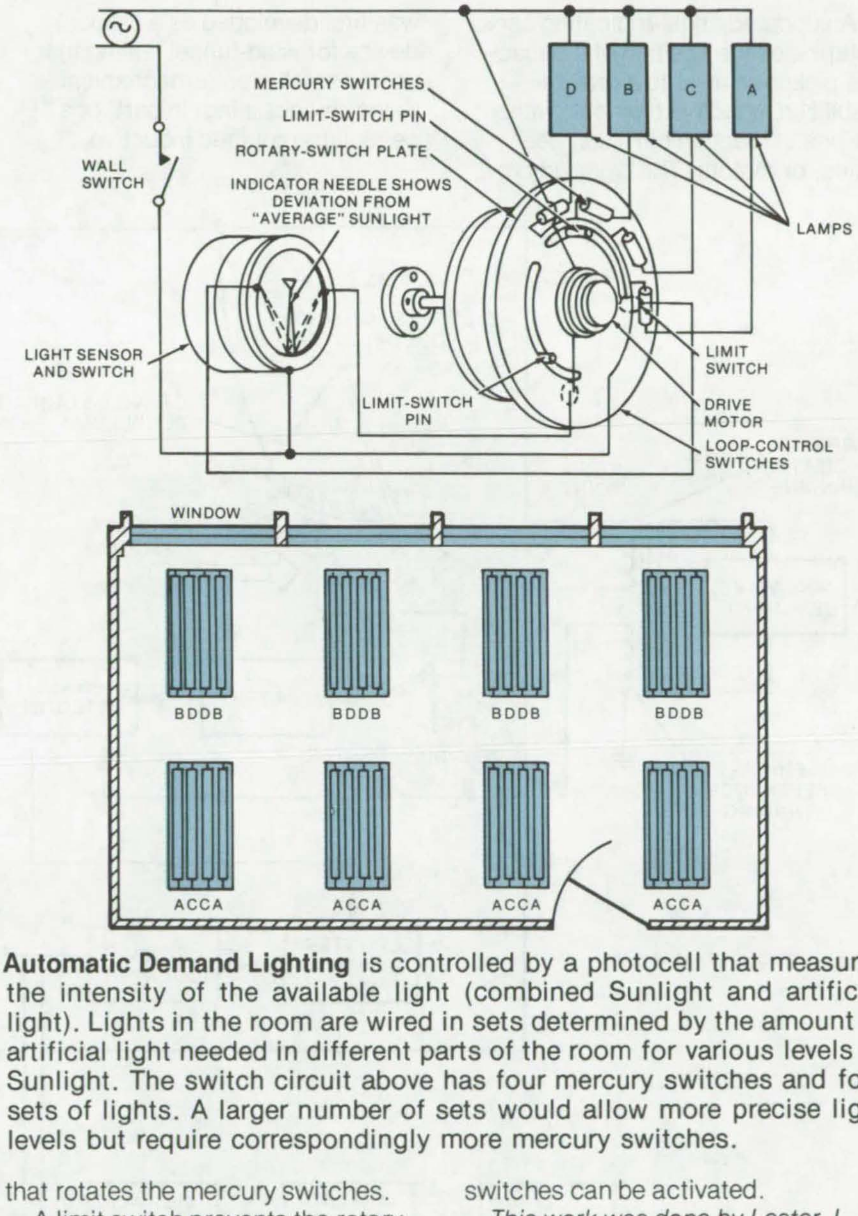

Automatic Demand Lighting is controlled by a photocell that measures the intensity of the available light (combined Sunlight and artificial light). Lights in the room are wired in sets determined by the amount of artificial light needed in different parts of the room for various levels of Sunlight. The switch circuit above has four mercury switches and four sets of lights. A larger number of sets would allow more precise light levels but require correspondingly more mercury switches.

This work was done by Lester J. Owens of **Kennedy Space Center.** *For further information, Circle 15 on the TSP Request Card.*

This invention is owned by NASA, and a patent application has been filed. Inquiries concerning nonexclusive or exclusive license for its commercial development should be addressed to the Patent Counsel, Kennedy Space Center [see page A8]. Refer to KSC-11010.

Angle-Indicating Digital Servo

A self-nulling bridge with digital readout is faster and more accurate than its electromechanical equivalent.

Ames Research Center, Moffett Field, California

An updated angle-indicating servo determines the position of a capacitive pickup relative to a gravity-stabilized inductive element, without the use of mechanical links, gear trains, or motors. The digital servo was first developed as a readout device for wind-tunnel testing that used a small electromechanical detector consisting, in part, of a pendulum-mounted inductive element, about which a capacitive pickup rotates.

The previously-used electromechanical servo was configured in a servo-nulled bridge circuit. As the

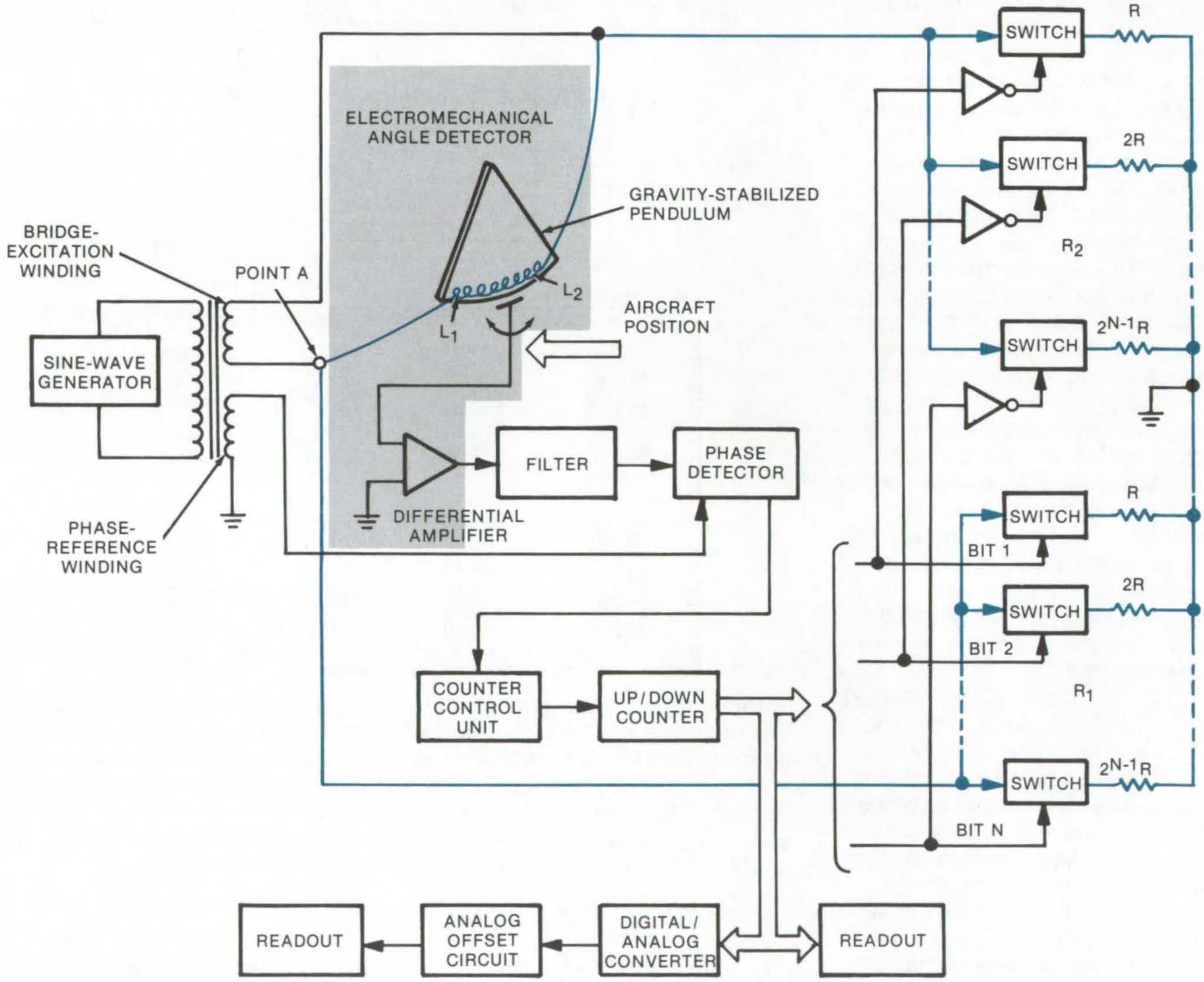

The **Angle-Indicating Digital Servo** uses an array of binary-weighted resistors to form two elements, R_1 and R_2, of an ac bridge circuit. The remaining elements, L_1 and L_2, of the bridge circuit are formed within the electromechanical angle detector between the position of the capacitive pickup and the two ends of the inductive element. The L_1/L_2 ratio varies with the angular displacement of the capacitive pickup. An ac source powers the bridge via the excitation winding. When the airplane-mounted capacitive pickup moves, the bridge is unbalanced. The resulting error signal is detected by the capacitive pickup and is amplified and filtered. Error-signal phase is determined relative to the reference-winding output. The bridge is nulled by switching binary-weighted resistors in (or out) of the resistor networks via commands from the up/down counter (which, in turn, is activated by the output of the phase detector). At bridge null, the pickup angle, relative to the gravity-stabilized pendulum, is read out directly in binary coded form from the up/down counter. Auxiliary circuits provide the angle readout in analog and BCD forms.

aircraft model moved, signals generated by the detector were mechanically translated via the servo to read out angular degrees. Detector error signals were used to position a potentiometer via the servo gear train to obtain bridge balance. Servo wear, gear-train friction, and mechanical hysteresis all contributed problems to this electromechanical system.

The improved angle-indicating digital servo uses two fixed-resistor networks to null out the detector output. The instrument is also connected in a bridge configuration like the earlier electromechanical servo. Bridge nulling is automatic, via the resistors (represented by the individual resistance units in networks R_1 and R_2) switched into (or out of) the network via an up/down counter to attain circuit null.

As the aircraft-mounted capacitive pickup is rotated about the inductive element, the element is split into two parts: L_1 and L_2. Pickup signals are amplified, filtered, and routed to a phase detector that senses the phasor difference between the pickup (error) signal and the phase of the reference winding voltage. The up/down counter outputs a new code in response to the phase detector and also sources the digital-to-analog converter plus readout circuits and displays.

Networks R_1 and R_2 shunt the detector elements L_1 and L_2, respectively, using binary-weighted resistors; each resistor is connected through a digitally controlled switch to remove (or add) resistance to the network. Resistor arrays R_1 and R_2 have resistors varying in resistance from R to 2^{N-1}R. Each series-connected switch has a control input that is coupled to one of the N lines from the counter, interfaced via the inverters in network R_2. When a "1" is transmitted on a control input, the switch is closed, and the series-coupled resistor is connected between ground and one lead of the transformer excitation winding. When a "0" is impressed on the control input, the switch is opened; the resistor is disconnected.

If a "1" is transmitted from the Nth line of the counter, the switch in series with resistor 2^{N-1}R closes and connects it between point A and ground. The same bit N, routed through the inverter, is seen as a "0" at 2^{N-1}R in network R_2. The resistor arrays work in push/pull: when R_1 decreases, R_2 increases; and so forth. By connecting only certain binary-weighted resistors in a network, the equivalent network resistance can vary from a very small resistance to an effectively infinite resistance, depending on the counter output code.

This work was done by Gilbert T. Parra of **Ames Research Center.** *For further information, Circle 16 on the TSP Request Card.*

This invention is owned by NASA, and a patent application has been filed. Inquiries concerning nonexclusive or exclusive license for its commercial development should be addressed to the Patent Counsel, Ames Research Center [see page A8]. Refer to ARC-11036.

Gain and Phase-Margin Measurements

Open-loop gain of precision servos can be measured in field by inserting self-powered test amplifier into loop under analysis.

Caltech/JPL, Pasadena, California

The simple battery-powered test circuit (shown in the figure) will contribute negligible error when taking open-loop measurements of gain and phase parameters. This is especially helpful when measuring high-gain circuits containing integrators. Ordinarily, such a circuit will saturate when the loop is opened. This can be prevented by opening the loop and inserting the operational amplifier shown in the figure at the point where the loop is broken.

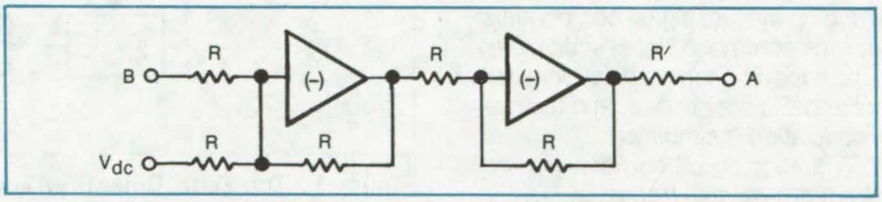

The **Gain and Phase Margin** test circuit can be battery powered for field use. In the case of noisy signals, identical filters can be attached between points A and B and the gain-phase meter. The configuration can also be used to take the frequency response of an unstable circuit by adding compensation to the test amplifiers as necessary to prevent the circuit from oscillating.

Resistor R should equal the impedance when driving from the break at B. Resistor R′ should match the driving impedance normally at the loop break point. (Impedance matching is not difficult if the loop is broken at a point of low impedance to ground.)

With no applied ac reference signal, V_{ac}, the circuit is unchanged because of unity gain of the inserted test circuit. When an ac signal appears at V_{ac}, the loop is completed through the test circuit. Open-loop gain and phase measurements are then taken of B with respect to -A (to account for circuit negative feedback), using a conventional gain-phase meter.

(continued on next page)

The open-loop transfer function is then given by

$$\frac{B(j\omega)}{A(j\omega)} = \left|\frac{B}{A}\right| \frac{\angle B - 180^\circ}{\angle A} = \left|\frac{B}{A}\right| \angle B - A - 180^\circ$$

The inserted test amplifier does not contribute error. Large phase lags may cause oscillation at higher frequencies; however, it is usually possible to take measurements over a two-decade frequency range centered around the open-loop 0-dB crossover point. Using small batteries to power the operational amplifier, this method lends itself to field use. Usually, only one wire needs to be removed to make measurements.

This work was done by Billie D. Pierce of Ball Brothers Research Corp. for **Caltech/JPL.** *For further information, Circle 17 on the TSP Request Card.*
NPO-13296

Simplified Command and Range Detection System

Both range and command data are combined into one subcarrier.

Caltech/JPL, Pasadena, California

In communicating with spacecraft, a separate unmodulated carrier uplink signal was required for the spacecraft's narrow-band phase-locked loop receiver to track signals from the ground. Transmitted commands are low-frequency signals and must fall outside the tracking-loop bandwidth. Therefore these signals are modulated onto an intermediate subcarrier before being modulated onto the carrier. The spacecraft must have independent tracking loops to demodulate all the carriers and also needs a second subcarrier channel for ranging information.

The functions of ranging and command demodulation can be combined by using the uplink sequential-ranging-system signal components for the command signal subcarrier. The separate command subcarrier channel is not needed, and the demodulation is simplified.

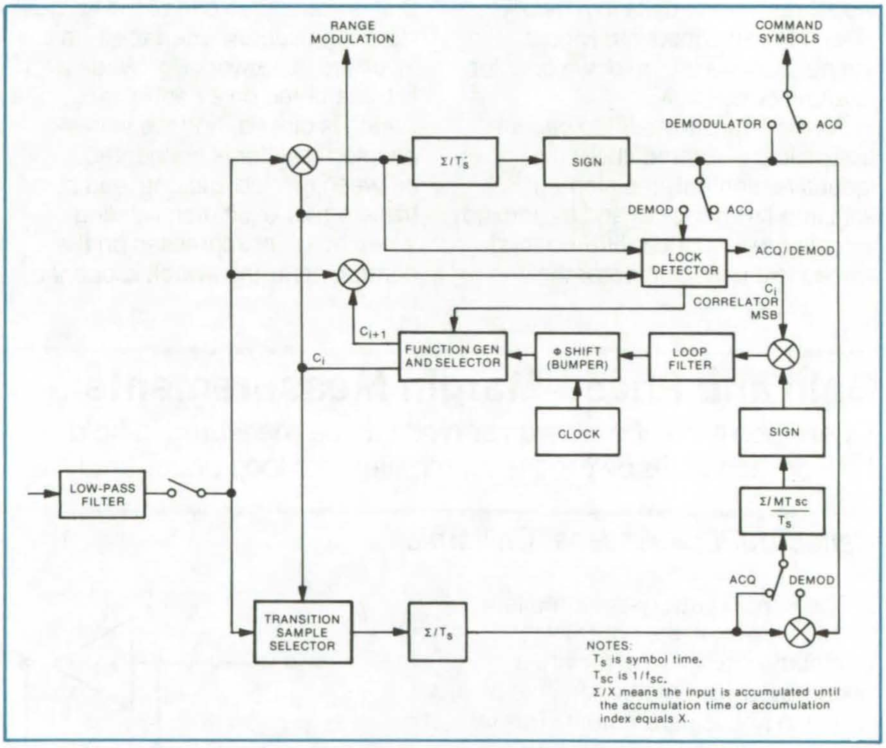

Figure 1. The **Data Detection and Range Cleanup Loop** processes a subcarrier that is modulated with a sequential range code and with command data. The loop locks in on the range codes as they occur in sequence. When the range code modulated with the data-rate frequency arrives, the loop switches to DEMOD to receive data.

The ranging subcarrier signal is a square wave of frequency, f_{SC}, phase modulated by one of its own subharmonics. If c_i denotes the ith possible composite signal, it is derived by

$$c_i = f_{SC} \odot f_{SC}/2^i$$

where $\odot$ indicates modulo 2 addition for (0,1) data levels and multiplication for (+1,-1) data levels on the square wave. The ranging system is sequential because initially c_1 is transmitted; then after a period of time, c_2 is transmitted; etc.

The system, as shown in Figure 1, is a phase-locked loop (PLL) in which the VCO has been replaced with a combination VCO/function generator. The function generator provides a synchronous signal modulated identical to the c_i that is being received. In addition, it provides a second signal, c_{i+1}.

The loop also has two correlators: One correlates the received signal with c_i from the generator, and the second correlator compares the received signal with c_{i+1}. If the first correlator output is high enough, the proper code is being tracked; but if the output of the second correlator becomes higher, the code has shifted. This condition causes both function-generator outputs to shift to the next code in the sequence, so that the new code is being tracked and the next-expected code is being looked for.

This loop is similar to a conventional PLL, with a detector to sense when it is in lock. By adding a phase-data integrator leg (in the lock-detector circuitry) and a way of removing the effect of data modulation from the error channel, the loop becomes a subcarrier demodulator and bit detector in which the subcarrier is actually the composite range system.

The operation of the system is shown in the flow chart in Figure 2. Initially the switches in Figure 1 are in the acquisition (ACQ) position, and the function generator is producing components c_1 and c_2. As long as no signal is received by the demodulator, neither c_1 nor c_2 correlators will accumulate high values. As soon as c_1 is received, the signal is applied to the transition sample selector of the PLL.

After a sufficient length of time, the tracking loop will lock onto the received subcarrier component c_1 and will continue in this mode until the signal is lost or the c_2 correlator detects the presence of c_2. Note that by supplying the signal c_1 to the transmitter, the "cleaned-up" range signal can be transmitted back to the originating station.

The command-symbol rate is selected to be the same as one of the subharmonic frequencies ($f_{SC}/2^i$) that are used to construct the composite subcarrier. Because symbol (bit) and subcarrier timing are in sync, the detection of c_i corresponds to detection of the rate associated with c_i as well as the sequential determination of the symbol timing at that rate. (Sequential symbol timing is determined by examining the sign of the c_{i+1} correlator at the time c_{i+1} is detected. This is the same process by which range ambiguity is removed in the sequential ranging system.)

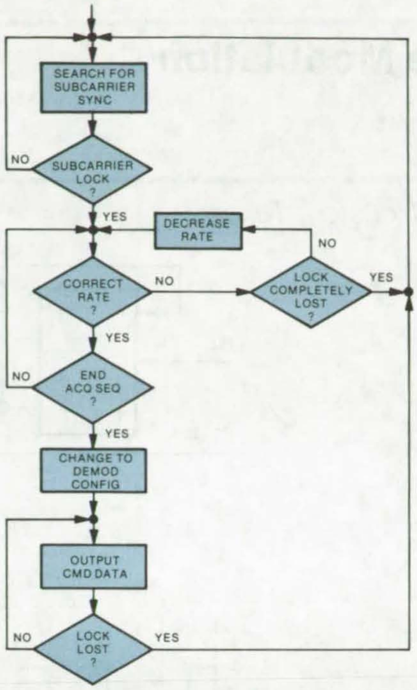

Figure 2. The **Search Sequence** keeps the loop tracking on one composite carrier code and searching for the next-expected one. When the end-of-acquisition sequence (the complement of the composite subcarrier) arrives, the loop switches to the demodulation configuration to output command data.

The switches in Figure 1 are initially set to ACQ to allow efficient detection of the code sequence; once the data rate desired for command signals is reached, the switches are changed to the DEMOD position. This is done by transmitting the complement of c_i when the composite includes the desired data-transmission rate.

Thus, the c_i correlator also serves as an end-of-acquisition detector. Once in the DEMOD position, the system is ready to demodulate and detect command data as well as track the c_i range code component.

The command-symbol stream is integrated (accumulated) over the appropriate symbol time, T_S, and the symbol is detected. The symbol sign is then applied to the lock detector to remove the effects of data modulation on the lock-detector accumulators. The sign is also injected into the loop to remove the effects of data modulation on the loop-error signal.

From this simplified description of the loop operation, it can be seen how the same subcarrier signal is used both for ranging and to carry command data. The demodulator has false-acquisition and failure-to-acquire probabilities that are compatible with most requirements. Furthermore the acquisition time of this scheme is comparable to the acquisition times of existing command detector designs.

This work was done by Stanley A. Butman and James R. Lesh of **Caltech/JPL.** *For further information, Circle 18 on the TSP Request Card.*

This invention is owned by NASA and a patent application has been filed. Inquiries concerning nonexclusive or exclusive license for its commercial development should be addressed to the Patent Counsel, NASA Resident Legal Office-JPL [see page A8]. Refer to NPO-13753.

Null-Balancing Microwave Radiometer

A new microwave radiometer performs absolute temperature measurements over the range of zero to 300 K. A prototype, built for remote temperature sensing of the Earth's surface from an aircraft, operates at 2.695 GHz. Besides measuring the temperature of arctic icepacks, the radiometer detects oil slicks on water and monitors the atmosphere.
(See page 49.)

Simultaneous EKG and Ultrasonoscope Display

A new real-time system simultaneously displays a two-dimensional image of the heart and an EKG waveform on a cathode-ray screen so that dimensional changes of the heart can be continuously compared with the EKG waveform. The apparatus combines EKG monitoring with appropriate logic and an ultrasonoscope.
(See page 98.)

Remote Surface-Height Measurement

Airborne synthetic-aperture radar statistically measures the height of terrain above an arbitrary level and is not limited to surface roughness or minimum area. Although developed for use on a spacecraft to observe ocean-wave heights, it can be adapted to measure vegetation size, urban development, and geological roughness.
(See page 54.)

Differential Pulse-Code Modulation

A new differential PCM encoding scheme conserves bandwidth.

Lyndon B. Johnson Space Center, Houston, Texas

An improved differential pulse-code-modulation (DPCM) encoding and decoding method allows data to be transmitted with less bandwidth than required for conventional PCM codes and is not affected by the data-transition density. In addition, it requires no direct-current response of the transition link, and there is little ambiguity in resolution of the digital data.

The differential code represents information by the presence or absence of change in signal-level transitions between successive data-bit intervals. The code is derived from an NRZ-Mark Code, in which a "1" is represented by a change in level and a "0" is represented by no change in level. (A similar code is derived from an NRZ-Space Code, the converse of the Mark Code.)

The encoder and waveforms are shown in the figure. A flip-flop receives data in an RZ (return-to-zero) format and converts it to an NRZ (nonreturn-to-zero) Mark format by changing digital levels for each "1" signal in response to the leading edge of the half-bit-wide RZ "1" pulse at the beginning of each bit interval. The flip-flop does not change levels for a "0" input.

As is evident from the Mark Code waveform and the input RZ waveform, the encoder encodes differentially by causing a transition in signal-level changes in response to a digital "1", namely a transition from the presence of a level change to the absence of it, or the converse, between successive bit-time transition points. The bit-time transition points occur at times defined by the clock waveform during successive bit-data intervals. Similarly, there is no transition in signal-level changes between successive bit-time transition points in response to a "0", so that the data are represented by the presence or absence of data-level

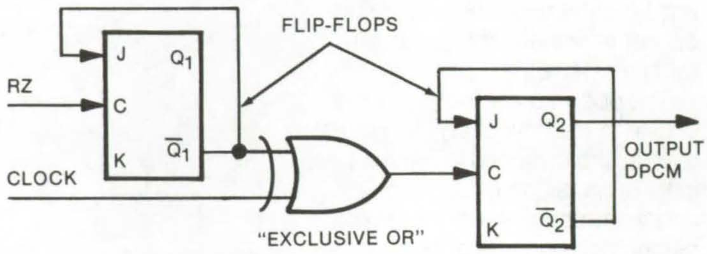

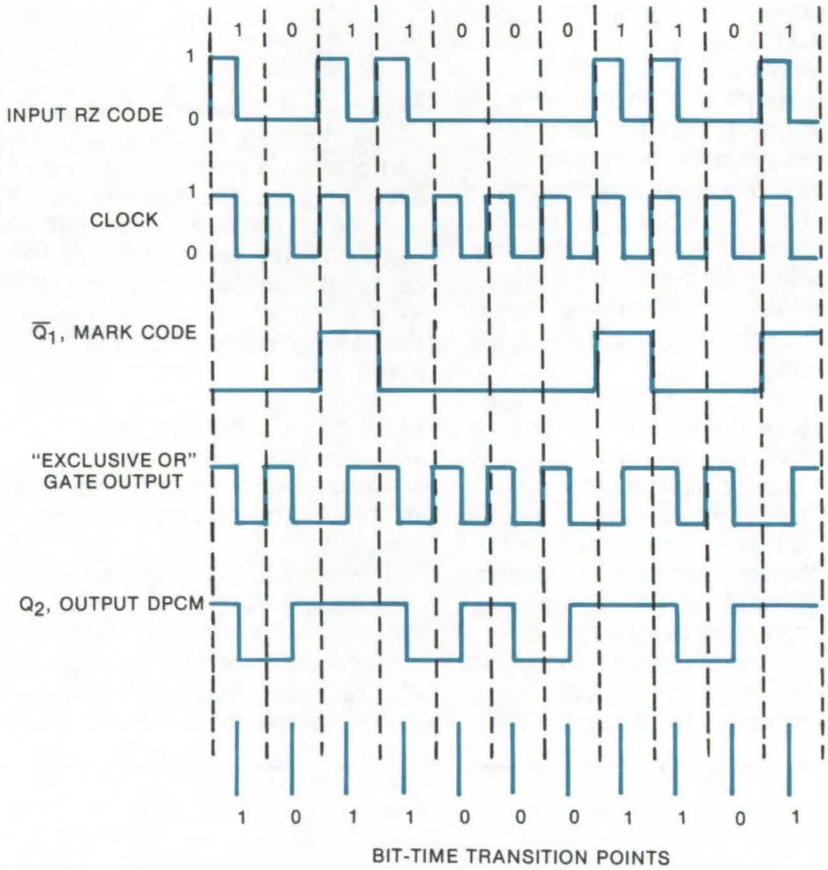

The **Circuit and Waveforms** for the DPCM encoder illustrate the logic used to derive the code. Data are represented by the presence or absence of a change in signal-level transitions in the middle of a data-bit interval. For instance, a series of "1's" would be represented by a change in signal level, followed by no change in signal level, followed by a change in signal level, etc. A series of "0's" is represented by a change in signal level each bit interval.

changes between successive bit-time transitions during successive data-bit intervals.

After encoding, the data are transmitted and received for decoding. The decoder compares the received successive data-bit intervals to determine the presence or absence of transitions in data-level changes between successive bit-time transition points. The received signal is then converted into an NRZ data format for subsequent processing or analysis.

Since information is transmitted as a differential change or a lack of change of the state of data levels at bit-time transition points, no decoding ambiguity occurs. The system requires no dc response, and the spectral energy of the transmitted signal is concentrated in a narrow bandwidth. The technique eliminates the sensitivity of the receiving system to transition density, since the presence or absence of transitions defines the data content rather than the actual transitions. Accordingly, system transmission power requirements are reduced, while data-handling capabilities are increased. Further, since the output encoded data transmits clock-rate information directly, system synchronization reliability is increased.

This work was done by Calvin F. Herman of **Johnson Space Center.** *Further information may be found in the U.S. Patent referenced below, which may be purchased from the U.S. Patent and Trademark Office, Washington, D.C. 20231 for $0.50 a copy.*

This invention has been patented by NASA [U.S. Patent No. 3,988,729]. Inquiries concerning nonexclusive or exclusive license for its commercial development should be addressed to the Patent Counsel, Johnson Space Center [see page A8]. Refer to MSC-12506.

Aircraft-Noise Synthesizer

Digital synthesis system simulates aircraft flyover noise.

Langley Research Center, Hampton, Virginia

A digital aircraft-noise synthesizer using a general-purpose minicomputer with special digital-to-analog hardware has been developed and is currently in use at Langley Research Center. It is extremely desirable, especially for research into the effects of aircraft noise on people, to have a means of simulating the flyover sounds that new or modified aircraft will make prior to flight and the actual field recording of the prototypes. It is also desirable to be able to eliminate or control some of the problems inherent to actual field recordings, such as wind noise, background noises, equipment limitations on acoustical range, and difficulties in obtaining optimal field locations. The digital synthesis system for simulating aircraft flyover noise is a major development in overcoming these problems.

Programs for time-dependent generation and modification of aircraft noise are loaded into the computer via a paper-tape reader; aircraft flight parameters and acoustical reference parameters are then entered into the system by the operator, using a keyboard or the paper-tape reader. Input parameters include the following:

- aircraft position as a function of observer time
- speed of approach or departure (Doppler effect)
- observer distance from threshold
- observer distance from ground-track
- broadband and narrow-band random-noise generation
- harmonically-related pure-tone generation
- source directivity
- atmospheric attenuation and amplitude fluctuation

The system currently in use employs relatively simple models for atmospheric effects and source directivity. Also the current hardware/software configuration limits the noise generation to an upper frequency of 5,000 Hz, with a maximum of 10 harmonically-related pure tones. Only 10 narrow-band noise signals are being generated, with a minimum bandwidth of 12.5 Hz. However, these restrictions are not inherent to the synthesizer, and the system can be modified or expanded with improved programs and hardware as new requirements arise.

This digital aircraft-noise synthesizer has been designed, and it is being used, for aircraft-noise simulation. However, it could be modified for use with road vehicles, rail vehicles, and most other applications that involve time-varying acoustical parameters.

This work was done by Thomas J. Brown and Clemans A. Powell of **Langley Research Center** *and P. A. Bickford of Time Data Corp. No further documentation is available.* *LAR-11858*

Combined PAM/PCM Audio Switching System

Economical electronic switching offers extensive conference capability in telephone communications.

John F. Kennedy Space Center, Florida

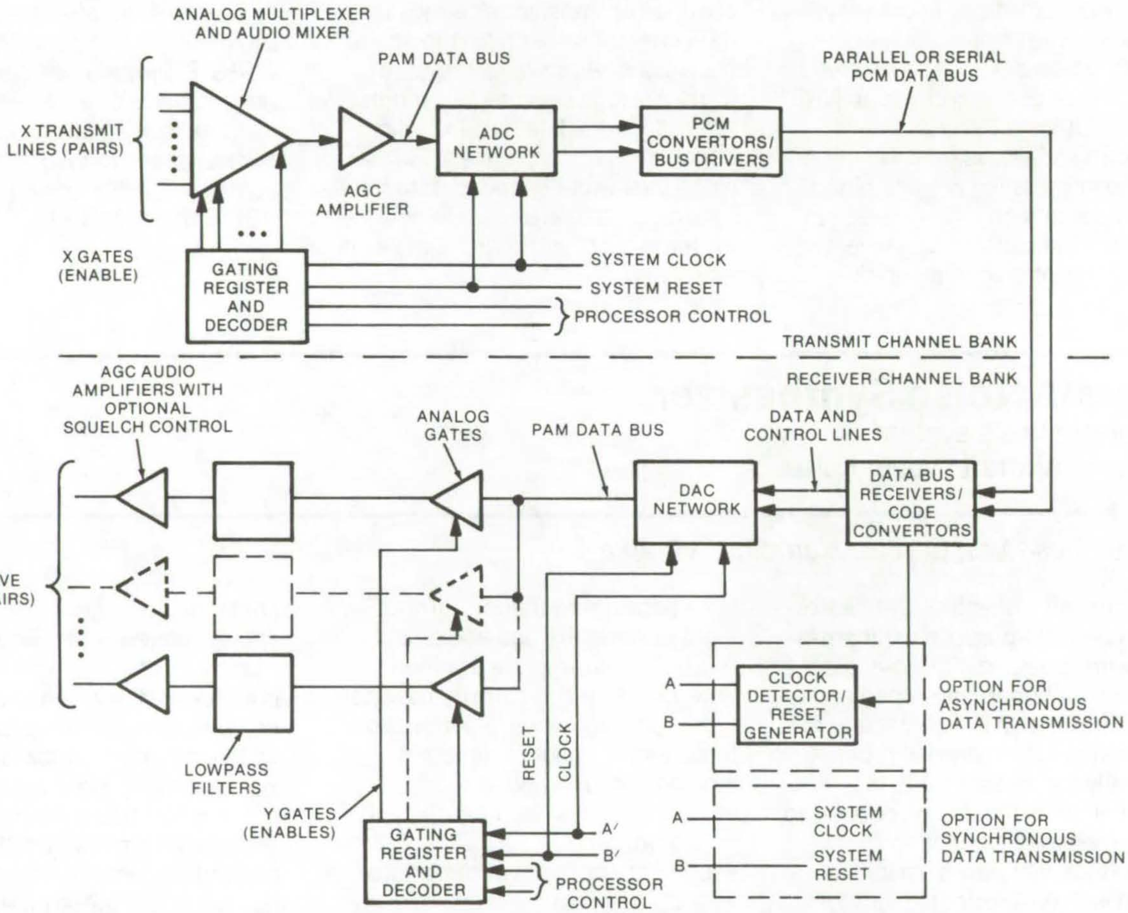

A **Single Data Channel Audio Switching System** may be used for party-to-party calls and several large conferences. The configuration features random sampling of the input audio under processor control, rather than sequential sampling, analog-to-digital conversion, storage, and subsequent processor-controlled random selection of the stored digital data. Another feature is the ability to conference "unlimited" numbers of audio inputs on the same network, while making a large number of different networks available. This is possible through a linear summation of audio inputs at the time of sampling.

A new electronic switching system makes simultaneous use of pulse amplitude or time-division and pulse code, or space-division, multiplexing (PAM and PCM), for economical electronic switching in a telephone communications system. It connects normal two-party stations as well as many very-large-conference calls.

The system (a single channel bank is shown in the figure) uses PCM for transmission between channel banks and is therefore well suited to modern long-distance communications, using repeaters and a transmission clock. The system operates at the standard 1.544 M-bits/s. However, it is not confined to this transmission rate, and higher rates will increase the permissible number of channels per bank.

For a 4-kHz audio bandwidth (filter-limited to avoid aliases), 1.544 M-bits/s allow 193 time slots. Reserving 1 slot for synchronization, 192 slots are available for audio transmission. Assuming a non-blocking switch, up to 96 party-to-party lines are available per channel bank. Clearly, the number of lines per channel bank can be doubled by allowing blockage and can be otherwise increased by using higher clock rates. Additional 96-line channel banks can be connected in parallel, permitting a simple modular approach to increase system capacity.

The switching system has the capability of conferencing many

telephone lines in the same network, over 6,000 in some examples. By using the channel-bank counters to preset and delay, the system may use DAC's that are too slow to keep up with the clock bit rate, at the expense of a few microseconds of delay time.

The channel-bank gating register and decoder, which controls the various time and space slots, handles party-to-party, conferencing, and combined systems, affording considerable hardware savings over conventional systems. The system is therefore well suited to PBX telephone exchange use, especially where large-conference calls occur.

This work was done by Duane L. Abbey of Rockwell International Corp. for **Kennedy Space Center.** *For further information, Circle 19 on the TSP Request Card.*
KSC-11015

Priority Protocol and Control Circuit

Ambiguity-free handling of requests in an intercomputer communications link

Caltech/JPL, Pasadena, California

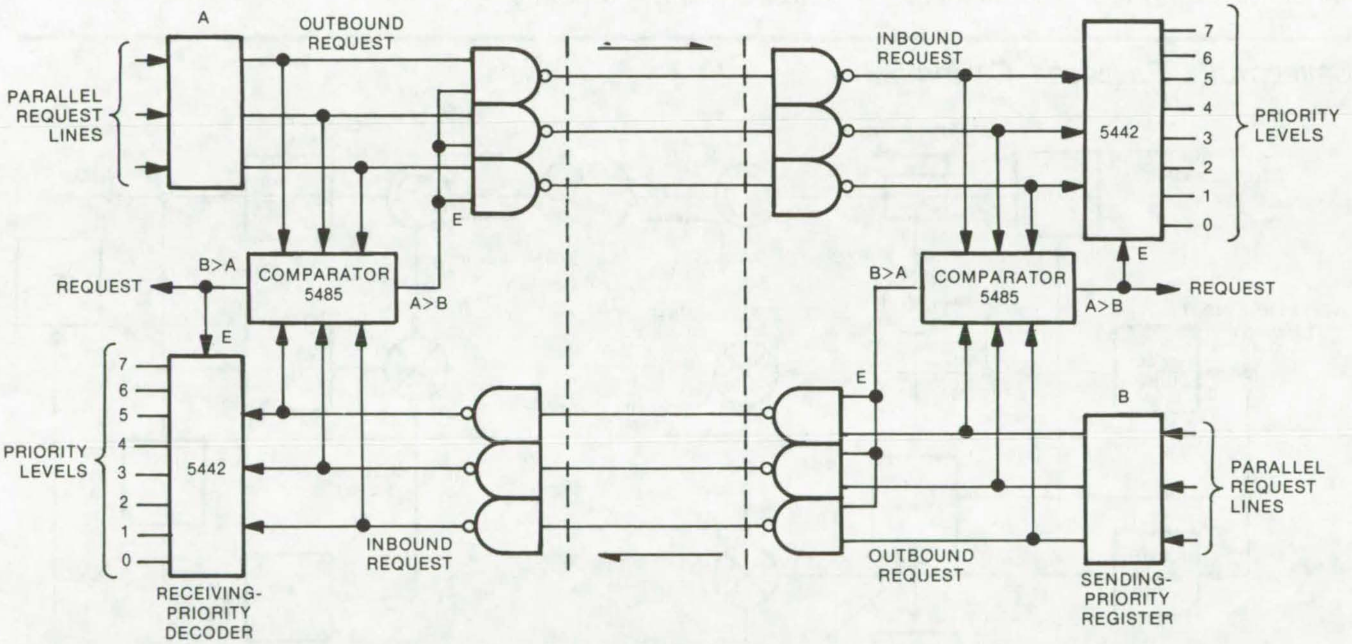

The Computer Interface Priority Protocol Control Circuit consists of three request lines in each direction, interlock comparators, and priority decoders. The outbound request from one device becomes the inbound request line for the device at the receiving end. To maintain bistable operation, wires are not crossed in cables; cables are equipped with a male connector at one end, a female socket at the other end. This assures the distinction between inbound vs. outbound terminals. The weight of the request code determines the data-transfer direction through the traffic controller.

In a conventional half-duplex intercomputer data-transfer system (bidirectional with data flow in one direction at a time permissible), the calling or request-to-transmit signal is unidirectional, or one request per direction. In a proposed modification, the calling signal is carried over three parallel lines, thus permitting the link to be priority coded. These parallel lines form the equivalent of a bistable flip-flop system. The flip-flop configuration precludes ambiguities that result from receiving simultaneous requests. Once a data path has been established through a data-traffic controller, the controller monitors the priority-request-coded lines and locks out all other requests. In the proposed system (see the figure), data-traffic direction may be reversed instantaneously by interchanging the inbound with the outbound address register.

When establishing a triple-line priority protocol, the output from a simple OR gate between the three lines constitutes a single-request signal. The three lines are decoded; into seven priority levels. The levels, ranging from one to seven, identify the type of data being transmitted, such as ordinary data, status information, command information, or addressing information for a data-traffic controller.

Binary comparators between the three lines (one in each end) are used to resolve the priorities as well as to establish the bistable condition that

(continued on next page)

resolves the ambiguity of simultaneous requests. Since the A>B and A<B outputs are used exclusively (leaving the A=B output unused), a bistable condition is assured.

One output from the comparator can also serve as the basic request command. If none of the six request lines is asserted, the comparator is reset. If the same set of lines is asserted simultaneously from each end, the bistable configuration of the circuit favors one set of lines and locks out the others. An increase in the request code, however, can change the directional priority.

The request lines are also used with a data-traffic controller. Once a data path has been established, the traffic controller can monitor the lines from both the transmitting and receiving device. As a priority change occurs, a reversal in traffic is implemented by interchanging the inbound and outbound addresses.

For a "ones" status of all request lines (i.e., all lines grounded), priority level seven may be reserved to indicate that power is off at the device at the opposite end. A dropout relay is used to ground the three lines in the power-off end.

This work was done by Tage O. Anderson of **Caltech/JPL.** *For further information, Circle 20 on the TSP Request Card.*
NPO-13901

Ultrastable-Frequency Distribution System

A highly accurate reference can be transmitted at costs much lower than for a sophisticated onsite frequency standard.

Caltech/JPL, Pasadena, California

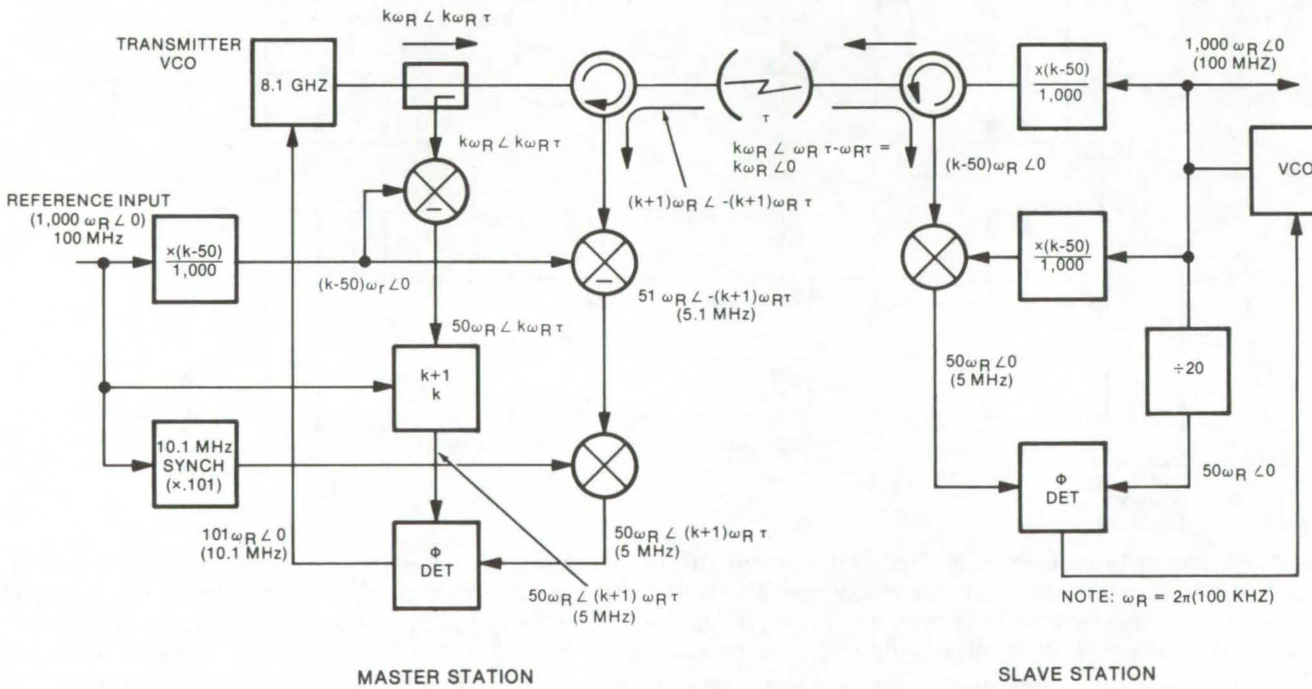

A **Frequency Transmission System,** used to distribute a highly-accurate RF reference between a master site and a slave site, automatically compensates for path perturbations between the transmitting (master) and receiving (slave) stations. The phase of the transmitter RF output is shifted forward (phase leading) via a phase-locking technique. The degree of phase shift is proportional to the instantaneous path-length perturbation and is measured as one-half the round-trip phase delay. The original signal is thereby reproduced at the slave site minus the phase shift.

A single, highly-accurate frequency reference, available as a transmitted signal, would be much less costly than building separate standards for each site in a communications or navigation system. However, when the distance between sites is greater than 0.5 km, perturbations in the path between sites are sufficient to degrade the transmitted signal beyond the tolerances required for much of today's equipment.

A promising new frequency transmission system automatically compensates for path perturbations between the transmitter (master) and receiver (slave) sites, and thereby allows a single source, such as a hydrogen maser, to serve as the frequency reference for multiple users. A phase-lock technique is used to introduce a phase lead at the master station. The degree of phase

change is proportional to the instantaneous path-length perturbation and is measured as one-half the round-trip phase delay, in order to reproduce the original signal at the destination with no phase shift.

A voltage-controlled oscillator (VCO) at the master station generates a signal that is sent to the remote-site (slave) receiver where it is received modified by the path time delay. The receiver local oscillator (LO) is phase locked to the signal with a -5.0-MHz offset and is derived from the receiver VCO. This VCO signal is also multiplied and transmitted back to the master station. This signal is received at the master station after experiencing a delay due to the path and is mixed with an LO to give an intermediate frequency (IF) of 5.1 MHz. This IF signal is then mixed with a 10.1-MHz signal (generated from the reference), yielding a 5-MHz IF with the proper phase relationship.

The LO used to generate the 5.1-MHz receiver IF is also mixed with a sample of the transmitted signal. The resultant signal is operated on by a synthesizer that multiplies only the phase of this signal. The output of this synthesizer is then phase detected against the output of the receiver IF and is used to control the transmitter VCO. The result is a transmitted signal, $k\omega_R \angle k\omega_R \tau$, where τ is the path delay. This signal experiences a phase shift due to the path ($-k\omega_R \tau$), yielding

$$k\omega_R \angle k\omega_R \tau - k\omega_R \tau = k\omega_R \angle 0,$$

the desired signal. Using the bidirectional link, path stability is about 10^{-15} over a 50-km path.

This work was done by John W. MacConnell and Richard L. Sydnor of **Caltech/JPL.** *For further information, Circle 21 on the TSP Request Card.*

This invention is owned by NASA, and a patent application has been filed. Inquiries concerning nonexclusive or exclusive license for its commercial development should be addressed to the Patent Counsel, NASA Resident Legal Office-JPL [see page A8]. Refer to NPO-13836.

Time-Division Multiplexer Uses Digital Gates

Eliminates errors caused by analog gates in multiplexing a large number of channels at high frequency

John F. Kennedy Space Center, Florida

Unless complex and expensive circuitry is added, time-division multiplexers tend to become inaccurate at frequencies above 20 kHz when 100 or more channels are combined. A new circuit design employs digital instead of analog gates to eliminate this problem. The circuit uses standard, readily available components, including logic elements and a digital-to-analog converter.

The new design has been used in aerospace work to multiplex signals for monitoring such variables as fuel consumption, pressure, temperature, strain, and stress. The circuit may be useful in other fields as well, for example in monitoring variables in process control and medicine.

In conventional time-division multiplexers, analog gates, one for each channel, feed an analog-to-digital converter (see Figure 1). A gate turns on when a signal arrives. However, the gate cannot respond instantaneously, since the capacitance of the gate output bus must be charged and the shunt impedance of all the off gates must be

(continued on next page)

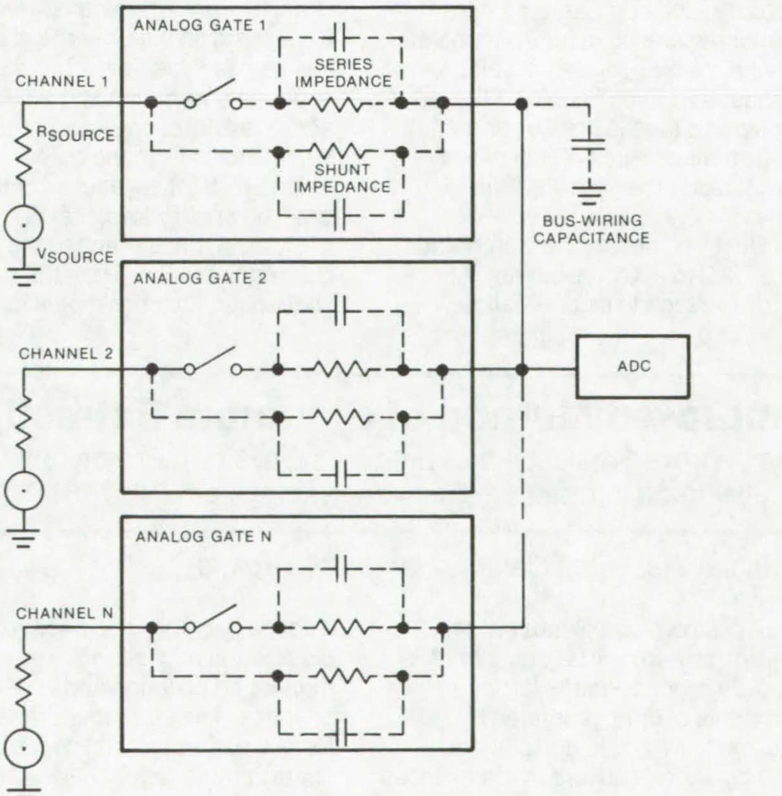

Figure 1. In the **Conventional Time-Division Multiplexer,** error is introduced by series and shunt impedances in the analog gates and by bus wiring capacitance.

driven. In addition, the drive current must pass through the series impedance of the on gate. These capacitances and impedances combine to create an error in the voltage on the output bus.

The new multiplexer design (see Figure 2) employs the "half-split" approximation process to avoid voltage errors. The analog inputs are applied to analog comparators - one comparator for each channel.

The circuit operates by comparing an analog input with a reference voltage and adding to or subtracting from the reference until the reference and the input match with the desired precision. With each addition or subtraction, digital pulses are generated and stored. When the match is complete, the pulses are an accurate digital replica of the original analog input.

The circuit operation can be understood in greater detail with reference to Figure 2: A sequencer turns digital gate 1 on and commands a digital-to-analog converter to apply one-half the full-scale reference voltage to the analog comparators. Analog comparator 1 compares the analog input from channel 1 with the half-reference voltage and produces a "yes" output if the input analog voltage is greater or a "no" if it is smaller. Since digital gate 1 is on, it feeds the "yes" or "no" to the DAC.

Next, the sequencer commands the DAC to add one-quarter full-scale voltage to its one-half full-scale output (if a "yes" is present) or to subtract one-quarter full-scale voltage (if there is a "no"). The DAC output and the analog signal on channel 1 are again compared. Depending on whether the answer this time is "yes" or "no," the sequencer commands the DAC to add or subtract one-eighth full-scale voltage to or from the output.

This half-split process continues until the analog-to-digital conversion of channel 1 has reached the desired precision. Then the sequencer switches digital gate 2 on, and so forth. When the last channel has been converted, the sequencer starts again at channel 1.

The output of the on digital gate is a PCM wave train. The DAC stores the binary digits and releases them as a parallel digital pulse stream at the end of each conversion.

This work was done by Claiborne E. Myers and Arthur E. Vreeland of Federal Electric Corp. for **Kennedy Space Center.** *For further information, Circle 22 on the TSP Request Card.*
KSC-10878

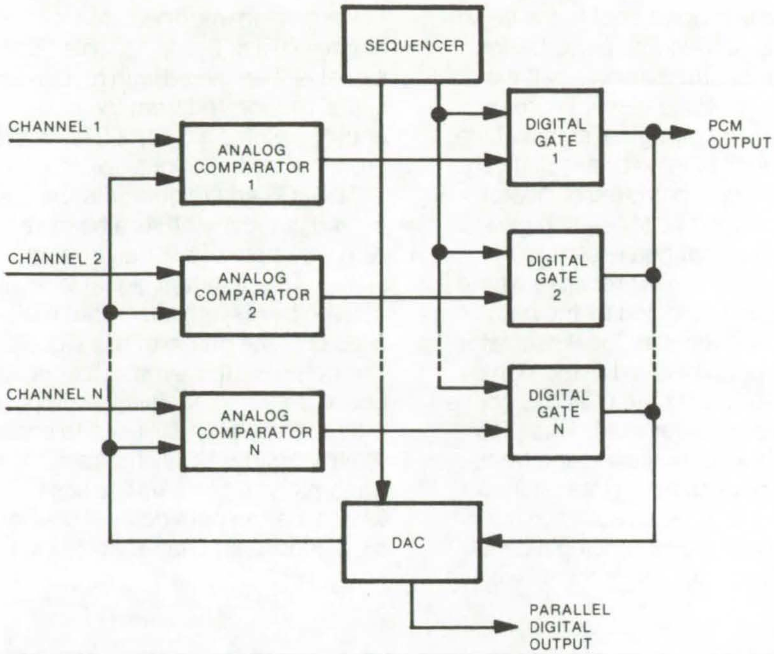

Figure 2. The **Time-Division Multiplexer With Digital Gates** avoids error by comparing the input with an adjustable reference. When the input and reference are equal, the value of the input is released in digital form.

Improved Method of Signature Extraction

An improved multispectral processing system: Prototype multivariate interactive digital analysis system (MIDAS).

Langley Research Center, Hampton, Virginia

A prototype multispectral processing system will be capable of rapidly processing the large amounts of data generated by currently available and planned multispectral sensors, such as those utilized on aircraft and spacecraft. Relative to the number of subject classes, an inordinate amount of operator time is required to classify a scene into finer and finer subject classes, as may be required for monitoring pollution and vegetation changes. The techniques developed for this system greatly decrease the operator time required for signature extraction from a multispectral data base.

The primary area of improved operator efficiency is in the determination of spectral signatures for subject classes contained within a remotely sensed scene. Such a determination usually requires that the operator display all or a portion of the data base, identify in the display-coordinate system the coordinates of each sample data element, translate the display coordinates into the data base coordinate

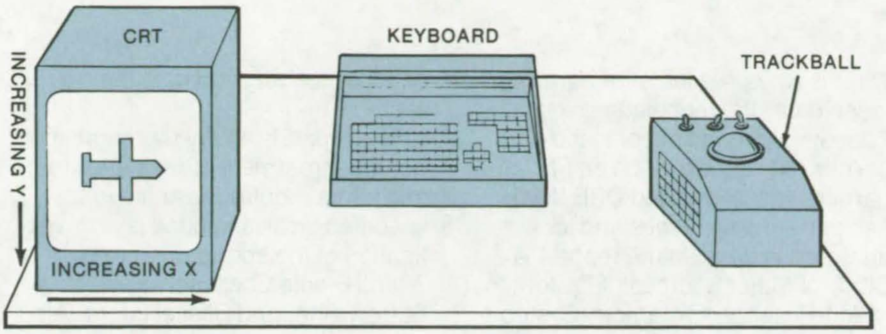

Figure 1. The **Operator-Control Hardware** includes a three-color cathode-ray tube (CRT) screen for display of multispectral data, a trackball cursor for delineation of subsets of data displayed on the CRT, and an alphanumeric keyboard for communication between the operator and the central processing system.

system, and then compile the sample elements for a subsequent statistical analysis. This sequence is greatly accelerated with the new technique.

The spectral signatures of the various subject classes are computed by employing a user-interactive subsystem made up of commercially available units (Figure 1).

To determine the spectral signatures for a desired subject class, the operator follows the steps shown in Figure 2. First, a subset of the base of multispectral data that is believed to contain a subject class is displayed on a CRT. The operator selects the data subset, based on prior knowledge of the scanned scene; e.g., as derived from a ground-truth photograph.

The operator identifies the sample on the CRT. This is the basis of the methodology. Using the trackball cursor, the operator delineates the sample-area data elements from other data elements by defining the vertices of a polygon representing the sample area. It is then the task of the system software to identify the coordinates of the data elements contained within the polygon.

The data elements identified in the polygonal sample are translated from the display-coordinate system to a random-access file-coordinate system. Then, the spectral signature for this subject class is computed and the signature is stored on file. The last decision in the sequence is whether there are additional classes for which signatures are to be obtained. If yes, the process is repeated; if no, this phase of the overall processing sequence is completed.

The MIDAS multispectral data processing system demonstrates greatly increased throughput efficiency via improvements in the method of operator/machine interaction. The technique takes advantage of commercially available hardware to provide a rapid method for extraction of spectral signature of a subject class from a large base of multispectral data, and it is suitable for a wide range of applications in the processing of remotely sensed data.

This work was done by D. Christianson, M. Gordon, R. Kistler, F. Kriegler, S. Lampert, R. Marshall, R. McLaughlin, and V. Smith of Environmental Research Institute of Michigan for **Langley Research Center.** *For further information, Circle 23 on the TSP Request Card.*

Inquiries concerning rights for the commercial use of this invention should be addressed to the Patent Counsel, Langley Research Center [see page A8]. Refer to LAR-12101.

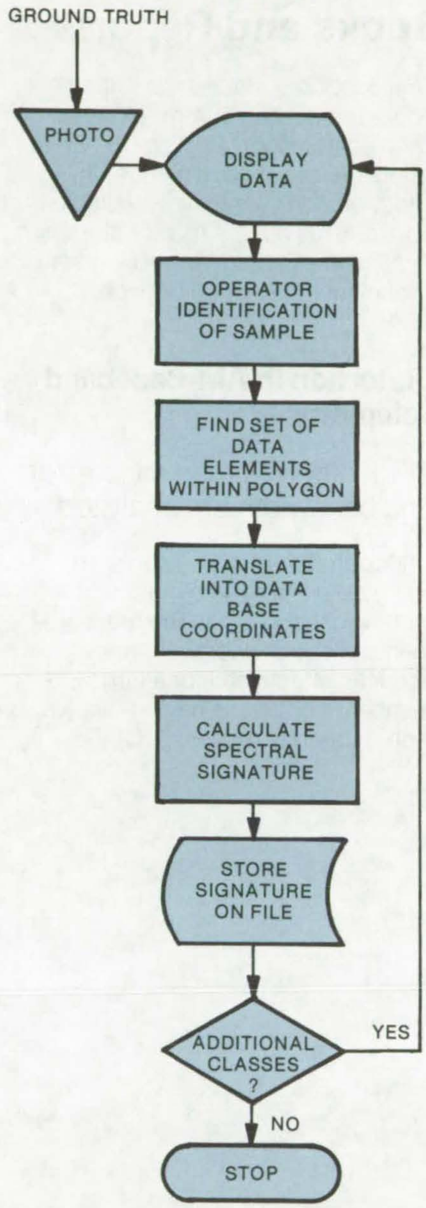

Figure 2. The **Sequence of Spectral Signature Computation** is a rapid and efficient interaction of the operator and the computerized data base and processing.

Books and Reports

These reports, studies, and handbooks are available from NASA as Technical Support Packages (TSP's) when a Request Card number is cited; otherwise they are available from one of NASA's Industrial Application Centers or the National Technical Information Service.

Distortion in AM-Baseband Telemetry

Tradeoffs with respect to error and bandwidth are analyzed.

Modern telemetry systems are being asked to handle more and more wideband data. The measurements of shock, vibration, and acoustic effects call for a large number of channels having relatively high frequency response. Of the various ways available for handling these data, the technique using "double-sideband suppressed-carrier AM subcarrier on an FM carrier" (usually called DSB/FM) has certain advantages and is analyzed in detail in the report "A Study of Major Sources of Distortion in AM-Baseband Telemetry Systems And Techniques for Optimum Baseband Design."

The four primary sources of distortion in a DSB/FM system are identified as channel filter distortion, adjacent channel crosstalk, intermodulation distortion, and RF fluctuation noise. The major tradeoff in a telemetry system is error versus bandwidth. To obtain small errors, a large bandwidth is required. Careful filtering and channel separation can be used to reduce distortion, but any system will still have a "nonremovable error" that is a function of channel spacing and data bandwidth.

The report is a very thorough and rigorous treatment of the bandwidth and filters required to achieve a specified error. Included is an investigation of the contribution to error of 3- and 6-pole Chebyschev, Butterworth, and Bessel filters. Also included is a methodology for designing DSB/FM telemetry systems to make optimum use of available bandwidth while reducing the error toward its theoretical minimum. Several design examples show how the information can be used.

This work was done by William E. Salter of Sperry Rand Corp. for **Marshall Space Flight Center.** *To learn how to obtain a copy of the report, Circle 24 on the TSP Request Card.*
MFS-22180

Physical Sciences

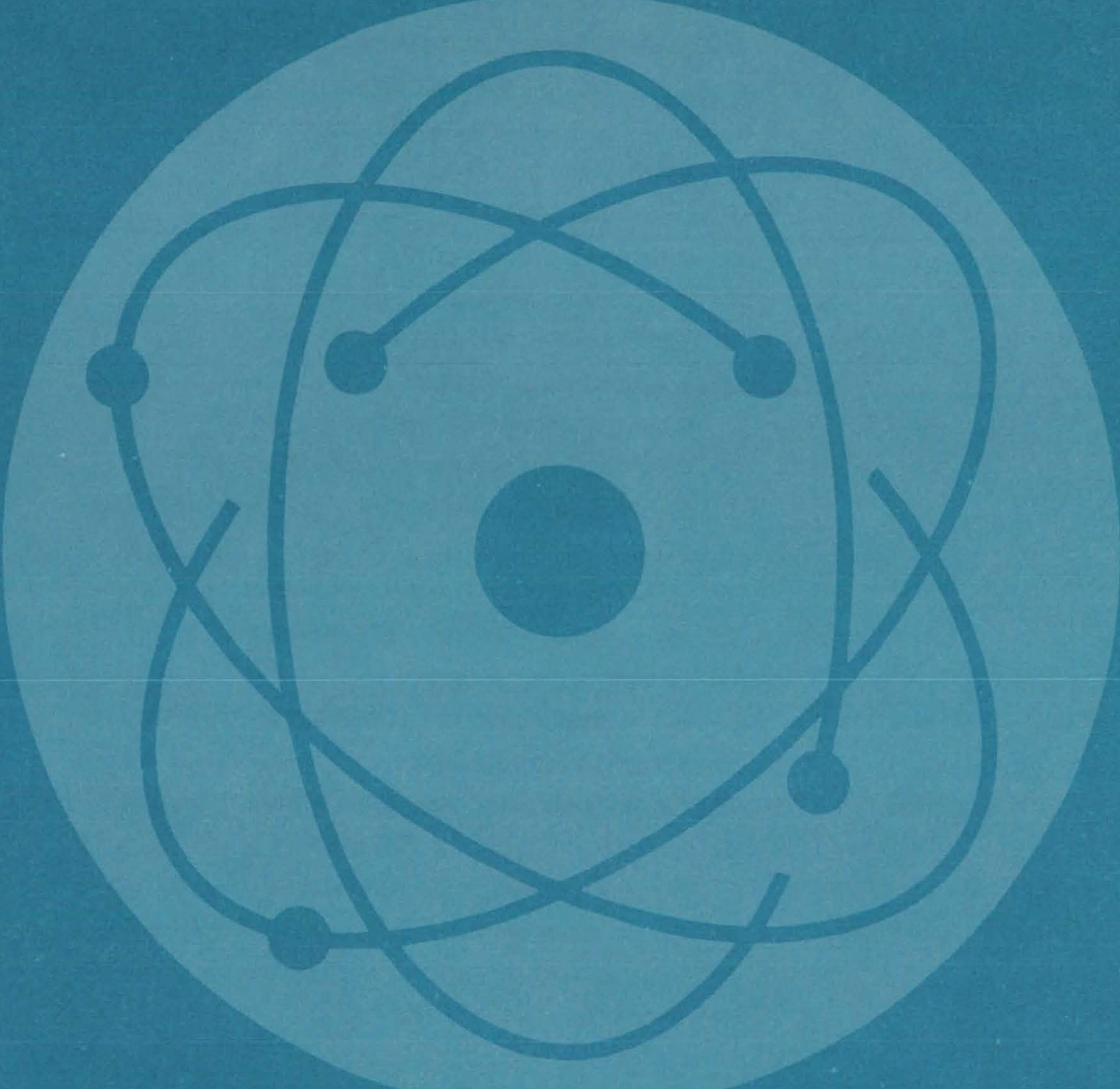

Hardware, Techniques, and Processes

Books and Reports

Computer Programs

High-Performance Flat-Plate Solar Collector

Absorber material, selective coating, and collector design are combined to improve efficiency.

Caltech/JPL, Pasadena, California

By refining and combining several known techniques, a proposed solar collector could be more efficient and could operate at a higher temperature than previous collectors. The collector, as shown in the illustration, would comprise three basic approaches:

- a vacuum to reduce convection losses,
- a selective coating, and
- a porous absorber.

All three concepts are implemented and combined with improvements that should increase the cost effectiveness of the system.

The collector is an evacuated, concentric tubular envelope surrounding a flat-plate absorber. The evacuated envelope is used to reduce heat losses from convection and conduction. In contrast to existing systems that used the inner tube as a heat exchanger, the use of the flat plate is expected to enhance the absorber-to-gas heat exchange.

The other primary source of heat loss in solar collectors is the reradiation of absorbed energy. Like many other systems, a thin selective coating would be used to achieve high absorbance of solar radiation and low emittance of the reradiated longer wavelength radiation. However, one of the problems with selective coatings is that their effectiveness increases rapidly as the angle of incident solar energy approaches the plane of the collector. This increases the long-wavelength emittance of the system and reduces the efficiency of the system. The coating emittance and angular dependence can be lowered by making it thinner, but this also reduces the amount of absorbance.

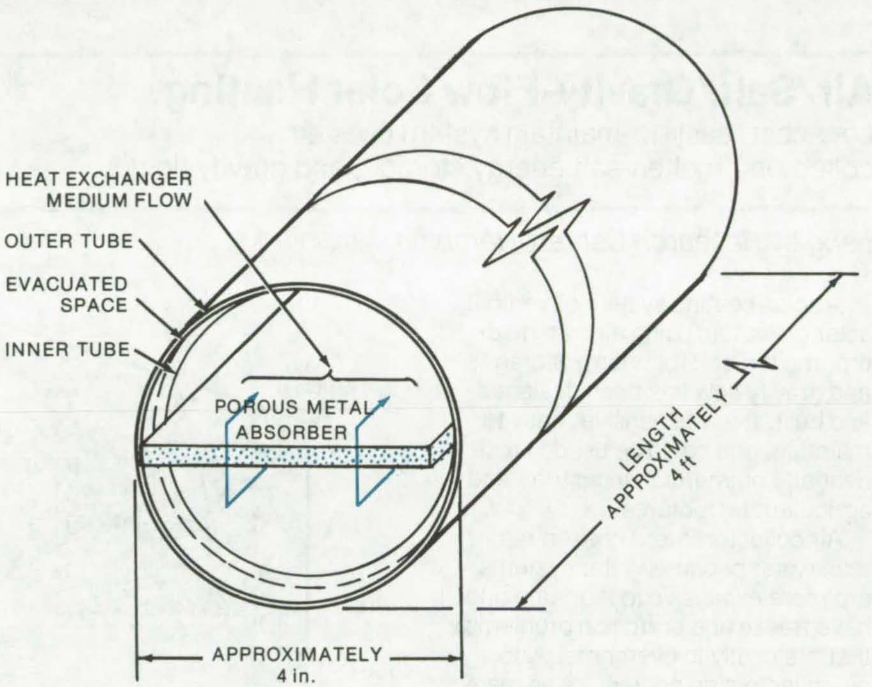

The **Concentric Glass-Tube-Envelope Collector** surrounds a flat-plate absorber having a spectrally selective coating. The envelope is transparent with an antireflection coating. The heat-transfer medium is a gas, such as air, that circulates along a hairpin path as shown by the arrows.

These contradicting requirements could be resolved by using a porous metal as the substrate on which the coating is deposited. The porosity increases the absorption surface area and increases the absorbance of the copper by "trapping" radiation in the pores (multiple internal reflections). On the other hand, copper emittance will not increase much, as it occurs mostly on the outermost sufaces of the plate and will not be appreciably enhanced by the pores.

This increased absorption allows effective use of a selective coating. For instance, a thin dielectric coating that absorbs (appears black to) wavelengths shorter than 3 μm could be placed over porous copper. This same coating can be selected to be transparent to the longer infrared wavelengths emitted by the copper. Thus, the coating will absorb solar radiation; but because of the transparency region of the coating, the emittance will be that of the longer wavelength source, the copper. The emittance of polished copper is about 0.04 at solar-collector temperatures, and the absorbance of typical coatings is

(continued on next page)

around 0.9. Thus, the absorbance-to-emittance ratio can be made quite high.

However, the real advantage of the porous copper accrues when the coating is made very thin to insure that the collector emittance is that of the copper and is not increased by the coating thickness. Polished copper has an absorbance of only 0.35; and when combined with a thin coating with a much-reduced absorptance, the total absorbance-to-emittance ratio drops significantly. With the porous substrate, a thin dielectric coating can be used while retaining significant absorbance.

This work was done by Rollin K. Reynolds of Kentron-Hawaii, Ltd., for **Caltech/JPL** *and Glen McDonald of* **Lewis Research Center.** *For further information, Circle 25 on the TSP Request Card.*
NPO-13883

Air/Salt/Gravity-Flow Solar Heating

Low-cost, easy-to-maintain system uses air collectors, molten-salt energy storage, and gravity flow.

Langley Research Center, Hampton, Virginia

A solar-heating system of vertical solar collectors using air as a medium, molten-salt for energy storage, and gravity flow has been designed and built. It is inexpensive, easy to maintain, and could be used in residential, commercial, industrial, and agricultural structures.

Air collectors were chosen rather than water because water systems are more expensive to fabricate and have freeze and corrosion problems that are costly to overcome. Also, air collectors do not require as many "nonrenewing" resources, such as copper, aluminum, and other metals. Molten-salt storage of energy was chosen because it reduces the weight required for energy storage by utilizing heat of fusion rather than heat capacity only, as is the case with water or rocks.

Gravity flow eliminates high pumping costs otherwise required to move large quantities of hot air from the top of the collectors to the basement for storage. In addition, the hot air is circulated in a closed system and utilizes radiator surfaces, eliminating the dirt and other problems associated with the introduction of hot air directly into the occupied space.

The operation of the system can be followed through the accompanying diagram. When solar energy is available, heat is concentrated in the absorber plate and is transmitted to the surrounding air. The heated air rises and passes through ports and the collector valve into the

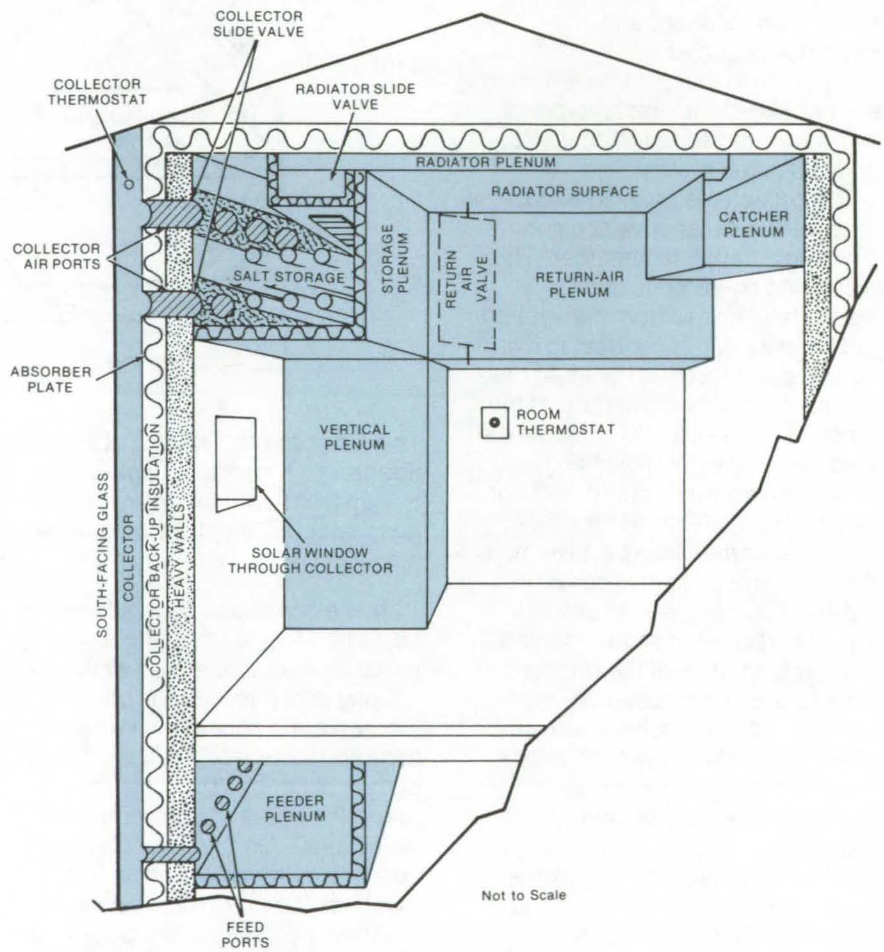

The **Gravity-Flow, Molten-Salt Storage** solar-heating system uses a collector on a vertical wall. Air carries the heat collected from the Sun and passes through the radiators to heat the room. Heat can be stored by closing the radiation valves and passing the heat over salts that heat and melt as they absorb the solar energy.

energy-storage plenum. It continues through the radiator valve into the radiator plenum. The hot air transmits heat to the radiator surface or panel, which heats the occupied space by radiation. The then cooler air continues into the catcher plenum and into the return-air plenum. There, the air passes through the return-air valve and is directed down through the vertical plenum to the feeder plenum, which feeds the cooled air back into the collector.

As room temperature rises and demand for heat is satisfied, the room thermostat closes both the radiator valve and the return-air valve, preventing hot-air flow to the radiator surfaces. In this case, the hot air is used to heat the energy-storage salts. From the storage plenum the air flows down through the vertical plenum to the feeder plenum and back to the collector.

When there is a demand for heat, and solar energy is not available, the collector temperature drops, and the collector thermostat closes the collector valve. The room thermostat activates both the radiator valve and the return-air valve. Hot air from storage flows through the radiator valve onto the radiator surfaces, heating the room. The air continues to flow into the catcher plenum and return-air plenum and is directed, in this case, by the return-air valve into the storage plenum for reheating. Auxiliary fans could be used to increase airflow and improve efficiency. Heavy walls with outside insulation are recommended so that the structure becomes an important part of energy storage. Windows in the wall covered by the solar collector can be made of heat-absorbing glass at the absorber plate.

The test system was used to heat a 400-ft^2 (37.2-m^2) room used for equipment storage. The solar-collector area was 210 ft^2 (18.6 m^2) Various types of solar collectors were tried, and the best design used perforated metal as an auxiliary absorber panel between the south-facing glass and the absorber plate. Air in excess of 200° F (93° C) could be dumped from the collectors with 50° F (10° C) outside ambient temperatures, but the most efficient operation was with discharge temperatures between 130° and 150° F (54° and 66° C). Summer stagnant temperature did not exceed 120° F (49° C) because of the high divergent angle between the Sun's rays and the normal to the collectors.

The energy-storage medium was sodium sulphate salts that melt at 89° F (32° C). They were loaded in plastic bags. However, after a few cycles of freezing and thawing of the sales, the bags failed. Concrete blocks were used to replace the salts until a better holding device can be developed. The reduced heat-storage capability and extra weight of the rock storage caused an overall loss of system effectiveness, so other methods of handling the salts successfully are now being considered.

The overall temperature of the solar-heated room was compared to that of a similar unheated room. The solar-heated room temperature ran 15° to 20° F (8° to 11° C) higher than that of the unheated room, but the rooms were still somewhat cooler than is normally considered comfortable.

This system can be retrofitted to existing buildings and can be used on high-rise buildings. An important feature is that the weight of the vertical collector imposes a relatively minor load on the building structure and presents few installation problems.

This work was done by Ronald N. Jensen of **Langley Research Center.** *For further information, Circle 103 on the TSP Request Card.*

This invention is owned by NASA, and a patent application has been filed. Inquiries concerning nonexclusive or exclusive license for its commercial development should be addressed to the Patent Counsel, Langley Research Center [see page A8]. Refer to LAR-12009.

Solar Radiation Shadow Detector

An optical sighting technique determines the amount of annual shadow at a location.

Marshall Space Flight Center, Alabama

The task of choosing the optimal location for solar-energy collector panels is one of the major design decisions required when planning the installation of a solar-energy system. The location for the collectors must be chosen so that they will receive the maximum insolation during the year. At many installation sites, this decision will be influenced by the presence of shadow-creating objects, such as neighboring buildings, trees, and hills. A visual inspection of candidate collector sites will not always be sufficient to insure the absence of shadows during the year, since the shadow position is a function of the calendar date and hour.

Presently, a graphical technique is used to determine the time and location of shadows. This method requires drawing a shadow mask of nearby objects, which is superimposed over a Sun-path diagram. The time, date, and location of the shadow are then read from the composite drawing. This method is time consuming, requires much skill, and its accuracy depends on one's ability to prepare an accurate shadow mask.

The portable shadow-surveying instrument shown in the accompanying figure can be quickly and easily set up at a proposed collector site. It requires a relatively unskilled operator and provides immediate and accurate shadow determination.

To use the instrument, one must first level and aline the baseplate, using the bubble level and compass.

(continued on next page)

The baseplate is orientated such that the inscribed line is pointing toward true north. Correction of the magnetic compass reading to true north will generally be required for precision measurements. The outer gimbal is then set, using the latitude scale, to the indicia corresponding to the latitude of the installation site. This operation alines the axis of rotation of the inner gimbal parallel to the Earth's axis of rotation.

The sight tube is then adjusted and set to a specified declination angle, using the declination scale. The declination angle setting determines which of the diurnal Sun paths the sight tube will track. For example, a 0° declination angle setting alines the sight tube to track the Sun's path at equinox; a setting of $\pm$ 23 1/2° corresponds to the Sun's path at winter and summer solstices.

Having completed the setup, the operator then looks into the mirror, which is mounted in the sight tube, and rotates the inner gimbal $\pm$ 90°; i.e., the sight tube scans the sky from east to west horizons. If an object is sighted through the tube, that object will cast a shadow at the location of the instrument. The time and day when the shadow will appear are determined from the elevation and declination angle settings.

This work was done by Richard A. Campbell of **Marshall Space Flight Center.** *For further information, Circle 26 on the TSP Request Card.*

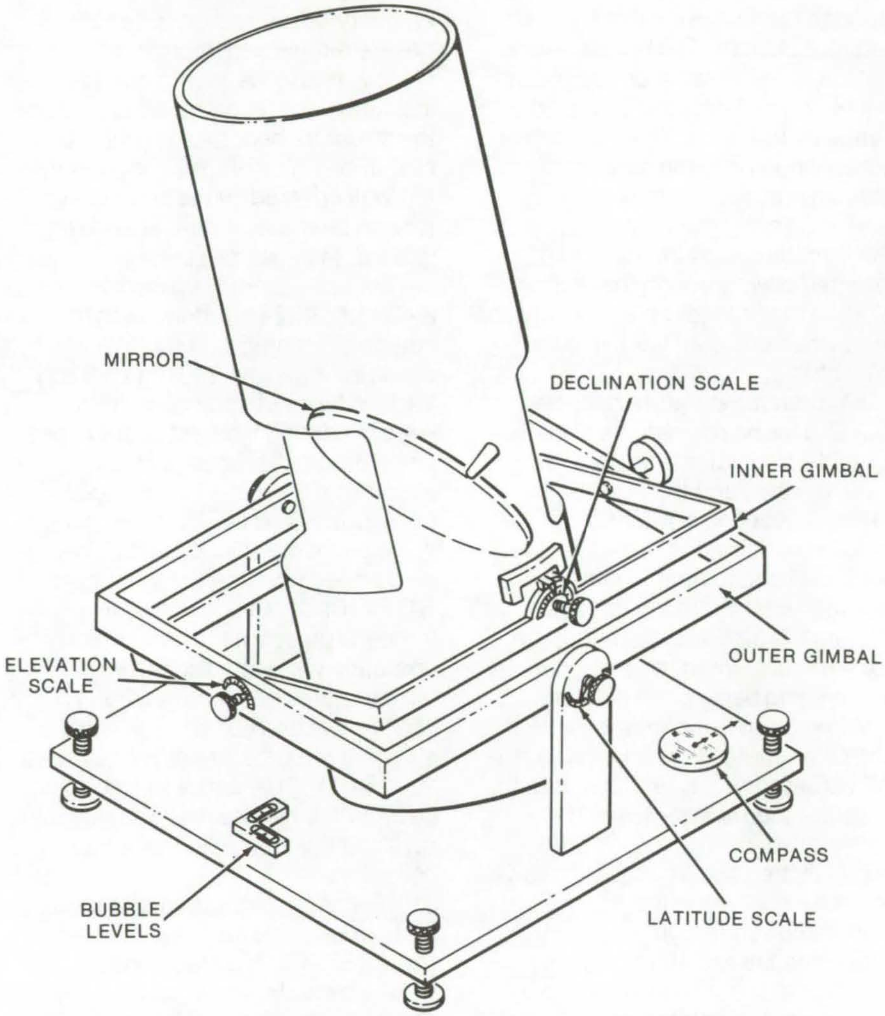

The **Solar Radiation Shadow Detector** has a gimbal-mounted sight tube, through which the operator views the surroundings and locates nearby objects that will produce shadows at the detector's location.

Inquiries concerning rights for the commercial use of this invention should be addressed to the Patent Counsel, Marshall Space Flight Center [see page A8]. Refer to MFS-23546.

Tower-Supported Solar-Energy Collector

Booms support several improved collectors on a single tower to increase efficiency.

Caltech/JPL, Pasadena, California

When considering a large thermal solar-energy plant, one of the first problems to come to mind is how to concentrate as much radiation as possible in a small area. This concentration is necessary to achieve the efficiencies of high-temperature operation. One promising approach has been to place an array of solar reflectors on the ground and aim the reflected radiation to a collector supported high in the air by a tower.

This extension of a solar collector into a third dimension has the advantage of providing an unobstructed, relatively short path to the collector for each of many reflectors covering a large amount of ground and intercepting substantial Sunlight. As might be expected, however, the design of a cost-effective and efficient collector, supported on a huge tower, is attendant with many problems.

For instance, the base of the tower takes up a lot of ground space that might be more effectively used by reflectors. A related problem is

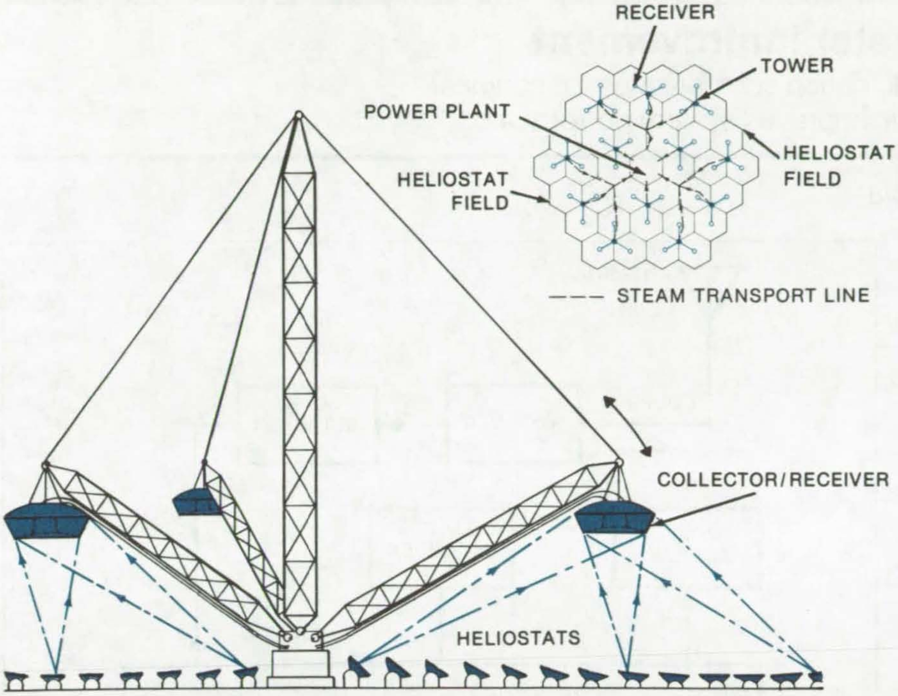

Figure 1. The **Multiple-Collector Tower** supports three receiver/concentrators that absorb solar energy reflected from a surrounding field of heliostats. The heliostats are hexagonal to allow dense packing. Several such tower-and-heliostat units could be arrayed in a hexagonal field as shown in the insert. Heated vapor from all would be conducted to a central powerplant.

the poor intercept angle of reflectors near the base of the tower and the resulting loss of energy reflected to the collector. Even with reflectors placed further away, beam dispersion due to pointing errors tends to dilute the solar flux. Another drawback to towers is the cost of making them able to withstand high winds.

None of these problems, however, is insurmountable, and they could well be overcome with a proposed modular tower system and an improved collector. The suggested tower, shown in Figure 1, is a guyed arrangement with three suspended collector arms constructed from commercially-available crane booms. The open lattice reduces wind loading, and the collector booms could be lowered during heavy winds to protect both the arms and the collectors.

The tower is placed in the center of a field of heliostats, Sun-tracking reflectors that direct the solar energy over a substantial ground surface to a single collector. Because there are three collectors to a tower, the ground space lost to the tower base is considerably less, and the intercept angles can be improved.

The collector, or receiver, proposed for this system is able to accept beams from a wide range of angles of incidence. Each collector, as shown in Figure 2, has an energy-absorbing surface that consists of a closely spaced network of conduits through which the working fluid flows. The flux distribution is such that at the outer edges of the receiver where the flux is more diluted, pressurized fluid may be preheated to the saturation temperature. Near the center, the flux is greater, and the working fluid is vaporized. Then superheated vapor goes to the tower, from where it is directed to a central powerplant along with the output of the other towers in the solar-power array.

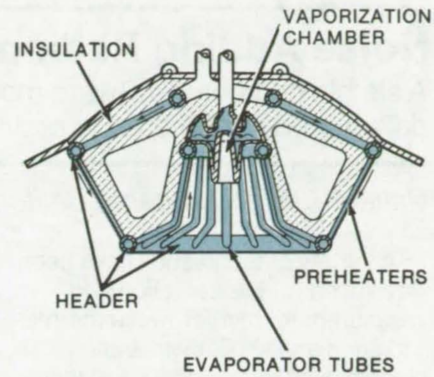

Figure 2. The **Solar Collector** used with the tower is circular (cross section shown above) and generally concave. Received flux is highest near the center where the vaporization chamber is located.

This system as proposed should overcome many of the disadvantages of tower-supported collectors and make their implementation cost-effective. By using the hexagonal arrangement of towers and heliostats shown in Figure 1 and by employing the new receiver design, which combines the advantages of cavity and vertical target collectors, efficiency should be improved markedly.

This work was done by M. Kudret Selçuk of **Caltech/JPL.** *For further information, Circle 27 on the TSP Request Card.*

This invention is owned by NASA, and a patent application has been filed. Inquiries concerning nonexclusive or exclusive license for its commercial development should be addressed to the Patent Counsel, NASA Resident Legal Office-JPL [see page A8]. Refer to NPO-13810.

Noise Adding Radiometer Improvement

A simple computer software modification compensates for nonideal detector characteristics to provide improved system performance.

Caltech/JPL, Pasadena, California

A variety of techniques have been developed for the detection and measurement of microwave thermal radiation and similar wideband signals. However, because of their low energy and quasi-random composition, these signals are often masked by receiver-generated noise. Thus a major goal of researchers is the development of systems with increased sensitivity and/or selectivity.

A recent innovation improves the performance of a noise adding radiometer (NAR) by suppressing much of the nonlinearity introduced into the system by departure of the detector characteristic from a true square-law function. This improvement is achieved by applying a simple analytical expression for detector nonlinearity in a calibration procedure, implemented by appropriate modifications to computer software.

The figure shows a simplified block diagram of a NAR. Output for a perfect square-law detector is given by

$$T_{op} = \frac{T_N}{Y-1}$$

where $Y = V_2/V_1$, and

V_2 = averaged detector output voltage with noise diode on,
V_1 = averaged detector output voltage with noise diode off,
T_N = noise temperature increase with noise diode on, and
T_{op} = system operating noise temperature.

Where the detector characteristic deviates from a perfect square law, improved radiometer performance can be obtained by accounting for this in the above equation. For the diode detector presently used,

$$Y = \frac{V_2 + aV_2^2}{V_1 + aV_1^2}$$

Substituting into the equation for T_{op},

$$T_{op} = \frac{T_N}{\dfrac{V_2 + aV_2^2}{V_1 + aV_1^2} - 1}$$

To determine a, choose two operating levels, V_2'' and V_2', and hold T_{op} constant

$$\frac{T_N}{\dfrac{V_2'' + a(V_2'')^2}{V_1'' + a(V_1'')^2}} = \frac{T_N}{\dfrac{V_2' + a(V_2')^2}{V_1' + a(V_1')^2}}$$

Since V_2'' and V_2' are arbitrarily selected, let

$$\frac{V_2''}{V_2'} = \frac{V_1''}{V_1'} = 2$$

and

$T_{op}'' = T_{op}$
when $a = 0$, high detector level, and
$T_{op}' = T_{op}$
when $a = 0$, low detector level.

Solving for a, substituting and simplifying through approximation,

$$a = \frac{2}{V_2''} \; \frac{T_{op}'' - T_{op}'}{T_{op}''}$$

Once determined, the a correction is readily implemented in computer software. In one application, radiometer linearily has been improved by a factor of about 50.

This work was done by Robert A. Gardner and Charles T. Stelzried of **Caltech/JPL.** *For further information, Circle 28 on the TSP Request Card.*
NPO-13108

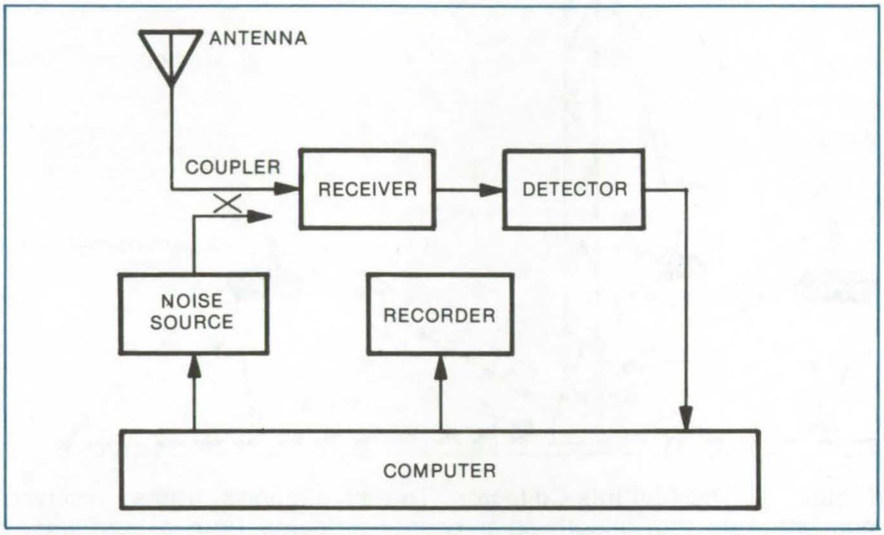

Noise Adding Radiometer block diagram shows the interconnection of the detector and computer. The computer software has been modified to compensate for nonideal detector characteristics.

Null-Balancing Microwave Radiometer

Remote absolute temperature measurements from 0 to 300 K with accuracy near 0.1 K

Langley Research Center, Hampton, Virginia

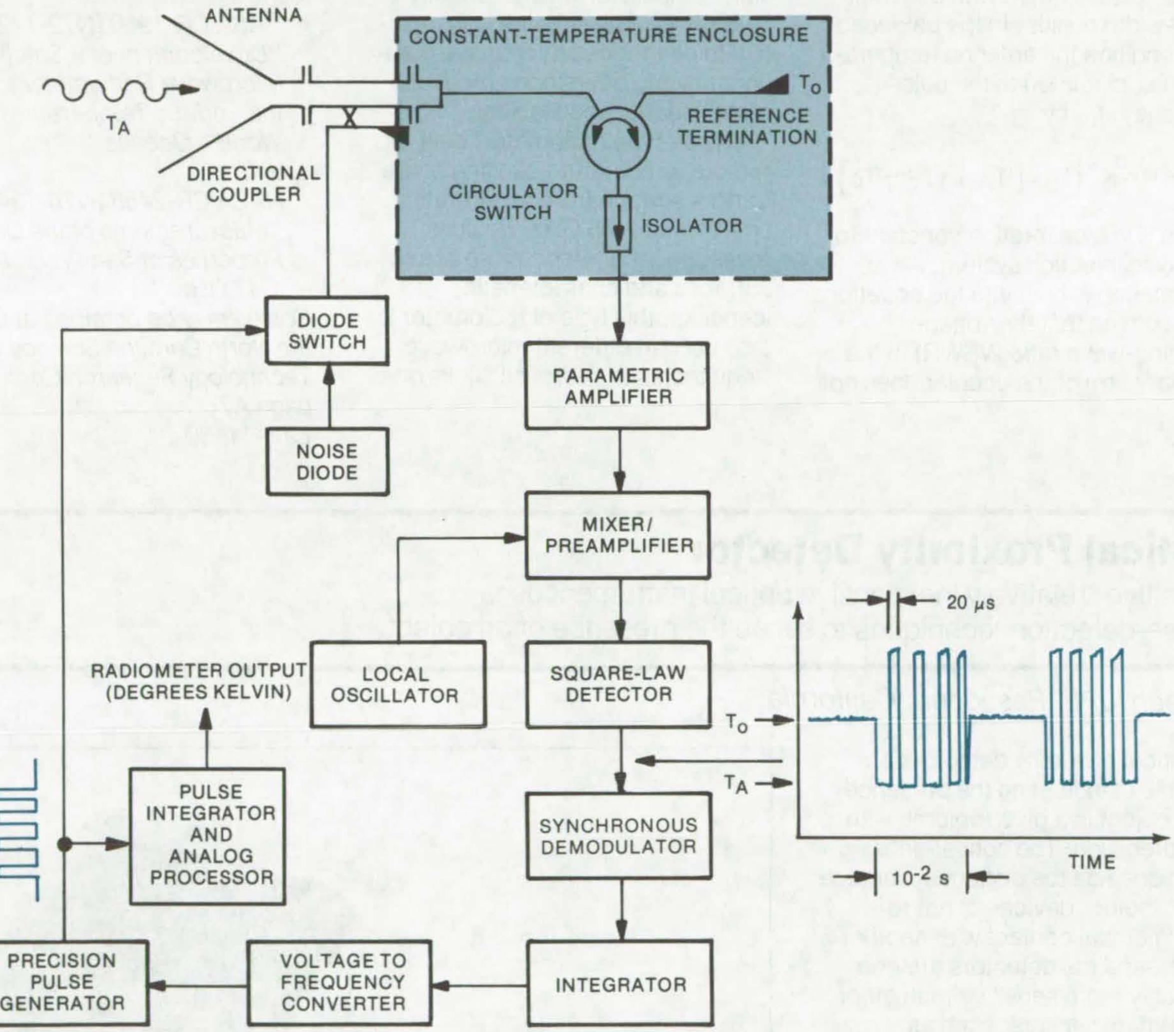

In the Microwave Radiometer a microwave switch is used to compare the thermal noise power of the antenna arm of the radiometer to that of a reference termination. By using a directional coupler and an attenuator, noise from a broadband noise source is added to the thermal noise from the antenna until the total power matches that of the reference termination. The equality is determined by amplifying and detecting the isolator output and then demodulating it at the switching frequency.

A new microwave radiometer may be used for the remote measurement of thermal emission. Conventional microwave radiometers are available with very high resolution but can only perform temperature measurements relative to two reference noise levels. The null-balancing radiometer described performs absolute temperature measurements over the range of zero to 300 K. The stability of the radiometer approaches 0.1 K.

The basic configuration of the radiometer is illustrated. A circulator switch is used to compare the thermal noise power of the radiometer antenna arm to that of a reference termination. Noise from a broadband source is added (via a directional coupler and a diode switch) to the thermal noise received by the antenna until the total power matches that of the reference termination. The isolator output signal is amplified and detected by synchronous demodulating it at the frequency of the circulator switch generator (not shown).

(continued on next page)

The output of the noise diode is switched in the form of 20-μs pulses and injected into the antenna via the directional coupler. An error signal at the output of the synchronous demodulator causes the frequency of the pulses to vary in such a way as to reduce the error signal.

The noise is gated with constant-pulse-width pulses. In the balanced null condition the antenna temperature, T_A, is related to the pulse frequency, f_p, by

$$f_p = KT = K\left[T_O - \left[tT_A + (1 - t)\,T_p\right]\right]$$

where K is a calibration constant for the noise injection system. An approximation is built into the equation by assuming that the voltage standing-wave ratio (VSWR) in the auxiliary arm of the coupler does not change when the diode is pulsed and therefore that t (which includes losses to the coupler) does not change.

The constant-temperature enclosure and a variable-frequency pulsed-noise injection scheme result in the circuit operating as a precision comparator with essentially zero offset. The scheme is insensitive to deleterious microwave components and offers good measurement linearity and stability.

A prototype radiometer, built for remote temperature sensing of the Earth's surface from an aircraft, operates at 2.65 GHz. Besides measuring the temperature of sea surfaces and characteristics of icepacks, this type of radiometer is also used at different microwave frequencies to detect oil slicks on water and to determine cloud water content and water vapor content of the atmosphere.

This work was done by Walter N. Hardy, Allan W. Love, and Albert C. Jones of Rockwell International Corp. for **Langley Research Center.** *Further information may be found in:*

NASA CR-1960 [N72-17271] "Development of a Satellite Microwave Radiometer to Sense the Surface Temperature of the World's Oceans,"

and

NASA CR-2458 [N75-13496] "Measurements of the Dielectric Properties of Sea Water at 1.43 GHz."

Copies may be obtained at cost from the North Carolina Science & Technology Research Center [see page A7].

LAR-11130

Optical Proximity Detector

Sensitive, relatively inexpensive optical instrument uses phase-detection techniques to sense the presence of an object.

Caltech/JPL, Pasadena, California

Optical proximity detectors are capable of indicating the presence of an object in a given volume with high precision. The optical-sensing technique has the distinct advantage over "feeler" devices of not requiring actual contact with another object, and the detectors are considerably more sensitive than other noncontact sensors, such as capacity-operated switches. Possible applications include control of remote hand manipulators, monitoring machine-tool carriage movements, and use as a vehicular collision-warning device.

The detector shown in Figure 1 employs a small light source consisting of a gallium arsenide, light emitting diode (LED), with an output pulsed at 1,500 Hz. A converging lens focuses the light to a predetermined detection point. A second lens, mounted in the same housing, is aimed at the focus point and yields an image on a silicon PIN photodiode. When an object moves into

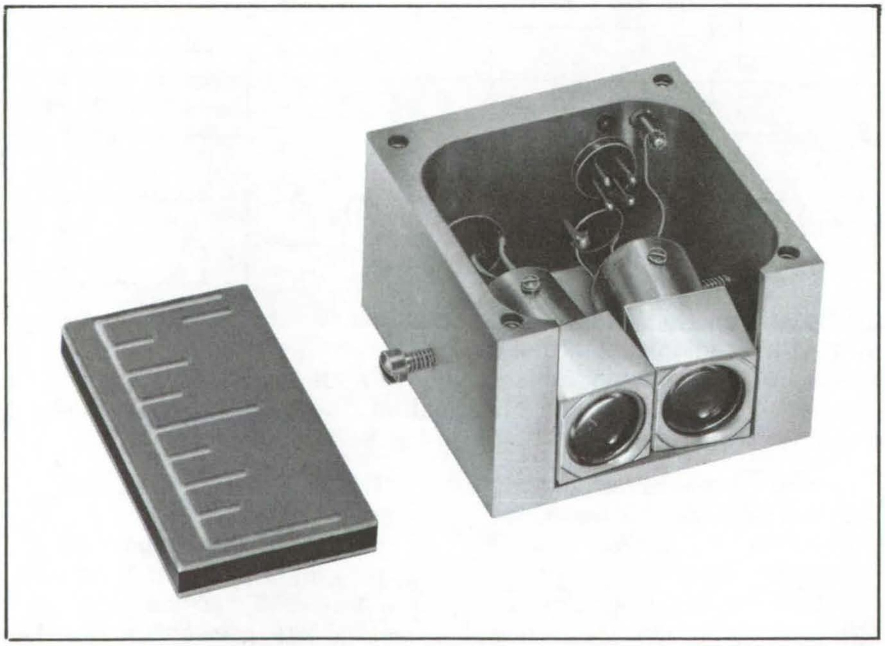

Figure 1. The **Optical Proximity Detection** has an LED light source aimed at a focus point in common with a detection lens. The instrument is about 1 by 1.5 by 2 cm in size and focuses on an object, typically 10 cm directly ahead. The detection region is a volume 0.5 mm by 3 mm in lateral dimensions.

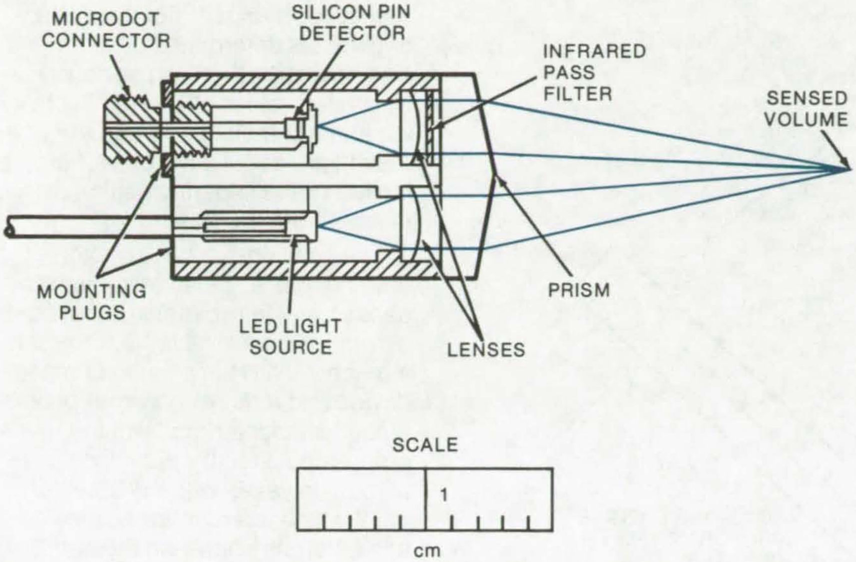

Figure 2. A **Prism-Aimed Optical** system, geometrically equivalent to aimed-lens system in Figure 1, can be modified with Fresnel grooving over 20 percent of the prism to result in detection of objects anywhere between the instrument and the focus point.

the focus-point region, it reflects light to the photodetector, which generates a signal to indicate its presence.

The electronics make use of a phase-sensitive detector which is tuned to respond only to the pulsing frequency. This helps to insure that the sensor is not confused by ambient light which may enter the detector lens. In addition, the LED, the photodiode with response matched to the LED output, and the filtering lens allow the detector to operate over a rather narrow radiation band, giving further selectivity over stray light.

In a second version of the optical system, outlined in Figure 2, the source and detector lenses are mounted parallel, and a prism directs the lens images to the desired point. With this arrangement, it is possible to construct a sensor that responds not only to an object at the sensing point but also to objects at all points inward to the detector. This is accomplished by cutting parallel grooves, similar to those of a Fresnel lens, over a region on the face of the prism. These grooves fan the light inward across the detector and collect light reflected from an object anywhere within the field of view.

The sensor output may be used in a variety of ways to provide a warning or panic-stop indication. It might be included as part of a feedback loop to an operator or control system to make motion corrections, or possibly to generate an audio tone indicating impending contact.

This work was done by Wilbert A. Hermann and Alan R. Johnston of **Caltech/JPL.** *For further information, Circle 30 on the TSP Request Card.*
NPO-13306

Large-Area Soft X-Ray Imaging System

Two-dimensional focusing collector can be adapted for crystallography or biological studies.

Goddard Space Flight Center, Greenbelt, Maryland

A new reflection-based detection and imaging system for soft X-ray photons (0.1 to 4 keV) consists of a large-area focusing X-ray collector and a position-sensitive proportional counter. It has an effective area of 150 cm^2 (1.2 keV) and was originally built for observing cosmic X-rays from a sounding rocket, but it could be used to study plasmas or with X-ray imaging in the biological sciences. As constructed, true images of X-ray sources are recorded with an angular resolution of 3 minutes of arc in two dimensions over a 1.5° by 1.5° field.

X-rays are imaged in two dimensions so that parallel beams are focused into points; and the detector, built into the new system, records the position of individual photons. Spatial resolution is about 1 mm for photon energies exceeding 0.25 keV.

The new X-ray telescope is larger than former similar telescopes, and the materials and methods used in its construction can be easily applied to yet larger instruments. Radiation is focused by successive reflections from orthogonal plates that are slightly curved. Theoretically, for radiation on axis, resolution is perfect in one dimension, degrading to about 1 second of arc in the other. For radiation off axis, the resolution degrades as the first power of the angle. In a practical instrument, alinement errors and imperfections in the reflecting plates result in a resolution of a few minutes of arc everywhere within the field of view.

The two-dimensional telescope is built of materials similar to those of the former telescope. Commercially-available float glass is used as the reflecting surfaces without further polishing. The active glass surfaces are coated with 500 Å of gold, stabilized by a 500-Å undercoat of chromium. The reflecting plates are housed in a 25-cm by 40-cm rectangular box that is strengthened by

(continued on next page)

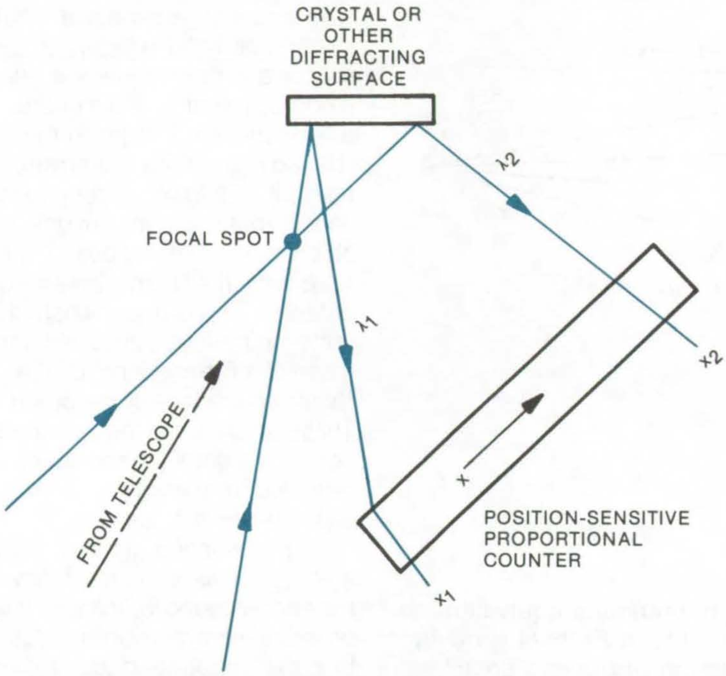

Figure 1. **Analysis of Crystals** or other diffracting surfaces, using the modified Rowland geometry: The imaging telescope and proportional-counter detector permit high system throughput. X-rays diverging from the small focal spot reflect from the crystal (or other surface) when the Bragg condition is satisfied. Following reflection, the position at which X-rays enter the counter indicates wavelength. Thus the position distribution (as indicated by x) across the counter is an indication of the wavelength distribution of the reflected X-rays, which is uniquely characteristic of the reflecting surface. The high system throughput is useful when data is taken quickly, such as observing the structure of a diffracting surface that changes with time.

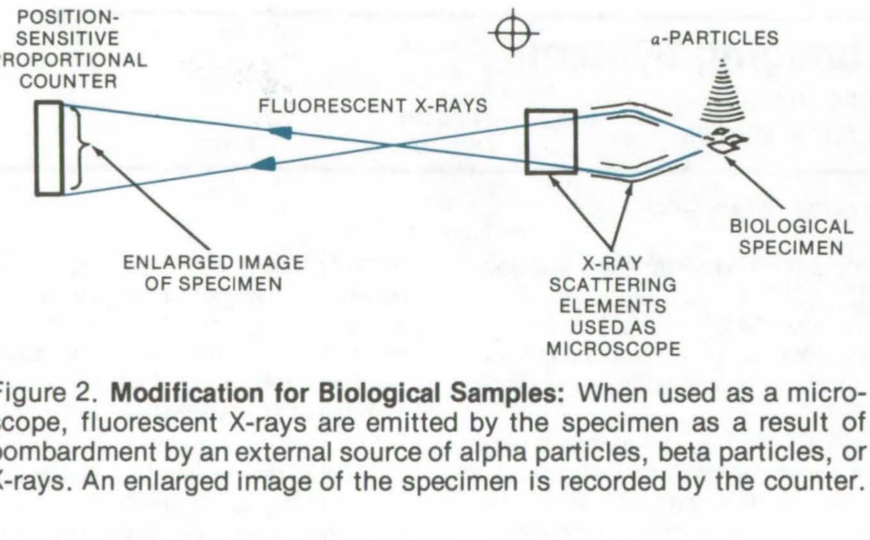

Figure 2. **Modification for Biological Samples:** When used as a microscope, fluorescent X-rays are emitted by the specimen as a result of bombardment by an external source of alpha particles, beta particles, or X-rays. An enlarged image of the specimen is recorded by the counter.

four support rings. Effective collecting area is determined by ray-tracing analysis, using previously measured values of X-ray reflectivity vs. angle of incidence. Angular resolution, about 3 minutes of arc, is limited by the superimposition of the images from the plates.

The position-sensitive photon detector has a spatial resolution of about 1 mm in two dimensions; the detector active area is 100 cm^2. It is a mechanically simple and compact device and requires only four preamplifiers to interface with the processing circuitry. Position resolution varies with the detector gain, which is a function of the voltage difference between the anode and cathode. The operating point is the highest detector gain that can be achieved without breakdown.

The imaging system can also be adapted to study crystal structures or other diffracting surfaces. As illustrated in Figure 1, the telescope is used to image an X-ray beam (having a broad-wavelength distribution) down to a small point. X-rays diverging from the spot reflect from the crystal or other surface when the Bragg condition is met. Following reflection, the position at which X-rays enter the counter is an indication of their wavelength. In this application, the two-dimensional detector is used to derive information about the nature of the reflecting surface from the X-ray position distribution.

Biological specimens are studied by replacing the crystal specimen with the biological one, as shown in Figure 2. The telescope is also modified for use as a microscope. Pictures recorded by the detector are characteristics of the molecular structure; a sequence of recorded images reveals the dynamic changes of the specimen.

This work was done by P. Gorenstein, H. Gursky, and F. R. Harnden, Jr., of the Smithsonian Astrophysical Observatory and P. Bjorkholm and A. DeCaprio of American Science and Engineering, Inc., for **Goddard Space Flight Center.** *For further information, Circle 31 on the TSP Request Card.*
GSC-12093

Portable Mass Spectrometer

Eighteen-pound unit can give real-time onsite sample analysis.

Caltech/JPL, Pasadena, California

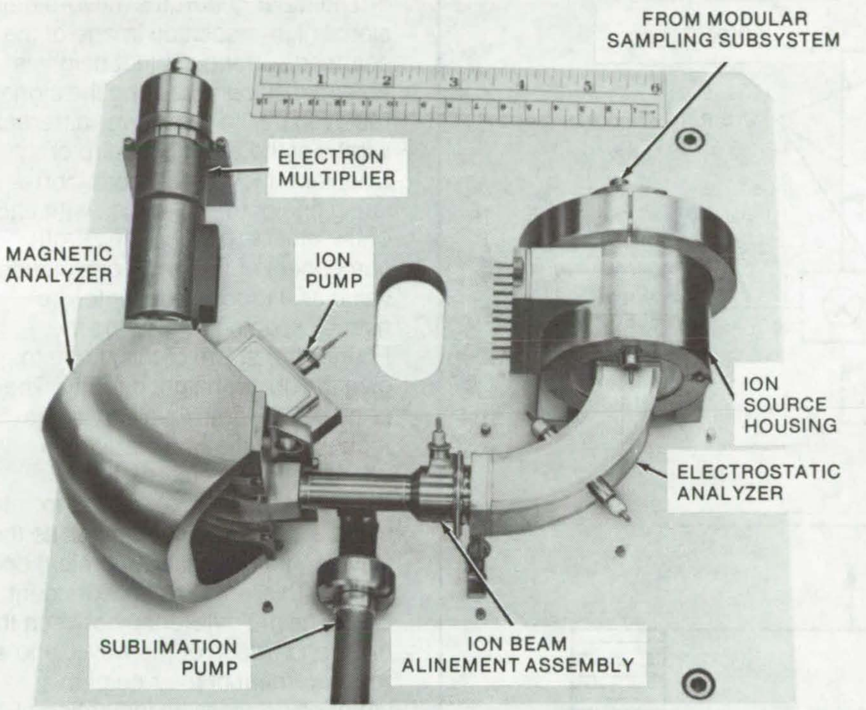

The **Portable Mass Spectrometer** is used with a modular sampling subsystem such as a gas chromatograph. The titanium sublimation pump is used only in the event of a gas overload.

A new portable mass spectrometer, originally designed for use with the Viking Spacecraft, should prove valuable in many terrestrial applications. Mass spectrometers have traditionally tended to be rather bulky machines intended for use in research work. They have generally been operated in fixed laboratory environments and therefore have not been designed for portability. However, for such modern applications as air-pollution monitoring and onsite toxic gas analysis in industrial plants and mine shafts, there is a need for a mass spectrometer of moderate resolution that may be easily transported for use in the field.

This new instrument packs ion source and ion beam alinement units, electric and magnetic field sectors, an electron multiplier, and a ion pump into a single housing (see figure) weighing a total of only 5 lb (2.3 kg). The complete mass spectrometer couples this assembly with the associated electronics and a modular sampling subsystem, which could be a gas chromatograph, to accommodate solid, liquid, or gaseous samples. The complete instrument could weigh as little as 18 lb (8.2 kg) and occupy a volume of 4 by 12 by 18 in. (10 by 30.5 by 45.5 cm).

The mass range is 12 to 200 atomic mass units (amu) with a resolution ($M/\Delta M$) of 200. It can quantitatively analyze sample inputs as low as 4.0 picograms/s when used with an electrometer amplifier having a gain of 10^8 volts/ampere. The values of these parameters should be more than adequate to meet the needs of many gas analysis applications and problems involving in situ analysis of volatile and volatizable liquids and solids. In addition to the uses already mentioned, the spectrometer has been suggested for several biomedical applications, such as the determination of the alcohol and gas content of the blood and breath and of traces of organics in the air or other gaseous media.

The unit is intended for use with state of the art data acquisition, processing, and display equipment, which would provide real-time output information. A self-contained data subsystem and telemetry link would supply remote monitoring and data reduction capability.

This work was done by Charles E. Giffin and Leonard M. Sieradski of **Caltech/JPL.** *For further information, Circle 32 on the TSP Request Card.*
NPO-13664

Remote Surface-Height Measurement

Radar-generated images are unaffected by weather conditions, cloud coverage, or solar illumination.

Caltech/JPL, Pasadena, California

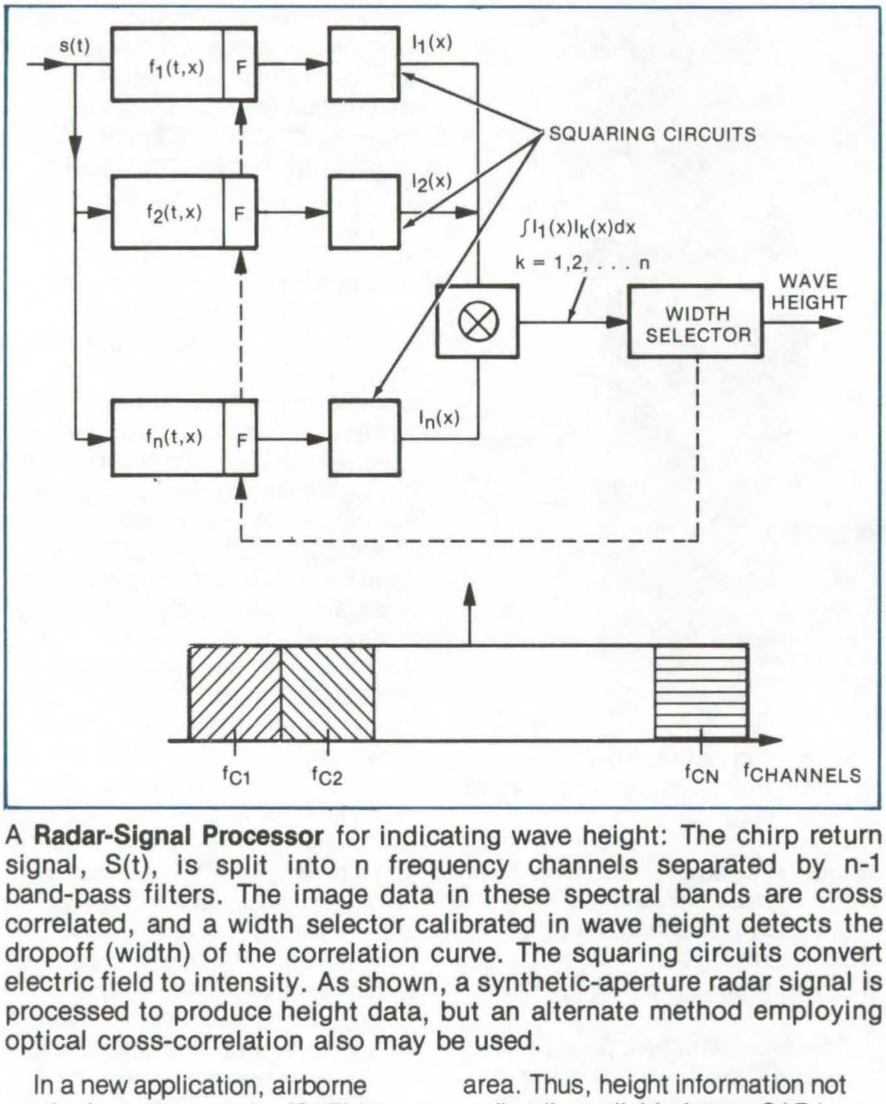

A **Radar-Signal Processor** for indicating wave height: The chirp return signal, S(t), is split into n frequency channels separated by n-1 band-pass filters. The image data in these spectral bands are cross correlated, and a width selector calibrated in wave height detects the dropoff (width) of the correlation curve. The squaring circuits convert electric field to intensity. As shown, a synthetic-aperture radar signal is processed to produce height data, but an alternate method employing optical cross-correlation also may be used.

In a new application, airborne synthetic-aperture radar (SAR) is used to measure the height of terrain features by comparing the variation of the image intensity pattern with frequency. When observing ocean-wave heights, for instance, large waves have a pattern that show more rapid variations with frequency, as compared to variations displayed for small waves. The radar system statistically measures the height of peaks above an arbitrary level and is not limited to surface roughness or minimum area. Thus, height information not ordinarily available from a SAR is obtained.

The technique, although developed for use on a spacecraft to observe ocean-wave heights, can be adapted to measure vegetation size, urban development, and geological roughness. It may be necessary to utilize a different microwave frequency per height measurement. Vegetation size, for example, would require a different frequency (and thus scale of height), compared to geological formations.

The radar generates a two-dimensional high-resolution image of the scanned surface. Object height is obtained by compressing the signal received by the radar over different widths of the available chirp or Doppler bandwidths, cross-correlating one of these images with each of the others, plotting the zeroth component of the cross correlation value as a function of center frequency spacing, and using the Fourier transform of this curve to give the object height directly. The principal concept involved in this technique is that the resultant intensity for the electric field scattered by the ocean wave to some arbitrary point changes as the wavelength or angle of illumination varies. This variation is dependent on the height difference between the crest and trough of the wave, and a measurement of the rate of this variation provides an indication of the ocean wave height.

This work was done by Atul Jain of **Caltech/JPL.** *For further information, Circle 33 on the TSP Request Card.*

This invention is owned by NASA, and a patent application has been filed. Inquiries concerning nonexclusive or exclusive license for its commercial development should be addressed to the Patent Counsel, NASA Resident Legal Office-JPL [see page A8]. Refer to NPO-13862.

Subsurface "Radar" Camera

Underground stratified layers are mapped via multiple-frequency synthetic-aperture radio ranging.

Caltech/JPL, Pasadena, California

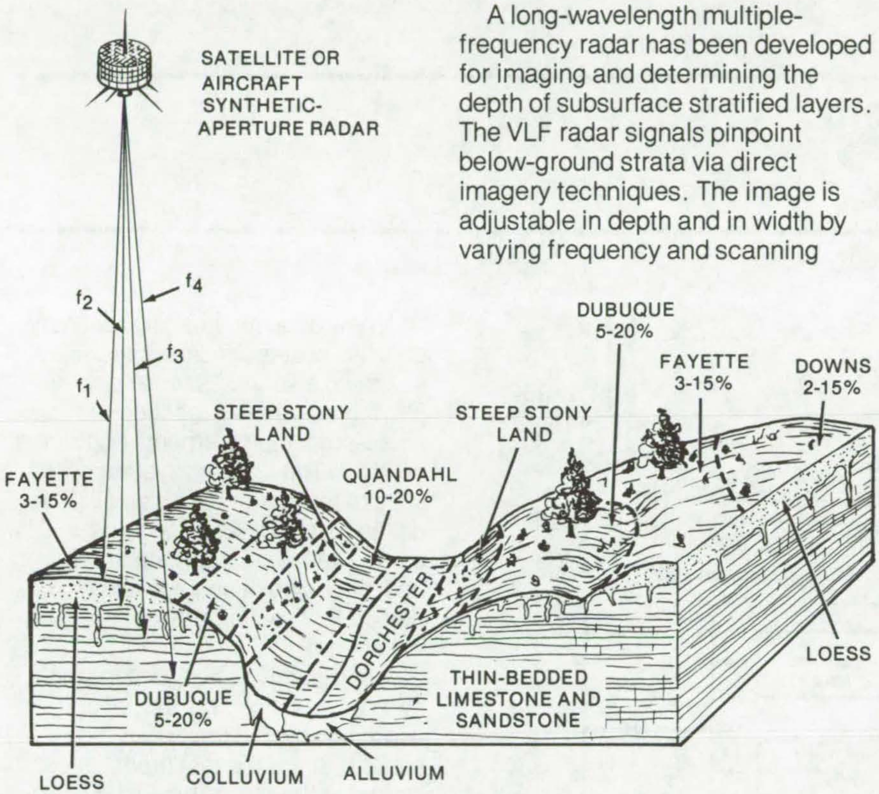

Figure 1. A **Very-Low-Frequency [∼ 40-kHz] Radar** transmits a pulse at frequency f_1 and receives an image at that frequency. Simultaneously, frequencies of penetration — f_2 through f_4 — may be transmitted and their received images differenced to obtain the relative depth of the reflecting strata. This method is based on the use of a plurality of synchronized synthetic-aperture radars.

A long-wavelength multiple-frequency radar has been developed for imaging and determining the depth of subsurface stratified layers. The VLF radar signals pinpoint below-ground strata via direct imagery techniques. The image is adjustable in depth and in width by varying frequency and scanning angle, respectively. The absorption per unit depth for electromagnetic radiation depends upon the angle or frequency of the radiation. The frequency dependence of the power returned by a subsurface scatterer is different from the frequency dependence of the power received from a surface scatterer, and this dependence is used to identify on the radar imagery features due to subsurface objects. The method uses two discrete frequencies or two look-angle synthetic-operative radars which may operate from an aircraft or from a satellite. The radar may prove useful in petroleum or mineral prospecting, flood control studies, agricultural planning, and the like (see Figure 1).

As depicted in Figure 2a, the images formed via the multiple-frequency radar are subtracted to provide subsurface imagery; or, as in Figure 2b, a single-frequency chirped-pulse synthetic-aperture radar may also be used. It processes the return signal over different bandwidths of the chirp or Doppler and subtracts the images formed from these bands to obtain depth data.

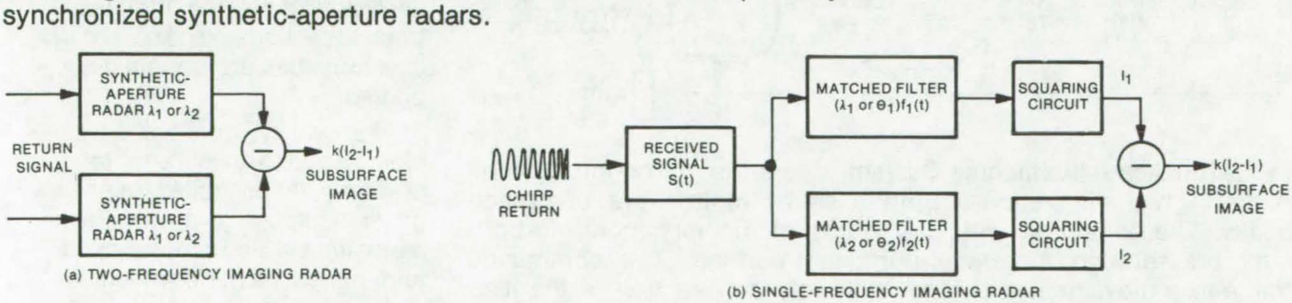

Figure 2. The **Synthetic-Aperture Radar** is used to determine the relative depths of underground geological phenomena. A two-frequency imaging radar signal (a) or a single-frequency chirped-pulse radar signal centered at about 40 kHz (b) is beamed Earthward from an aircraft or a satellite. In either method, the return pulse is match filtered, each filter operating at the discrete (or chirp) frequencies. The filters separate the frequency spectra which are then subtracted pixel by pixel to obtain the relative depth between strata.

(continued on next page)

In the single-frequency method, the chirp signal return is split into images covering two or more spectral bands. As the chirp signal is received by the radar, it is match filtered according to frequency or look angle at penetration frequency band f_1. The processed signal is simultaneously match filtered at penetration frequency f_2. The matched filters separate the frequency spectra, which are then subtracted pixel by pixel or differentiated with respect to radar frequency to obtain the relative depth information between two or more strata. The squaring circuits change amplitude to intensity.

This work was done by Atul Jain of **Caltech/JPL.** *For further information, Circle 34 on the TSP Request Card.*

NPO-13864

Acoustic Imaging System

Noise sources are pinpointed, and their positions are displayed visually.

Caltech/JPL, Pasadena, California

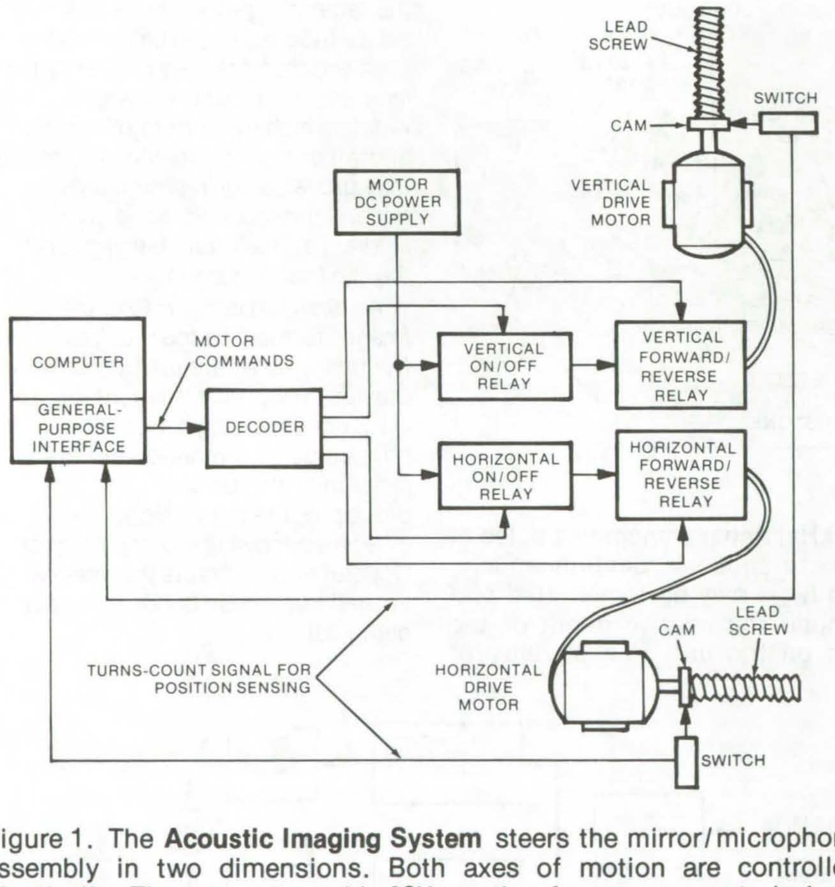

Figure 1. The **Acoustic Imaging System** steers the mirror/microphone assembly in two dimensions. Both axes of motion are controlled identically. The computer, with 32K words of memory, controls both drive motors through a general-purpose interface. The commands determine axis movement and forward or reverse direction of the lead screw (and thus of the mirror/microphone). All motion is relative to the initial placement and is determined by the operator prior to taking measurements.

A new acoustic imaging tool may be used to detect noise sources by scanning a sound "scene" and displaying the relative location of the noise-producing elements contained within it. The imaging system consists of two major parts: an ellipsoidal acoustic mirror aimed at the source with a microphone at the near-focus point and a display device for creating a visual image of the scene.

A computer is used to steer the microphone along horizontal and vertical axes and thus scan the source. Since the test model is placed at the mirror far-focus point, noise that originates at any location other than that point does not return to the microphone and is effectively rejected in measurement. As the noise source is scanned, a spectral analysis is generated. After subtracting background noise, the frequency distribution is plotted and printed.

As shown in Figure 1, the two motors used to drive the mirror assembly are controlled via a general-purpose computer. Each motor turns a lead screw that, in turn, moves the mirror-mounted

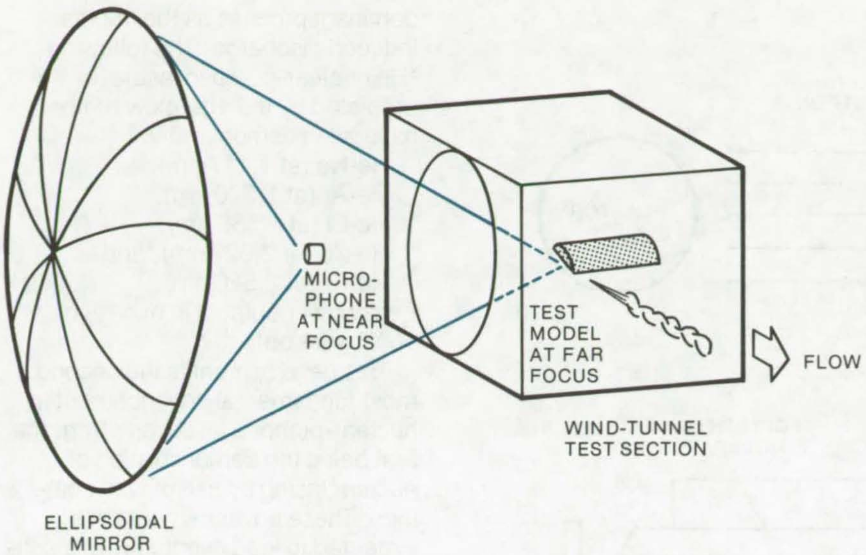

Figure 2. The **Acoustic Measurement Technique** used to study aircraft noise employs a microphone and a mirror located outside a wind tunnel. The ellipsoidal mirror faces a test model. Incident acoustic energy is collected at the farthest focal point and is concentrated at the nearest focal point. The mirror and microphone are supported within an enclosure that shields against room noise. The enclosure is mounted on wheels that run in a guideway, and it is driven in the upstream/downstream direction over a 50-cm range. Vertical movement of the aiming point is 15 cm.

microphone. The distance traveled is sensed by the computer via cam-operated switches that are mounted to the screws. As the microphone scans a scene, the computer counts the number of times the switches open and close. After the desired number of cycles have been counted (each cycle corresponding to instrument displacement), a new command is issued, and the motors are deactivated.

In one application of the imaging system, the mirror/microphone assembly is located external to the test site: a 60 by 60 cm wind tunnel for aircraft airframe-noise studies (see Figure 2). The 1-m-diameter mirror scans the airframe under test as the microphone picks up frequencies between 1 and 50 kHz.

This work was done by James M. Kendall, Jr., of **Caltech/JPL.** *For further information, Circle 35 on the TSP Request Card.*
NPO-13888

Nuclear-Pumped Gas Lasers

A new class of direct nuclear-pumped gas lasers uses a volumetric ^{3}He reaction.

Langley Research Center, Hampton, Virginia

Attempts at pumping gas lasers by charged particles created from nuclear reactions have been made for many years. Significant progress has been achieved in direct nuclear excitation with the development of nuclear-pumped lasers using either uranium-235 or boron-10 coatings on the internal walls of the laser cell. However, coatings are basically inefficient, since fissions occur primarily inside the coating itself, and most of the charged particle energy (approximately 80 percent) is lost within the coating. A much more efficient means of laser pumping incorporates the volumetric ^{3}He(n,p)^{3}H reaction.

Since helium is a major constituent of many gas lasers, it is convenient to replace the usual ^{4}He with the ^{3}He isotope. The ^{3}He reaction is initiated by a thermal neutron which is absorbed by the ^{3}He nucleus. The nucleus then disintegrates, producing a proton of 0.57 MeV and a triton of 0.19 MeV. Both these charged particles ionize and excite the gas medium homogeneously. Thus the ^{3}He reaction deposits energy nearly uniformly throughout the laser volume. By this method, direct nuclear pumping was first achieved with a ^{3}He-Ar (10 percent Ar) laser. Argon has many laser transitions which operate with high gain in the infrared region of the spectrum. Thus it is a good candidate for volumetric nuclear pumping.

The laser produced an essentially steady-state output, since the atomic and molecular processes operate on a very short time scale. Lasing took place from 200 torr to 4 atm (26.5×10^3 to 400×10^3 N/m^2) in ^{3}He-Ar. Further studies are needed to determine the minimum and maximum pressures for laser operation and the optimal ^{3}He-Ar mixture, although tests indicate that a 1 percent Ar concentration is near optimum. Also, the addition of chlorine to the ^{3}He-Ar laser was

(continued on next page)

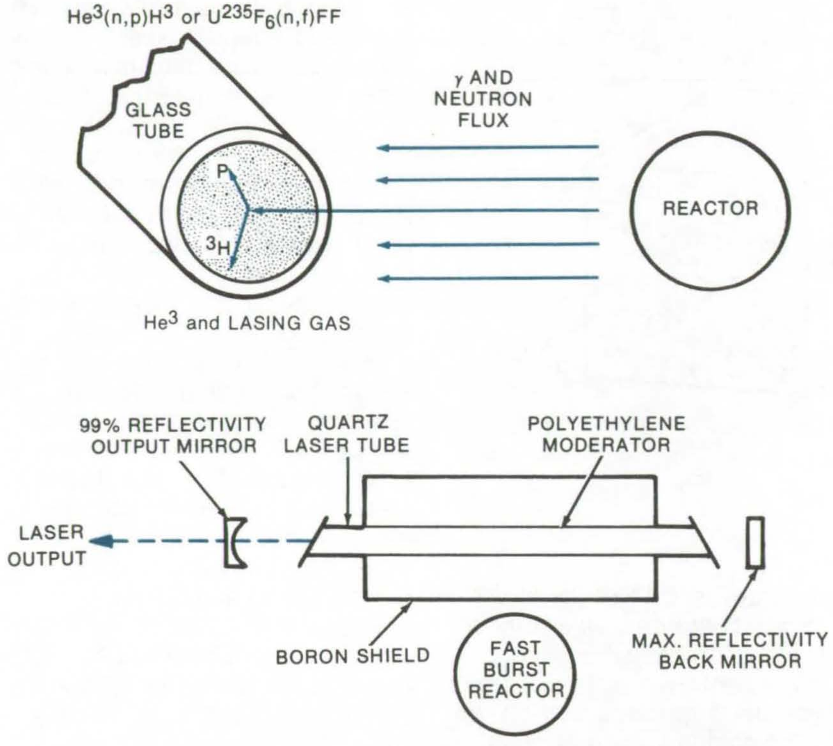

The **Volumetric ^{3}He Reaction** is initiated by a thermal neutron absorbed by ^{3}He isotope. Disintegration produces charged particles that excite the lasing gas.

found to produce a substantial improvement in the laser output. This phenomenon has been attributed to an interaction with the argon energy levels.

Using a fast-burst reactor to pump a laser medium is a slow process; only about five reactor pulses per day can be achieved. Thus it was desirable to use other means to study and optimize the laser parameters. With the ^{3}He-Ar laser it was found that a high-pressure (> 50-torr) electrically pulsed laser lasing in the afterglow could be used for this purpose. Test results indicate that the electrically pulsed discharge may have the same dominant process as the nuclear-induced discharge. The following ^{3}He nuclear-pumped lasers predicted by the afterglow method have been demonstrated:

He-Ne (at 1,117 nm),
He-Ar (at 1,270 nm),
He-Cl (at 1,586 nm),
He-Xe (at 2,027 nm), and
He-Kr (at 2,520 nm).

Peak power outputs in excess of 10 W were obtained.

This development is the second most fundamental advancement in nuclear-pumped laser research, the first being the demonstration of nuclear lasing by use of wall coatings. These advancements are expected to lead eventually to a self-critical nuclear-pumped laser system. This achievement would be of major significance because one of the most important features of a nuclear-pumped laser is that it has the potential of being the only practical steady-state high-power laser system.

This work was done by Frank Hohl, Nelson W. Jalufka, and Michael D. Williams of **Langley Research Center** *and R. J. De Young of Vanderbilt University. For further information, Circle 36 on the TSP Request Card.*
LAR-12131

Humidity-Resistant Black-Nickel Coatings

A black-nickel coating for solar collectors can withstand exposure to high humidity and temperature without degradation of optical properties. Under conditions where the solar adsorption of a conventional coating deteriorated from 0.96 to 0.72 in two weeks, the new formulation remained unchanged at over 0.92.
(See page 87.)

Differential Sound-Level Meter

The relative difference between sound-pressure levels at two microphone sites is measured precisely by continuously monitoring the gains of the two acoustical channels. The difference between two pilot voltages is used in a regulating loop to force the gain of the second channel to track the gain of the first channel.
(See page 108.)

Absorption Generator for Solar-Powered Air-Conditioner

A new generator for absorption air conditioners uses water at a somewhat low temperature — 185° F (85° C). Because solar collectors absorb more heat from the Sun at this temperature, the overall collector area can be decreased, making the overall cost of the solar powered air-conditioner more attractive to home-owners.
(See page 104.)

Burst Simulator for Laser-Doppler Velocimeter

Simulator allows for precheck of velocimeter electronics.

Langley Research Center, Hampton, Virginia

A laser-Doppler velocimeter (LDV) burst simulator has been developed for prechecking an LDV before an actual test run is performed. A known signal is introduced into the electronics of the LDV to determine whether they are functioning properly. Adjustments for maximum performance of the LDV can then be made.

This versatile simulator uses voltage-controlled oscillators (VCO's) to generate the fundamental frequency and the pedestal frequency independently. Previous simulators were limited to a fixed ratio between these two frequencies. In addition, the magnitude of each signal can be adjusted, and this burst simulator has the capability of producing single bursts, double bursts, or continuous waves of bursts.

Asymmetric burst is found frequently in LDV measurements. However, earlier simulators could not produce asymmetry in the pedestal of the burst signal; this system allows variable asymmetry in the burst signal to the point of producing the "double-pulse burst."

The LDV burst is simulated by mixing the outputs of two VCO's, one generating a high-frequency (up to 1 MHz) signal, the other a low-frequency (up to 10 kHz) signal. The pedestal is obtained by adding a portion of the low-frequency signal to a portion of the mixed signal. The electronic circuitry allows for single, multiple, and continuous burst modes of operation, with the timing obtained from a zero-crossing detector. The asymmetry is obtained by the introduction of a nonsymmetrical voltage pulse at one of the amplification stages.

Accurate and easy readout of both the fundamental frequency and the pedestal frequency of this versatile LDV burst simulator is accomplished through the use of an LED digital display.

This work was done by Otto Youngbluth, Jr., of **Langley Research Center.** *For further information, Circle 37 on the TSP Request Card.*
LAR-11859

Electrically-Controlled Variable-Color Optical Filters

The optical transmission characteristics of a birefringent element are changed by applying voltage to the plate.

Lyndon B. Johnson Space Center, Houston, Texas

Spectral transmission characteristics of optical filters may be changed electrically by using birefringent elements. A typical birefringent element uses a lanthanum-modified lead zironate titanate (PLZT) ceramic plate having a high index of refraction and a high dielectric constant. Its optical transmission characteristics are changed by applying voltage. The plate (acting as a half-wave plate) retards certain wavelengths when a given voltage is applied. In addition to the electrically controlled elements, fixed birefringent elements are also used. These are designed to retard specific wavelengths, without electrical control.

An entire filter is made from one or a number of birefringent elements mounted between two optical polarizers (see figure). The elements are arranged in certain orders to obtain the desired filter response. For example, electrically controlled elements may be interspersed between a number of fixed elements. The performance of the entire filter also depends on whether the polarizers are crossed or parallel. Certain color sequences may be generated when the polarizers are crossed, while different color sequences may be generated with parallel polarizers. A sequence of colors resembling a standard visible spectrum is best obtained with parallel polarizers.

A similar arrangement can be used with colored polarizers made from standard polarizer sheets. An oriented array of dye molecules is formed on the sheet. Depending on the dye, the colored polarizer can be made to transmit certain wavelengths when the incident light is of one polarization and to transmit different wavelengths, or none at all,

(continued on next page)

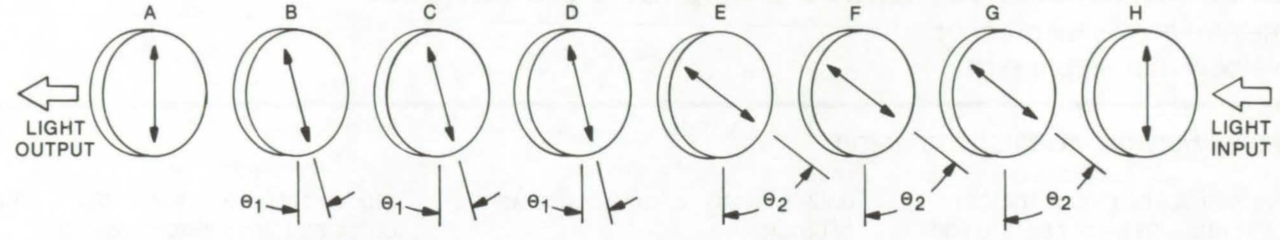

The **Birefringent Optical Filter** consists of elements A through H. Elements A and H are polarizers with their electrical vectors oriented vertically, as depicted by the double-ended arrows. Elements B, C, and D comprise, in combination, a birefringent assembly with a variable rate of light retardation of from about 800 to 1,400 nm. The slow axis is indicated by Θ_1. Elements E, F, and G comprise an identical assembly to B, C, and D except that the slow axis is inclined Θ_2 degrees to vertical. Different values of Θ_1 and Θ_2 result in different transmission functions.

when the incident light is of different polarization. For example, a vertically polarized light may be transmitted as red, while horizontally polarized light may be transmitted as yellow. Such polarizers can be used in combination with conventional polarizers and PLZT plates to form color filters.

The newly proposed filters can be used on sequential-color TV cameras and in color displays. Preliminary studies show that the filters are more convenient and less costly than mechanical color wheels and crystal-based filters.

This work was done by Arthur Miller of RCA Corp. for **Johnson Space Center.** *For further information, Circle 38 on the TSP Request Card.*
MSC-14944

Field-of-View Divider

A relatively-inexpensive mirror system splits the scene of a single camera into three parts.

Lyndon B. Johnson Space Center, Houston, Texas

A cost-effective optical system for use with training simulators presents the trainee with a view as seen from three windows. In an earlier version, the multiple scenes were created by separate imaging systems and scene models for each window. The new system splits the output scene of a single optical probe into three separate parts by using sharp-edged mirrors.

In the original optical system, a high-resolution, color, window view was derived by using a beam splitter to divide the output flux of the optical probe into two parts: one for the color cameras and one for the high-resolution black-and-white luminance vidicon camera. In the improved system, as shown in the illustration, each of the light portions from the beam splitter is further divided into three spatially distinct fields by sharp-edged mirrors.

Mirrors are used in the luminance channel and in the color (chrominance) channel to separate physically three sections of the field-of-view of the single optical probe and to relay these sections to three cameras in each channel. Unlike the beam splitter, the locations of these "field-splitter" mirrors are critical. Ideally, the best place to cut the image into more than one section is at an image plane. The further away from the image plane, the more the field splitter will act like a beam splitter, separating the flux of the beam but not splitting the image.

The mirrors in the luminance channel are placed very close to the central vidicon, and the reflected images are received by identical vidicons positioned orthogonally. The mirrors in the chrominance channel are likewise placed near the central color camera, and the reflected images are relayed by one-power lenses to the outer color cameras, which are physically located side by side because of their larger size compared with the luminance cameras. The principle of field splitting is the same in both the luminance and chrominance channels, though the mirror arrangements are different.

The principle of operation may be understood from the light paths shown for the chrominance channel in the illustration. The entire bundle of light within the angle subtended

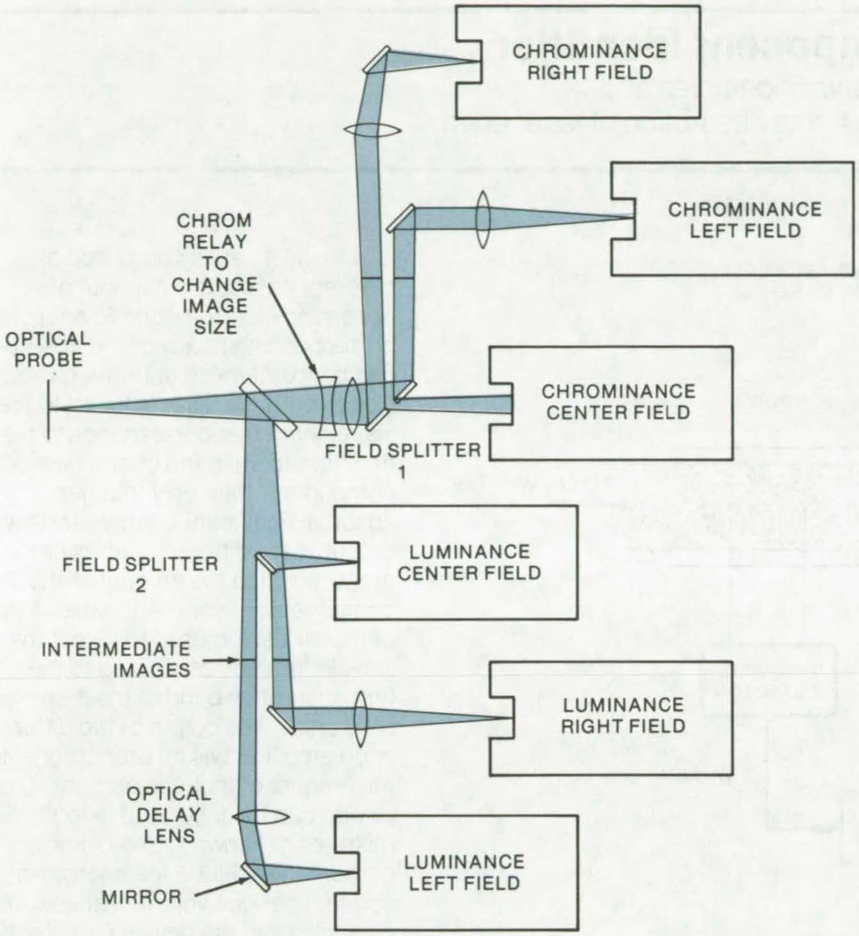

The Multiple-Window Display creates three separate images from a single optical signal by using sharp-edged mirrors as "field splitters." Slightly different mirror arrangements are used for the luminance and chrominance channels because of their different geometries; but the principle of operation is the same for both.

by the gap in field splitter 1 strikes the center-field camera. Likewise, light rays outside of this angle will be reflected off one of the field-splitter mirrors and will enter either of the other two cameras. At certain intermediate field angles the converging light bundle from the optical probe will be only partially reflected by the mirrors, and the rest of the bundle will pass the mirror and impinge on the central camera. Thus, there is an area of overlap of field points on the central and side cameras.

Going out from the center of the field, there will be full illumination on the central camera until a certain angle is reached, where part of the bundle is reflected off a mirror and is imaged on a side camera. Continuing on, there will be a point in the field where none of the light reaches the central camera, and the entire bundle for this and larger field angles will be imaged on the side camera. The area of overlap amounts to about 5° to 10° and is dependent on the distance of the field-splitter mirrors from the camera face.

Most of the overlap region occurs at angles that coincide with window structure, so that the falloff in illumination due to the overlap is not seen. The net effect is a continuous picture for the observer through all three windows. It entirely eliminates the point-by-point replication, alinement, and registration of multiple-model board assemblies.

This work was done by Victor Italiano and Robert E. Klemm of The Singer Co. for **Johnson Space Center.** *No further documentation is available.*

Title to this invention has been waived under the provisions of the National Aeronautics and Space Act [42 U.S.C. 2457(f)] to: The Singer Co., Binghamton, N. Y. 13902.
MSC-16106

Laser-Excited Gas-Component Identifier

Portable, continuous-sampling analyzer identifies and quantifies gas components by measuring absorption of laser energy.

Langley Research Center, Hampton, Virginia

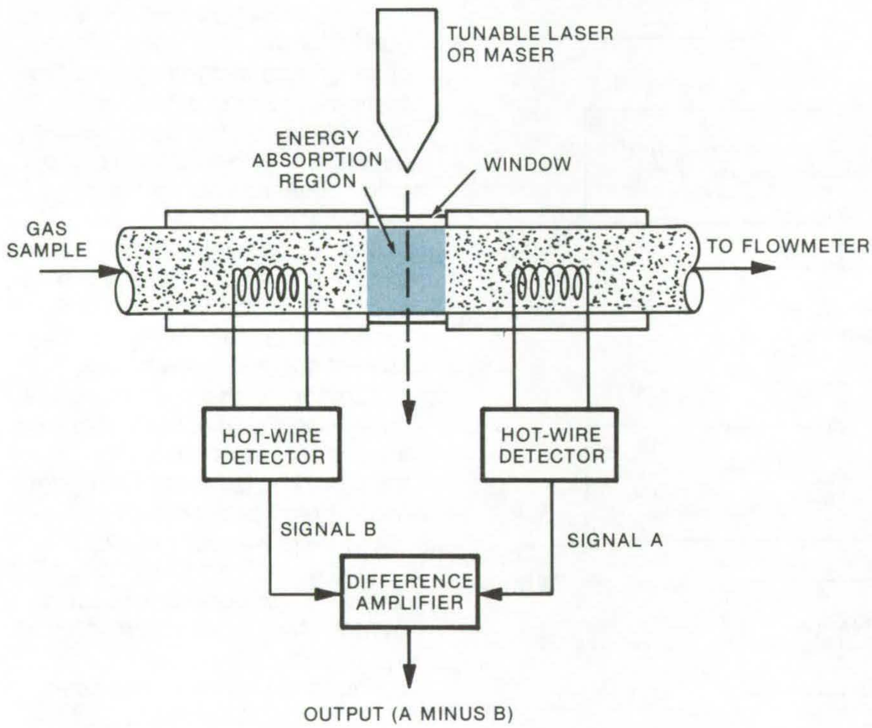

The **Laser-Excited Gas-Component Analyzer** combines some of the features of a conventional absorption spectrometer and a hot-wire aneometer. As a gaseous mixture flows through the sample tube, it absorbs quanta of energy from a tunable laser or maser. Flow rate is known, so the cooling effect on the hot-wire aneometers can be used to calculate the heat absorbed by the gas. By proper selection of the laser wavelength, only one gas component can absorb energy, and the gas volume, flow rate, and heat-absorption rate can be used to find the amount of that component present.

A laser-excited or maser-excited gas-component identifier features portability, continuous analysis, and application limited only by the laser (maser) frequencies obtainable. Prior methods utilizing gas chromatography, mass spectrometry, flame ionization, and so forth, lack some or all of the above features. The laser-excited device is contemplated for use as a gas analyzer and possibly as an explosive or drug detector.

The gas to be analyzed flows through a detector housing and volume flowmeter to a pump or vacuum. The housing contains optical windows to allow a laser beam to traverse the gas channel; it also contains two thermistors, or "hot-wire" detectors, one on either side of the path of the beam. As the gas passes the first detector, its cooling effect on the hot wire determines the output of the detector, which is then fed to the B input of a difference amplifier. Similarly, the output of the second detector is fed to the A input of the difference amplifier. The output from the second detector differs from that of the first because the laser adds energy to the gas. The difference amplifier produces the output (A minus B).

If the test gas is composed of different gases, it is capable of absorbing electromagnetic energy corresponding to any of the absorption bands of these different gases. However, if the laser is tuned to the wavelength that corresponds to the first absorption band of one gaseous component, then only that gas absorbs significant energy, and the output of the difference amplifier is proportional to the amount of the component present. A tunable laser or maser can be used to select the wavelength corresponding to the first absorption band of most any gas of interest. The output of the difference amplifier will be proportional to the amount of that gas present. The device can be calibrated using mixtures of known gases of known percentages. Since the energy absorption per gas volume varies with gas flow rate, the device can also be calibrated against different flow rates.

An alternate configuration of this instrument would have a series of detectors and lasers or masers to simultaneously test several or all gas components in the same sample.

As currently envisioned, the output of the difference amplifier will be compared against calibration charts showing percentage curves of known gases at different flow rates. However, the difference-amplifier output signal and the simple data inputs required lend themselves readily, with the addition of analog-to-digital circuitry, to digitization and automatic readout of the percentages of components in the gas mixture.

This work was done by Renaldo V. Jenkins of **Langley Research Center.** *No further documentation is available.*

Inquiries concerning rights for the commercial use of this invention should be addressed to the Patent Counsel, Langley Research Center [see page A8]. Refer to LAR-12035.

Multiple-Laser-Energy Detection System

Fiber optics attached to output mirrors transmit an optical signal proportional to the output energy.

Langley Research Center, Hampton, Virginia

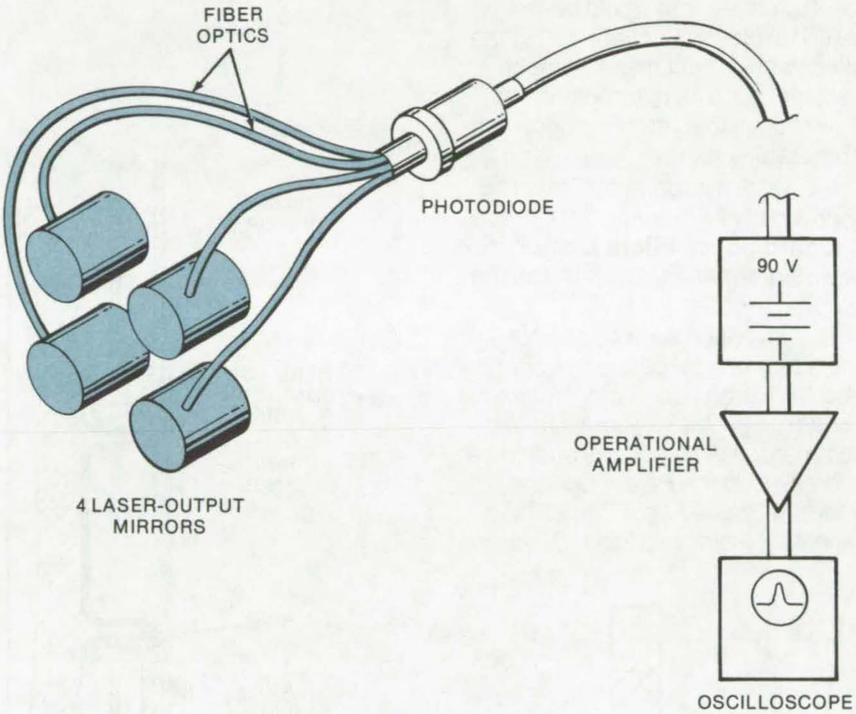

The **Multiple-Laser-Energy Detection System** employs fiber optics as "sensors" on the periphery of the laser-output mirrors. After calibration, the optical energy transmitted through the fibers is used to determine the energy of the lasers.

Development has been completed of a laser-energy detection system used to monitor the energy output of each of four sequentially-pulsed dye lasers for the ALOPE (Airborne LIDAR Oceanographic Probing Experiment) system. The overall goal of the ALOPE system is to remotely determine the density of *chlorophyll a* (the blue-black ester $C_{55}H_{72}MgN_4O_5$) according to the color group of phytoplankton in a body of water. The energy output of the sequentially pulsed lasers is one of the required parameters.

Previously, laser-output energy was determined as a function of the charge on the capacitor powering the laser flashlamp. This method not only lacked the capability of automatically recording the capacitor voltage but introduced error as high as ±10 percent.

In this newly developed system, a piece of fiber optics consisting of four fiber bundles of nominal 3.2-mm diameter was specially fabricated. Each bundle is attached to the perimeter of one of the four sequentially-pulsed laser-output mirrors, and the collected light is transmitted to a photodiode. A 90-V battery pack, connected to the photodiode by BNC cable and located at the console, powers the photodiode. An operational amplifier with a nominal 5-MHz maximum band pass amplifies the signal and acts partially as a filter.

This system was calibrated by firing the laser into a laser-energy meter and comparing the readings with the photodiode output measured by an oscilloscope. A worst-case correlation coefficient of 0.975 was achieved.

High-frequency noise was reduced by using the filtering capability of the operational amplifier and by locating the battery pack away from the diode. This same problem was encountered in development as a result of the proximity of the photodiode to the laser spark gap and flashlamp. It can be reduced by increasing the length of the fiber optics in order to remove the photodiode from the vicinity of the laser.

This system is believed to be the first to use fiber optics to transmit light scattered from the perimeter of a laser-output mirror to a photodiode for the purpose of monitoring the laser output. The fiber-optic coupling scheme and the electronic filtering scheme developed for this application are adaptable for use in other LIDAR systems.

This work was done by Olin Jarrett, Jr., and G. Burton Northam of **Langley Research Center.** *For further information, Circle 39 on the TSP Request Card.*
LAR-12017

Isothermal Optical System

Beryllium mirrors and structural mount reduce thermal stresses and misalinement.

Goddard Space Flight Center, Greenbelt, Maryland

When an optical system is subjected to thermal variations, it can easily lose its alinement. This thermal problem has been solved for a laser system by fabricating both the mirror and the structural mount from the same highly heat-conductive material.

Of the various materials available, beryllium was found to have the best combination of properties (see table). In addition to the selection of a suitable material, the thermal coupling of the parts has been improved to allow better heat conduction. Thus, when temperature varies, the focal distances of the optical elements change in exactly the same way as the spacing of the elements, and there is little optical distortion.

Two examples of the new coupling schemes are shown in the illustration. Materials are made of beryllium, and the mating-surface areas are made as large as possible. In the illustrated joint between a vertical and a horizontal wall section of the mount, a beryllium reinforcing block is used. This block not only improves the strength of the joint but provides an increased area of thermal contact that greatly improves heat transfer at the joint.

A typical mirror mount is also illustrated. A cylindrical flange is cast as an integral part of the back of the mirror. This flange increases the area of the contacting surface, yet it allows the mount to be made adjustable. The flange is held in position by a slipring and a clamp ring that are mounted to the wall of the support structure with a fairly-large contact area.

By making all the optical mounts and structural joints similar to these two examples and by using beryllium as both the optical and structural material, an optical system can be made relatively resistant to thermal gradients. Such a design might be useful with remote-monitoring spectrometers that would be exposed to intense Sunlight during the day or with optical measurement systems, such as pyrometers, that are exposed to a unidirectional high-temperature source.

This work was done by Francis E. Goodwin of Hughes Aircraft Co. for **Goddard Space Flight Center.** *For further information, Circle 40 on the TSP Request Card.*

This invention is owned by NASA, and a patent application has been filed. Inquiries concerning nonexclusive or exclusive license for its commercial development should be addressed to the Patent Counsel, Goddard Space Flight Center [see page A8]. Refer to GSC-12059.

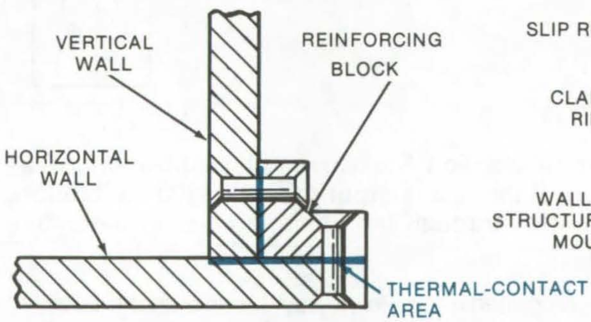

(a) Wall Joint for Structural Frame

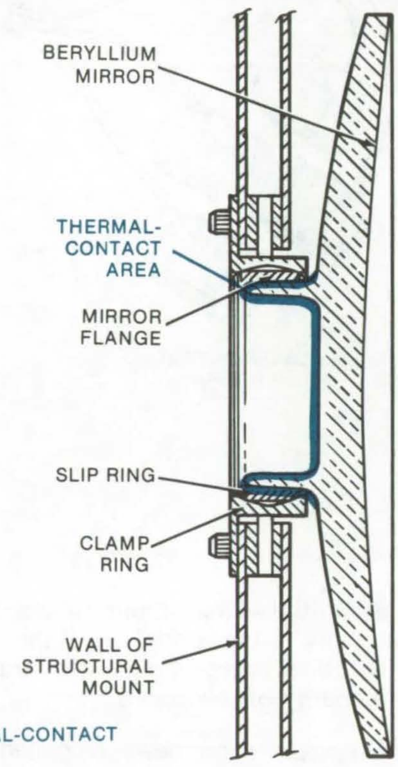

(b) Beryllium Mirror and Mount

The **Two Isothermal Joints** shown above were designed for a laser optics system. All materials are made from beryllium, including the mirror. Heat transfer is improved by the relatively-large surface area of the mating parts.

PROPERTY	BERYLLIUM	ALUMINUM	MAGNESIUM
Modulus (Stiffness)	1	0.245	0.155
Strength	1	0.71	1.14
Thermal Conductivity	1	1.17	0.65
Expansion^{-1}	1	0.48	0.51
Density^{-1}	1	0.68	1.06
Overall Merit	1	0.067	0.067

A **Comparison of Relevant Characteristics** was made for three materials considered as mounts and mirrors for the isothermal laser system. The data above have been normalized about the properties of beryllium, and the overall superiority of beryllium for this application can be seen to be about 15 to 1.

Beam-Splitter for Infrared Detection of Pollutants

Germanium optical elements at proper tilt angles minimize effects of polarization and radiance variations of background scene.

Langley Research Center, Hampton, Virginia

Two of the major causes of erroneous data in the detection of pollutants by remote instruments, such as those in orbiting spacecraft, are polarization and radiance variations in the background scene. Monitoring air pollution from satellites (MAPS) is an optical system designed for measuring pollutants from a space platform, but improvements made in this instrument might be adaptable to other optical monitoring systems. In MAPS, the infrared energy generated by the ground scene and intervening atmosphere is divided into three branches by a three-way beam-splitter that minimizes the dependence on entrance angle to the objective lens. A computer analysis was performed to determine the changes in the relative fractions of energy falling upon the three detectors of the MAPS optical system due to possible polarization and radiance variations of the background scene.

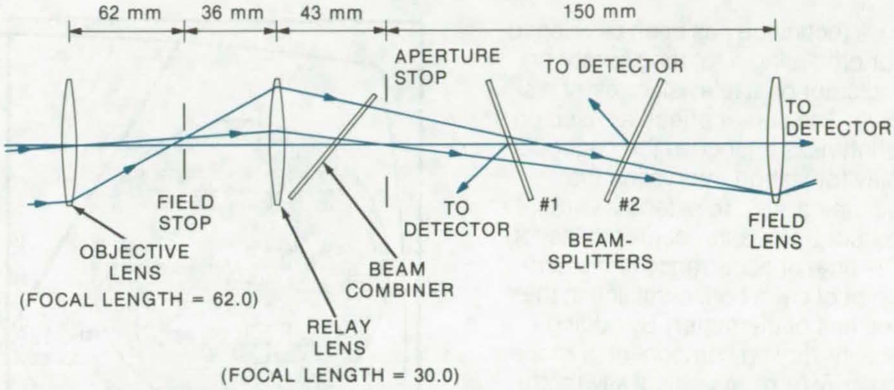

The **Best Optical Arrangement** for a three-way beam-splitter/combiner in a remote pollution-monitoring instrument was determined by computer analysis. As shown above (not to scale), the beam-combiner is tilted -45° to the optical axis, and the beam-splitters are tilted +20° and -25°.

Simple thin lens theory was converted to a computer program, making it possible to trace a bundle of rays at any field angle through the objective and relay lenses of the optical system. The full field view of the MAPS system was divided into 21 equal regions for ray tracing. The square entrance pupil of the optical system, located at the objective lens, was divided into 25 equally spaced squares so that a total of 525 rays passing through the lens represented the energy from the entire object scene. Two different object-plane radiance levels were used in the analysis, with ratios as high as 6:1. For the MAPS application, polarization of the object scene is expected to be nearly zero. For this analysis, values of zero and 2 percent were used.

In addition to the above variations, beam-combiner and beam-splitter tilt angles were varied, and various combinations of materials for the beam-combiner and beam-splitters were used. For example, one case investigated the use of a zinc selenide beam-combiner with germanium beam-splitters, and another case investigated a germanium beam-combiner with zinc selenide beam-splitters. The germanium objective and relay lenses, as well as the germanium beam-combiner, were considered to have antireflection coatings, allowing 100 percent incident-light transmittal. The germanium beam-splitters were considered to have antireflection coatings on the back surfaces, resulting in zero internal reflection. All zinc selenide elements were considered to have no antireflection coatings.

The best optical configuration determined by this analysis is shown in the diagram. The beam-combiner is tilted at -45°, while beam-splitters 1 and 2 are tilted at +20° and -25°, respectively. This baseline configuration contains all germanium elements.

Results indicated that this scheme has an advantage over conventional infrared beam-splitters in that the energy-division ratio is less dependent on the angle of incidence of the entrance beam. The change in energy distribution on the three detectors due to the 2 percent polarization of the object scene was calculated to be less than 0.1 percent. The change in energy distribution on the three detectors due to dividing the object scene into two different intensities was less than 0.006 percent, even in the presence of a 6:1 ratio of object-plane radiance levels.

This work was done by Wayne A. Massey of TRW, Inc., for **Langley Research Center.** *For further information, Circle 41 on the TSP Request Card.*

Inquiries concerning rights for the commercial use of this invention should be addressed to the Patent Counsel, Langley Research Center [see page A8]. Refer to LAR-12073.

Rotating-Vector TV Cursor

The indicator can be used as a wiping signal to cover an adjustable 0°-to-360° arc of the TV raster.

Lyndon B. Johnson Space Center, Houston, Texas

A technique has been developed for producing a rotating cursor or indicator on a television raster display. The cursor effect is based on a brightness change in the raster display for a short interval on the scanning line. To extend a vertical cursor from raster center to the top, the time of occurrence is the midpoint of each horizontal line in the top half of the raster. By adding a slowly varying component of proper polarity (e.g., a vertical sawtooth), the time of occurrence per line is made earlier (or later) at the top of the raster and then returns to normal mid-raster timing.

Three representative timing waveforms, shown in the figure as A, B, and C, are used to generate a vertical cursor. Horizontal sawtooth signals of period H are used to trigger a pulse at a level corresponding to the center of the negative-going waveform. Each time a negative-going horizontal sawtooth reaches this level (at raster center), a narrow pulse is generated. It may be added to the video information fed to the display, with appropriate polarity, to generate a white dot on each scanning line. The total of these dots, one for each raster scan line, comprises a vertical scan line in the display.

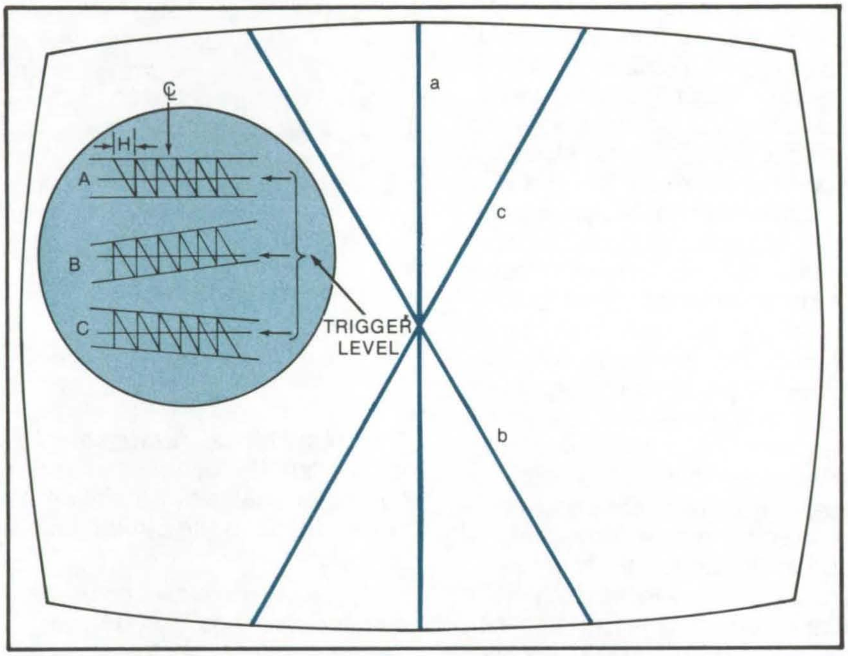

Cursor-Generating Timing Waveforms, left above, are shown with their respective raster indicators. The cursor is used in one application to generate a TV alinement reference to assist remotely-controlled payload operations. Slightly modified, the cursor can be used as a special-effects-generated wiping signal to cover (or uncover) an adjustable 360° arc of the TV raster.

Rotating vectors a, b, and c, corresponding to their respective waveforms, are shown on a TV raster. The vertical cursor (b) has rotated counterclockwise relative to the position of vector a. Vector c is the result of an opposite-polarity additive component that results in later firing for scan lines above center. The cursor thus rotates clockwise. An interruption in the triggering process for scan lines after the center results in the cursor appearing as a vector extending from the raster center toward the top edge. To maintain cursor rotation, the vector-generating device used must pass the cursor through the horizontal and continue smoothly through all remaining quadrants of the raster.

A single-turn motor-driven potentiometer may be used to implement this rotation. The potentiometer is grounded at the 0° (reference) and 180° points. A triangular waveform of opposite polarity is impressed at the 90° and 270° points. The waveform repetition rate is the TV field rate, with the peak occurring at raster center.

Voltage picked off by the wiper is added to the horizontal sawtooth. The firing level, advanced at the top of the raster, is retarded linearly so that the cursor passes through the center.

For raster lines below center, the firing time advances; the raster lower half is a mirror image of the top half. For a single vector to appear, the raster lower half is blanked until the potentiometer passes through the maximum value, after which the top half is blanked. Then the vector appears only in the raster third quadrant and continues to rotate counterclockwise as the potentiometer reaches the vertical position at the lower (180°) point. Blanking is switched from the top to the bottom half of the raster as the potentiometer passes through 270° of arc, allowing the vector to pass through the final quadrant.

This work was done by Larry A. Freedman and Marvin Kravitz of RCA Corp. for **Johnson Space Center.** *For further information, Circle 42 on the TSP Request Card. MSC-16119*

Closed-Cycle Refrigerator for Masers

Reducing maser temperature from 4.5 to 3.0 K increases gain from 45 to 72 dB.

Caltech/JPL, Pasadena, California

In radio astronomy 4.5-K closed-cycle helium refrigerators (CCR's) are used to cool a maser operating at the S, X, and K_u bands. The performance of the maser can be substantially improved by reducing its temperature from 4.5 to 3.0 K. An X-band maser, for instance, operating at 4.5 K has a 45-dB net gain and a theoretical noise temperature of 3.5 K. When cooled to 3.0 K, net gain increases to 72 dB, while maser noise temperature is reduced to 2.0 K.

A 200-mW-capacity CCR progressively cools the helium at 70-K, 15-K, and 4.5-K stations. The refrigerator, as shown, includes a station for cooling the maser magnet pole pieces and portions of waveguides to 4.5 K, except the amplifier which is cooled to 3.0 K. Apparatus utilized for 3.0-K cooling includes a pressure regulator, heat exchangers, an expansion valve, and a vacuum pump.

The parts added for additional chilling capacity were used to modify a conventional CCR. Improved performance is thus gained at a relatively small increase in cost.

This work was done by Ervin R. Wiebe of **Caltech/JPL.** *For further information, Circle 43 on the TSP Request Card.*

This invention is owned by NASA, and a patent application has been filed. Inquiries concerning nonexclusive or exclusive license for its commercial development should be addressed to the Patent Counsel, NASA Resident Legal Office-JPL [see page A8]. Refer to NPO-13839.

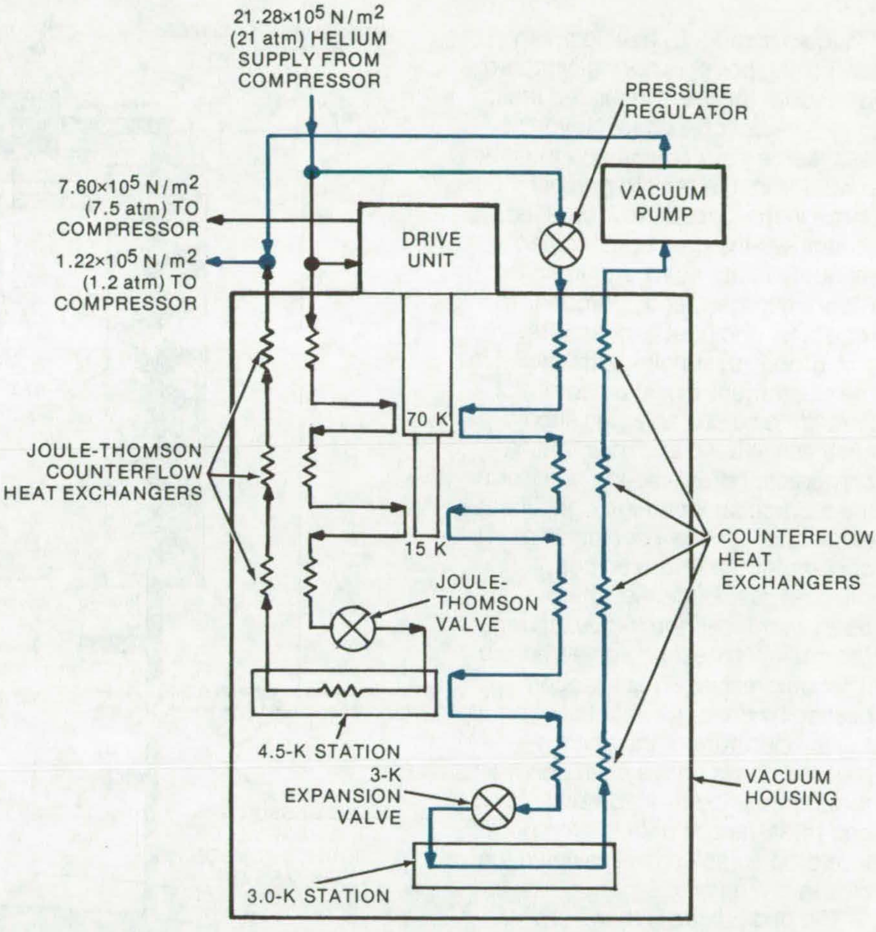

The **Combined 4.5-K and 3.0-K CCR System:** Compressed helium gas is supplied by (and returned to) a CCR compressor. A pressure regulator reduces the supply to 3 atmospheres for use in the 3-K portion of the system. Helium gas is cooled by the 70-K, 15-K, and 4.5-K stations and liquefies at about 5 K. The liquid experiences a partial vacuum in the 3-K station after passing through the expansion valve. The temperature of the boiling liquid in the 3-K station is determined by the absolute pressure at the station. Counterflow heat exchangers permit helium cooling to the 3.0-K station, with a minimum of heat delivered to the other stations. Gas flow through the 3-K system is about 8 standard liters per minute. A mechanical vacuum pump easily handles this gas flow.

Liquid-Hydrogen Boiloff Reliquifier

Pressure-relief cooling and
Joule-Thomson expansion simplify system.

John F. Kennedy Space Center, Florida

Liquid hydrogen, having a very low boiling point, is normally stored in vacuum-jacketed insulated tanks to reduce boiloff losses. Nevertheless, some gas boils off and must be vented from the tank to prevent damage from pressure increases. To recover the gas, complicated reliquefiers are used, requiring Freon, nitrogen, and hydrogen refrigerants and heat exchangers.

A proposed simpler unit, shown in the illustration, would be compact enough to be portable and should cost less to build and maintain. A compressor draws boiloff gas from the storage tank and through a heat exchanger. There it serves as a coolant for the returning compressed gas. Because it has been warmed in the heat exchanger, the gas must next be cooled before it is compressed. This is accomplished by pressure-relief cooling. If the temperature of the uncompressed gas is above a set point, a temperature-controlled valve opens and releases gas until the temperature drop sufficiently. The valve then closes.

The cooled gas is then compressed to approximately 600 psig (4.2×10^6 N/m^2) and passes through the tubes in the heat exchanger, where it is cooled to approximately 35 K by gas leaving the liquid-hydrogen tank. The cooled and compressed gas is finally expanded at constant enthalpy through a pressure-controlled Joule-Thomson valve. The valve opens at approximately 600 psi and closes at about 575 psi (4.2×10^6 and 3.9×10^6 N/m^2). The pressure and temperature of the hydrogen must be kept in the supercritical region in order for the constant-enthalpy expansion to liquefy a portion of the gas. About two-thirds of the hydrogen will be liquefied, and the remaining unliquefied portion mixes with the boiloff gas and is drawn through the heat exchanger to repeat the cycle.

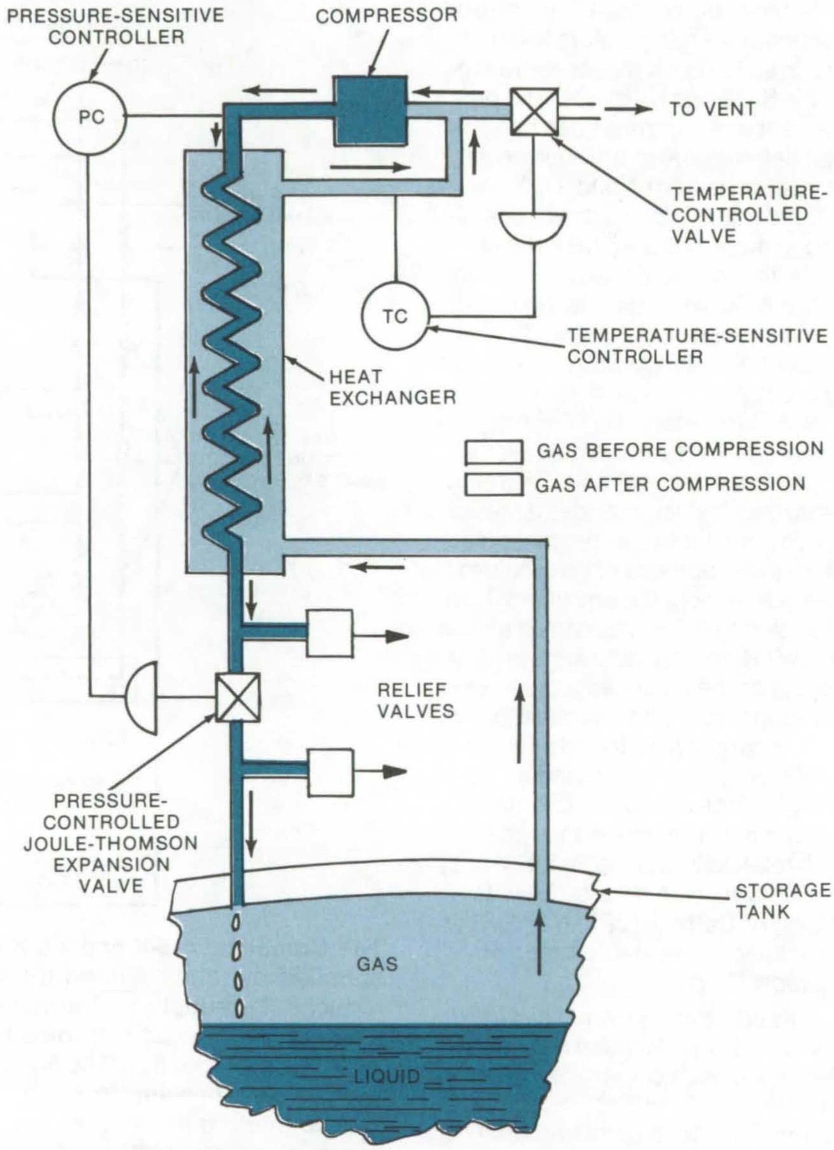

The **Cryogenic Boiloff Reliquefier** uses Joule-Thomson expansion of compressed and cooled boiloff hydrogen to condense a portion of the gas. The system could also be used with other cryogens, such as liquid helium, nitrogen, and oxygen.

This work was done by Frank S. Howard of **Kennedy Space Center.** *No further documentation is available.*
KSC-11021

Simplified Sensing for Cloud Chamber

Electromagnetic delay line greatly simplifies electronics for sensing particle-trajectory data.

Lyndon B. Johnson Space Center, Houston, Texas

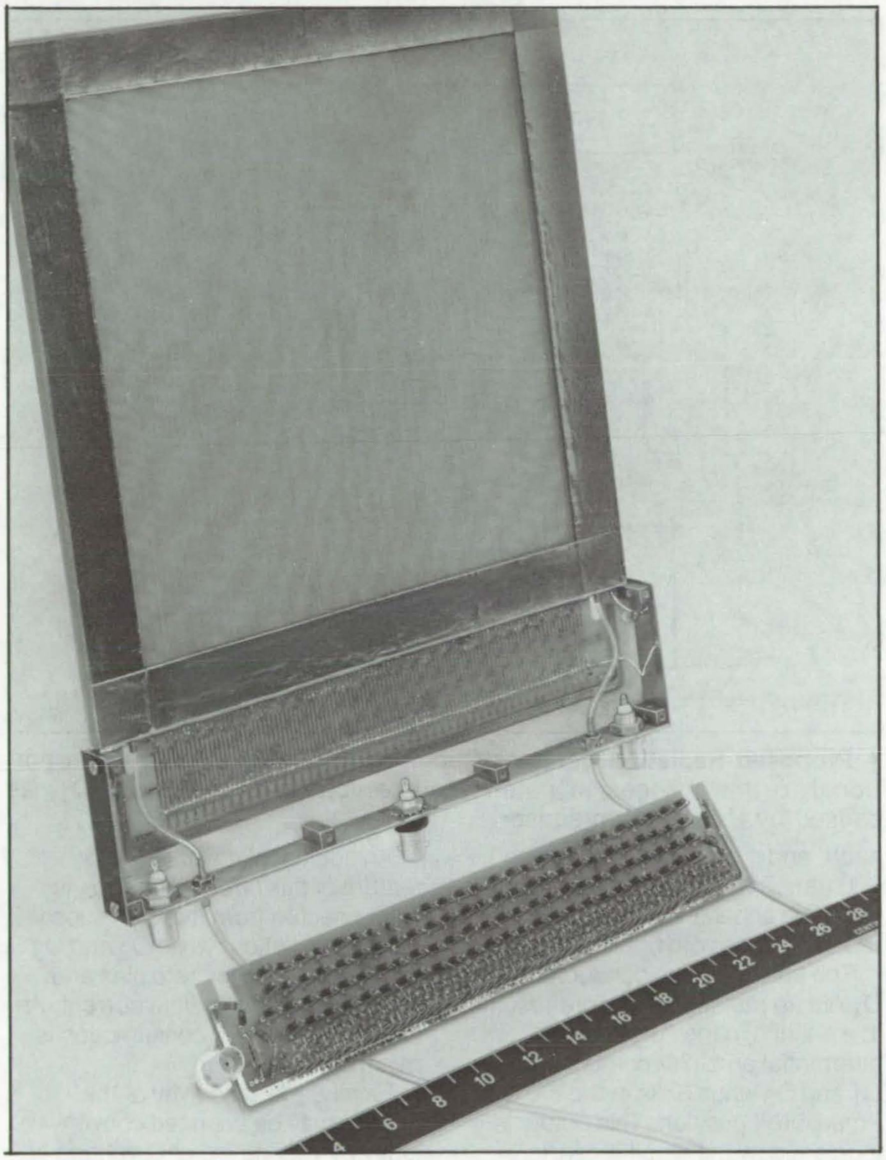

Anode Plane and Delay Line combination is expected to give 100-micron resolutions of the trajectories of elementary particles, cosmic rays, and X-rays.

The key characteristic in determining the energy of elementary particles, cosmic rays, and X-rays is their trajectory. As a particle moves through a gas-filled chamber (cloud chamber), it ionizes some of the atoms or molecules along its path. To calculate the path of the particle, the ionization must be detected and analyzed.

Large-area multiwire proportional chambers have been used for this purpose since about 1968. In this technique thin wires are strung side by side to form planes, and a number of planes are placed at right angles to each other. Voltage is applied to the wires, and when a passing particle creates local ionization, nearby wires are affected and currents can flow. These signals in turn are the raw data from which the path and energy of the particle are calculated. In some chambers as many as 50,000 wire may be used.

In early verions of proportional chambers, each wire was connected to its own amplifier. Time sharing was used in later models, but even then the amount of support electronics was large. For measurements in space or in balloons sent into the atmosphere, reductions in size, weight, and complexity were desired.

In the simplified chamber shown in the photo, an electromagnetic delay is used to collect the signals from the wires. Instead of attaching an amplifier to each wire in the plane, a lumped-element delay line is used. The resulting voltage impulses created by a passing particle are effectively integrated in such a fashion that relatively-simple electronic circuits can calculate the spatial position of the particle. The calculation takes into account the rise time and impedance of the delay line, the amplitude of the signal, circuit noise, and the jitter of the constant fraction discriminator.

This work was done by Alan J. Eskovitz and Arpad G. Pallai of TRW, Inc., for **Johnson Space Center.** *Further information may be found in NASA CR-128899 [N73-22210], "Multiwire Proportional Chamber Development," $5.50, a copy of which may be purchased [prepayment required] from the National Technical Information Service, Springfield, Virginia 22151.*
MSC-14708

Differential Multi-MOSFET Nuclear Radiation Sensor

Proposed circuit could allow improved
sensitivity and stability with MOSFET sensors.

Lyndon B. Johnson Space Center, Houston, Texas

A proposed circuit could substantially increase the effectiveness of the metal-oxide-semiconductor field-effect transistor (MOSFET) as a nuclear radiation detector. With the new arrangement, it should be possible to measure radiation doses as low as 10^{-3} rad; and other advantages, such as the minimization of thermal-drift errors, low power consumption, and operation over a wide dynamic range, may be realized.

Radiation bombardment is known to affect the MOSFET by generating a concentration of electron/hole pairs in the oxide layer. If a gate-to-source bias is applied simultaneously, the electrons are drawn off into the external circuit, while the less mobile holes remain trapped in the oxide. The holes, which can remain permanently trapped for periods of several months, set up image charges in the substrate which change the conductance and turn-on voltage of the transistor. While this can often be a problem for circuits employed in radiation environments, it is also possible to make use of this effect in determining doses of radiation by measuring these changes in the MOSFET's characteristics. Circuits to accomplish this have been used in the past, and the new design, shown in the figure, represents an improvement over these in a number of aspects.

Under irradiation, MOSFET's Q_1, Q_2, and Q_3 are all exposed. However, the switch settings are such that Q_2 and Q_3 are zero biased while Q_1 is biased negatively by virtue of battery B_1. Since the effects of radiation are two or three orders of magnitude greater under negative bias, only Q_1 effectively builds up a radiation dose. The devices Q_1, Q_2, and Q_3 are each actually multiple transistors connected in parallel, all contained in the same large-scale integrated (LSI) package. The multiplicity increases the effective conductance (g_m) of each, and it is estimated that with 200 transistors in parallel, the circuit would be capable of measuring radiation doses of 10^{-3} rad.

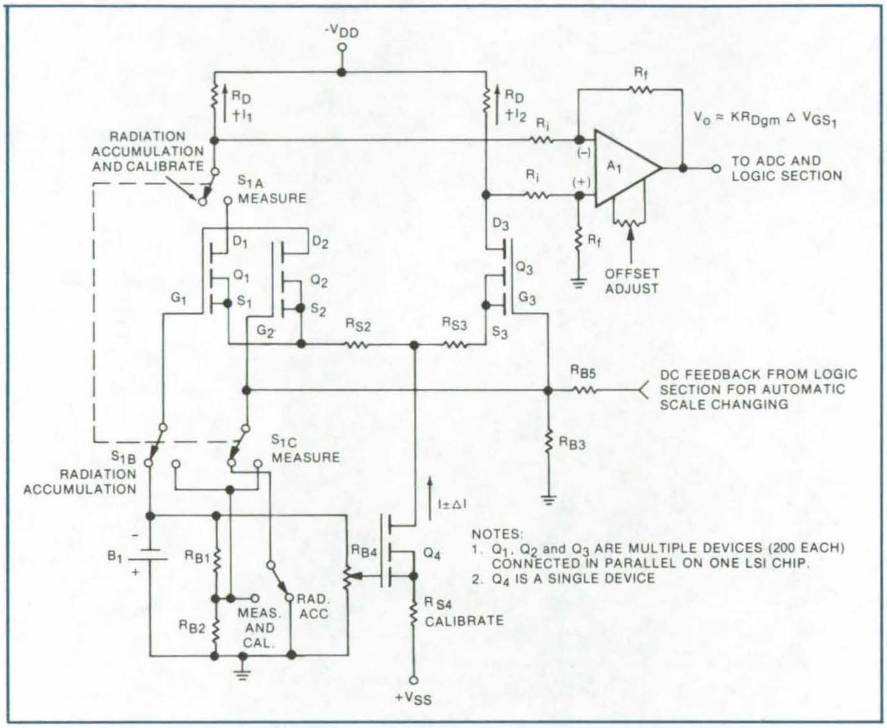

A **Proposed Radiation-Detector Circuit** would have an output proportional to the changes in gate-to-source voltage of transistor Q_1, as caused by the radiation sensor.

The change in the conductance of Q_1 due to radiation exposure results in a change in the output of the differential amplifier composed of Q_1 and Q_3 when S_1 is in the "measure" position. This output is increased by the amplifier A_1 to generate the signal V_0. This may be related back to the unknown dosage once the system has been calibrated against a known radiation source. The output V_o could also be fed through an analog-to-digital converter and appropriate logic to drive a digital display. The inherent stability of the differential amplifier contained in a single LSI package represents an improvement over previous measuring systems which had no built-in compensation for drifts due to time and temperature.

An additional advantageous feature of this circuit is that Q_1 is disconnected from the V_{DD} supply during irradiation, while Q_2 and Q_3 are operated under zero bias and therefore draw very little current. As a result, the power consumption is minimal.

Finally, the sensitivity of the system may be changed conveniently by varying the gate voltage of the differential amplifier, thereby adjusting its operating point. Overall, five decades of dynamic range (10^{-3} to 10^2 rad) may be realized with a single circuit bias configuration, and an expansion seven decades (to 10^4rad) can be achieved if the bias configuration is altered.

This work was done by Wilson A. De Oliveira of **Johnson Space Center.** *No further documentation is available.*
MSC-14444

Spectrally-Balanced Chromatic Approach-Lighting System

Red and blue light combinations enhance pilots' depth perception during landing approaches.

Ames Research Center, Moffett Field, California

Rows of red lights are ordinarily used at airports to define the boundaries of runway landing approaches. However, these lights have been known to cause errors in estimating altitude and distance on the part of pilots attempting nighttime landings. The reason for this is that the natural chromatic aberration of the human eye makes red-colored objects appear closer to the observer than they actually are, causing the pilot to perceive his orientation to the runway incorrectly. However, a new approach lighting system employing combinations of red and blue lights has been designed, which substantially reduces this problem. The system exploits the inherent chromatic aberration of the eye to create a three-dimensional effect that gives a pilot valuable visual cues concerning his position with respect to the runway.

Referring to the accompanying figure, it can be seen that when red lights are used alone, the effects of chromatic aberration are such that the runway appears inclined at an angle to its true orientation. As a result of this illusion, the pilot may believe that he is coming in too high or that the nose of the plane is pitched up, and he may be led to take erroneous corrective measures that could result in a landing short of the runway.

In a simple form of the proposed system, each red light would be replaced by adjacent red and blue lights acting as a bicolored point source. The red lights would still appear above their actual positions while the blue lights would be only slightly displaced, as the effects of chromatic aberration are much smaller at the blue end of the visible spectrum. It can be seen that in this case, the pilot is presented with a three-dimensional array, which gives him added visual cues concerning his position above the runway approach. In experiments under simulated night-flying conditions, it was found that pilots performed substantially better in approach maneuvers when the combination of red and blue lights was used compared to using red lights only or blue lights only.

This system also gives greater visibility than red lights alone when used in fog or poor weather, since there is greater scattering of the blue radiations by the water droplets which contributes toward a greater penetration thru the fog, while the red light is more readily absorbed. If it is desired to eliminate the red light entirely in certain installations, green and blue combinations may be substituted. These give an almost equivalent three-dimensional effect at some sacrifice of chromatic spectral separation.

Specific recommendations have been proposed for incorporating red and blue combinations into existing American and European approach-lighting systems, along with a plan for approach lighting around short-takeoff and landing (STOL) ports. There are also potential applications beyond airport use to other situations where accurate perception of distances is necessary. Suggestions have included automobile and boat collision-warning systems, spacecraft docking lights, and warning lights on stationary obstacles.

This work was done by Wendell D. Chase of **Ames Research Center.** *For further information, Circle 44 on the TSP Request Card.*

This invention is owned by NASA, and a patent application has been filed. Inquiries concerning nonexclusive or exclusive license for its commercial development should be addressed to the Patent Counsel, Ames Research Center [see page A8] Refer to ARC-10990.

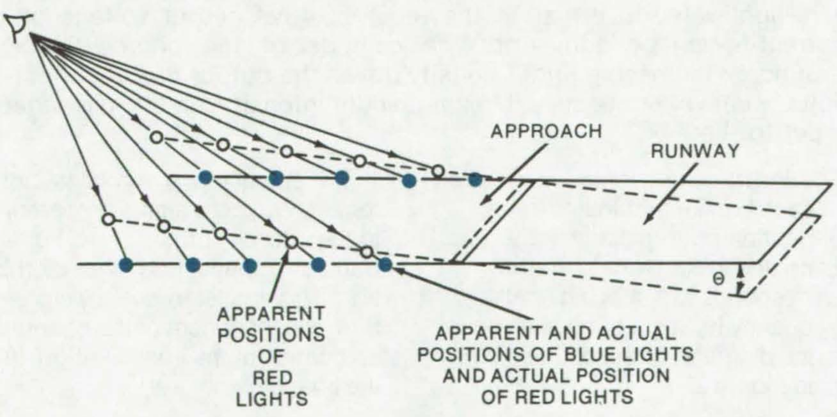

Lighting on Aircraft Runways can cause color-based optical illusions that make the pilot perceive the runway plane incorrectly. When red lights are used alone, they appear displaced. When red and blue pairs are used, the red lights still appear displaced, but the blue lights appear nearer their true positions.

Hybrid Optical/Digital Detector

Optical diffraction patterns of photographs are sampled in real time, using an optical Fourier-transform detector.

Marshall Space Flight Center, Alabama

A hybrid optical/digital Fourier-transform detector for automatic diffraction-pattern recognition is designed around a concentric-ring fiber-optic array. In this system, coherent light passes through the film-image transparency and then through a lens that optically produces the Fourier transform of the image. By using a special optical detector array, the optical transform is converted to digital data that is the basis of a diffraction-pattern recognition program performed in a computer.

The optical detector is an array of approximately 89,000 optical fibers of 3-mil (0.007-cm) diameter. The fibers are sorted into 168 concentric rings about a single fiber. One end of all the fibers in each ring is collected in a bundle and is terminated into a photodetector. The termination is made by bonding one end of the bundles in 169 holes laid out as a rectangular matrix in a mounting plate. An identical plate with photodiodes in the holes is then mated to the bundle-mounting plate.

An optical/digital interface, consisting of a high-speed multiplexer and analog-to-digital converter, samples the outputs of the photodetector/operational-amplifier pairs placed at the end of each ring of the fiber-optic array. Two pairs of photodetector/operational-amplifier interface circuits are shown in Figure 1.

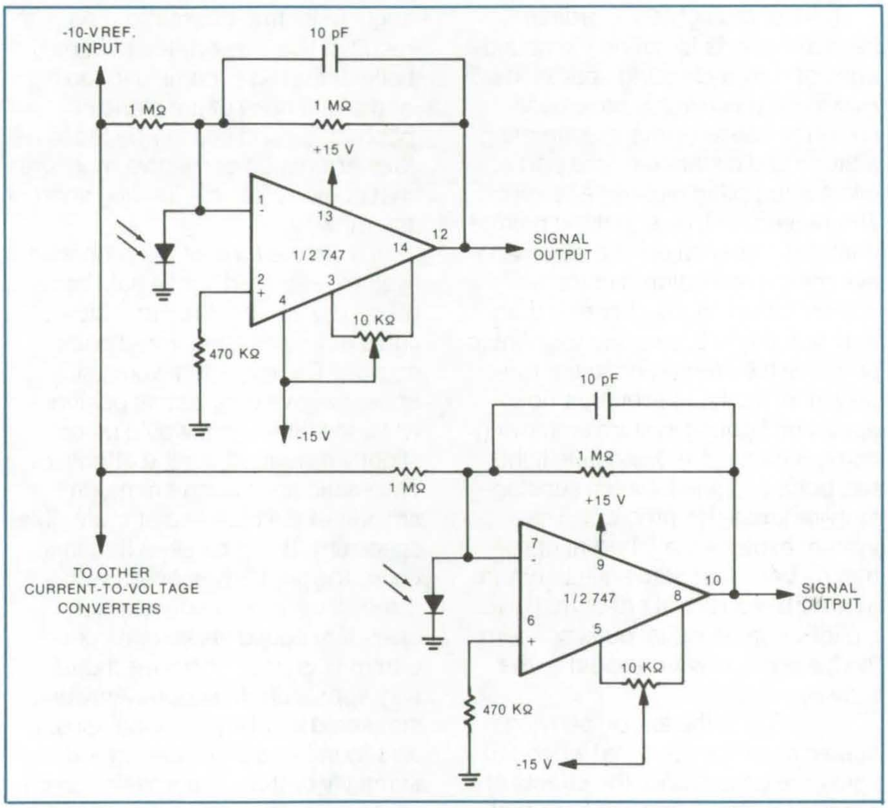

Figure 1. In the **Hybrid Optical/Digital Detector,** 2 of the 169 current-to-voltage converters are shown. To use the full range of the converter, the zero-light value is offset to the most positive output voltage of the current-to-voltage converter. The cathode of the photodetector is grounded; increasing light intensity drives the output of the current-to-voltage converter negative. Maximum light intensity results in a negative input to the ADC.

The fiber bundles are oriented with the axes of each fiber coincident with the optical axis of the Fourier-transform lens. The ring end of each bundle terminates in the diffraction-pattern plane of the lens. Each ring in the plane therefore corresponds to a specific spatial frequency having a bandwidth equal to the diameter of the optical fiber (see Figure 2).

The output of the photodetector for each ring is a signal proportional to the intensity profile of the Fourier-transform spatial frequency distribution. This spatial frequency signature is independent of the orientation or location of the image feature in the image plane.

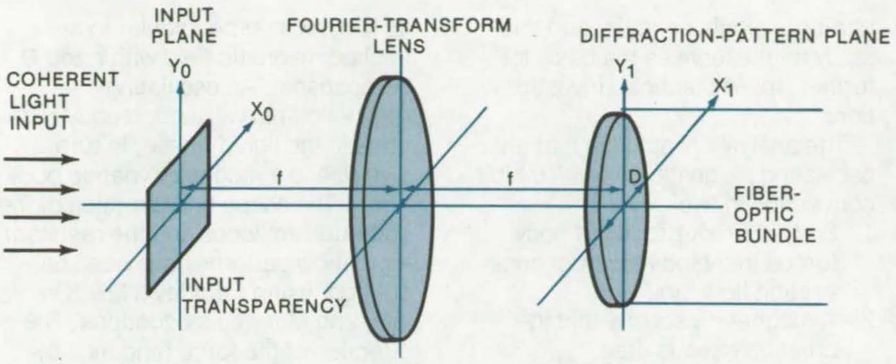

Figure 2. The geometry of the **Fourier-Transform Processors,** as shown above: The separation of adjacent maximums of a Fourier-transform diffraction pattern corresponding to an object feature of dimension ΔX_0 is approximately $\Delta X_1 = \lambda\ f/\Delta X_0$, where λ is the optical wavelength and f is the focal length of the Fourier-transform lens. The optical processor uses an argon-ion laser source operating on the 488-nm transition and a Fourier-transform lens of 59.89-cm focal length. Setting ΔX_1 equal to the radius of the fiber-optic bundle [0.5 in. (1.2 cm)], the smallest feature that results in at least one secondary maximum falling on the fiber-optic array is 0.023 mm.

The optical/electronic interface consists of 169 photodiodes, each connected to its own current-to-voltage converter. The converter outputs are fed to an analog-to-digital interface subsystem that includes six multiplexers (up to 32 inputs each), sample-and-hold amplifiers, and an analog-to-digital converter. The next stage in the electronics is a computer that provides sampling and timing control, performs the actual pattern analysis, and controls oscilloscope and teletypewriter outputs.

This work was done by R. G. Shackelford and J. R. Walsh, Jr., of Georgia Institute of Technology for **Marshall Space Flight Center.** *For further information, including algorithms and software for pattern recognition, Circle 45 on the TSP Request Card.*
MFS-23439

Books and Reports

These reports, studies, and handbooks are available from NASA as Technical Support Packages (TSP's) when a Request Card number is cited; otherwise they are available from one of NASA's Industrial Application Centers or the National Technical Information Service.

Fresnel-Lens Solar-Energy Concentrator

Theoretical and experimental evaluations are described.

An analytical and experimental evaluation of a plastic Fresnel lens has produced lens and concentrator data that help to improve collector performance. In addition, the methodology described in the report will be useful to the designers of other Fresnel-lens solar concentrators.

A grooves-down planocylindrical collector lens of compression-molded optical-grade methyl methacrylate was the test subject. The lens was 22 by 15 in. (56 by 38 cm) in size and had a groove density of 34.5 per in. (13.6 per cm), a center thickness of 0.171 in. (0.434 cm), an F number of 1.0, and a design wavelenght of 5,893 Å.

In the analytical study, Snell's law and Fresnel formulas were used to determine the groove angle and the total fraction of incident Sunlight transmitted through the lens. The concentrated solar energy at a position beneath the lens was calculated by summing the intensity contributions from each serration and for each wavelength interval of the solar spectrum. A computer program was then used to develop performance data for the Fresnel lens under study. These data included lens-transmission and focal-plane-intensity profiles for various wavelengths and amounts of defocusing.

The experimental evaluation was conducted by using natural Sunlight reflected from a tracking heliostat to maintain a constant angle of radiation incidence. Tests were conducted at Marshall Space Flight Center in Alabama from 10 a.m. to 2 p.m. on cloudless days to minimize variations in incident flux intensity.

As a result of these studies, several conclusions were drawn. The analytical baseline profile indicated that the refraction of wavelengths far removed from the design wavelength is the primary factor determining the image width.

A baseline peak concentration of 57 and a 90-percent target width of 1.4 cm were calculated for the 56-cm lens. The measured concentration and target width were 47 and 3.6 cm, respectively. Spreading at the experimental profile base resulted in a lower concentration and an increased image width relative to the analytical baseline.

Manufacturing modifications satisfactorily corrected the profile-spreading difficulty. Preliminary testing with a second-generation lens indicated a marked reduction in profile spreading.

The sensitivity of image properties to small transverse tracking errors (<1°) was low. The primary effect was the lateral shift of the profile and a corresponding increase in interception target width. The reduction

(continued on next page)

of peak concentration ratio and increased profile skewness occurred for greater misalinement.

For deviations of 5° or less, longitudinal orientation effects on lens performance were insignificant.

High lens transmittance was computed (87 percent) and measured (85 percent) and was not significantly affected within the range of tracking errors evaluated.

Slight defocusing can result in more desirable profile characteristics from a thermal design standpoint; i.e., equal energy interception can occur with decreased thermal gradients.

This work was done by Steve L. Allums and Leon J. Hastings of **Marshall Space Flight Center** *and Ronald M. Cosby of Ball State University. To learn how to obtain a copy of the report, Circle 46 on the TSP Request Card.*
MFS-23575

Effects of Oscillating Magnetic Fields on Liquids

Gravity-induced convection may be inhibited in molten crystals.

A theoretical study suggests that gravity-driven convection in crystal melts and other dense liquids could be reduced by the application of oscillating magnetic fields. Such convection is responsible for imperfections during the production of ultrapure single crystals, and this study might serve as the basis for further, more practical, investigations.

The analysis concludes that an oscillating magnetic field will inhibit convection in two ways:
1. Eddy-current-produced body forces that tend to disrupt convection flow, and
2. A magnetic viscosity that increases viscous drag.

The model for the study was a liquid-filled cylindrical container with

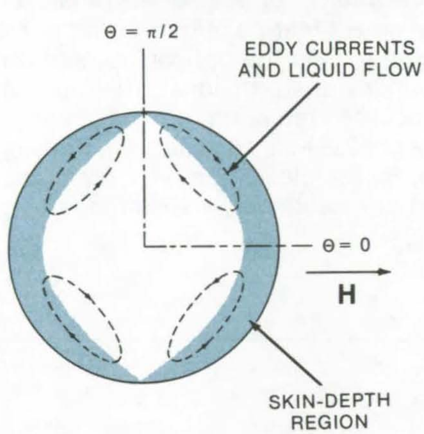

Skin Depth and Liquid Flow can be seen in this top view of a hypothetical liquid-filled cylinder. The color region shows the variation of skin depth with Θ.

its long axis perpendicular to an applied magnetic field with $\hat{r}$ and $\hat{\Theta}$ components. An oscillating magnetic field will induce eddy currents in the liquid; these, in turn, give rise to a magnetodynamic body force. The shape and direction of the eddy-current loops and the resultant liquid-flow patterns have been calculated, using Faraday's law, Ohm's law, and Maxwell's equations. The direction of the force (and thus the direction of liquid flow in the absence of any other forces) will be perpendicular to the direction of the magnetic field and in the $\hat{r}$-$\hat{\Theta}$ plane. The skin depth will vary as shown in the figure.

A second analysis, using Maxwell's equations and the Navier-Stokes equation, indicates that the oscillating field will induce drag in the liquid. This effect can be interpreted as a magnetic viscosity that increases viscous drag through the liquid and rapidly decays all motion transverse to the field lines.

This work was done by Ronald I. Miller of The Boeing Aerospace Co. for **Marshall Space Flight Center.** *To learn how to obtain further information, Circle 47 on the TSP Request Card.*
MFS-15235

Computer Programs

These programs may be obtained at very reasonable cost from COSMIC, a facility sponsored by NASA to make new programs available to the public. For information on program price, size, and availability, circle the reference letter on the COSMIC Request Card in this issue.

Stray Optical-Radiation Suppression

Five programs for the study of scattered radiation

The first of five basic programs for the study of stray-radiation suppression is the only one that does not create or depend on any external files. The remaining four are written to be run separately but sequentially as one job train, each creating files for the succeeding programs.

Program one looks out from a point in the image plane and determines which objects are seen from that point. These are the sources of scattered radiation reaching that point in the image plane. This program, along with the remaining programs, can handle only rotationally symmetric objects. Program one computes those surfaces that are seen and the angles at which they are seen in real space. Any such surface is divided into five segments; the position and angle of each segment is printed out. This initial program helps one to see quickly any major flaws in the design

(from a scattered-radiation standpoint), and it will reduce the amount of calculations needed to be executed by the succeeding programs.

Program two is similar to program one; both use the same data deck input, and both lay out the imaged space as seen from the image plane. Program two, however, does not calculate what segments are seen or any angular information; instead, it lays out the image space as seen from object space. That is, "Looking into the first imaging aperture, what do the imaged spaces look like?" This is necessary to determine to what sections the radiation can scatter. This is also done for the space between the primary and secondary, which turns out to be a partial combination of the other two cases. Although this may appear redundant in the case of two-mirror systems, it may not be so for other systems. The output is plotted for each space so that one may see how and where real space objects are imaged or reimaged. The printout gives numerical data about the imaged objects. These include distances, heights, y-$\bar{y}$ values, and any objects with images that pass through infinity. It creates an important file (BASICA) that is necessary for the succeeding programs.

Program three attaches most of the information it needs from BASICA. It will take any object from program two and treat it as a source of radiation to any other object, including imaged objects. The data input at this stage can be as simple as two numbers — source object number and collector object number. This program creates four important files: (1) the geometrical percentage of power transferred from each segment of the sources to each segment of the collectors (BDRDF), (2) the angle out of the source (ANGOUT), (3) the angle into the collector (ANGIN), and (4) more information is added to BASICA.

Program four loads the Sun shield with power. Any section on the object can be described with a specified amount of power. When loading of the source object is complete, the program processes the data and creates tape two for use by program five.

Program five is the driver program for determining the scattered-radiation levels throughout the system. The amount of power reaching the image plane from scattered radiation is printed out so that major contributing surfaces can be determined along with how much power is received from each section. It requires the following files: (1) BDRDF, ANGIN, and ANGOUT from program three, (2) BASICA from programs two and three, and (3) the input file. The input to this part of the program can be large. The program considers only those radiation paths that contribute scattered radiation to the image plane for the level of scattering being considered; this avoids unnecessary and expensive calculations of scattered energy to surfaces that are not seen from the image plane and do not scatter to surfaces that are seen. This provides the opportunity to study individual radiation paths.

Program five also needs information as to vane configuration, such as position, vane angle, and reflectance of the coating. The total output map of all the energy transfer to each segment is put on tape by a utility program for later analysis.

The APART program is written in FORTRAN, operates in batch mode, and has been implemented on a CDC 6400 computer. It requires a minimum of 33K 60-bit words.

This program was written by R. P. Breault, B. B. Fannin, and D. B. Griner of the University of Arizona for **Marshall Space Flight Center.** *For further information, Circle A on the COSMIC Request Card.*
MFS-23495

Radiation Shielding Methods

Design and analysis of charged-particle radiation and shields

This system can be used as an aid in charged-particle radiation transport analysis and shielding design. SIGMA II was used to perform radiation analyses on virtually all the engineering and science subsystems of the Mariner Jupiter/Saturn 1977 (MJS '77) spacecraft. System level and subsystem level shielding for the MJS '77 spacecraft were based on these radiation shielding calculations. This system could be adapted for use in shielding design and analysis in any charged-particle radiation environment. Given the radiation environment and the geometry descriptions, SIGMA II will calculate an optimum shield configuration for a set of allowable radiation criteria.

Processing in the SIGMA II system occurs in three phases. The first phase is a kernel-generation program called SHIELD. Input to this phase consists of data on the unshielded electron and proton radiation environments in the form of flux and fluence energy spectra. The SHIELD program output includes one-dimensional attenuation kernels, such as dose or fluence, versus absorber thickness for electrons, protons, and secondary photons (bremsstrahlung radiation). These kernels are obtained by subdividing materials into many small layers. Within each layer, incident particles are transported using the continuous slowing down approximation for a set of solid-angle bins. The angular distribution is revised at the surface of each layer using angular straggling distributions.

The second phase of the SIGMA II system consists of computing the local radiation levels using the program SIGMA. Inputs to this phase consist of the one-dimensional kernal data along with the geometry or mass-distribution descriptions. The geometry section can recognize multiple-bay configurations and shapes with multiple bounding surfaces. The program SIGMA uses a three-dimensional ray tracing technique to obtain dose and fluence estimates at internal locations. SIGMA output includes mass path distribution (both slant path and minimum path) and sensitivity of radiation levels with respect to

(continued on next page)

shielding added to particular (user-specified) surfaces. This shield-sensitivity output includes recognition of shield crossing combinations.

The final phase in the SIGMA II system is shield optimization by the program SOCODE. The shield-sensitivity data from SIGMA are used to perform optimization calculations for multiple dose points, shields, and criteria. The user specifies the geometry and minimum and maximum shield thickness at each candidate shield location. The optimum shield configuration is calculated by iteratively incrementing shield thickness until all criteria are met.

This program is written in FORTRAN and has been implemented on a UNIVAC 1108 under control of EXEC 8 with a minimum core requirement of approximately 65K of 36-bit words. This program has plotting capabilities using the SC4020 plotter.

This program was written by Herbert S. Davis and Thomas M. Jordan of **Caltech/JPL.** *For further information, Circle B on the COSMIC Request Card.*
NPO-13923

Four-D Global Reference Atmosphere

Model of atmospheric pressure, temperature, density, and winds

The Four-D Global Reference Atmosphere Program was developed from an empirical atmospheric model which generates values for pressure, density, temperature, and winds from surface level to orbital altitudes. This program can be used to generate altitude profiles of atmospheric parameters along any simulated trajectory through the atmosphere. The program was developed for design applications in the Space Shuttle Program, such as the simulation of external tank reentry trajectories. Other potential applications would be global circulation and diffusion studies and generating profiles for comparison with other atmospheric measurement techniques, such as satellite-measured temperature profiles and infrasonic measurement of wind profiles.

Two previously-existing empirical atmospheric models for the low (25 km) and the high (90 km) atmosphere are combined with a newly-developed latitude/longitude-dependent model for the middle atmosphere. The high atmospheric region above 115 km is simulated entirely by the Jacchia (1970 model. The Jacchia program sections are in separate subroutines, so that other thermospheric/exospheric models could easily by adapted if required for special applications. The atmospheric region between 30 and 90 km is simulated by a latitude/longitude-dependent empirical model modification of the latitude-dependent empirical model of Groves (1971). Between 90 and 115 km a smooth transition between the modified Groves values and the Jacchia values is accomplished by a fairing technique. Below 25 km the atmospheric parameters are computed by the 4-D worldwide atmospheric model of Spiegler and Fowler (1972). Between 25 and 30 km an interpolation scheme is used between the 4-D results and the modified Groves values.

The output parameters consist of components for:
- Latitude, longitude, and altitude-dependent monthly and annual means;
- Quasi-biennial oscillations (QBO); and
- Random perturbations to simulate partially the variability due to synoptic, diurnal, planetary wave, and gravity wave variations.

Quasi-biennial and random variation perturbations are computed from parameters determined from various empirical studies and are added to the monthly mean values.

This program is written in UNIVAC FORTRAN and has been implemented on a UNIVAC 1110, under control of EXEC 8 with a central memory requirement of approximately 30K 36-bit words.

This program was written by B. Robertson and O. E. Smith of **Marshall Space Flight Center** *and C. G. Justus, R. G. Roper, and A. W. Woodrum of Georgia Institute of Technology. For further information, Circle C on the COSMIC Request Card.*
MFS-23336

Materials

High-Temperature Glass and Glass Coatings

Family of reaction-cured glasses resists thermal shock and maintains properties above 1,450° C.

Ames Research Center, Moffett Field, California

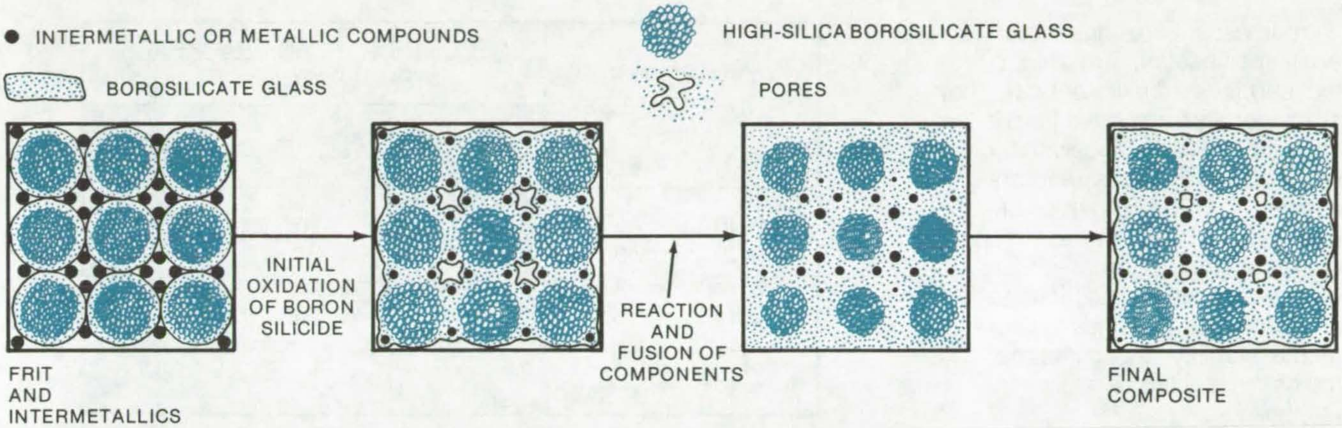

The **Composite-Glass Forming Reaction** of the dispersion of glass frit and intermetallic compound is characterized by an initial oxidation of the intermetallic compounds that react with the outer boron-oxide-rich layers of the frits. Upon further heating, the components fuse into a continuous mass. The boron-oxide-rich matrix prevents devitrification of the more-refractory high-silica core in each particle.

A new group of composites, called reaction-cured glass, have outstanding thermal and physical properties that make them excellent materials for high-temperature glassware and tubing or for coatings for porous materials, such as porous insulation tile. They can be used over a temperature range of -150° to 2,700° F (-100° to 1,480° C), have low thermal-expansion coefficients to resist thermal shock, and can be made highly opaque with a high surface emittance, or translucent, or transparent.

The glass is a composite material comprising a borosilicate glass matrix containing regions of high-silica borosilicate glass with intermetallic or metallic compounds dispersed throughout. The intermetallic compounds may be silicon tetraboride or other boron silicides, boron, or a mixture of these.

The glassy composites are prepared by combining about 100 parts of high-silicate borosilicate glass with two to ten parts of boron oxide. These are mixed to form an aqueous dispersion and are dried, dispersed, screened, and fired at 2,000° F (1,090° C) for over an hour after grinding and powdering, the resulting sintered material, or frit, is a two-phase glass with a very-reactive boron-oxide-rich borosilicate layer on the outside and a high-silica borosilicate core in each particle (see figure).

This frit is used to form a glass coating or glass article by reacting it with the appropriate intermetallic compound. Typically, a glass coating is prepared by blending the glass frit and 2.5 percent, by weight, of silicon tetraboride with an ethanol carrier and a methylcellulose prebinder. The mixture is ball milled and sprayed on the surface to be coated with an airbrush or a spray gun [coatings have been applied in thickness of 0.1 to 0.3 lb/ft^2 (0.05 to 0.15 g/cm^2)]. The coated article is dried and glazed at around 2,225° F (1,215° C) for about 1-1/2 hours.

This process forms an opaque, waterproof coating with an emittance of about 0.90 to 0.93 from room temperature to above 2,300° F (1,260° C). Its thermal-expansion coefficient is below 9×10^{-7} cm/cm/°C from room temperature to 1,500° F (820° C). The coating resists devitrification and does not bubble, foam, or change dimensions during glazing.

This work was done by Howard E. Goldstein and Victor E. Katvala of **Ames Research Center** *and Daniel B. Leiser of Stanford University. For further information, Circle 48 on the TSP Request Card.*

This invention is owned by NASA, and a patent application has been filed. Inquiries concerning nonexclusive or exclusive license for its commercial development should be addressed to the Patent Counsel, Ames Research Center [see page A8]. Refer to ARC-11051.

Improved Intumescent Coating

New fire-retardant intumescent coating has increased environmental stability.

Ames Research Center, Moffett Field, California

Intumescent coatings, which swell upon heating, are used to protect surfaces from fire or heat. They are generally formulated from a combination of chemicals that react when heated to release a foam-causing gas. The properties of a particular formulation depend on the characteristics of its constituent compounds, and it is difficult to find a coating that combines environmental stability, a long lifetime, and the necessary temperature response.

A new composition employing 4,4′ dinitrosulfanilide as intumescent agent is stable in the presence of water (one of the main causes of environmental degradation), adheres well, and is durable. The coating begins to swell at around 200° C, which is hot enough to prevent unwanted intumescence but is a low-enough temperature to insure protection against heat and fire for most applications.

The coating can be applied, by spraying or brushing, on wood, plastic, cardboard, and metals. The protective film is best applied in thicknesses of 30 to 70 mils (0.8 to 1.8 mm); when heated, it expands by a factor of 10 to 30 to form a tough insulating char.

Although the coating can be made with various ratios of constituents, the best formulation has been found to be 55 percent by weight of the dinitrosulfanilide combined with a binder system. The binder should be nonflammable or self-extinguishing and should exhibit little or no exothermic behavior upon thermal decomposition. A suitable binder has been prepared from a chlorinated polyolefin mixed with a bisphenol-A epoxy resin for flexibility and adhesion during thermal decomposition; a rubberlike amine hardener is also added.

The composition is normally blended in an organic solvent such as toluene. When properly formulated and applied, the coating not only has superior stability but has improved insulative characteristics when compared to existing intumescent coatings (see table).

COATING TYPE AND THICKNESS (MILS)		SECONDS TO REACH BACKFACE TEMPERATURE OF:		
		100° C	150° C	200° C
DNSA	62	50	110	170
DNSA	60	30	80	150
DNSA	43	20	50	80
DNSA	56	40	80	110
NSA	60	30	60	120

The **Insulative Efficiency** of the new intumescent coating (DNSA) is compared above to a coating based on the ammonium salt of 1,4-nitroaniline-2-sulfonic acid (NSA in the table).

This work was done by Paul M. Sawko and Salvatore R. Riccitiello of **Ames Research Center.** *For further information, Circle 49 on the TSP Request Card.*

This invention is owned by NASA, and a patent application has been filed. Inquiries concerning nonexclusive or exclusive license for its commercial development should be addressed to the Patent Counsel, Ames Research Center [see page A8]. Refer to ARC-11042.

Heat-Moderating Filler for Intumescent Coatings

An endothermic filler improves insulative efficiency when added to intumescent coatings.

Ames Research Center, Moffett Field, California

Intumescent coatings are used to make metals, plastics, woods, and other materials more fire-retardant. When exposed to high temperature, these coatings undergo a chemical reaction and swell to many times their original thickness to produce a nonflammable insulating char. (One such coating is described in the preceding article: "Improved Intumescent Coating," ARC-11042.)

Intumescent coatings based on a nitro-aromatic amine are generally more efficient than other known intumescent coatings. However, they are not as efficient as they might be, because they give off heat upon activation. This reduces the insulative efficiency of coating. The effect of this exothermic (heating-releasing)reaction can be substan-

tially countered by adding compounds that react endothermically (absorbing heat). An inorganic filler, such as ammonium oxalate, can be added to most existing intumescent coatings in sufficient quantity to result in an endothermic reaction that compensates for much of the exothermic char-producing reaction of the nitro-aromatic intumescent agent.

Such ablator additives have been used previously in other types of coatings with proved effectiveness. When added to an intumescent coating, they effectively reduce the heat transfer to the backside of the coated surface as shown in the figure.

In addition to ammonium oxlate, the filler may be potassium fluoborate, ammonium fluoborate, zinc borate, and most any other "endothermic" water-insoluble compound compatible with the coating formulation. Properly formulated, the fillers do not adversely affect the functional properties of the coating, and they even add to the oxidative stability of the char.

The amount of filler added should be based on the total exotherm of the coating, without interfering with the intumescent properties of the particular coating, generally in the range from 5 to 30 percent by weight. The preparation of a coating with filler depends on the process used to formulate the base coating without filler.

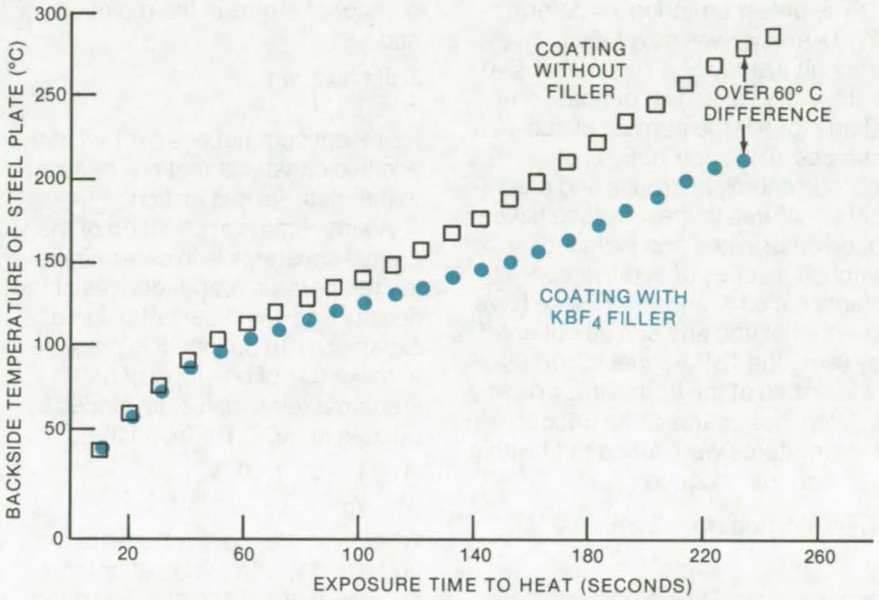

The **Improved Insulative Ability of a Filler Coating** is illustrated by the above comparison of an intumescent composition containing KBF_4 with one with no filler. The temperature on the vertical axis is that measured on the backside of steel panels with intumescent coatings. The panels were subjected to a heat flux of 110 to 120 kW/m^2, generated by burning jet fuel.

For example, using a base intumescent coating containing 4,4′-dinitrosulfanilide (as described in the preceding article, "Improved Intumescent Coating"), the filler is added to a dispersion of the intumescent material, binder, and solvent. Otherwise, preparation is as for the coating without the filler.

This work was done by Paul M. Sawko and Salvatore R. Riccitiello of **Ames Research center.** *For further information, Circle 50 on the TSP Request Card.*

This invention is owned by NASA, and a patent application has been filed. Inquiries concerning nonexclusive or exclusive license for its commercial development should be addressed to the Patent Counsel, Ames Research Center [see page A8]. Refer to ARC-11043.

Determining Critical Temperatures and Volumes

Estimates are made without the need for experimental data.

Caltech/JPL, Pasadena, California

Methods for evaluating the thermodynamic critical constants of a material have heretofore required the input of a certain amount of experimental data, such as for example the normal boiling point. However, a technique has been developed for estimating the critical temperature and volume of a fluid entirely from its chemical composition and structure and, significantly, without the need for any additional empirical data. As such, the method may be of use to designers interested in materials for which the critical constants are unavailable.

The critical point is a unique combination of temperature and pressure at which the liquid and gas phases of a substance have the same densities. At lower pressures, the material may be cooled through its boiling point, and an abrupt change from gas to liquid is observed. Above the critical point, no such sharp transition is seen, and in its place a gradual change from a tenuous vapor phase to the liquid condition occurs. The unique values of the temperature and pressure at the critical point are known as the critical temperature (T_c) and critical pressure, respectively, and the volume of 1 mole of the substance at the critical point is the critical molar volume (v_c).

(continued on next page)

The present method for determining T_c and v_c was developed through a study of a comprehensive compilation of known critical constants for a large number of substances. The contributions of various chemical groups and chemical structures to these values have been determined and included through a series of additive constants called δ_i and v_{ci}. (These have been tabulated and can be obtained by using the TSP Request Card as referenced at the end of this article.)

With these values, the critical temperatures were found to fit within 10° C to the equation

$$T_c = 535\,[\log(m + \sum_i \delta_i) - 0.350]$$

and the critical volume to within 5 percent

$$V_c = \sum_i v_c$$

In these equations, m is the total number of atoms in the molecule, and

$$\sum_i \delta_i \text{ and } \sum_i v_{ci}$$

represent summations over all of the additive constants that are relevant to the material in question.

An immediate application of the critical constants is in determining the temperature dependences of the density and coefficient of volume expansion. To do this, it is possible to make use of one form of an empirical relationship developed by Sugden in 1927. He found that

$$\frac{1}{v} = \frac{1}{v_o}\left(1 - \frac{T}{T_c}\right)^{0.3}$$

where v is the molar volume of the liquid and v_o is a hypothetical molar volume at absolute zero. The quantity v_o may be determined from the relationship

$$V_o = \sum_i v_{oi}$$

where v_{oi} is a sum over additive constants. Equation 3 and the critical temperature allow an evaluation of the molar volume and therefore the density as a function of the temperature.

The coefficient of volume expansion is defined by

$$\beta = \frac{1}{v}\left(\frac{\delta v}{\delta T}\right)_p$$

and may also be determined if equation 3 is differentiated once, giving

$$\beta = \frac{0.3}{T_c}\left(1 - \frac{T}{T_c}\right)^{-1}$$

With this equation, the only quantity needed to determine β at some temperature is the value of T_c.

This work was done by Robert F. Fedors of **Caltech/JPL.** *For further information, Circle 51 on the TSP Request Card.*
NPO-13405

Determining Viscosities of Liquids

Accuracies of 15 percent or better are obtained without experimentation.

Caltech/JPL, Pasadena, California

The viscosity of a liquid is often of interest to designers, yet it is not always known or easily accessible to measurement. Now a method has been developed which allows an evaluation of the viscosity for many liquids yet requires no input of experimental data other than the chemical composition and molecular structure. The evaluations are generally valid to within 15 percent and are therefore useful for many design applications and feasibility studies.

This technique complements that described in the preceding article, "Determining Critical Temperatures and Volumes" NPO-13405, which presents a method for determining the critical temperature (T_c) and critical volume (v_c) of a substance without the need for experimental measurements. It makes use of an empirical relationship first developed by Batschinski in 1913 which relates the viscosity of a liquid to its specific molar volume. This relationship takes the form

$$\eta = \frac{c}{v - \omega} \qquad (1)$$

where η is the viscosity in poise, v is the molar volume, and c and ω are temperature-independent constants characteristic of the liquid. This equation is valid for a wide class of substances excluding very strongly associated liquids.

Work by Sugden in 1927 showed that v could be determined as a function of temperature from the empirical relationship

$$\frac{1}{v} = \frac{1}{v_o}\left(1 - \frac{T}{T_c}\right)^{0.3} \qquad (2)$$

where v_o is a hypothetical molar volume at absolute zero which can be determined from a table of additive group and structural constants that apply to the substance in question. [This equation was alluded to in the preceding article (NPO-13405) and can be obtained by circling the TSP Request Card number for that article.]

The work has also been expanded to include a way of evaluating the constants c and ω in equation 1 from a knowledge of T_c and v_o. It was found from a study of viscosity data for over 60 liquids that the constant ω fits the empirical relationship

$$\omega = 1.130\,\frac{v_o}{M} \qquad (3)$$

within 5 percent, where M is the molecular weight; the constant c is given to an accuracy of 10 percent by the relation

$$c = 2.52 \times 10^{-5}\left(\frac{T_c v_o}{M}\right)^{1/2} \qquad (4)$$

Once T_c and v_o have been evaluated, it is possible to use equations 2, 3, and 4 to determine v, ω, and c for use in equation 1 to calculate the viscosity. The combined error for all factors falls within the range ±15 percent.

There is an alternate method for determining the viscosity which uses the "rheochor" concept introduced by Friend in 1946. It is found that the viscosity also fits the expression

$$\eta = 10^{-3} \left(\frac{R}{v^{*}m}\right)^{8} \left(\frac{v^{*} - \omega}{v - \omega}\right) \qquad (5)$$

where v* refers to the molar volume at the normal boiling point and R is the rheochor constant which can be evaluated from a table of additive constants. The quantity ω can be determined from equation 3, and v* from equation 2, provided the normal boiling point is known.

This work was done by Robert F. Fedors of **Caltech/JPL.** *For further information, Circle 52 on the TSP Request Card.*
NPO-13406

Estimating Molar Volume and Expansion

Molar volumes and expansion coefficients of polymers are estimated quickly from minimal experimental data.

Caltech/JPL, Pasadena, California

Engineers often require quick estimates of the molar volumes and expansion coefficients of polymers. The experimental determination of these properties can be time-consuming and may require complicated and unavailable equipment. A new fast and efficient technique requires but a single experimental determination: the glass transition temperature of the polymer. It is used in conjunction with tabular data to calculate both the molar volume and the expansion coefficient. Estimates of molar volumes are generally within 5 percent of the experimentally determined molar volume, and the expansion coefficient is generally within 15 percent of the experimentally determined parameter.

If the T_c is the hypothetical critical temperature of the polymer, then the molar volume, V_c, at this temperature can be estimated by adding the contributions of each atom or group within the polymer to this volume. Thus, if the chemical structure of the polymer is known, the molar volume at the critical temperature can be calculated:

$$V_c = v_{c1} + v_{c2} + \ . \ . \ . \ v_{cn}$$

Likewise, if T_0 represents absolute zero, then the molar volume at this temperature, V_0, can be calculated in the same way:

$$V_0 = v_{01} + v_{02} + \ . \ . \ . \ v_{0n}$$

Given V_c and V_0, the molar volume at the glass transition temperature, V_g, can be calculated from the relation:

$$V_g = K(V_c - V_0)$$

where K is a constant having an average value of 0.368. An analysis of available data indicates that the majority of values of K lie within 5 percent of the mean, and all values lie within 10 percent.

The expansion coefficient, β, of a polymer at temperature T can be determined as follows:

$$\beta = \frac{0.3V}{T_c\left(1 - \frac{T}{T_c}\right)} = \frac{0.108V}{T_g\left(1 - \frac{0.36T}{T_g}\right)}$$

where V is the molar volume of the repeating unit. Only T_g need be determined experimentally.

Two similar techniques are described in the preceding articles: "Determining Critical Temperatures and Volumes" (NPO-13405) and "Determining Viscosities of Liquids" (NPO-13406).

This work was done by Robert F. Fedors of **Caltech/JPL.** *For further information, Circle 53 on the TSP Request Card.*
NPO-13404

Removing CO_2 and Moisture From Air

An improved closed-cycle atmospheric scrubber reduces the levels of carbon dioxide and water vapor in an air stream without affecting its temperature. Impurities are drawn from the air and removed to an outside site; chemical filters, desiccants, and additional heaters are not required.
(See page 105.)

Quantitative Measurement of the "Feel" of Fabric

A new methodology measures fabric "handle": the combined effects of drapability, flexibility, compressibility, foldability, and pliability. Quantitative measurements of knits, films, composites, and laminates are made with a bench type or a portable instrument.
(See page 116.)

Transducer for Ultrasonic Inspection of Porous Material

New ultrasonic nondestructive inspection techniques are useful with materials having high acoustic losses, such as surface insulators. An ultrasonic transducer array is used with an echo technique, or a pair of ultrasonic transducers are placed on opposite sides of a specimen for an electrodynamic technique.
(See page 107.)

Solubility-Parameter "Spectroscopy"

Experimental determination of polymer solubilities

Caltech/JPL, Pasadena, California

When choosing polymers to be used in the fabrication of biomedical implants such as heart valves and other devices, the solubility of the polymer is an important consideration. In fact, in most every application of polymers where extended contact with potentially damaging liquids is expected, the designer must consider the solubilities of the polymers.

A new technique for measuring the solubility of solids is particularly useful for polymers, especially for measuring solubilities in nonvolatile liquids for which heats of vaporization are not well known. The technique comprises the measurement of the "solubility parameter" δ defined as

$$\delta^2 = -E/\overline{V}$$

where E is the thermodynamic potential energy of a mole of the material and $\overline{V}$ is the molar volume.

A series of measurements is taken to determine a solubility-parameter profile or "spectrum" of the material, thus the term "solubility spectroscopy." The polymer under test is immersed in a series of mixtures of two solvents, of varying solvent ratios. The effective solubility parameter of each different mixture δ_m is

$$\delta_m = \gamma_1\delta_1 + \gamma_2\delta_2$$

when δ_1 and δ_2 are the solubility parameters of the two pure liquids and γ_1 and γ_2 are their volume fractions.

Using a suitable number of binary solvent mixtures, a "solubility spectrum" such as that shown in the illustration may be prepared. The polymer is immersed in the solvent mixture, and the resultant swelling, or the weight increase, is measured to determine the amount of solvent absorbed.

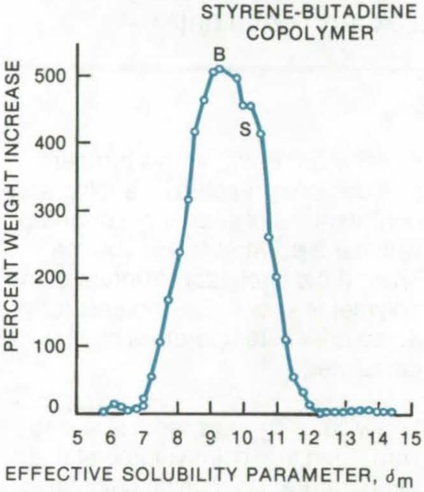

The **"Solubility-Parameter Spectrum"** of styrene-butadiene copolymer exhibits a peak representing the butadiene block and a shoulder representing the styrene block.

This work was done by John D. Ingham, Daniel D. Lawson, and Jovan Moacanin of **Caltech/JPL.** *For further information, Circle 54 on the TSP Request Card.*
NPO-13829

Predicting Hydrogen-Storage Capabilities of Metals

A simple method can aid designers of hydrogen-storage facilities for electric power plants.

Caltech/JPL, Pasadena, California

Solubility-parameter comparison has been successfully used to predict the absorption of hydrogen into metals. This process is of particular interest because of proposals currently under study to produce hydrogen at electric power plants during off-peak hours. If it could be stored economically, the hydrogen could be used during peak hours to provide extra electricity. Absorption in metals is a particularly attractive storage method because neither the cooling energy needed for cryogenic storage nor the volume needed for high-pressure storage are required.

Currently, designers must test each candidate metal composition experimentally, since absorption cannot generally be predicted on the basis of stoichiometry. However, by treating the absorption of hydrogen as a solution process, solubility parameters can be used to identify those compositions that will absorb appreciable amounts of H_2.

For metals, the solubility parameter, δ, is defined as

$$\delta^2 = \frac{\Delta H_S - RT}{\overline{V}}$$

where

ΔH_S is the heat of sublimation,
R is the universal gas constant,
T is the kelvin temperature, and
$\overline{V}$ is the atomic volume;

and δm, the solubility parameter for a mixture or alloy, is

$$\delta_m = a_1\delta_1 + a_2\delta_2 + \ldots a_n\delta_n$$

where

a_n is the volume fraction of the nth component and

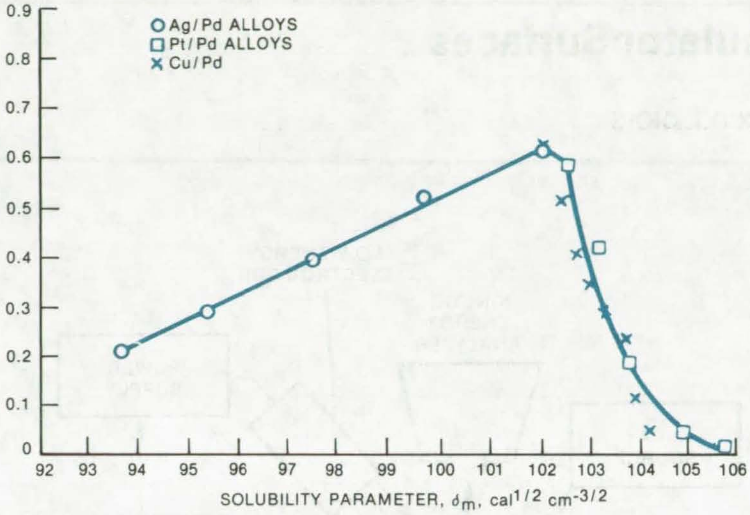

Hydrogen Absorption is shown as a function of solubility parameter for three binary alloys. The ratio of hydrogen atoms to metal atoms at 25° C is given by H/M, and the solubility parameters for several different metal-composition ratios are given for each alloy.

δ_n is the solubility parameter of the nth component.

Theory predicts that those metals having solubility parameters close to that of dissociated hydrogen will be the best absorbers. When the solubility parameters of metals shown experimentally to be desirable for hydrogen storage are calculated, they are found to lie between 100 and 118 $cal^{1/2}$ $cm^{-3/2}$, near the δ values for hydrogen.

The utility of the method can be further appreciated by the illustrated graph of the solubility parameters of three series of binary alloys. For each alloy type, the amount of hydrogen absorbed varies with the solubility parameter and thus the relative amounts of the two components. The absorption can be seen to peak around δ values of 102 $cal^{1/2}$ $cm^{-3/2}$.

This work was done by Robert F. Landel, Daniel D. Lawson, and Charles G. Miller of **Caltech/JPL.** *For further information, Circle 55 on the TSP Request Card.*
NPO-13893

Porous Poly-HEMA Bead Synthesis

Low-cost reagent is useful in labeling cells for research and diagnostic purposes.

Caltech/JPL, Pasadena, California

Microbeads of poly-HEMA, produced by a new process, can be used for the labeling of cells by immunological techniques. The small spherical beads are from 0.05 to 10 microns in diameter. They are produced from freshly distilled HEMA dissolved in H_2O; polyethylene oxide is added, and the mixture is subjected to ionizing radiation.

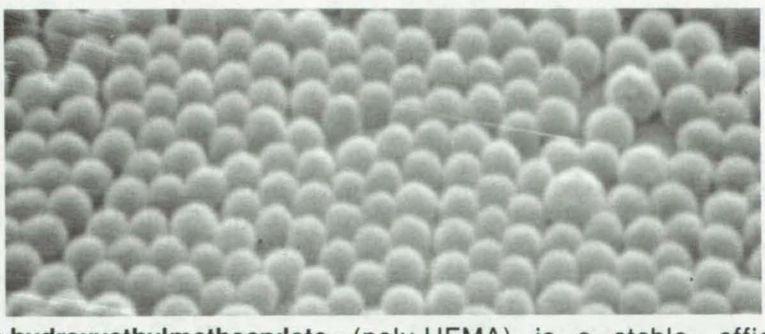

Poly-hydroxyethylmethacrylate (poly-HEMA) is a stable, efficient, economical polymer reagent in the form of 0.05- to 10-micron spherical porous beads.

The resulting material is diluted, filtered, and washed with water to remove the polyethylene oxide. The remaining dry material is composed of spherical beads of poly-HEMA (over 90 percent yield). By adjusting reaction conditions, spheres from 1 to 10 microns in diameter can be prepared; an emulsion polymerization system can also be used.

Due to cross-linking, the beads are insoluble and swell in water and common organic and inorganic solvents. The process can be modified in order to introduce carboxyl groups into the beads. The presence of both hydroxyl and carboxyl permits the formation of covalent bonds with large biomolecules such as antibodies and enzymes, making the beads suitable for the labeling of cells in the scanning and light microscope, as well as for the immobilization of enxymes.

This work was done by Alan Rembaum and S-P. S. Yen of **Caltech/JPL** *and William J. Dreyer of the California Institute of Technology. For further information, Circle 56 on the TSP Request Card.*

Title to this invention has been waived under the provisions of the National Aeronautics and Space Act [42 U.S.C. 2457(f)], to the California Institute of Technology, Pasadena, California 91109.
NPO-13383

ESCA Measurement of Insulator Surfaces

Precision ESCA of insulators, as well as improved results with metals and semiconductors

Caltech/JPL, Pasadena, California

Electron spectroscopy for chemiical analysis (ESCA), also referred to as X-ray photoelectron spectroscopy (XPS), has been a powerful tool for measurement of the chemical properties of the surfaces of materials. However, the technique is relatively new and has been largely confined to use with metals and semiconductors.

The difficulty in applying ESCA to studies of insulators can be understood from a brief review of the experiment. For analysis, the sample is attached to the spectrometer with an ohmic contact. It is then bombarded with an X-ray source. Electrons in the sample absorb the X-ray photons; part of the photon energy goes into the ionization energy required to remove the electron from its atom, and the remainder goes into the kinetic energy of the ejected electron. The kinetic energies of the ejected electrons are analyzed, to produce a distribution plot (by kinetic energy). Since the X-ray photon energy is known, this is also a plot of the chemical bonding energy of the electrons and can thus be used to identify the types and quantities of chemical species in the sample.

To allow a comparison of data between samples, some reference energy level is required. In the case of metals and semiconductors, this is the Fermi level at the surface of the sample. However, when the sample is an insulator, the surface potential (and correspondingly the vacuum energy level at the surface) is constantly altered by the ejection of electrons and the accumulation of positive charge on the surface. (For metals and semiconductors this charge is neutralized through the ohmic contact to the spectrometer ground.) The amount of surface charge on the insulator can be varied by spraying it with electrons, but the magnitude of the charge can be neither controlled nor measured.

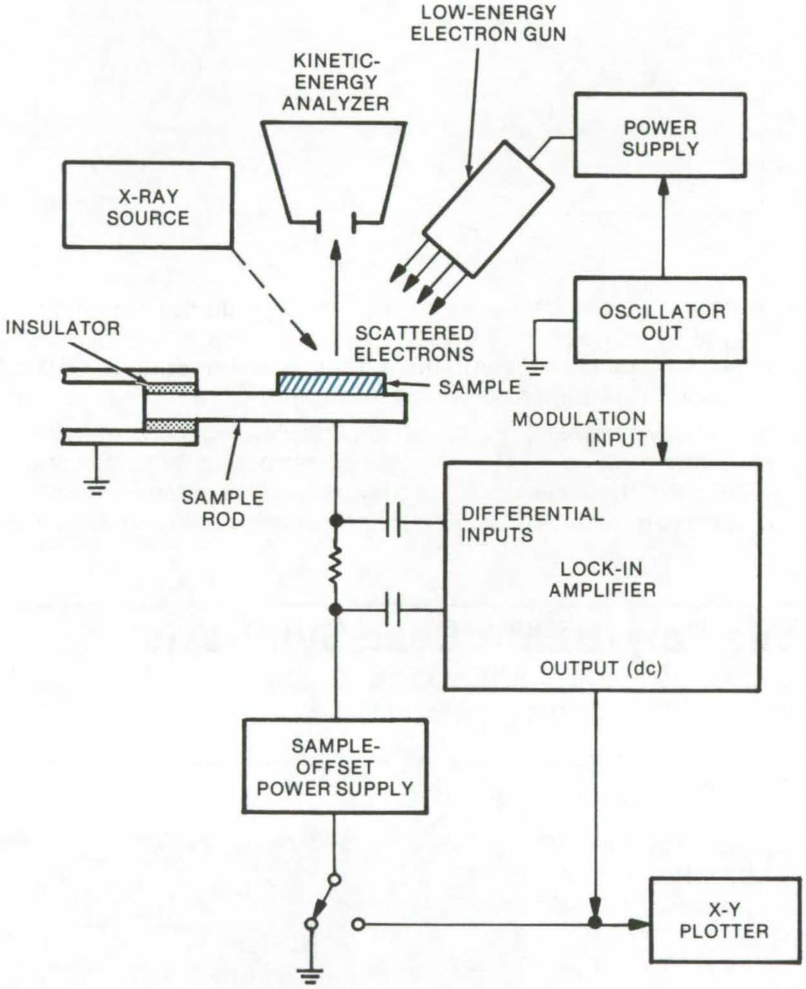

In the **Improved Photoelectron Spectrometer,** the sample is insulated from ground. Photons are directed to the sample from an X-ray source, and low-energy electrons are directed to the sample from an electron gun. The gun potential is modulated by an oscillator, and the current passing through the sample is detected, using phase-sensitive techniques. The sample-surface potential is varied until the ac current reaches a peak amplitude, which occurs when the vacuum levels of the sample and gun are equal. A feedback signal from the lock-in amplifier to the sample offset voltage supply keeps the vacuum levels of the sample and gun equal. The gun vacuum level and the sample vacuum level are known and presumed constant during the measurement; thus the surface potential of the sample may be determined with precision.

A new approach to a reference energy level allows, for the first time, precision ESCA of insulators as well as improved results with metals and semiconductors. The vacuum level at the surface of a sample can be determined to varying degrees of spatial resolution, using a new electron flood gun (the source of the electrons spray used to vary the surface charge on the insulator).

The electron beam from the gun is modulated by a reference oscillation. The alternating current from the gun passes through the sample and sample rod and is detected by a phase-sensitive technique, using a lock-in amplifier. The potential difference between the sample surface and the gun is controlled by a dc bias supply as indicated in the figure.

The vacuum energy level at the surface of the sample is determined by plotting the first derivative of the detected current as a function of the potential difference between the sample and the gun. This signal is at a maximum when the vacuum level at the sample surface is the same as at the gun cathode. Thus, a hard energy reference is determined by using the Fermi level of the gun cathode as the electronic state in equilibrium with the spectrometer Fermi level.

The bias voltage is varied to determine the bias at which the vacuum levels of the gun and the area of the sample surface being probed are the same. The width of the signal peak at this potential depends on the spatial resolution of the gun and the charge distribution on the sample surface. By determining the minimum detectable width of the reference peak for a well-characterized metal surface, the charge distribution on the surface of the sample can be measured as a function of the spatial resolution of the electron gun.

In a refinement of the technique, a fine-focus gun with an x-y raster scan can be used to map the vacuum level with high spatial resolution, to reduce spurious electron background and improve sensitivity.

This work was done by Frank J. Grunthaner of **Caltech/JPL.** *For further information, Circle 57 on the TSP Request Card.*

This invention is owned by NASA, and a patent application has been filed. Inquiries concerning nonexclusive or exclusive license for its commercial development should be addressed to the Patent Counsel, NASA Resident Legal Office-JPL *[see page A8]*. *Refer to NPO-13772.*

Humidity-Resistant Black-Nickel Coatings

Coatings for solar collectors are improved by increasing metal hydroxide concentrations.

Marshall Space Flight Center, Alabama

	BEFORE HUMIDITY		MIL-STD 810B HUMIDITY		NASA STANDARD HUMIDITY				
			1 day	4 days	4 days	10 days	14 days		20 days
	α	ε	α	α	α	α	α	ε	α
NASA standard	0.900	0.097	0.846	---	0.891	0.783	0.721	---	0.670
New formula	0.902	0.10	0.842	0.751	---	0.924	0.917	0.10	0.906

The **Humidity Resistance** of the new black-nickel coating is compared to the previous standard formulation.

Black nickel is one of the best selectively absorbing coatings for solar energy use, since it is efficient and relatively inexpensive. However, electroplated black nickel (a Ni/Zn/S/O complex) will degrade in less than ten days at 38° C and 95-percent relative humidity.

A new black-nickel formulation withstands such exposures without sacrificing optical properties. It has a solar absorption greater than 0.92 and an infrared emmitance (at 100° C) less than 0.10. This improved humidity resistance is achieved by increasing the concentration of metal hydroxide in the coating.

The improved coating was developed as a result of an experimental study on the effects of changes in the electroplating parameters. Plating time, current density, bath temperature, pH, and the concentraton of SCN^-, Zn^{++}, and Ni^{++} were all found to affect the coatings significantly. The role of these parameters is to control the relative proportions of metal hydroxides, metal sulfides, and free metals in the coating.

The main effect of humidity on black-nickel coatings is to convert metal sulfides near the surface of a coating to metal hydroxides. The extent of this problem was found to be reduced when the initial concentrations of metal hydroxides were increased. Such a coating (see table) was prepared by increasing the pH and the plating-current density.

After 14 days at 95 percent relative humidity and 38° C the optical properties of the coating were essentially unchanged. The solar absorption of the conventional formula degraded from 0.96 to 0.72 under the same conditions.

This work was done by James R. Lowery of **Marshall Space Flight Center** *and J. H. Lin and R. E. Peterson of Honeywell Inc. For further information, Circle 58 on the TSP Request Card.*
MFS-23650

Improved Processability of Addition Polyimides

Melting point depression of addition-type polyimides through the use of proper amine mixtures improves processability.

Langley Research Center, Hampton, Virginia

A highly cross-linked, thermoset polymeric material used for fabricating consolidated composite parts results from the preparation of polyimides by the addition-polymerization method. This method basically involves the preparation of an oligomeric imide which has alkenyl endcaps (see Figure 1). In this general case, such an oligomer will melt when heated and, when sufficient temperature is reached, will polymerize through the alkenyl linkage in Figure 2.

In the preparation of fiber-reinforced composites, the polymerization encapsulates the reinforcement and is set. A particularly attractive, commercially available addition-type polyimide has the structure shown in Figure 3. Fabrication of composite parts with this material generally requires temperatures of 550 to 600° F (280 to 315° C) at pressures exceeding 1,000 psi (6.9×10^6 N/m^2). At these temperatures the imide ring forms, liberating water, and the alkene portion of the molecule undergoes polymerization, producing a highly cross-linked, thermally stable polymer. However, in this case, the oligomer is a solid, and the resin system undergoes little or no melt, necessitating the use of the extremely high pressure for fabrication. A lowering of the melting point for this type resin system could significantly reduce the pressure required for molding.

The depression of melting points by mixing two or more pure components is a well-known technique in the alloying of metals and in organic chemistry. The mixture, in such a case, has a lower melting point than either separate component, the ratio of components demonstrating the lowest melting point being commonly known as the eutectic mixture. It is believed that the interaction of the two components in the liquid state disrupts the ability of either component to assume the preferred crystalline configuration.

Obviously, for high molecular weight polymers, this type of depression is not pronounced unless the polymer is crystalline. The high molecular weight polyimides, being amorphous, i.e., having no apparent crystalline form, would not be expected to undergo any significant melting point depression when mixed.

However, for an addition-type polyimide a significant melting point depression was achieved by using a mixture of isomeric diaminodiphenylmethanes as the diamine portion of the oligomer instead of using pure p,p′-methylene dianiline (p,p′-MDA). The amine mixture that has been used successfully is the isomeric mixture of methylene dianilines, i.e., o,o′-MDA; o,p′-MDA; p,p′-MDA, as well as di- and tri-methylene bridged aromatic polyamines. This technique resulted in an oligomer which was liquid as a prepreg even after solvent loss. Pressures of under 200 psi (1.4×10^6 N/m^2) were adequate to fabricate composites with properties equal to or better than those of the polymer in Figure 3 made at the higher temperatures and pressures (see Figure 4).

In addition to the advantage of lower temperature and pressure

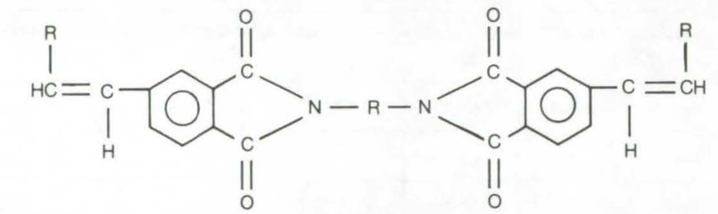

Figure 1. An **Oligomeric Imide** with alkenyl endcaps is a starting material for the preparation of polyimides used in composites.

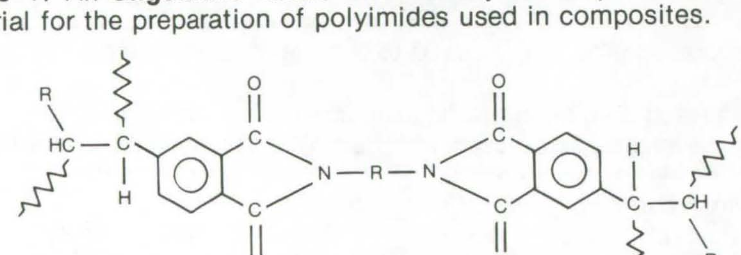

Figure 2. The **Polymerized Oligomer** is formed by heating the monomer in Figure 1.

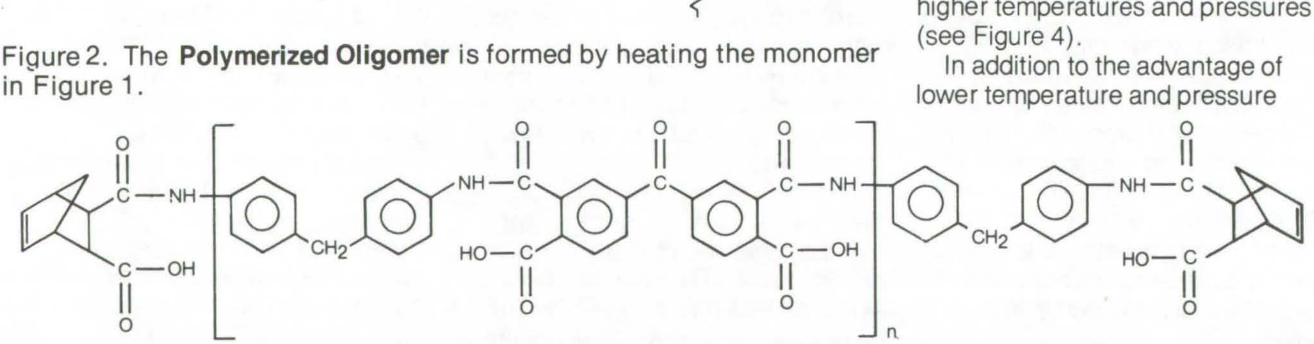

Figure 3. **Addition-Type Polyimide** used for the preparation of fiber-reinforced composites.

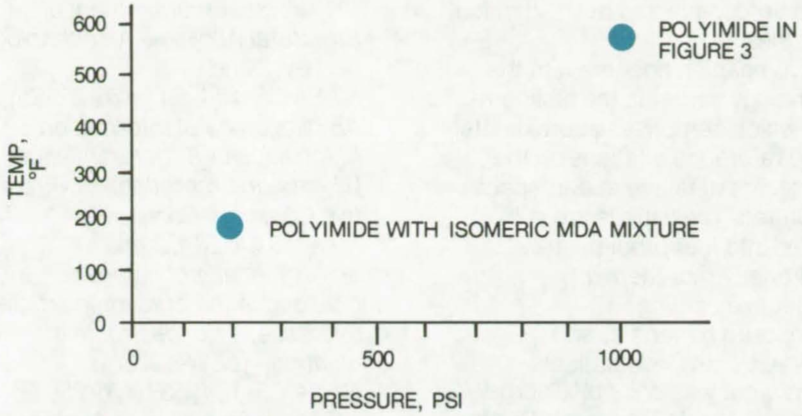

Figure 4. **Temperature/Pressure** diagram compares the processing requirements for consolidation of composite parts, with and without the addition of MDA to lower the melting point.

requirements for fabrication of composites, depression of the melting point of the polyimide system through the use of the isomeric mixture of methylene dianilines produced a polymeric material that could be thermoformed at elevated temperatures after an initial consolidation at lower temperatures.

This work was done by Terry L. St. Clair of **Langley Research Center.** *For further information,* Circle 59 *on the TSP Request Card.*

Inquiries concerning rights for the commercial use of this invention should be addressed to the Patent Counsel, Langley Research Center [see page A8]. Refer to LAR-12054

Extraction of Trace Elements from Ores

Low-temperature vaporization separates trace elements from ores.

NASA Headquarters, Washington, D.C.

A process developed for the analysis of trace elements in stony meteorites may be useful for the recovery of trace elements in ores and minerals. Elements such as Ga, Se, Bi, Tl, and In can be extracted by low-pressure, relatively low-temperature vaporization from compositions in which they may occur in trace amounts only, such as interstitial impurities.

The process has been tried on a laboratory scale, where samples of stony meteorites are sealed in a container under 10^{-5} atm of hydrogen. They are then heated in a muffle furnace to between 400° and 1,000° C, and are kept at that temperature for about a week. When samples thus treated are analyzed for the trace elements (by neutron activation), a reduction in the trace-element content of the meteorites indicates the elements removed by vaporization.

Plots of the vaporization loss and temperature indicate that the loss is a diffusion-controlled process and can be used to calculate the activation energies for loss of each element.

The reaction vessel may be made of any material that does not react with the sample (generally silicates) at the process temperatures. By establishing a thermal gradient in the vessel, the vaporized elements can be collected on the cooler region. By varying the temperature in the hot region, it should be possible to mobilize particular elements selectively, for separation as well as extraction.

This work was done by Mohammed Ikramuddin and Michael E. Lipschutz of Purdue Research Foundation for **NASA Headquarters.** *No further documentation is available. HQN-10875*

Books and Reports

These reports, studies, and handbooks are available from NASA as Technical Support Packages (TSP's) when a Request Card number is cited; otherwise they are available from one of NASA's Industrial Application Centers or the National Technical Information Service.

Hydrogen Embrittlement of Structural Alloys

A technology survey and bibliography

The effect of hydrogen embrittlement on structural metals has become a subject of significant interest due to the potential uses of hydrogen as a primary energy source. An understanding of hydrogen embrittlement is important to designers and operators of hydrogen propulsion systems and hydrogen storage and transfer systems.

A technology survey has been assembled that reviews information covering the three types of hydrogen

(continued on next page)

embrittlement: hydrogen environment embrittlement, internal reversible hydrogen embrittlement, and hydrogen reaction embrittlelent. In addition, major consideration is given to three specific hydrogen effects that have received widespread attention:

- stress corrosion cracking,
- crack growth and fracture mechanics, and
- ductile fracture.

The survey summarizes the accumulating knowledge about hydrogen embrittlement as reflected in the technical literature covering the time period from 1962 to 1975, with most attention devoted to the last 5 years and highlighting the applications and service experience in the aerospace and petrochemical industries.

A companion document to the technology survey is the bibliography, which comprises approximately 1,600 reference citations on the mechanics of failure in aerospace structures. The listings are subdivided into four problem areas:

- hydrogen embrittlement,
- protective coatings,
- composite materials, and
- nondestructive evaluation.

This work was done by George Mandel of **Lewis Research Center** *and James L. Carpenter, Jr., and William F. Stuhrke of Martin Marietta Corp. Copies of the two reports:*

NASA CR-134962 [N76-25375], "Hydrogen Embrittlement of Structural Alloys — A Technology Survey," and

NASA CR-134964 [N76-28565], "Bibliography of Information on Mechanics of Structural Failure [Hydrogen Embrittlement, Protective Coatings, Composite Materials, NDE]," and

of an additional technology survey, announced in the preceding article in this issue, "Nondestructive Evaluation" [LEW-12766]:

NASA CR-134963 [N76-25577], "NDE — An Effective Approach to Improved Reliability and Safety — A Technology Survey,"

can be obtained at cost from the New England Research Application Center [see page A7].

LEW-12767

Computer Programs

These programs may be obtained at very reasonable cost from COSMIC, a facility sponsored by NASA to make new programs available to the public. For information on program price, size, and availability, circle the reference letter on the COSMIC Request Card in this issue.

Paralinear Oxidation Behavior

COREST emphasizes long-time behavior.

A new program, COREST, was developed for analyzing paralinear oxidation, with emphasis on long-time behavior. The high-temperature, isothermal oxidation of metals and alloys is generally analyzed on the basis of oxygen weight gain as a function of time. For many high chromium content, heat-resistant alloys, the scale formed is predominantly a chromium oxide (Cr_2O_3) which does not follow standard parabolic kinetics. Once formed, the oxide can further react with oxygen and volatilize. In this process, weight gain due to oxygen pickup and weight losses due to oxide volatilization occur simultaneously. This volatilization process is of special concern in the high-velocity environments that are encountered by orbital reentry vehicles and gas turbine engines. Thus, this program can be used to estimate long-time oxidation at high temperatures of chromite-forming alloys, with emphasis on metal consumption (corrosion).

COREST was developed for analyzing paralinear oxidation based on the mass-balance expression ΔW (net sample-weight change) $= W_r$ (specific weight of the retained oxide) - W_m (specific weight of the metal consumed). Starting from the basic mass equation, the basic differential equations for W_r and W_m are solved separately. This basic paralinear model gives an exact solution as a function of time for ΔW, W_r, and W_m. These basic equations are generalized by dimensional analysis so that the W_r and W_m values can be generated independently as a function of time from a minimal amount of input data with a known scale.

With a stoichiometric constant calculated from the composition of the oxide, the following types of input data can be completely analyzed by COREST:

- Maximum estimate values of ΔW with its corresponding time
- Any paired values of the parabolic scaling constant K_p and the linear vaporization-rate constant K_v ($K_v \neq O$)
- Any value of K_p or K_v, along with any one set of ΔW with its corresponding time
- Any two sets of ΔW values with their corresponding times

From this input the program calculates and lists:

- K_p and K_v
- Maximum positive ΔW with corresponding time and W_r and W_m
- The time for ΔW to return to zero and its corresponding W_r and W_m
- The limiting value of W_r and its corresponding thickness
- The time to reach any requested fraction of the limiting value of W_r
- The time to reach any requested value of W_m
- The ΔW, W_m, W_r, effective metal-thickness loss, and oxide thickness at any requested time

The program has also been used to analyze cyclic oxidation where oxide growth and spalling between heating cycles approximates paralinear behavior.

This program is written in FORTRAN to run in the batch mode and has been implemented on a UNIVAC 1100 series computer with a central memory requirement of approximately 13K of 36-bit words.

This program was written by Charles A. Barrett and Alden F. Presler of **Lewis Research Center.** *For further information, Circle D on the COSMIC Request Card.*

LEW-12677

Life Sciences

Skin-Implant Multiwire Connector

A magnetically latched connector for multiwire skin implants is easy to use and is reliable.

John F. Kennedy Space Center, Florida

Skin implants are used to connect external electronic systems to sensors and wires implanted in tissue or within the body. They are used with bioelectronic data monitors, to exercise paralyzed muscles, to block pain, to stimulate nerves, to transmit measurements, and to convey nerve impulses to amplifiers for prostheses. When two or more connections are required at a single site, an electrical connector that would appear simple and effective for conventional electronics can become complex and troublesome when implanted through the skin.

For skin-implanted connectors, there are several special criteria: They must be biocompatible and hygienic; they must be easily connected and disconnected in darkness, from any direction, and with one hand; they must not be likely to catch or snag on clothing; and they must be easy to clean and maintain. These requirements are, of course, in addition to more conventional standards of functional reliability, cost, and durability.

Work by the Rancho Los Amigos Hospital of Downey, California has shown the biocompatible high-purity carbon (developed for aerospace use) provides an ideal hygienic material for implants; but until the development of a new connector, the problems of ease of use, snagging, and cleaning have been difficult to achieve in a device meeting all the other requirements of a multiwire percutaneous (through-the-skin) connector. The illustrated three-wire connector is a relatively inexpensive device that meets all these criteria.

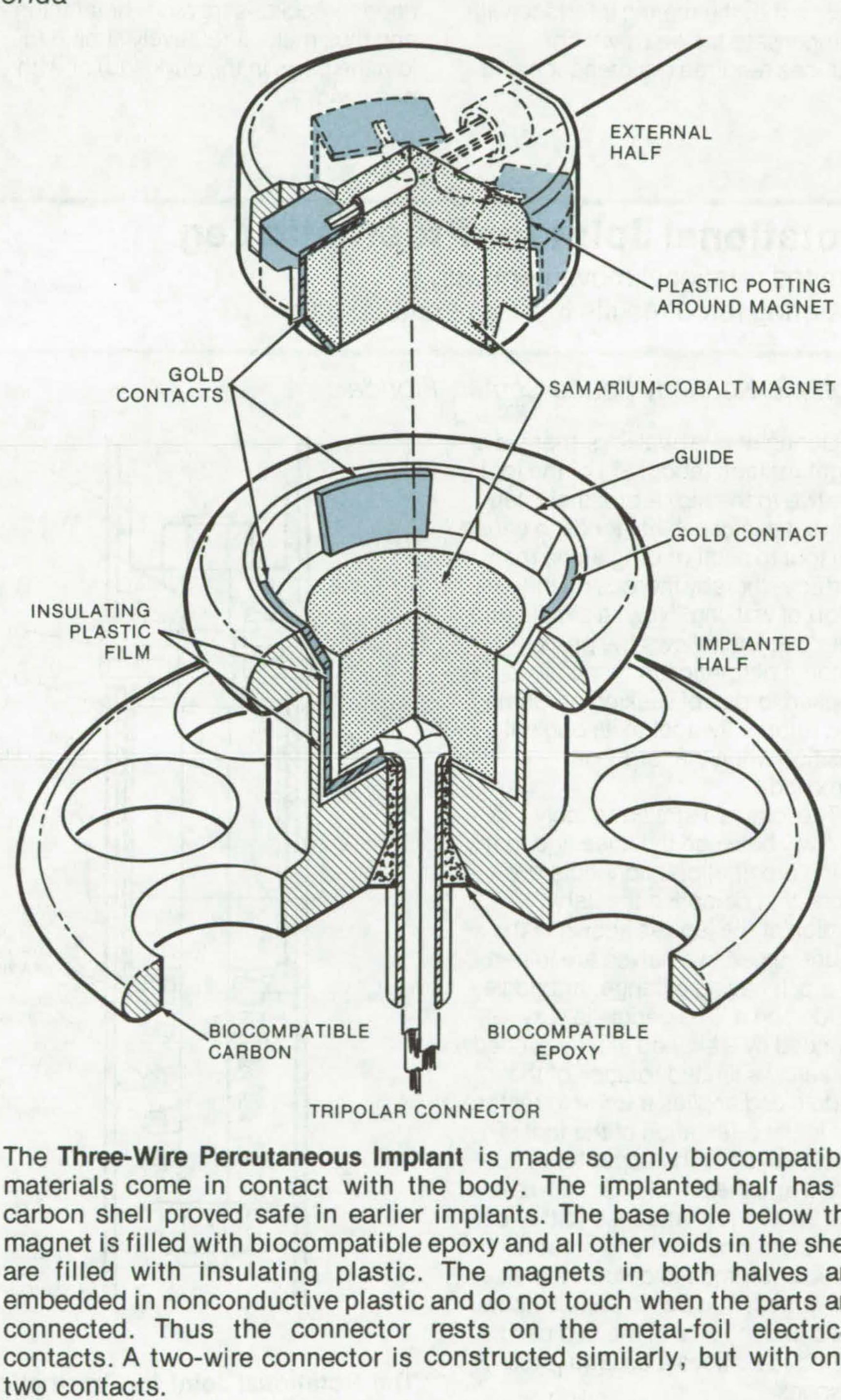

The **Three-Wire Percutaneous Implant** is made so only biocompatible materials come in contact with the body. The implanted half has a carbon shell proved safe in earlier implants. The base hole below the magnet is filled with biocompatible epoxy and all other voids in the shell are filled with insulating plastic. The magnets in both halves are embedded in nonconductive plastic and do not touch when the parts are connected. Thus the connector rests on the metal-foil electrical contacts. A two-wire connector is constructed similarly, but with only two contacts.

The implanted half of the connector is shaped like a cylinder on a disk. The disk offers stability and support; and the cylinder, which protrudes through the skin, is only as large as is required for simple use and good electrical connection. The part is embedded so that the bottom of the rim around the top of the cylinder is flush with the surface of the skin, which will heal around the rim to form a relatively unobtrusive profile. The external male connector fits within a conical well in the implanted half, thus solving the problem of snagging on clothing and other objects.

(continued on next page)

Magnets in both the implanted and external halves exert a constant and controlled force yet allow disconnection without damaging the implanted half. The electrical connections (gold foil) are mating "wedges." Their conical shape means that the mating interface will compensate for wear, which reduces required maintenance and manufacturing tolerances. Furthermore, the conical depression is shallow and easily cleaned with a cotton pad. Slot guides facilitate proper alinement of the pieces and hold them there. The guides and magnetic coupling preclude the need for locks, screwing, or latching and thus make it relatively simple to join the parts in the dark and/or with one hand.

This work was done by Lester J. Owens of **Kennedy Space Center.** *For further information, Circle 60 on the TSP Request Card.*

This invention is owned by NASA, and a patent application has been filed. Inquiries concerning nonexclusive or exclusive license for its commercial development should be addressed to the Patent Counsel, Kennedy Space Center [see page A8]. Refer to KSC-11030.

Rotational Joint for Prosthetic Leg

Limited rotational movement with a restoring force results in a more natural gait.

John F. Kennedy Space Center, Florida

During normal walking, there is a slight rotation (about 3°) of the foot relative to the hip. A prosthetic leg without this capability tends to cause the foot to scuff or drag along the surface, thereby increasing the effort of walking. Now, a simple and effective joint allows the proper amount of rotation in response to the applied torque of walking or running and returns the foot to its original position when the torque is removed.

The joint is installed roughly halfway between the knee and foot of the prosthetic; it connects two tubes that comprise the "shin" portion of the leg. As shown in the figure, these two halves are joined by a bolt having a flange, or paddle, welded on it. The paddle is surrounded by a shaped elastomer bed that allows limited rotation of the paddle and applies a force to restore the initial orientation of the foot. The bolt is keyed to the upper tube, so that it and the paddle do not rotate. The lower tube, attached to the foot, will rotate when walking creates sufficient torque to deform the elastomer bed. The particular elastomer used and the size of the bed can be varied to achieve a desired force response.

The deformation of the elastomer, and thus the amount of foot rotation, is proportional to the applied torque, much as in natural walking. The

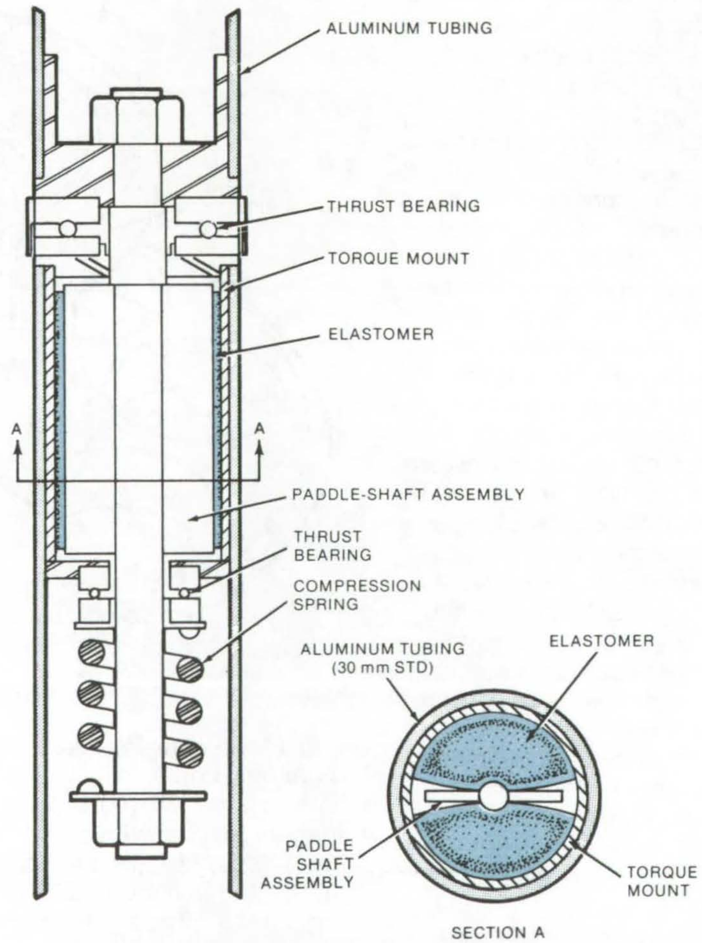

The **Rotational Joint for Prosthetic Legs** is installed in standard 30-mm tubing used for lower leg prosthetics. Rotation is controlled by a flanged bolt embedded in a shaped bed of elastomer. The elastomer is thicker toward the center of the flange (paddle) so that the antirotational force increases as the rotational angle increases. The compression spring prevents looseness in the joint.

elastomer is shaped so that its restraining force (against rotation) increases with the amount of foot rotation. Thus rotation is effectively limited, and the force restoring the foot to its initial position is responsive to the demands of the stride.

A tension preload is applied to the paddle shaft by the compression spring. This preload assures compression between the two sections of the rotational joint. The compression prevents looseness; it also assures that the joint always acts as a column in compression, with no bending moment on the paddle shaft when side loads are applied.

This work was done by William C. Jones and Lester J. Owens of **Kennedy Space Center.** *For further information, Circle 61 on the TSP Request Card.*

This invention is owned by NASA, and a patent application has been filed. Inquiries concerning nonexclusive or exclusive license for its commercial development should be addressed to the Patent Counsel, Kennedy Space Center [see page A8]. Refer to KSC-11004.

Isoelectric Leukocyte Focusing

A modification of standard isoelectric focusing procedures provides a reproducible separation of peripheral leukocytes.

Marshall Space Flight Center, Alabama

There is an increasingly urgent need in the fields of immunology and genetics for a successful technique to separate and characterize morphologically-similar, but functionally-different, peripheral leukocytes. Common separation techniques involve centrifugation, a process that takes its toll on cell viability. Isoelectric focusing techniques have been commonly applied in the separation of soluble macromolecules, but are not generally used for the separation of viable cells. A new modified electrophoretic separation procedure yields 70 to 80 percent viable cells for small-scale immunologic and clinical profiling.

Leukocyte layers are removed from whole blood preparations previously subjected to conventional erythrocyte sedimentation techniques. The separation leukocytes are washed several times in RPMI-1640 tissue culture medium containing 25 mM Hepes buffer, are counted, and are suspended in a small volume of midpoint gradient solution immediately before their addition to the fractionation column.

Unlike conventional electrophoretic techniques that use an isotonic buffer of physiologic pH, isoelectric focusing uses a nonionic density gradient solution of dextran 40 and an appropriate ampholine or polyaminopolycarboxylic acid mixture. Dextran 40 acts as a cell-surface stabilizer and tends to prevent lysis. Ampholine mixtures will produce pH density gradients as broad as 3 to 10 and as narrow as 2.5 to 4. Cathode solution, gradient solution, suspended cells, additional gradient solution, and anode solution are added sequentially to a previously detergent-washed, siliconized, and alcohol-sterilized 110-ml mechanical-gradient device. An antibiotic solution of penicillin-streptomycin is added to all four solutions to maintain sterility.

In order to achieve optimal viscosity, the temperature is maintained at 7° C by pumping refrigerated water through the outer and inner cooling jackets of the device. A small (4-mA) constant current is passed through the column, and after the voltage reaches a maximum of 1,200 V, the current flow gradually decreases and stabilizes around 1 to 1.5 mA. The pH gradient is fully established, the system is stabilized, and separation is complete in 24 to 48 hours. Electrophoresis is discontinued at that time, and 4-ml fractions of the graded preparation are collected as rapidly as possible under sterile conditions. The third or fourth collection exhibits the pH of the true ampholine gradient. Subsequent collections show smooth and regular decrements in pH until the anode solution is reached. In addition, there is an associated distribution of polymorphonuclear leukocytes, eosinophils, and subpopulations of lymphocytes.

The specific gravity of each fraction is determined from a standard curve that is prepared from the refractive index of each fraction. Results from routine Wright staining procedures and the measurements of protein concentration and enzyme (LDH) activity are used to characterize the cells in each fraction. Trypan blue staining procedures, in conjunction with cuture growth, the measurement of O_2 uptake, and the incorporation of labeled precursors are used to assess the viability of the cells. Fluorescent antibody staining is performed to determine the kinds and amounts of immunoglobulins present on the cell surfaces in the various fractions. Immunologic characteristics of the separated subpopulations of lymphocytes are studied, using hyperimmunization techniques with suspensions of sheep erythrocytes (SRBC) and immunization procedures with mycobacterium tuberculosis (PPD) and human serum albumin (HSA). All reagents and preparations used in the separation and characterization procedures are commercially available.

This work was done by Esther M. Leise of Georgetown University for **Marshall Space Flight Center.** *For further information, Circle 62 on the TSP Request Card.*

Inquiries concerning rights for the commercial use of this invention should be addressed to the Patent Counsel, Marshall Space Flight Center [see page A8]. Refer to MFS-23271.

Compact Prosthetic Hand

Reduced weight and increased flexibility result from redesign and rearrangement of components.

Caltech/JPL, Pasadena, California

Prosthetic hands are similar in many ways to the remote manipulators developed to handle hazardous materials and to perform complex operations from a distance, as on satellites. Based on experience with these manipulators, NASA has sponsored the design of an improved prosthetic that combines well-known and accessible components in a novel way to produce a more compact and usable device.

Three independent movement-producing mechanisms are rearranged within a single housing to reduce weight and bulk. Worm gears are substituted for spur gears to reduce size and to allow the drive mechanisms to be self-locking. Finally, by rearranging the motor and the speed reducer, there is continuous swiveling of the hand around the wrist axis, yet the grasping members can retain their grip without regard to wrist rotation or tilt.

These features are achieved by the arrangement of the mechanisms as shown in the illustration. For instance, continuous rotation about the wrist is possible and does not interfere with the hook because there are no mechanical or electrical cables to become entwined. Wrist motion is effected by a swivel motor connected through a series of four worm gears (only the first and last are visible in the illustration) to a rotatable frame on which the hooks and hook gears are mounted. However, the hook motor and drive train are on the axis of wrist rotation, making hook movement and position independent of the wrist rotation.

The hook is driven by two opposed worm gears that engage another worm gear in the axial drive train. The hand is supported in a yoke that permits tilt 90° to each side of the centerline. The yoke also operates with a series of worm gears, not visible in the view of the drawing.

This work was done by Wolfgang A. Mann and Gordon A. Wiker of **Caltech/JPL.** *For further information, Circle 63 on the TSP Request Card.*

Inquiries concerning rights for the commercial use of this invention should be addressed to the Patent Counsel, NASA Resident Legal Office-JPL [see page A8]. Refer to NPO-13906.

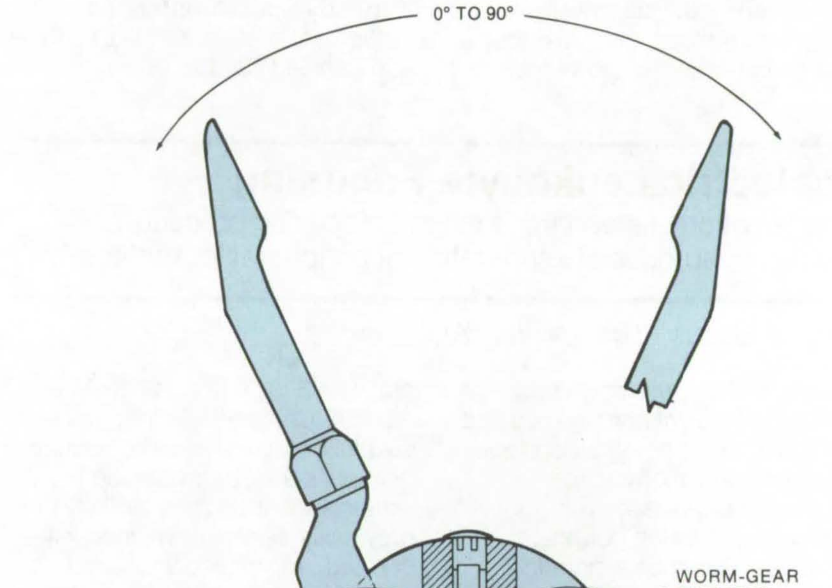

The **Compact Prosthetic Hand** combines tilt, wrist-rotation, and grasping mechanisms in a single housing. For wrist rotation, the housing remains stationary while the swivel motor drives a rotatable frame (shown in color). The main body of the device is about 15 cm long and 7.5 cm in diameter.

Dual-Purpose Laboratory Cage/Antenna

Part of a steel cage enclosing laboratory animals is used as an antenna to transmit biotelemetry data over short distances.

Langley Research Center, Hampton, Virginia

It is difficult, if not impossible, to transmit data via RF radiation through a metal container which is enclosed on all sides, as in experiments using laboratory animals in which the animals are confined in a steel cage. In one such laboratory experiment using bioelectronics to feed data outside the cage, a new technique is used in which the cage itself becomes the transmitting antenna.

Body-implanted electronics, which consist of two frequency-modulated telemetry systems, are used to encode animal ECG and body-temperature data and then to transmit the data via the cage to external receivers. One transmitter is used per body function. The data are collected by using two independent broadcast-band FM receivers which demodulate the signals and route them to bioelectronic analog signal processors.

A slot-pickoff method of transmitting data to the receivers is employed. Each section of the two-section antenna is 2 in. (5 cm) wide by 33 in. (83 cm) long. The antenna sections are connected at an angle of 135° to conform to cage geometry. The slot is located on one longitudinal wall of the cage which acts as one side of the electrical interface with other laboratory equipment and personnel.

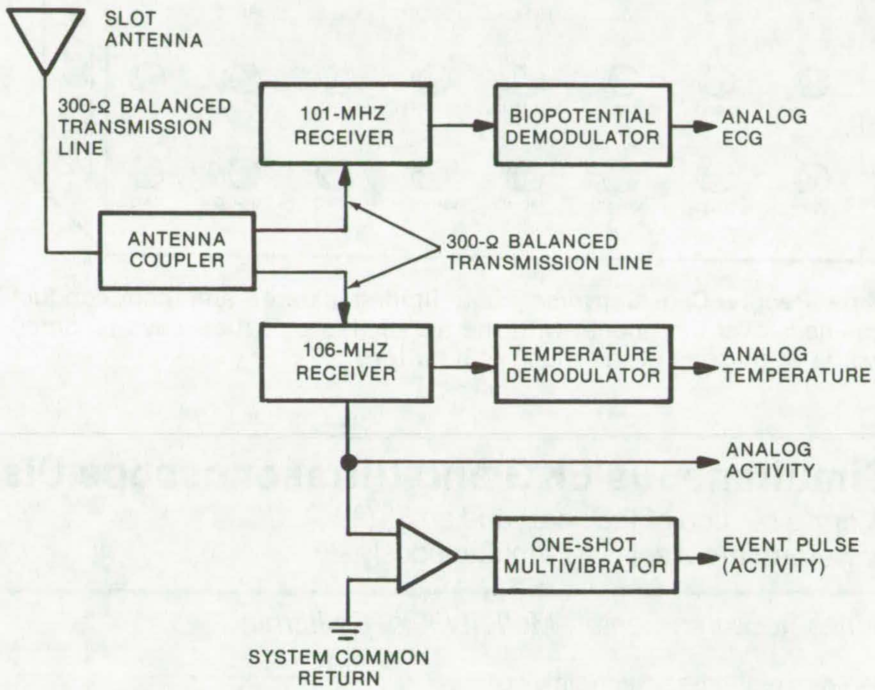

In the receiver portion of the **Laboratory Biotelemetry System,** both frequency-modulated signals are intercepted by a common antenna, split at the coupler, and processed to recover analog data via two separate receiver/demodulators. The receiving and signal-processing equipment are physically located above ground potential to avoid transmission-path difficulties.

The slot pick-off is isolated by series capacitors to the coaxial-transmission line. The entire telemetry system is isolated from ground potential via insulating material. System readout consists of a derived-AGC counter which, besides being mounted (above ground potential like the other equipment), is also isolated via a separate power supply.

This work was done by B. H. LaLande of Northrop Corp. for **Langley Research Center.** *For further information, Circle 64 on the TSP Request Card.*
LAR-11587

Record-Player "Voice" for Mutes

Words and phrases from record or tape player, selected by pushbutton, make conversation possible.

Marshall Space Flight Center, Alabama

A record player that reproduces a voice saying various words or phrases enables a mute person to answer the telephone and to carry on limited conversations. As indicated on the console in the illustration, pressing various buttons causes the unit to say particular words or phrases. For example, button A can trigger the phrase "How are you?" Button B can produce "I'm fine, thanks"; button C,

(continued on next page)

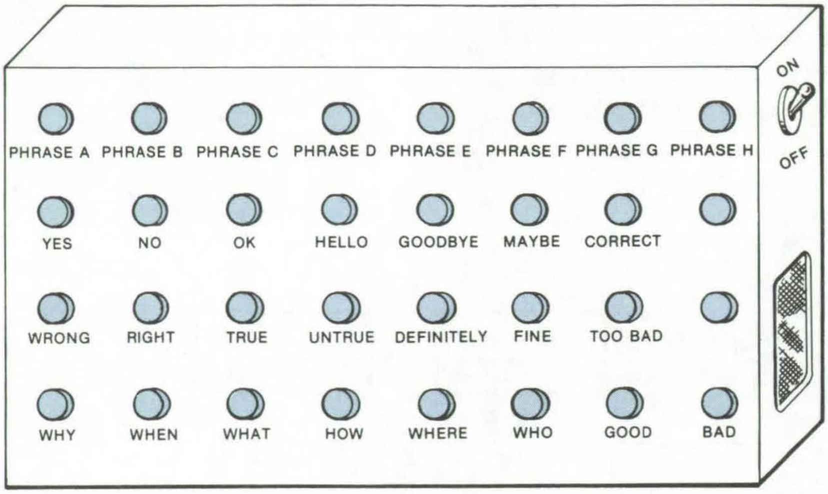

Mute People Can Converse to a limited extent, and can conduct business over the phone, with the aid of this unit that plays recorded words or phrases at the touch of a button.

"Nice day today"; and so forth.

When a button is pressed, a phonograph arm with needle drops at a selected point on a revolving record disk and then withdraws as soon as the word or phrase has been sounded. Alternatively, an appropriate tape reel system, such as those in some computer memories, can be used for accessing the desired message quickly and accurately.

This work was done by Sidney L. Hamilton of **Marshall Space Flight Center.** *No further documentation is available.*
MFS-21592

Simultaneous EKG and Ultrasonoscope Display

A cross section of the heart and an EKG waveform are displayed simultaneously.

Ames Research Center, Moffett Field, California

A new real-time system simultaneously displays a two-dimensional image of the heart and an EKG waveform on a cathode-ray screen (Figure 1). Thus, dimensional changes of the heart can be continuously compared with the EKG waveform.

The apparatus combines EKG monitoring with appropriate logic and an ultrasonoscope. A combination of digital and analog gating circuits for controlling display sequence permits two separate but simultaneous displays. The displays are made to appear simultaneous by the use of high-persistence phosphor on the face of the oscilloscope tube.

The ultrasonoscope utilizes a linear array of ultrasonic transducers to project sequenced acoustic pulses toward the patient's heart and to receive the echo pulses. EKG signals are derived from two input electrodes and a reference electrode, attached to the patient. The vertical axis in Figure 1 represents the position of the active transducers, and the horizontal axis represents time delay or depth.

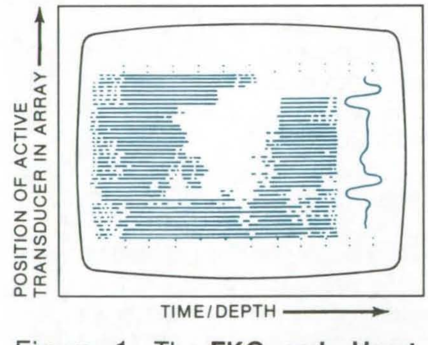

Figure 1. The **EKG and Heart Profile** are displayed together in real time. This simultaneous display allows continuous comparison of dimensional changes in the heart and the periodicity of the EKG waveform.

Figure 2 is a block diagram of the system. A master clock provides timing for both the ultrasonic and EKG portions. A sequencer controls the order and timing of the ultrasonic measurements and controls a depth-mark generator that creates depth-reference marks at the top and bottom of the display. The ultrasonic pulses are processed by a receiver, fed to the oscilloscope circuit, and displayed along with the depth marks. This portion of the circuit is essentially a conventional C-scan ultrasonoscope.

EKG measurements are controlled by a special EKG-logic circuit that receives timing signals directly from the master clock and receives other control signals from the sequencer, a staircase voltage generator, and a sweep generator. This logic circuit acts as a gate to control both the EKG-monitor circuit and the internal oscilloscope circuitry to provide sequenced display intervals for the ultrasonic and EKG images.

The ultrasonic image is generated in 48 milliseconds, while a complete EKG signal requires 1 full second. To overcome this problem, the EKG-logic circuit produces different-length display intervals for the two types of signals. This is accomplished by using interconnected one-shot pulse generators to produce pulses that control analog gates for both the sawtooth sweep generator signal and a staircase voltage signal. The outputs of the EKG-logic circuit trigger the EKG measurements via the monitor circuit and control the display via the receiver and sweep generator.

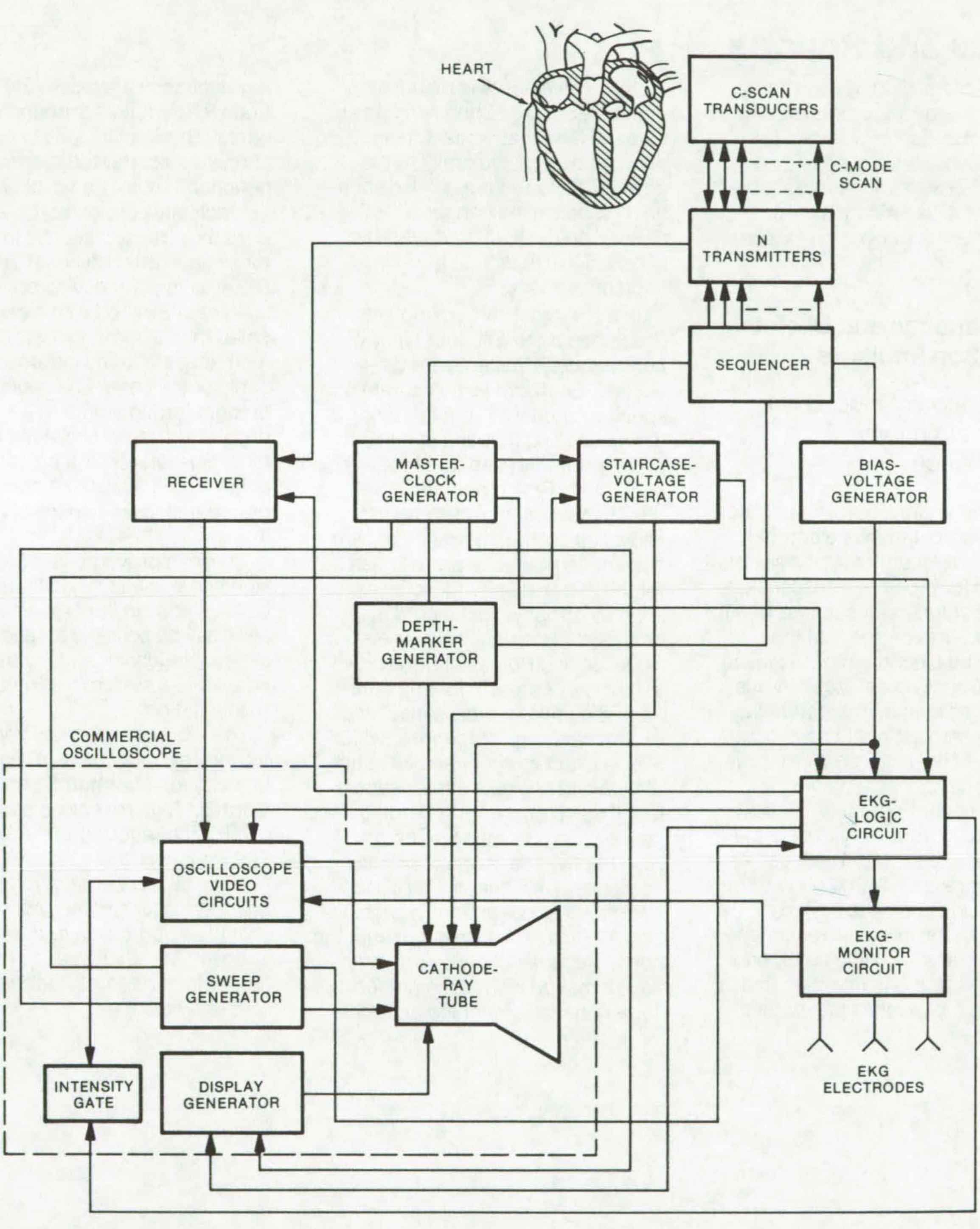

Figure 2. The **EKG and Ultrasonoscope** simultaneous display system includes an EKG-logic circuit coupled to the oscilloscope. The heart image information is displayed during a first timing interval; an EKG trace is displayed during a second timing interval.

This work was done by Robert D. Lee of **Ames Research Center.** *For further information, Circle 65 on the TSP Request Card.*

This invention is owned by NASA, and a patent application has been filed. Inquiries concerning nonexclusive or exclusive license for its commercial development should be addressed to the Patent Counsel, Ames Research Center [see page A8]. Refer to ARC-11137.

Books and Reports

These reports, studies, and handbooks are available from NASA as Technical Support Packages (TSP's) when a Request Card number is cited; otherwise they are available from one of NASA's Industrial Application Centers or the National Technical Information Service.

Percutaneous and Skeletal Biocarbon Implants

Modification of biocarbon implants improves performance.

Several improvements have been made in percutaneous electrical connectors, or buttons, and skeletal implants for prosthetic suspension. The first criterion for successful percutaneous passage is that the material be biocompatible. Clinical investigations reveal that vitreous carbon has unique characteristics from the standpoint of tissue compatibility. The major problem, however, remains mechanical.

New magnet-core biomedically pure carbon buttons eliminate the drawbacks associated with earlier connector systems that grew down into the skin and were buried by the subcutaneous tissue or remained at the skin surface only to catch on clothing, leading to infection and drainage around the base of the button. The magnet is mounted in the center of the button and has an external lead that centers itself when brought in close proximity to the device. It allows for a quick disconnect, should a sudden force be exerted on the lead, and thereby avoids skin irritation at the skin/implant interface.

In a review of carbon implants developed by NASA, four types of percutaneous implants are discussed. Each serves a separate and specific function. Type I permits generalized distribution of current and is primarily used for chronic pain relief. Type II permits more direct application of current and allows for greater tolerance of high current densities. Its primary use is for the stimulation of muscles weakened by atrophy, spinal cord injury, or stroke. Type III has a wire electrode leading from the button down to a nerve or muscle for implantation. The entire button is insulated except for the tip of the wire, which allows exact motor or sensory stimulation and avoids a defuse stimulus. It can be used for recording nerve action potentials (electromyography) and is an important component in a sensory feedback system for upper extremity prostheses. The implant does not disrupt the nerve sheaths nor cause any irritation or malfunction of the nerve. Type IV has a larger bipolar lead terminating in a wraparound electrode that is sutured around the nerve. This implant aids in a process of muscle contracture correction by peripheral motor nerve stimulation.

Medically pure carbon is also used as a transcutaneous interface for skeletal attachment of prostheses. The implant device consists of a stainless-steel rod with a carbon collar that is cemented with methylmethacrylate to the intramedullary canal of the bone. The implant is brought through the skin with an unpolished carbon collar as an interface. Suspension of a prosthesis is achieved via a quick-disconnect device that locks into the shaft of the implant.

These improvements could be of significant use to rehabilitation centers and similar organizations. It also may be possible to modify the sensory feedback system and to adapt it to a system of remote manipulation.

This work was done by Vert Mooney of Rancho Los Amigos Hospital for **Marshall Space Flight Center.** *To learn how to obtain a copy of the report, Circle 66 on the TSP Request Card.*

Inquiries concerning rights for the commercial use of this invention should be addressed to the Patent Counsel, Marshall Space Flight Center [see page A8]. Refer to MFS-23666.

Mechanics

Improving Efficiency of Existing Air-Conditioning

Inexpensive duct-work change improves hot-and-cold deck air-conditioning units.

Goddard Space Flight Center, Greenbelt, Maryland

Heating and cooling energy costs can be reduced in facilities using two or more air-conditioning units supplying hot-and-cold deck or multizone air-conditioners. These systems mix heated and cooled air to heat or cool an area to a desired temperature. As conventionally hooked up, air is both cooled and heated in both the summer and the winter, without regard to the indoor and outdoor temperatures.

The energy costs of reheating cooled air can be eliminated by tying all the cold decks to one air-conditioning unit and all the hot decks to another unit. The reconnections can be accomplished easily, especially when the units are near each other, as is usually the case. The connections can be best understood from Figures 1 and 2, which compare the conventional and improved arrangements for summer and winter cycles.

In the conventional summer arrangement (Figure 1), outside air in the conventional system is first cooled; then part of it is reheated. The cooled air and the reheated air are combined in a mixing box and used to cool the building. In the revised system, the hot-air distribution ducts from two units are hooked to the reheat coil directly, without being cooled first. The cold air from both units is cooled and passed directly to the mixing box, without reheating.

Further savings may be realized by using the return air (which is generally cooler than outside air in the summer) as the input to the cold deck and by using the hotter outside air as input to the hot deck.

In the winter (Figure 2), the hookup is similar, except the warmer return air is heated instead of cooled as in the summer arrangement. If the outside temperature is

(continued on next page)

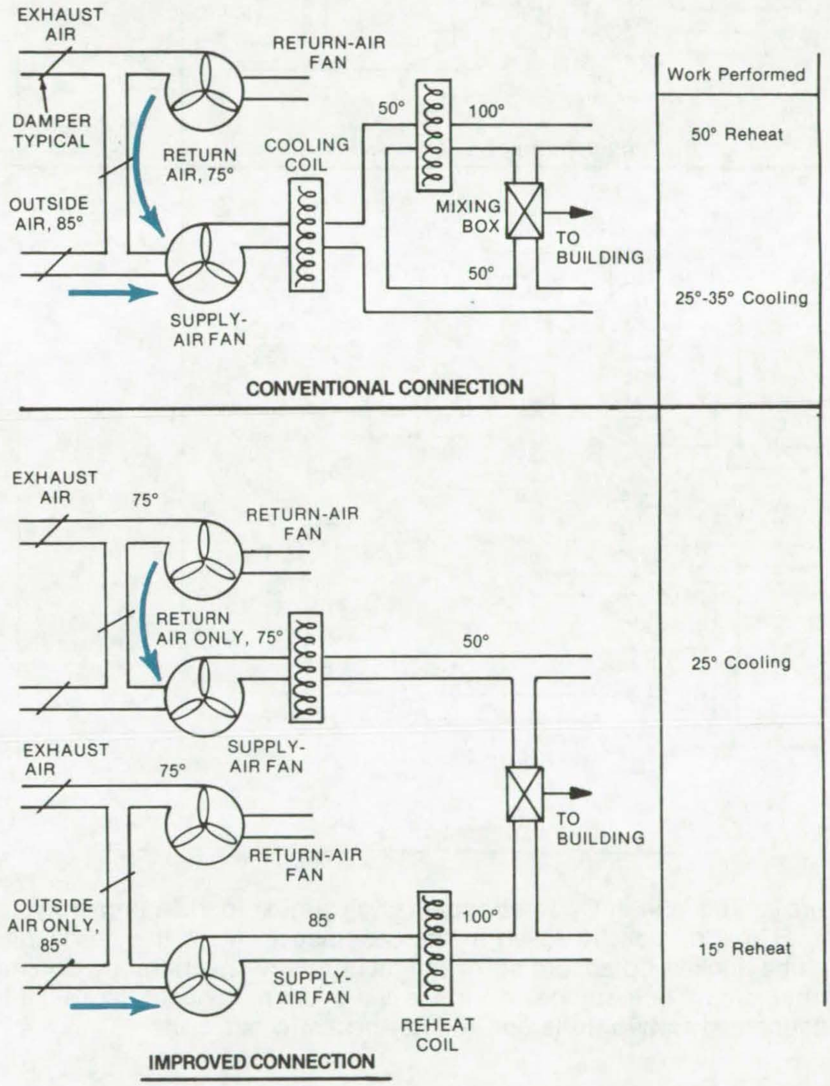

Figure 1. The **Summer Cycle** hookup of hot-and-cold deck air-conditioners avoids reheating cooled air. In the case shown above, heating and cooling savings amount to from 25° to 45° F, depending on the amount of fresh/recycled air mixing that would have been set with the conventional system. Savings are greater for hotter temperatures.

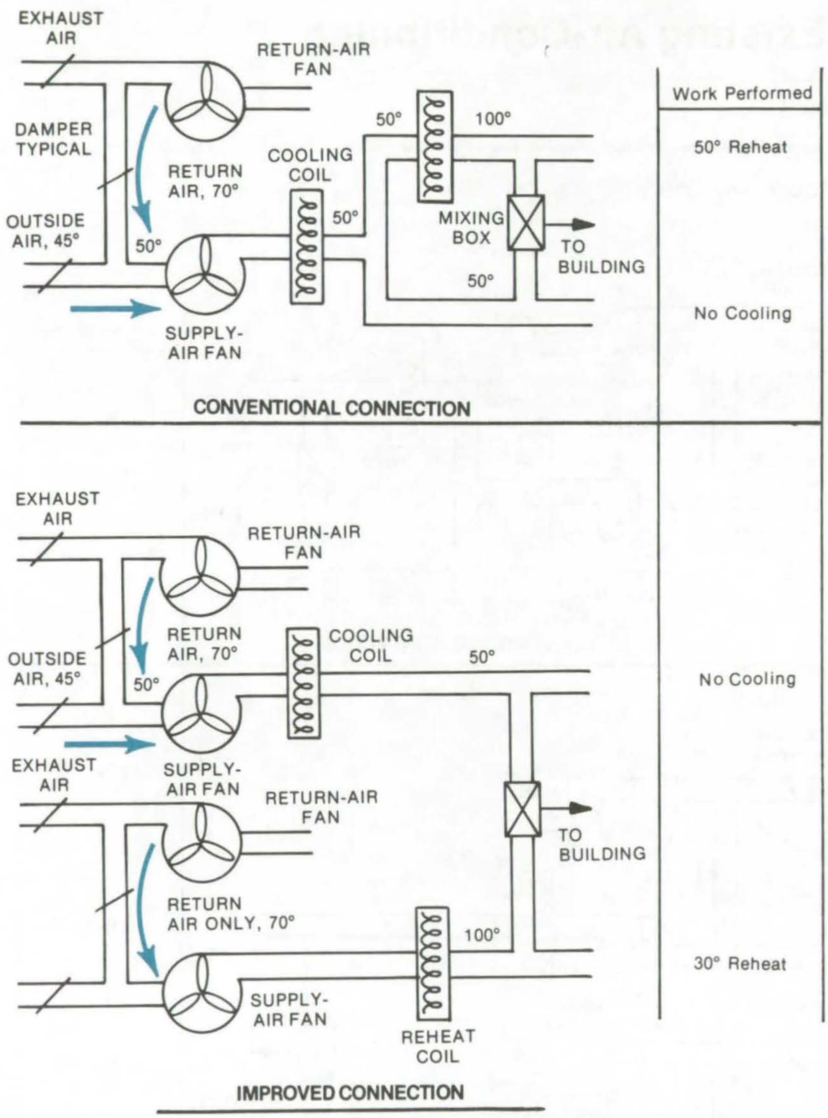

Figure 2. The **Winter Cycle** arrangement is similar to the summer cycle; a 30° F heating cost is saved in the case above. More than two units could be hooked up according to the local relative heating and cooling requirements. For instance, in a three-unit system, the cold decks could be connected to two units and the hot decks to one unit.

not so low as to freeze the cooling coils, the air to be cooled may be taken from the outside; otherwise it must be mixed with the return air. In any case, it is never necessary to reheat previously cooled air.

The resultant energy savings are easily possible with two or more units only, because a single unit does not have the two supply fans needed. Of course, manufacturers could incorporate the fans and other energy-saving measures in new units, but the simple alteration could save substantial energy costs in facilities with existing systems.

This work was done by Henry D. Obler of **Goddard Space Flight Center.** *No further documentation is available.*
GSC-12217

Absorption Generator for Solar-Powered Air-Conditioner

Matching generator temperature
to collector efficiency helps cut costs.

Marshall Space Flight Center, Alabama

Generators for absorption-cycle residential air-conditioners pose a problem when they are used in solar-powered systems instead of gas-fired systems. The generators are designed to operate with water at 210° F (99° C). Most solar collectors that would heat the water in a solar-powered system do not function efficiently at that high temperature.

Now, a new generator has been developed that uses water at a somewhat lower temperature — 185° F (85° C). Because solar collectors absorb more heat from the Sun at this temperature, the overall collector area can be decreased,

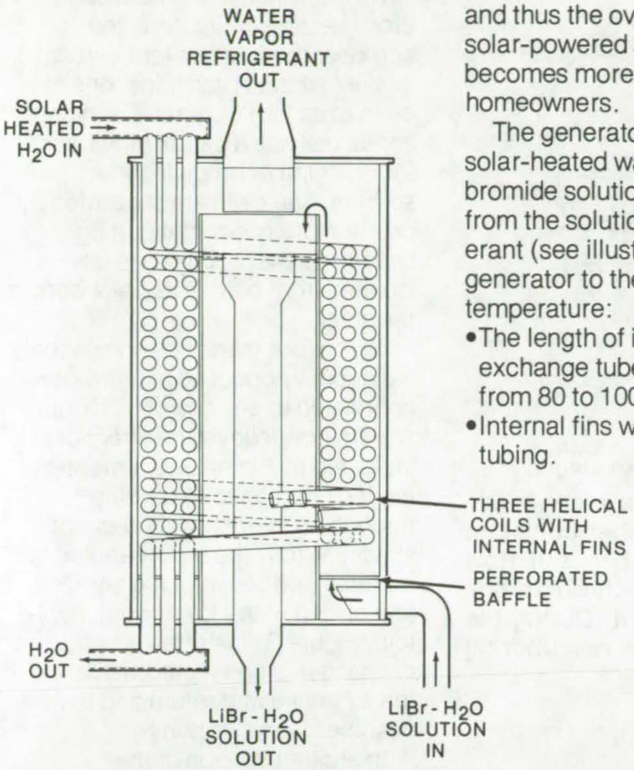

The **Low-Temperature Absorption Generator** passes solar-heated water through coils. Hot LiBr/H_2O solution leaves through a central standpipe, and water vapor leaves through a refrigerant outlet at the top. The generator is 23 in. (58 cm) high.

and thus the overall cost of the solar-powered air-conditioner becomes more attractive to homeowners.

The generator transfers heat from solar-heated water to a lithium bromide solution, evaporating water from the solution for use as a refrigerant (see illustration). To adapt the generator to the lower operating temperature:

- The length of its coiled heat-exchange tubes was increased from 80 to 100 ft (27 to 33 m).
- Internal fins were added to the tubing.
- A baffle was added to the tank to increase the turbulence of the LiBr solution as it flows through the coils, thereby increasing the heat transfer.

The overall air-conditioning system includes the modified low-temperature generator, a new solid-state control system, flat-plate collectors, an insulated steel storage tank, and a cooling tank. The system is designed to maintain 78° F (25.5° C) temperature in a 1,000-ft^2 (93-m^2) house for a 98.25-percent design outdoor summer temperature of 94° F (34.5° C).

This work was done by D. J. Lowen and J. G. Murray of Chrysler Corp. for **Marshall Space Flight Center.** *To learn how to obtain further information, including detail drawings of the generator and specifications for the overall system, Circle 67 on the TSP Request Card.*

Inquiries concerning rights for the commercial use of this invention should be addressed to the Patent Counsel, Marshall Space Flight Center [see page A8]. Refer to MFS-23417.

Removing CO_2 and Moisture From Air

Foamed-aluminum blocks act as a passive heat exchanger to improve efficiency.

Lyndon B. Johnson Space Center, Houston, Texas

In an improved closed-cycle atmospheric scrubber, the levels of carbon dioxide and water vapor are reduced without affecting the temperature of the airstream. The exchanger draws impurities from the air without additional heaters or auxiliary equipment, and it collects the impurities for removal to an outside site. Chemical filters and desiccants and the like are thus not required. The exchanger operates as two subsystems: One-half collects CO_2 and H_2O from the airstream while the other, having already absorbed impurities, is desorbed via a vacuum pump; the pump purges the products to an external environment. Sorption and desorption require about 30 minutes, at the end of which time the subsystem halves are alternated.

The major improvement in this system is the integral incorporation of a passive heat exchanger. Sorption generates heat, and desorption requires heat. The role of the heat exchanger is to transfer heat from the half of the scrubber that is in the sorption cycle to the half that is in the desorption cycle. This improves the overall efficiency of the process and helps to maintain the airstream at a constant temperature.

The scrubber is a stack of horizontal cells connected to a valve system that switches alternate cells from the sorption to the desorption cycle. The sorbing material is typically polyethyleneimine-coated inert granules. The heat exchanger is a foamed-aluminum matrix in which the granules are dispersed; the matrix "fills" the cell but occupies only 4 percent of its volume. The aluminum is an excellent heat conductor and absorbs heat from (or transfers heat to) neighboring cells to help achieve an isothermal condition throughout the scrubber.

In one version, foamed aluminum is cut into blocks as thick as 2 in. (5 cm) in the heat-transfer direction. The material, with a compression strength of 800 psi (5.5×10^6 N/m^2), is a reticulated network of duodecahedrally configured spaces. All the spaces are interconnected, and the metal defining the edges defines a continuous-wire network.

(continued on next page)

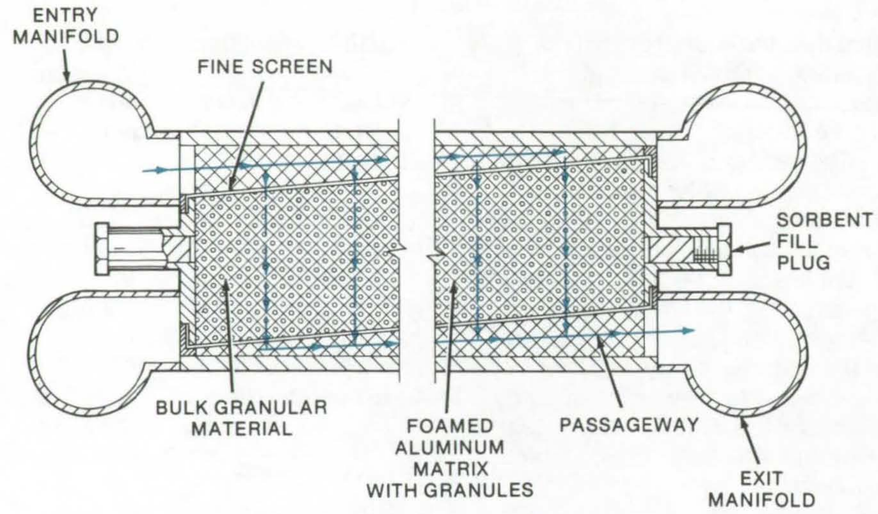

Figure 1. A **Horizontal Cross Section of One Cell** of the regenerable exchanger shows the flow through the cells. The exchanger consists, typically, of four such cells stacked on top of one another, but flow isolated. The airflow, as shown by the arrows, is in through one manifold and out through the diagonally opposed manifold. During the sorption cycle, the foamed aluminum conducts heat to neighboring cells where it is used in the desorption cycle.

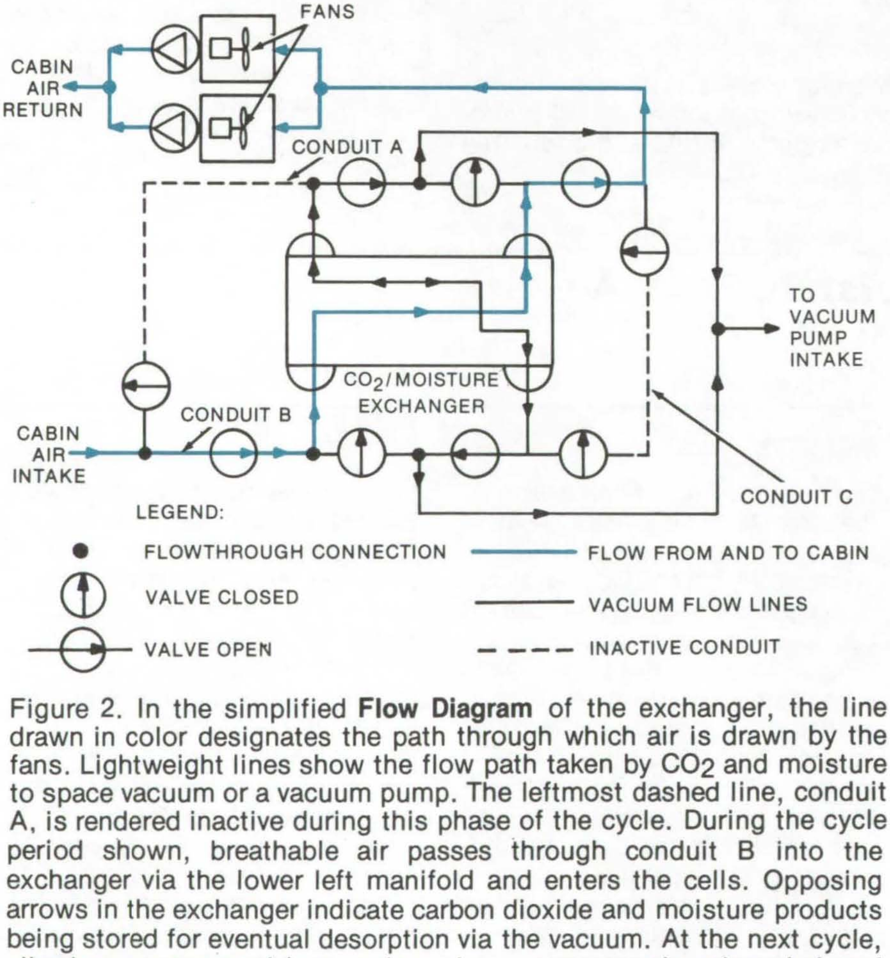

Figure 2. In the simplified **Flow Diagram** of the exchanger, the line drawn in color designates the path through which air is drawn by the fans. Lightweight lines show the flow path taken by CO_2 and moisture to space vacuum or a vacuum pump. The leftmost dashed line, conduit A, is rendered inactive during this phase of the cycle. During the cycle period shown, breathable air passes through conduit B into the exchanger via the lower left manifold and enters the cells. Opposing arrows in the exchanger indicate carbon dioxide and moisture products being stored for eventual desorption via the vacuum. At the next cycle, all valves are reversed (e.g., valves shown open are closed, and closed valves are opened). Cabin air then flows into the exchanger via conduit A and exits via conduit C; conduit B is deactivated. The bottom half of the exchanger desorbs via the pump.

As illustrated in the horizontal cross section in Figure 1, the scrubber module has four vertical intake/exhaust manifolds, one at each of its four corners. Each horizontal cell has a pair of filler necks for charging or emptying the sorbent. The cells are separated by one or more horizontal parting sheets, so that each cell is flow isolated from both of its neighbors in the stack.

Of the four manifolds shown, only a diagonally opposed pair are flow connected to any one cell. The airstream flow follows the directions indicated by the arrows, entering at the top left manifold, passing through an internal wedge-shaped space, across the bulk granular material and between the screens, and exiting at the lower right manifold. Figure 2 illustrates how the exchanger is connected via valves to the air intake and return and to the desorber (vacuum pump).

In another version of the scrubber, the heat exchanger is a series of wavy fins fabricated from aluminum. One fin lies inside each cell in the plane of the cell. Otherwise, the scrubber operates in the same manner as the one described above.

This work was done by Edward H. Tepper of United Aircraft Corp. for **Johnson Space Center.** *For further information, Circle 68 on the TSP Request Card.*

This invention is owned by NASA, and a patent application has been filed. Inquiries concerning nonexclusive or exclusive license for its commercial development should be addressed to the Patent Counsel, Johnson Space Center (see page A8). Refer to MSC-14771.

Transducer for Ultrasonic Inspection of Porous Materials

Nondestructive test technique for materials with high acoustic loss

Lyndon B. Johnson Space Center, Houston, Texas

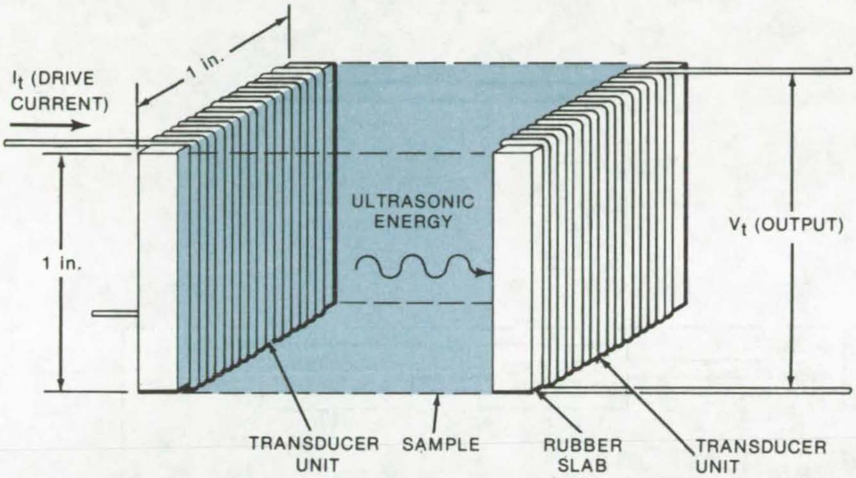

Figure 1. **Electronic Transducers** are shown as used to excite and detect ultrasonic signals in a porous test specimen. The drive current, modulated with the input electronic signal is converted to ultrasonic energy. This radiated strain wave propagates through the specimen and is converted to a voltage signal by the output transistor.

Low-density porous materials (e.g., high-temperature surface insulation) may be inspected for cracks by using newly-prepared electrodynamic or echo ultrasonic transducers. The electrodynamic transducer (see Figure 1) consists of many turns of fine wire bonded to the surface of a solid rubbery elastomer slab. The slab thickness is one-half the ultrasonic wavelength and has the same ultrasonic properties as water. Ultrasonic energy is generated by the slab in response to electronic signal input through the wire.

Porous samples are tested by using two electrodynamic transducer units placed on opposite sides of the sample. One unit transmits ultrasonic energy into the sample; the other receives this energy for visual display and analysis.

The echo transducer, on the other hand, is built to transmit and receive as a single unit. It comprises a piezoelectric array of 25 elements. The elements are bar shaped and are placed parallel to each other as shown in Figure 2. The array is placed in contact with the sample, and the elements are driven lengthwise by electronic signals to generate ultrasonic pulses. Energy reflected inside the sample is detected by the elements and is fed to the recording equipment. Transmission and reception are alternated.

The echo transducer includes mechanical damping by the use of neoprene rubber slabs bonded to each side of the elements. In addition, electrical damping is provided by matching (approximately) a series L-R-C circuit with a shunt inductor and a shunt resistor. Both of these measures help to damp the transducer vibration quickly so there is no interference in detecting the echo signals.

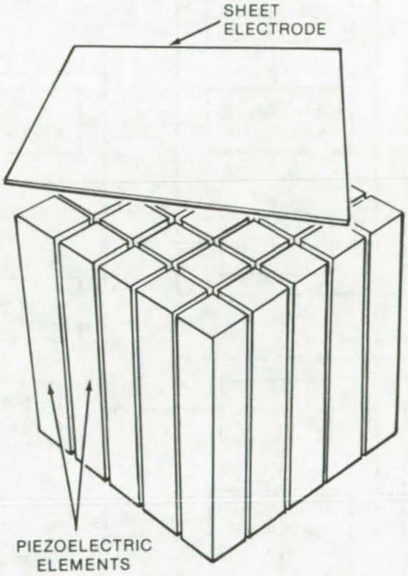

Figure 2. A **Transducer Array** is shown with a sheet electrode partially removed. The array is 7/8 in. (2.2 cm) on a side and consists of 25 elements connected in parallel by a 1-mil (0.0025-cm) steel sheet.

This work was done by George A. Alers and Robert B. Thompson of Rockwell International Corp. for **Johnson Space Center.** *For further information, Circle 69 on the TSP Request Card.*
MSC-19671

Differential Sound-Level Meter

Acoustical-channel gains are compared to measure difference between sound-pressure levels.

Langley Research Center, Hampton, Virginia

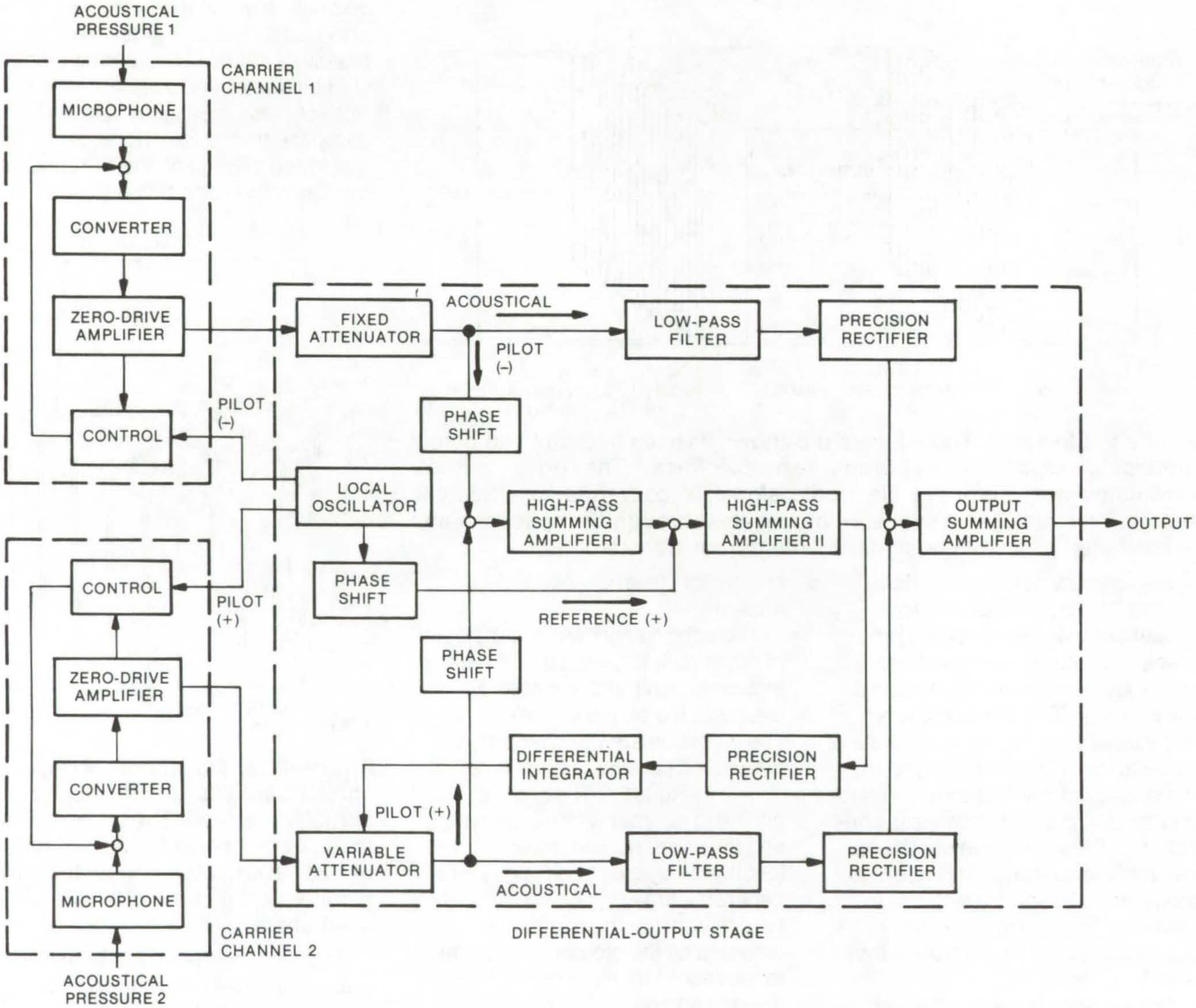

The Differential Sound-Level Meter consists of three basic components: carrier channels 1 and 2 and a differential output stage. The differential output stage is composed of conventional electronic circuits, tailored to this particular application.

The relative difference between sound-pressure levels at two different microphone sites is measured precisely with a circuit that continuously monitors the gains of the two acoustical channels. The difference between two pilot voltages is utilized in a regulating loop to force the gain of the second channel to track the gain of the first channel.

The carrier channels, as shown in the block diagram, convert instantaneous acoustical pressures into analog electrical signals. In each carrier channel, an acoustical pressure within the frequency band of 1 to 5 kHz causes variations in the capacitance of the condenser microphone. The converter produces an electrical current proportional to the instantaneous change in microphone capacitance. The zero-drive amplifier produces an output voltage proportional to the converter current.

The control circuit serves two purposes: It automatically keeps the converter optimally tuned to the carrier frequency to compensate against long-term drift in the static

capacitance of the microphone, and it also permits calibration of the carrier channel by means of an insertion voltage. This insertion voltage produces an output signal similar to that generated by the presence of sound at the microphone.

In the differential output stage, the acoustical signals from the outputs of the zero-drive amplifiers pass through the fixed attenuators, low-pass filters, and precision rectifiers to appear at the input of the output summing amplifier (in channel 1, as a positive direct voltage proportional to the incident acoustical pressure of channel 1, and in channel 2, as a negative direct voltage proportional to the incident acoustical pressure of channel 2). The precision rectifier outputs are summed at this point, and the output voltage of the output summing amplifier is proportional to the difference between the acoustical pressures at the microphones.

The gains of the two carrier channels will be continuously changing, primarily because the response of a condenser microphone is highly sensitive to variations in ambient conditions. This apparatus incorporates automatic gain regulation to lock the gain of channel 2 to that of channel 1 at all times. The regulating mechanism is based upon the insertion of pilot voltages of equal magnitude into the two carrier channels and comparing their magnitudes at the outputs of the attenuators. The difference between pilot voltages is used to regulate the variable attenuator of channel 2.

The local oscillator generates the pilot voltages, typically at 17 kHz, and the signals entering the two carrier channels are 180° out of phase with each other (positive and negative, respectively). The oscillator also provides a reference voltage of positive phase, at the input of the second stage of the high-pass summing amplifier, which is rectified and used to establish the reference attenuation of the variable attenuator for the matched condition. The phased (negative and positive) pilot signals are applied to the inputs of the control circuits and pass through the circuitry to the input of summing amplifier I.

The two pilot signals are summed at the input of the first stage of the high-pass summing amplifier where they are phase inverted. The negatively-phased pilot signal of channel 1, after inversion, adds to the reference signal; the positively-phased pilot signal of channel 2 subtracts from it. The pilot signals are summed to the reference signal at the input of the second stage of the high-pass summing amplifier. The composite signal is rectified in the precision rectifier and is applied to the differential integrator, at which output a direct voltage controls the level of attenuation of the variable attenuator. The phase-shift networks permit precise adjustment of the phases of the pilot and reference signals relative to one another.

If the pilot signals are equal at the summing point, they cancel, the reference signal alone controls the variable attenuator, and the two channels are matched. An increase in the pilot signal of channel 1 tends to increase the output of the variable attenuator; an increase in the pilot signal of channel 2 tends to decrease it. The response to a change in either pilot signal is directed toward a compensating change at the output of the variable attenuator. The differential integrator drives the variable attenuator until the difference in pilot signals is zero.

This work was done by Allan J. Zuckerwar of Old Dominion University for **Langley Research Center.** *For further information, Circle 70 on the TSP Request Card.*

Inquiries concerning rights for the commercial use of this invention should be addressed to the Patent Counsel, Langley Research Center [see page A8]. Refer to LAR-12106.

Life-Test Methodology for Mechanical Components

Accelerated life tests for instances where the number of parts is too small for statistical testing

Marshall Space Flight Center, Alabama

A methodology for predicting the service life of mechanical components for space applications with life requirements of up to 10 years may be applied to many other long-life mechanical components.

Conventional life-testing procedures are frequently impractical for components with expected lifetimes over a year. The common alternative, statistical reliability analysis based on relatively-short duration testing of large numbers of component samples, may be equally impractical due to the unavailability of the required numbers of samples. Another approach can be applied to hardware with life requirements greatly exceeding practical testing times by assuming that all hardware items meet specified material and tolerance requirements.

The methodology itself is based on examining and testing each part of the item under evaluation to determine whether aging processes, wear, or other inherent failure modes are likely to limit life to less than that required. The most significant advantage of the procedure is its ability to identify inherent design and material deficiencies.

The essential elements of the methodology are:

- Establish the component life cycle, which includes construction, testing, and storage; the environments to which it will be exposed; and the complete operating conditions such as cycle rate, temperatures, pressures, loads, and vibration.

(continued on next page)

• Forecast possible failure mechanisms, and identify the life-limiting parts by using the life-cycle information, including design and operational requirements.
• Perform an experimental failure analysis on a component subjected to a short-term normal duty cycle followed by a more severe duty cycle, with examination after each cycle for incipient failure.
• Develop a list of most-probable "critical" failure mechanisms, based on the forecast and failure analysis.
• Devise and conduct short-term accelerated life tests for each critical failure mechanism. Specific tests may cover low-cycle and high-cycle fatigue; metallic wear and corrosion; nonmetallic creep, wear, and aging (for which special test methods have been developed); radiation damage; and other mechanisms as applicable. During these tests, it is necessary to avoid unrealistically high stress factors.

This methodology has been demonstrated, using miniature needle valves as an arbitrarily-selected hardware component. Results are expected to be at least as reliable as those obtained from full-lifetime testing.

This work was done by Keith F. Dufrane and David B. Hamilton of Battelle Memorial Institute for **Marshall Space Flight Center.** *For further information, Circle 71 on the TSP Request Card.*
MFS-23082

Accurate RF Field Monitoring in Shielded Enclosure

Use of two separated sensing antennas averts errors due to reading of null caused by resonance.

Lyndon B. Johnson Space Center, Houston, Texas

In measurements using radio-frequency fields, such as measurement of the susceptibility of a dielectric, it is desirable to use the same field intensity at each test frequency. The RF field is produced by a transmitting antenna and is normally monitored by a receiving antenna at some fixed point. However, if the test is performed in a shielded enclosure (as is often done to avoid electromagnetic interference), the radio-frequency waves bounce back and forth and set up spatial resonances with nulls at various points in the enclosure.

When a null happens to occur at the sensing antenna, the indicated value of field strength is much lower than the average value throughout the enclosure. Therefore, if the input power level is set to give some particular field strength at the sensing antenna, the average field strength becomes far higher than intended. The sample of material under test is made large enough to respond to the space-averaged intensity, but because of the possibility of a null, this average level may not be the same at every frequency if it is monitored by the single antenna.

If a second sensing antenna is located elsewhere in the enclosure, it will give an accurate indication of average field intensity when the first sensor happens to be nulled. The arrangement for susceptibility testing shown in the figure illustrates the use of two sensing antennas equidistant from the power source. Power is fed into the enclosure via the transmitting antenna and is adjusted to provide the desired field level at the higher-reading sensor.

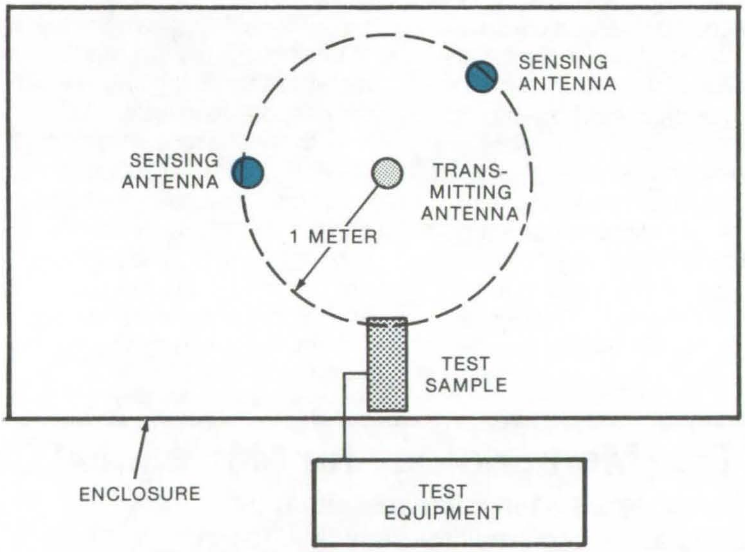

Test arrangement for **Radiated Susceptibility Measurements** has two sensing antennas for monitoring the RF field produced in the shielded enclosure by the transmitting antenna. The transmitter is adjusted to the minimum power that provides the desired field intensity at the higher-reading sensor.

Using the reading of the higher antenna avoids nulls, is simpler than moving a single antenna, and is accurate to within a factor of 2 (6 dB) produced by possible field reinforcement. This procedure meets the requirements of MIL-STD-461/2.

This work was done by Alfred P. Schmidt of Honeywell Inc. for **Johnson Space Center.** *For further information, Circle 72 on the TSP Request Card.*
MSC-16325

Infrared Temperature Maps of EHD Lubrication

Separate contact-surface and oil-film temperatures in an elastohydrodynamic conjunction

Lewis Research Center, Cleveland, Ohio

A more accurate and reliable infrared technique has been developed for separately mapping the contact-surface temperature and the average oil-film temperature in an elastohydrodynamic (EHD) conjunction. The technique uses an infrared detector with two specially-selected infrared filters. One filter permits mapping the contact-surface temperature; the second filter permits mapping the oil-film temperature. The technique aids research.

Elastohydrodynamic lubrication occurs between heavily-loaded moving surfaces with small contact areas, such as rolling-element bearings, mating gear teeth, and cams and followers. The contacting surfaces are separated by very thin films of oil under very high pressure. Breakdown of these films can cause damage to the contacting surfaces and failure of the contacting parts. The breakdown of these films is believed to be related to the temperatures within the contact region.

The apparatus used for mapping contact-area temperatures is shown in the figure. A conventional four ball bearing tester is equipped with a temperature-controlled lubricant supply system. A transparent sapphire flat is placed in contact with the test ball and weighted. The test ball is rotated against the weighted sapphire flat to produce an elastohydrodynamic conjunction. An infrared microscope detector with a spot size resolution of 38 μm traverses the contact area to map the infrared radiation and hence the temperature.

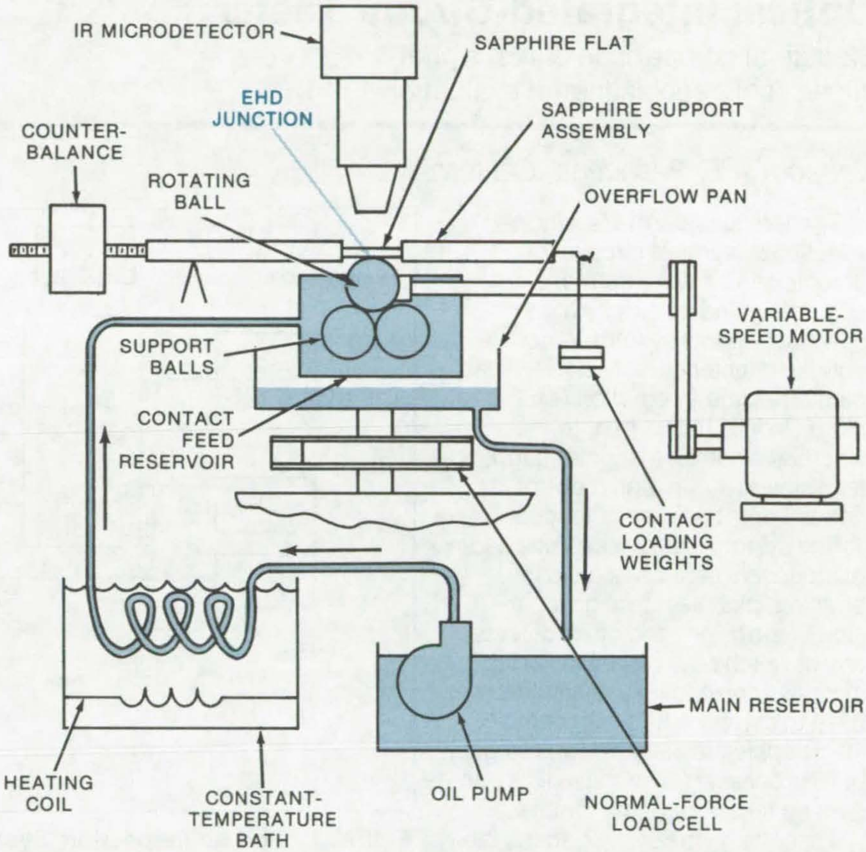

The **Sliding EHD Test Apparatus** for mapping contact-area temperatures includes a conventional four-ball bearing tester and a temperature-controlled lubricant system. An elastohydrodynamic (EHD) conjunction is created at the interface between a test ball and a sapphire flat.

The temperatures of the oil film and the ball contact surface are obtained individually by using two infrared filters. Each filter permits a specific bandwidth of infrared radiation to pass through to the detector. One filter (a wideband filter) covers a bandwidth in which the oil film is transparent and does not emit and which thus allows mapping the ball contact-area temperature. The second filter (a narrow-band filter) covers the emission band of the oil film and allows mapping the oil-film temperature. The narrow-band filter analysis is considerably more complicated than the wideband filter analysis since the spectral characteristics of lubricating oils vary with the oil chemistry. However, by calibrating the system for the effects of temperature and film thickness on emissivity, reliable determination of the oil-film temperature is obtained.

Using this technique, steady-state temperatures have been mapped at maximum pressures of 148,000 and 219,000 psi (1.05×10^9 and 1.51×10^9 N/m^2), sliding speeds ranging from 13.7 to 500 ips (0.35 to 12.7 m/s), with a lubricant supply temperature of 104° F (313 K). The temperatures mapped agreed with theoretical predictions.

An additional advantage of this technique is the ability to measure the local transient temperatures produced by high spots or asperities on the contacting surfaces. The thickness of elastohydrodynamic lubricating films is frequently not much greater than the height of surface asperities; thus asperities are vulnerable sites for initiation of surface wear or failure.

(continued on next page)

This work was done by David M. Sanborn and Ward O. Winer of Georgia Institute of Technology for **Lewis Research Center.** *Further information may be found in NASA CR-134882 [N76-10477], "Investigation of Lubricant Rheology as Applied to Elastohydrodynamic Lubrication," a copy of which may be obtained at cost from the New England Research Application Center [see page A7].*
LEW-12685

Optical Integrated-Circuit Tester

Statistical comparison of test signal allows more sophisticated evaluation.

Caltech/JPL, Pasadena, California

The tedious task of visually inspecting integrated circuits for defects can be done far more accurately and quickly by a computerized optical system. A computerized tester can check a typical medium-scale-integration (MSI) circuit in less than a minute, whereas a human inspector might take several hours and may not notice faults because of fatigue.

The system examines IC chips for microscopic scratches, voids, bridging, pinholes, foreign inclusions, corrosion, and other defects, any of which could eventually result in catastrophic failure. It also can be used to compare IC's with photolithographic masks at various stages of IC processing. Defective IC's can then be taken out of the process.

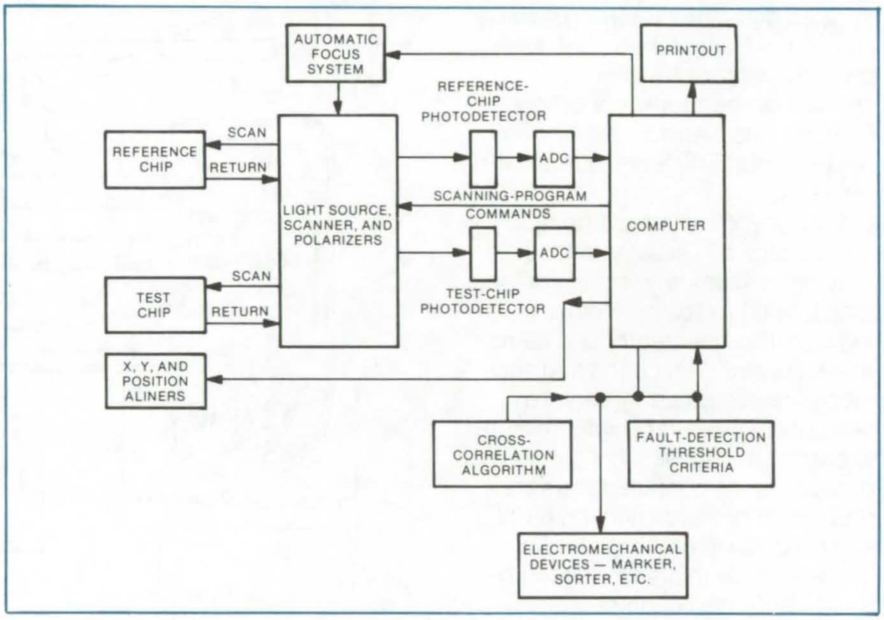

Figure 1. The **IC Inspection System** optically scans a reference chip and a test chip and statistically compares the reflected images to detect faults. The reference chip is mounted on a microscopelike stage that can also be manually rotated in the X-Y plane. The test chip is mounted similarly but is connected to a computer-controlled positioning motor to aline the chip in response to the scanning data.

Essentially, the system scans the circuit to be tested with a narrow beam of light at the same time it scans the reference chip. The light reflected from each IC is detected and converted into analog signals that are digitized for input to a minicomputer (see Figure 1). The computer compares the data from the test circuit with that from the reference circuit and decides whether any faults are present.

The chips are not compared point by point, because of the precise alinement required and the difficulty in distinguishing significant variances from those not related to chip faults. Instead, the computer uses a cross-correlation technique that detects statistical differences in dark or bright distributions. The statistical difference indicates the degree of dissimilarity between a given area on the reference chip and the scanned area on the test chip. Fault-detection criteria are stored in the computer so that it can decide whether the areas are dissimilar enough to disqualify the test chip.

The light source for the system is a high-intensity mercury lamp. Light from the source is directed to the two IC's by a lens system, which also directs reflected light from the IC's to photodetectors (see Figure 2). The light beam is deflected by galvanometer-driven mirrors so that it scans the IC's in the X and Y directions. The scanning spot size is adjustable between 2.5 and 7.5 μm.

A polarizing beam splitter separates the source beam into two beams by reflecting horizontally polarized rays and transmitting vertically polarized rays. One beam goes to the test chip, and the other to the reference circuit. A system of polarizers changes the polarities of the reflected beams to ensure that they are transmitted to the photodetectors.

The system automatically alines the test chip for inspection according to commands from the minicomputer, based on position information supplied by the optical scanner.

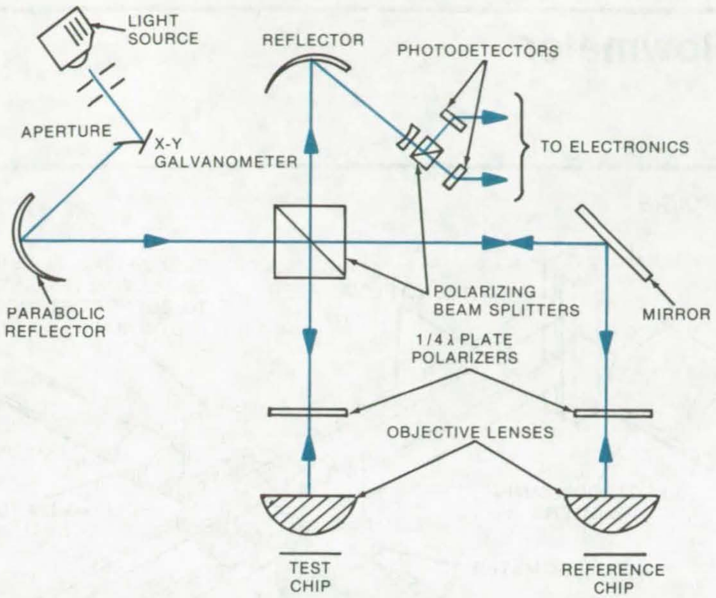

Figure 2. The **IC Optical Scanner** divides the light-source beam into a horizontally polarized component and a vertically polarized component, using a polarizing beam splitter. The horizontal component is deflected downward to the test IC, and the vertical component passes through to the reference. The reflected light from both will have passed through a quarter-wave plate before returning to the beam splitter, reversing polarization and causing the beam splitter to direct both beams to the detector. A final polarizer separates the reference and test beams.

This work was done by Ernest A. Micka, and Rollin K. Reynolds of **Caltech/JPL.** *For further information, Circle 73 on the TSP Request Card.*

Title to this invention, covered by U.S. Patent No. 3,909,602, has been waived under the provisions of the National Aeronautics and SpaceAct [42 U.S.C. 2457(f)], to the California Institute of Technology, Pasadena, California 91102.

NPO-13282

Particle Impact Noise Detection [PIND] Test

An acoustical nondestructive test technique for sealed and semisealed devices

Lyndon B. Johnson Space Center, Houston, Texas

An ultrasonic transducer, a detector, and a visual display are used in a nondestructive test technique to determine the presence (or absence) of foreign particles in industrial-grade and commercial-grade hybrid electronic devices having cavities. The test apparatus utilizes a number of conventional devices and subsystems, combined to form this diagnostic apparatus. Compared to previous PIND methods, the new, more-sophisticated test is easier to use, offers greater sensitivity to smaller particles, and shows improved repeatability of test results.

In the updated PIND test method, a water-soluble ultrasonic couplant is applied to the transducer, instead of a chemical bonding agent or double-sided masking tape. (The original ultrasonic couplant used was either DRC AVC-9, or equivalent, or double-sided masking tape. The ACV-9, however, an excellent sound-wave couplant, presented a cleaning problem when removing it from the devices under test. Double-sided masking tape is convenient, but it lacks sound-wave transmitting properties.)

A means has also been found to reduce the effects of static electricity on test results. Initially, a screwdriver was used to tap the device under test to free particles held by static electricity. A nylon rod 0.25 in. (0.63 cm) in diameter and 6 in. (15 cm) long is now used. A rubber tip first used to impart shock impulses to the device under test is replaced by a steel tip covered with a thin coating of Hysol DK4-03 (or equivalent). This latter material does not absorb the shock pulses as the rubber tip did.

When it was determined that static electricity is more prevalent at lower frequencies, the test frequency was increased from 40 to 60 Hz. Likewise, the applied acceleration was increased from 6 to 8 G's. Additionally, a 1-hour bake cycle at 85° C preconditions the devices to reduce further the effect of static electricity.

This work was done by Wilson Reilly of The Singer Co. for **Johnson Space Center.** *For further information, Circle 74 on the TSP Request Card.*

MSC-16208

Dynamic Calibration of Flowmeter

Noninterfering flowmeter is calibrated for oscillating flow.

Langley Research Center, Hampton, Virginia

In the investigation of the causes of longitudinal instabilities of aerospace launch vehicles, there had long been the need for a noninterfering flowmeter capable of measuring the magnitude of small perturbations in the flow velocity of the liquid propellant. Meters have been developed which, ideally, should have the same sensitivity to the oscillating component of flow velocity as to uniform flow velocity. Dynamic calibration of a flowmeter is complicated, however, by the difficulty in producing a fluid flow having an oscillating component of flow velocity of known magnitude. A dynamic calibration technique for flowmeters has been developed and tested whereby the fluid flows through the meter at a constant velocity while the flowmeter is forced to oscillate relative to the fluid.

The basic components of the test apparatus are illustrated in Figure 1. The flowmeter is supported in line with the fixed supply pipe by means of wide flex springs which permit only axial motion of the flowmeter. The apparent perturbation frequency of the fluid is the resonant symmetric bending frequency of a tunable spring-mass system consisting of a pair of parallel rectangular bars clamped to the flowmeter and movable masses clamped to the bars. The bars and masses are sized to give the lowest frequency of interest when the masses are positioned at the ends of the bars and the system is excited in the lowest symmetric bending mode. Higher calibration frequencies are obtained by sliding the masses inward and/or exciting a higher symmetric bending mode. The sinusoidal exciting force is provided by an electrodynamic exciter attached to one of the bars at a vibration antinode. The dynamic component of the fluid velocity relative to the flowmeter is determined from the output of an accelerometer attached to the flowmeter.

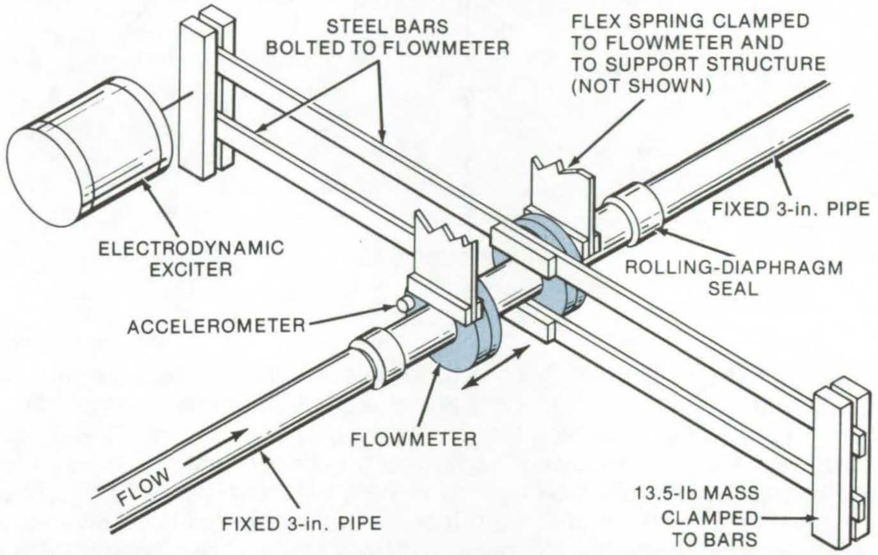

Figure 1. The **Dynamic Test Apparatus** for flowmeters is used to check measurements of the oscillating component of fluid flow by oscillating the flowmeters rather than the fluid. Flowmeters are vibrated by an exciter attached to the meters through steel bars. Flex springs (extending beyond the cut-off length shown above) restrict rotational movement of the meters, but allow axial movement.

Care must be exercised in the design of the seals between the axially oscillating flowmeter and the stationary supply pipes to prevent excessive leakage, friction, and pumping. Coulomb friction would not only increase the driving force required of the exciter but would distort the accelerometer output signal, rendering it impossible to obtain an accurate measurement of the perturbation velocity. The design illustrated in Figure 2 circumvents all of these difficulties by the use of Bellofram (or equivalent) rolling-diaphragm seals. These seals are long-stroke, deep-convolution, rubberized diaphragms which roll off the piston sidewalls onto the cylinder sidewalls with a continuous nearly frictionless motion. An auxiliary axial guide must be used with the seals as they provide no radial support.

As the pipe attached to the flowmeter is moved axially, the seal convolution acts as a piston, displacing fluid as it moves. This pumping action between the two seals would ordinarily result in an incremental flow velocity of unknown magnitude through the meter. If, however, the shoulder A is one-half the width of the convolution B, the volume of the chamber immediately to the right of the convolution will

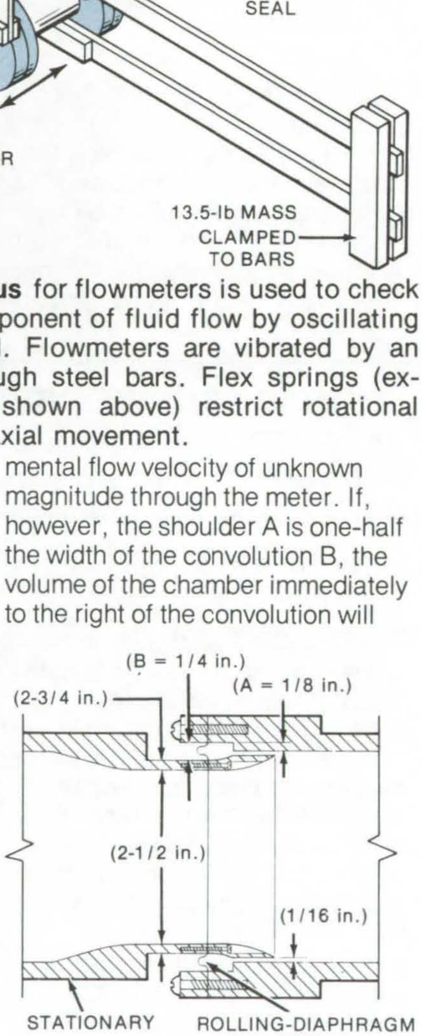

Figure 2. The **Rolling-Diaphragm Seals** allow the flowmeters to move relative to the fluid. Fluid pumping that might otherwise occur is virtually eliminated by the choice of relative widths of the shoulder, A, and the seal convolution, B.

remain virtually constant throughout the travel, thus eliminating the pumping.

The apparent perturbation velocity as indicated by a flowmeter (using the static calibration constant) was compared to the velocity determined from the accelerometer output at several amplitudes of oscillation and at several discrete frequencies between 7 and 30 Hz. Agreement was excellent.

This work was done by Robert W. Herr and David S. Vann of **Langley Research Center.** *For further information, Circle 75 on the TSP Request Card.*
LAR-12023

Inexpensive Mass Flowmeter

Force on a target in a moving fluid is measured to determine flow rate.

Marshall Space Flight Center, Alabama

The mass flow of fluids, such as water, oil, gasoline, and kerosene, can be measured directly with a simple flowmeter. Most of the parts for the flowmeter are available off-the-shelf, and the only component requiring special design and fabrication is a combination lever arm and diaphragm. Furthermore, a given target will be useful with many types of fluids and flow rates. The drag force on the target is measured by strain gages joined to a beam connected to the target. The strain-gage reading can then be used to determine the flow rate.

The flowmeter, as illustrated, is constructed from pipe fittings, strain gages, and a target. Moving fluid exerts a force on the target that depends on the fluid velocity head, the target area and drag coefficient, and the fluid density. The force on the target is transferred outside the flow tube by a lever arm with an integrally machined diaphragm.

At the external end, the lever arm is connected to a cantilever beam on which the strain gages are mounted. The diaphragm serves two purposes. It acts as a fulcrum for the lever, and it seals the flowmeter. The diaphragm is machined on the rod at a position and with a thickness that results in a full-scale deflection of the cantilever at rated flow.

The meter should be designed so that the expected stresses on the lever diaphragm are in a repeatable range for the lever material used. In a design prototype, there was a 2-mV output per 1 V excitation of the bridge. With the voltage limited to 10 V, the maximum design flow in the meter produced a 20-mV output.

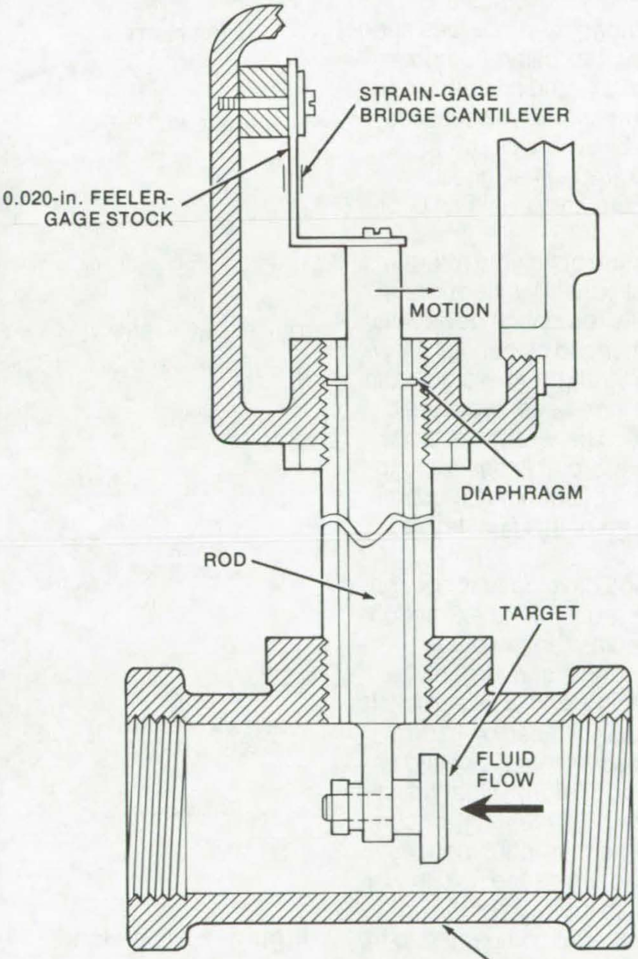

The **"Target" Flowmeter** measures drag of a body with a known drag coefficient to determine flow rate. Drag on the target is transferred by a cantilevered arm to a fully active strain-gage bridge.

This work was done by Harlan S. Harman of **Marshall Space Flight Center.** *For further information, Circle 76 on the TSP Request Card.*

Inquiries concerning rights for the commercial use of this invention should be addressed to the Patent Counsel, Marshall Space Flight Center [see page A8]. Refer to MFS-23528.

Quantitative Measurement of the "Feel" of Fabric

A new methodology and apparatus measure "handle" —
a property related to flexibility, pliability, and compressibility.

Langley Research Center, Hampton, Virginia

Increased activity in the research, development, and application of flexible materials for structural purposes has created a requirement for a quantitative measure of the textile concept "fabric hand," or "handle." Handle refers to the "feel" of a fabric, to properties such as drapability, flexibility, compressibility, foldability, and pliability, and it has been traditionally assessed subjectively by vision and touch. Nylon, for example, has good handle; a boardy material has poor handle.

The selection of flexible materials for use in balloons, decelerators, and inflatable aerospace devices is strongly influenced by handle. However, as the strength-to-weight ratio of materials increases, the handle characteristics generally become poorer. Therefore, it is desirable to have a means of obtaining a quantitative measure of this qualitative feature.

The method developed for quantifying handle requires the extraction of a flat, circular sample of the material through a convergent nozzle (see Figure 1). The sample is compressed and folded by extraction. The measurement is based on the hypothesis that the initial resistance to gathering, pleating, or compression of the material produces a pressure reaction on the nozzle wall, proportional to the ratio of the volume of material compacted to the respective nozzle volume at a point of interest. The integral of the axial components of these pressure reactions and their related friction forces is a measurable extraction force.

Laboratory tests made of numerous materials, with two test nozzles of different orifice size, yielded repeatable and predictable extraction

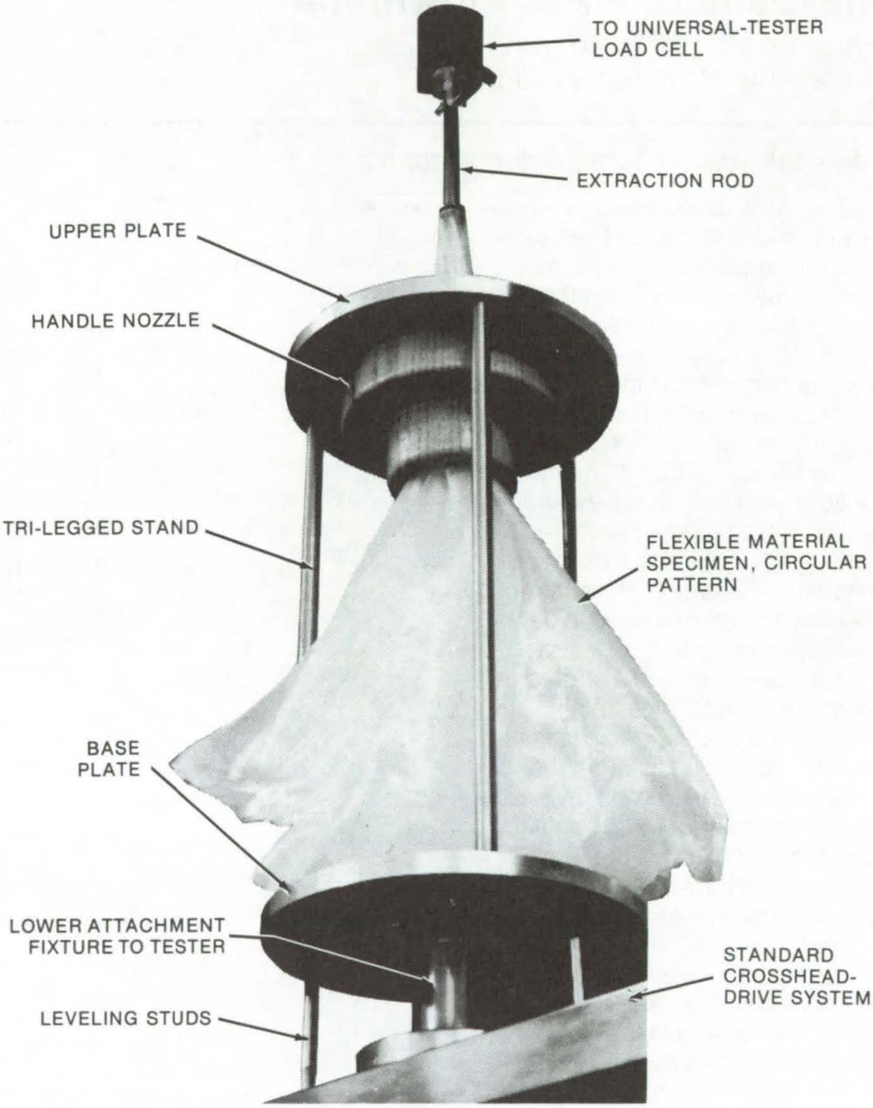

Figure 1. The **Handle Test** can be performed by drawing the test material through the apparatus shown above. A nozzle of a suitable diameter is placed in the upper ring plate of a tripod that is secured to a baseplate. The base of the tripod is attached to a load cell. The height of the apparatus is about 40 cm. A hole is cut in the center of the circular cloth specimen, allowing it to be attached to the extraction rod. The draped cloth is then drawn slowly through the nozzle, and force is plotted as a function of the extraction distance.

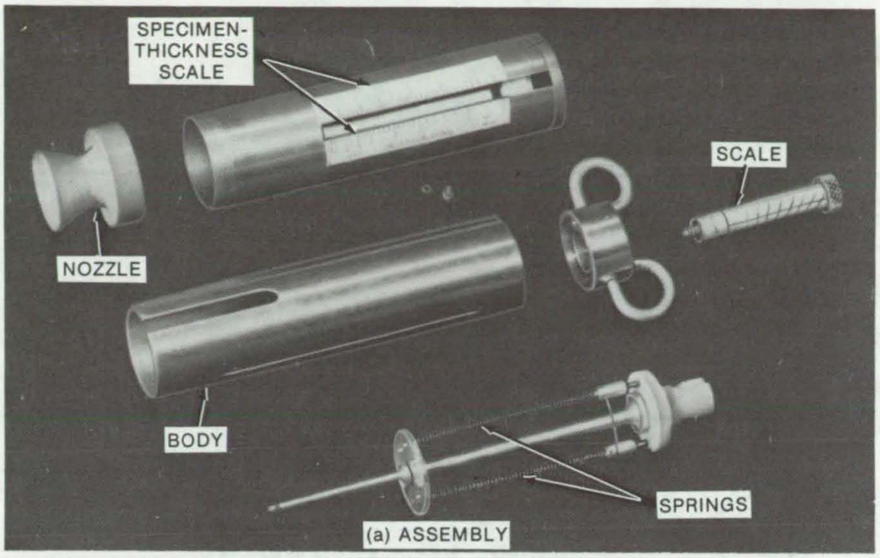

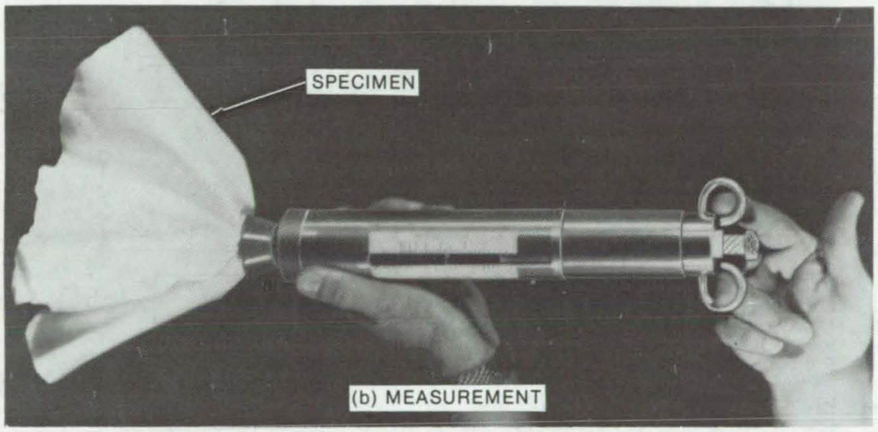

Figure 2. The **Handlemeter** is a portable device that takes advantage of the linearity (over a limited range of packing ratios) of the slope of the force-displacement curves measured with the apparatus in Figure 1. The meter consists of a set of nozzles with corresponding specimen-thickness scales, a telescoping body, and a finger grip/lock combination. A spring scale is used to measure the reaction force generated by expanding the telescoping body and causing the fabric to pass a prescribed distance through the nozzle. The product of the handle modulus and the effective thickness is read from the scale.

force-displacement curves and verified the basic hypothesis. The resultant force-displacement data are processed to yield the quantity termed "handle modulus." Dimensionless or relative handle characteristics are defined as the ratio of the handle modulus of the test material to the handle modulus of a reference material (nylon parachute cloth specified by MIL-C-7020).

A portable device for measuring handle, the "handlemeter," was developed (see Figure 2). It employs a set of nozzles of different sizes, to accommodate thin and thick materials, and a combination of springs to accommodate the full range of 3 orders of magnitude found for the handle moduli. Tests indicate that materials with handle modulus ratios in excess of 110 are not recommended for foldable, erectable, or inflatable applications and that packaging problems, crease damage, and repacking limitations occur at modulus ratios exceeding 40. Materials with ratios below 4.0 can be packaged repeatedly to high-compaction densities; and loose knits, nets, and meshes with handle modulus ratios as low as 0.2 are unencumbered in use from the geometric viewpoint.

Both a method and apparatus are now available for the quantitative measurement of fabric hand, and performance criteria can now be generated for research developments and procurement needs for a wide range of flexible materials, such as fabrics, knits, films, composites, and laminates.

This work was done by Vernon L. Alley, Jr., and Austin D. McHatton of **Langley Research Center.** *For further information, Circle 77 on the TSP Request Card.*

Inquiries concerning rights for the commercial use of this invention should be addressed to the Patent Counsel, Langley Research Center [see page A8]. Refer to LAR-12147.

Low-Power Anemometer

Alternate heating and measuring periods save power.

Langley Research Center, Hampton, Virginia

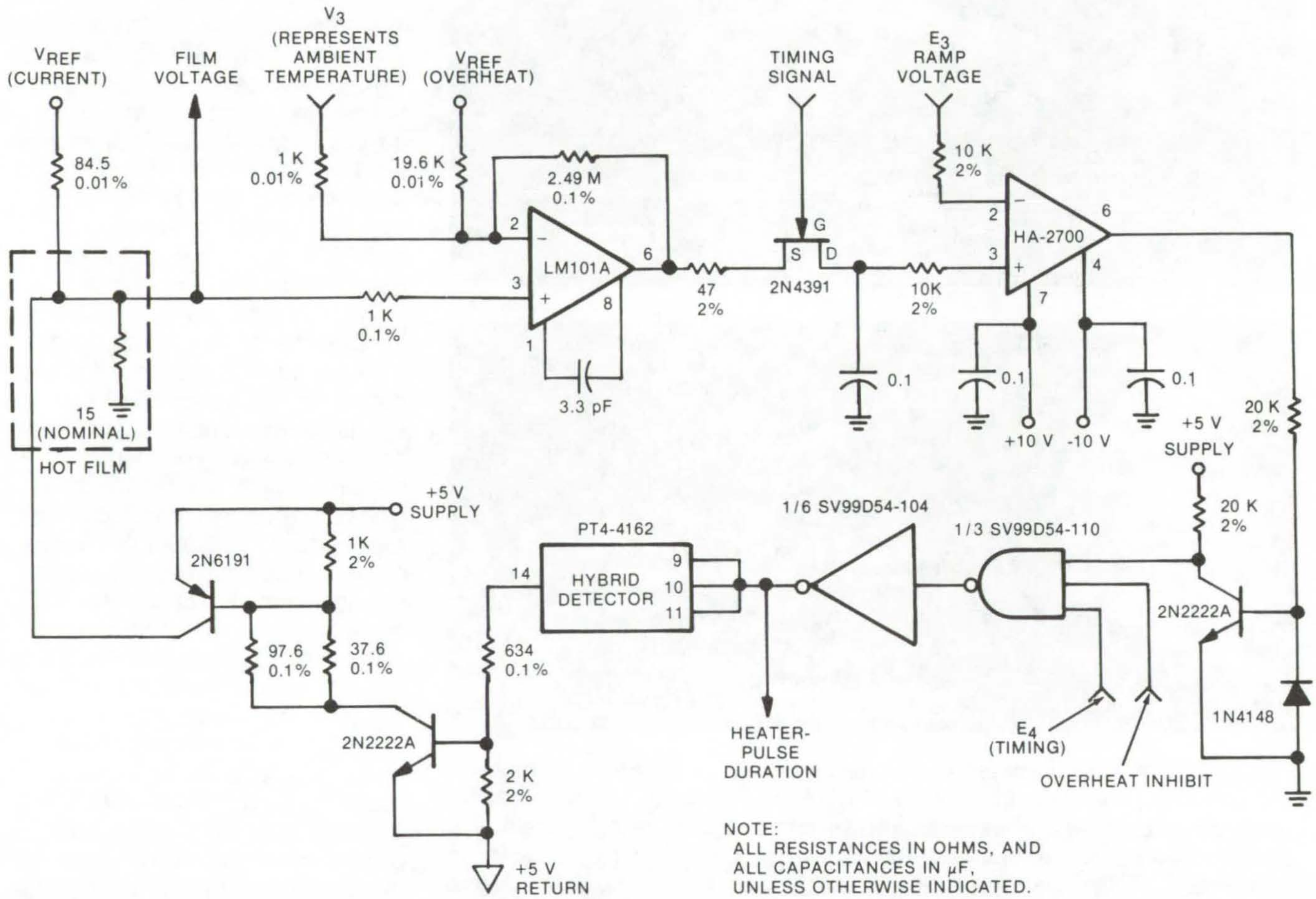

The **Anemometer Control Circuit** allows wind speeds to be measured with less power by alternating hot-wire or hot-film heating periods with measurement periods. In addition to the circuit shown, the system includes auxiliary circuits to generate V_{ref} and the ramp voltage (E_3) and reference half of the bridge circuit. The reference film has the same specifications as the measurement film, but it is operated at much lower current to avoid self-heating and save power. The reference-film output, after passing through a fixed-gain amplifier, is input above as V_3. The circuit permits the use of several sensing films with a common temperature compensating sensor.

Hot-wire or hot-film anemometers, commonly used to measure wind velocity, dissipate large quantities of power in their series resistors and in the linear amplifier that powers the bridge circuit. For this reason, they are not particularly suitable where power consumption is a prime consideration, such as on remote weather stations and ocean buoys.

These and other remote flow-sensing requirements are better fulfilled by a new low-power anemometer that alternates heating and measuring periods. This device further differs from conventional instruments in that heater power is applied to the hot wire directly rather than by heating the series resistors. Also, the linear amplifier is replaced with a pulse-width-modulated switching circuit that dissipates very little power.

Conventional hot-wire anemometers are fundamentally Wheatstone bridges with one element having a well-known and reasonably large temperature coefficient: the hot wire. The bridge is balanced if this element remains at a constant temperature (which is set to be well above ambient). If air flows by the hot wire, the element cools, and the bridge becomes unbalanced. A compensating voltage is applied to a power amplifier that raises the bridge voltage until it is balanced. The voltage across the hot wire is a measure of the electrical power applied, and thus of the thermal energy lost by cooling. This informa-

tion is used to calculate the wind velocity.

In the low-power anemometer, the illustrated circuit is used to alternate heating and measuring periods for a hot-film sensor. Timing is derived from a clock signal (E_4) that has a 500-Hz pulse-repetition rate and a 200-μs pulse width. During each pulse, the heater power is turned off and the voltage across the hot film is determined from its resistance; i.e., from its temperature and the current flowing through a selected series resistor (84.5 Ω) from a well-regulated reference voltage supply (3.200-V nominal). The hot-film voltage is compared with a voltage representing ambient temperature, augmented by an "overheat" increment which represents the temperature difference above ambient (supplied by V_{ref} and the 19.6K resistor). The voltages are compared in a high-gain amplifier that outputs 2.5 V per millivolt input, representing an approximately 1° C temperature error.

This output controls the duration of the heater pulse. It is compared with a ramp-voltage pulse that begins at 0 V at the end of the measuring period, and rises to 3 V by the end of the heating period. As soon as the ramp voltage exceeds the amplified temperature error voltage, a comparator circuit (HA-2700) causes the heater voltage to be applied to the hot film via a chain of logic elements and switching transistors. Thus, a temperature swing of 1.2° C in the hot film can cause the length of the heating pulse to go from minimum to maximum (0 to 1,750 μs). During operation, the heater pulse length will usually be between these extremes; it will not remain at either end of the range for more than a few periods. The heater power is computed from the known resistance of the hot film, the applied heater voltage (5 V nominal) and the heater-pulse duration.

This work was done by Ronald I. Gilje and Walter Lehman of TRW Corp. for **Langley Research Center.** *For further information, Circle 78 on the TSP Request Card. LAR-11473*

Use of Miniature, Single-Wire, Sheathed Thermocouples

Temperature measurement with small thermocouples is improved.

Lewis Research Center, Cleveland, Ohio

Thermocouples encased in a protective metal sheath to prolong thermocouple life have been used for temperature measurement in many severe applications; a standard two-wire sheathed thermocouple is shown in the figure. Special problems begin to occur, however, in applications where very-small sheathed thermocouples are required. A point is reached where the interelement insulation is not sufficient to provide adequate separation between two wires contained in one sheath. This results in high-temperature electrical shunting and diffusion between wires, insulation, and sheath, leading to thermocouple drift and eventual failure.

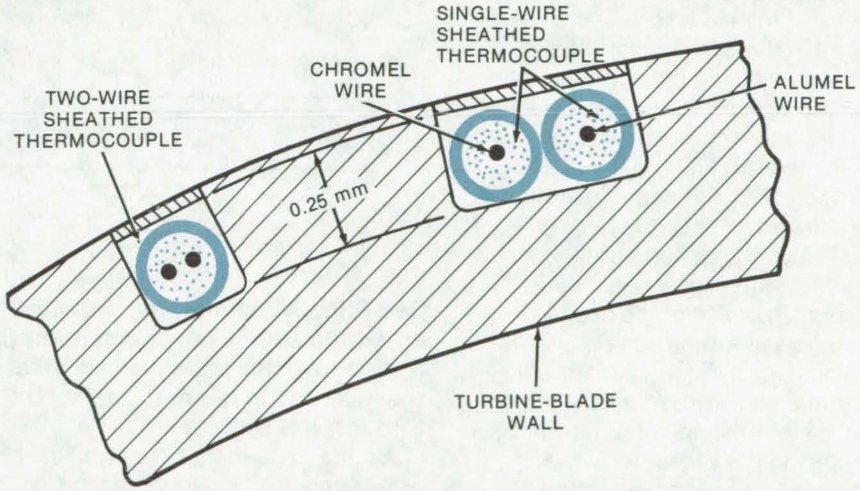

Miniature Sheathed Thermocouples are shown as used for temperature measurement of thin-walled turbine blades. In this application, the blade thickness limits the allowable groove depth for installation of the thermocouples. (The outside diameter of the sheath is the limiting parameter.)

In a miniature thermocouple development program, it was determined that such problems begin in two-wire commercial thermocouples with outside diameters of about 0.02 in. (0.5 mm) and smaller. It was found that whereas special-order two-wire thermocouples with outside diameters below 0.02 in. can sometimes perform satisfactorily, single-wire sheathed thermocouples with outside diameters down to 0.01 in. (0.25 mm) can be used with negligible degradation. In the miniature, single-wire, sheathed-thermocouple configuration, each wire is enclosed in a separate sheath (see figure), thus increasing the interelement insulation by a factor of 2-1/2 with the same sheath outside diameters. If desirable, each wire in its separate sheath can be brought to the junction region by independent paths.

Stringent acceptance tests for all thermocouple component parts have reduced failure rates of miniature, single-wire, sheathed thermocouples to a negligible level. To improve the long-duration perform-

(continued on next page)

ance of miniature, single-wire, sheathed thermocouples even further, a higher degree of fabrication quality control and the use of high-purity materials of construction are mandatory.

This work was done by George E. Glawe, Raymond Holanda, and Lloyd N. Krause of **Lewis Research Center.** *Further information may be found in NASA TN-D-7671 [N74-23050], "Miniature Sheathed Thermocouples for Turbine Blade Temperature Measurement," a copy of which may be obtained at cost from the Technology Application Center, University of New Mexico [see page A7].*
LEW-12436

Hydraulic Pressure Stabilization and "Pogo" Suppression

Accumulator for cryogenic liquid transport line damps low-frequency longitudinal oscillations in rocket-engine propellant feed system.

Marshall Space Flight Center, Alabama

Pressure fluctuations in a cryogenic liquid transport system can be eliminated by the use of an accumulator that is attached to the feedline and pressurized with gas from the liquid tank. This arrangement is useful in any cryogenics system or in any other liquid transfer system where a higher-pressure gas source and lower pressure drain exist. It is particularly important in large liquid-fuel rocket engines, however, for suppressing longitudinal oscillations ("pogo") in the vehicle. The system described here is simpler, lighter, and more reliable than other accumulator designs.

The figure shows an accumulator connected to a liquid-oxygen (lox) transport line. The accumulator is pressurized by gaseous oxygen continuously supplied from the lox-tank pressure supply and bled through an orifice at the desired liquid/gas interface position. If the lox liquid level rises in the accumulator, the orifice is blocked by liquid, and the interface is forced down by increasing gas pressure. If the orifice is totally uncovered, the gas quickly vents, allowing the liquid level to rise. This action helps to maintain a constant pressure in the feed system and to damp oscillations.

The gas that is bled from the accumulator is returned to a low-pressure point in the system. Heat transfer at the gas/liquid interface is controlled by the use of a float and/or baffles.

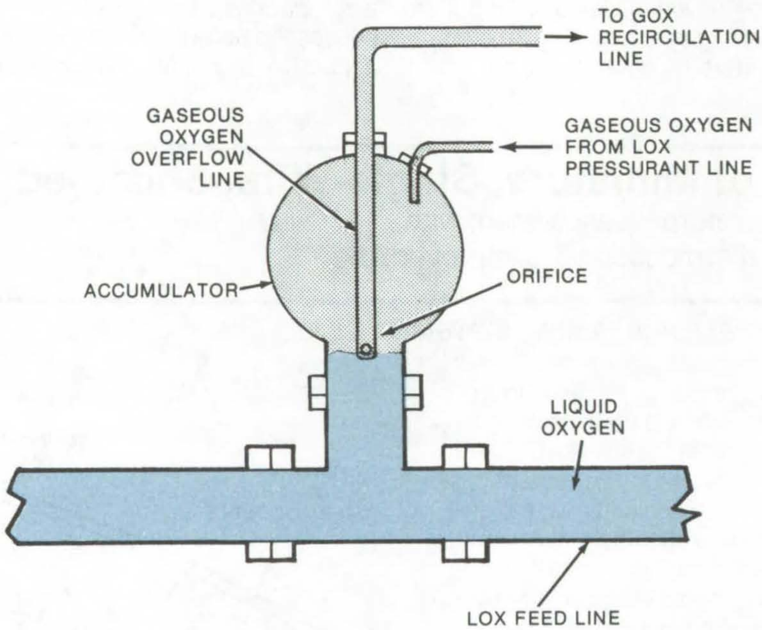

Gas-filled Accumulator Stabilizes Feedline Pressure passively and automatically. If the pressure on the lox line is too low, the liquid level rises above the gas-escape orifice, so gas pressure builds up. When gas pressure is too great, it pushes the liquid down, allowing the gas to vent through the orifice.

An accumulator is important in rocket engines because pressure variations may occur in the feed system during flight. Propellant feed-system oscillations can couple with combustion dynamics and vehicle structure to produce destructive low-frequency longitudinal oscillations ("pogo") in the vehicle. A lox accumulator is required to reduce these feed-system pressure oscillations.

Cryogenic accumulators used heretofore are complex and heavy. They use a helium-filled accumulator and sets of valves and level-control sensors to control pressure during flight; the helium requirements are high and uncertain. By contrast, in this newly-designed accumulator/"pogo" suppressor, the accumulator volume is controlled passively and automatically, the accumulator level sensor is

eliminated, and sensing and control electronics and the number of valves are minimized.

This "pogo" suppressor is the first to employ a gaseous propellant as the accumulator pressurant. Thus the system is simpler, more efficient (uses less power, and helium is used only during startup), and more reliable (fewer valves and sensors). It is practically self-sufficient during engine main-stage operation.

This work was done by James R. Fenwick and George H. Karigan of Rockwell International Corp. for **Marshall Space Flight Center.** *For further information, Circle 79 on the TSP Request Card.*
MFS-19287

Books and Reports

These reports, studies, and handbooks are available from NASA as Technical Support Packages (TSP's) when a Request Card number is cited; otherwise they are available from one of NASA's Industrial Application Centers or the National Technical Information Service.

Solar-Powered Air-Conditioning

A study of Rankine-cycle and lithium bromide absorption systems

A recent study on the development of solar-powered residential air-conditioners is based on selected literature through 1975. Its purposes are to characterize thermal and mechanical systems that might be useful in the development of a Rankine-cycle approach to solar cooling and, also, to establish baseline data defining physical characteristics, performance, and costs of using an $LiBr/H_2O$ absorption-cycle system.

The reviews of the literature on both the absorption-cycle and the Rankine systems include summary presentations of data and short descriptions of recent tests and development efforts in each area. Relevant data on nonsolar systems are also presented and discussed.

It was found that published cost/benefit data vary as much as an order of magnitude due to differences in basic assumptions, which fall into three areas:

- Projected costs of solar heat collectors
- Projected costs of fuel
- Efficiencies of heat-absorption systems

Approaching the problem from the standpoint of solar-collector size yields interesting results. For example, the solar collector used to power a heat-absorption (Rankine-cycle) air cooler can be reduced by 30 percent when the compressor and turbine efficiencies are increased from 70 percent to 80 and 85 percent, respectively.

The study concludes that, although commercial solar-powered air-conditioners are not yet widely available, the design and production of such equipment is within the current state of the art. For instance, one $LiBr/H_2O$ absorption system under development is a preexisting gas-fired model that has been modified with a water-fired unit for solar-collector interface.

This work was done by D. C. Clark of **Marshall Space Flight Center** *and J. Rousseau of The Garrett Corp. To learn how to obtain a copy of the report, Circle 80 on the TSP Request Card.*
MFS-23276

Nondestructive Evaluation

An effective approach to improved reliability and safety

The ability to predict the ultimate performance of an item without testing it to failure has been a long-sought goal. It is obvious, for example, that testing a nuclear-reactor containment vessel to failure is completely out of the question. This and similar challenges have led to the development of a variety of nondestructive-evaluation (NDE) techniques.

A technology survey has been assembled that summarizes the accumulating knowledge of NDE methodology, application, and reliability as it is presented in the literature covering the time period from 1962 to 1975. The report comprises technical abstracts of about 100 significant documents on the nondestructive testing of aircraft structures or on related structural testing; the abstracts also cover the reliability of the more-commonly-used evaluation methods.

Particular attention is directed toward six NDE techniques:

- acoustic emission,
- liquid penetrant,
- magnetic particle,
- ultrasonics,
- eddy current, and
- radiography.

The introduction of the report includes an overview of the current state of the art of NDE as reflected in the evaluated documents covered in the survey.

A companion document to the technology survey is the bibliography, which consists of approximately 1,600 reference citations related to four problem areas in the mechanics of failure in aerospace structures. The listings are subdivided into the four problem areas:

- hydrogen embrittlement,
- protective coatings,
- composite materials, and
- nondestructive evaluation.

This work was done by George Mandel of **Lewis Research Center** *and James L. Carpenter, Jr., and William F. Stuhrke of Martin Marietta Corp. Copies of the two reports:*

NASA CR-134963 [N76-25577], "NDE — An effective Approach to Improved Reliability and Safety

(continued on next page)

— A Technology Survey," and
NASA CR-134964 [N76-28565], "Bibliography of Information on Mechanics of Structural Failure [Hydrogen Embrittlement, Protective Coatings, Composite Materials, NDE]," and
of an additional technology survey, announced in the next article in this issue "Hydrogen Embrittlement of Structural Alloys" [LEW-12767]:
NASA CR-134962 [N76-25375], "Hydrogen Embrittlement of Structural Alloys — A Technology Survey,"
can be obtained at cost from the New England Research Application Center [see page A7].
LEW-12766

Dynamic Stability of Multilayer Sandwich Plates

Equations for analyzing the effects of periodic in-plane loads

A study of the dynamic stability of flat plates under the influence of time-dependent loads treats multilayer sandwich plates consisting of alternating hard and soft layers and includes the effects of in-plane inertia and damping. It is an extension of earlier work that considered either only homogeneous plates, elastic inhomogeneous plates, or three-layer plates consisting of only one soft-core layer, and neglected inertial and damping effects.

The work deals in part with setting up the governing differential equations of motion for a multilayer sandwich plate under the influence of a periodic in-plane load, using the complementary variational principle for dynamics. It is assumed that the soft-core layers carry only transverse shear stresses while the hard layers carry the in-plane normal and shear stresses. The equations that result are rather involved and are not subject to analytic analysis. However, they may be considerably simplified by neglecting second-order terms involving the transverse motion and rotations. The linearized equations are then solved for a given set of loading and boundary conditions.

Some interesting aspects of the motion of these plates are determined, including:

- The value of the static in-plane buckling load in terms of the elastic constants and dimensions of the plate,
- The in-plane resonance frequencies,
- The natural frequencies of transverse vibration under free unloaded conditions,
- The natural frequencies of transverse vibration under a time-independent in-plane load, and
- The principal regions of dynamic stability for a simply-supported rectangular plate under the influence of a periodic in-plane load.

In connection with this last analysis, it is found that the inclusion of in-plane inertia produces significant modifications of the instability boundaries of the first region, even in the presence of damping. The modifications are greatest in the neighborhood of the first in-plane resonance. The second and higher order regions are affected the least. Thus, in general the inclusion of in-plane inertia and damping is necessary for an accurate description of the instability boundaries. As an example, a core material with higher shear moduli is shown to exhibit correspondingly higher inertial effects, and some typical calculations are presented that compare a plastic core to an aluminum honeycomb core, separating aluminum hard layers in a rectangular multilayer sandwich.

This work was done by M. A. Salama and J. C. Chen of **Caltech/JPL.** *For further information, Circle 81 on the TSP Request Card.*
NPO-11625

Fluid-Connector Selection

Dynamic programing for complex systems with large numbers of variables.

The usefulness of dynamic programing for systems design is illustrated by a study on the selection of separable bolted connectors for an aerospace application. Although the major part of the report is confined to this specific connector system, it should be of general interest to those considering other dynamic programing applications in fields such as aeronautics, construction of refineries and chemical plants, and electronics.

Dynamic programing is the suggested design approach to highly complex problems involving numerous, and often unspecific, demands made by stringent requirements in the areas of environment, cost, materials, delivery date, reliability, safety, and numerous other constraints imposed upon the designer. In this report, analytical techniques based on dynamic programing provide the key to choosing the optimum connector design where the variables are imprecisely known and where there are a great number of acceptable configurations to consider.

For example, selecting the optimum design for the Saturn 1B space application required the investigation of 118 flange configurations, using 26 different materials and 30 different gasket materials. The study develops criteria for performance-parameter evaluation, stressing the maintenance of a "zero-leak" seal, and the simplest design approach is given preference by a "simplicity rating factor."

This work was done by Willibald P. Prasthofer of **Marshall Space Flight Center.** *To learn how to obtain a copy of the report, Circle 82 on the TSP Request Card.*
MFS-23072

Computer Programs

These programs may be obtained at very reasonable cost from COSMIC, a facility sponsored by NASA to make new programs available to the public. For information on program price, size, and availability, circle the reference letter on the COSMIC Request Card in this issue.

Atmospheric Interaction Plume

Shock structure, mixing chemical, and kinetic effects

This computer program can be used to predict the gas dynamic and chemical properties of underexpanded rocket plumes from sea level to the altitude above which the viscous continuum-flow assumption, with distinct shocks, is no longer valid. The plume shock structure is computed while simultaneously accounting for turbulent mixing, nonequilibrium chemistry, and gas/particle nonequilibrium effects. The program also has the ability to calculate plume properties in the subsonic region downstream from the Mach disk, downstream of the shock reflected from the triple point, and in the far field. It can readily be used to determine plume optical and electrical properties, which are necessary data for calculating the infrared radiation pattern and radar cross section. This program also has been used to calculate deposition rate of various nitrogen oxides into the stratosphere caused by the Space Shuttle exhaust plumes.

turbulent mixing effects within exhaust plumes. For the gas flow upstream of the Mach disk, the governing elliptic Navier-Stokes equations are reduced to a hyperbolic system (including lateral pressure gradients) by neglecting the diffusion of mass, momentum, and energy along streamlines as compared with that across streamlines. The conservation equations are then written in a streamline-oriented coordinate system. Shocks are treated as thin bounding surfaces of the flow across which the Rankine-Hugoniot relations are applicable. In the subsonic region behind the Mach disk, the inviscid-flow governing equations are taken to be elliptic. The equations of flow must be solved within the supersonic and subsonic regions, while simultaneously maintaining the equality of pressure and flow direction along the dividing streamline. In meeting these boundary conditions, several approximations are employed to reduce the amount of computer time and storage required. For the condensed phases present within the flow, a continuum particle-cloud assumption is made, and field-conservation equations for continuity, momentum, and energy can be written for the particles.

The "Atmospheric Interaction Plume Program" (AIPP) code is based on the Multitube code developed by Boynton (which incorporates the finite-difference stream-tube calculation technique) and has been expanded to treat particle/gas nonequilibrium, chemical kinetic, and

A finite-difference formulation of the gas-phase and particle-cloud governing equations is utilized on a grid that lies along and perpendicular to the streamlines. The gas-flow equations are solved via an explicit finite-difference marching technique. The chemical production terms utilize an implicit finite-difference formulation, because an explicit formulation leads to an impractically small integration step for near-equilibirum chemistry. The particle equations have no wave or diffusive nature and are solved explicitly via a finite-difference formulation. Initially, all flow properties, streamline positions, and angles must be known along an orthogonal surface. The streamlines are extended an incremental distance, forming a stream tube. The properties at the upstream surface are used, along with the governing equations, to determine all the necessary properties at the downstream surface. Below the Mach disk, a similar procedure using assumed streamlines is performed.

Only minimal judgment by the user is required to operate the program. The input data required are nozzle-exit conditions along a surface orthogonal to the exit streamlines, uniform supersonic external-flow conditions, and a suitable reaction mechanism and rate coefficients. The output contains the results of all calculations in a highly readable format. Care must be taken that the program is not used to predict plume characteristics at altitudes above which the assumption of continuum flow ahead of the Mach disk starts to break down.

This program is written in FORTRAN IV to operate in the batch mode and has been implemented on a CDC CYBER 175 with a central memory requirement of approximately 40K 60-bit words.

This program was written by J. T. Kelly and H. S. Pergament of AeroChem Research Laboratories, Inc., for **Langley Research Center.** *For further information, Circle E on the COSMIC Request Card.*
LAR-12203

Trim Conditions of Mated Vehicles

Effects of configuration and trajectory on vehicle separation

A flight-conditions program was developed to perform fast and accurate tradeoff studies on the effects of configuration and trajectory paramaters on the initial conditions at separation of mated vehicles. In particular, this program was designed to generate the trim-conditions data of the 747/Orbiter mated vehicle used in approach and landing tests of the space shuttle. It could be adapted to the study of trim conditions for any similar mated-vehicle configuration.

For a given mated-vehicle configuration, this program will define the rate-of-climb ceiling, corresponding trim attitude, and 747 control-surface deflections; it will define the attitude and 747 control-surface deflections for trim in straight and level flight at any attainable altitude;

(continued on next page)

and it will define the attitude and 747 control-surface deflections for equilibrium glide at any attainable altitude. The equations of motion used assume a flat nonrotating earth with flight limited to the vertical plane and mated-vehicle mass assumed constant. The forces accounted for include aerodynamic, thrust, and gravitational. The differential equations of motion are solved using a Newton-Raphson iteration technique that converges rapidly. If convergence does not occur by 50 iterations, an error message is printed and execution terminated. This usually indicates faulty input data or that a better first guess is needed for the Newton-Raphson routine.

Although designed primarily for conversational use on a demand terminal, a batch run can be set up. In the conversational mode, input is free format in response to program-generated questions. Output from each calculation is presented in a highly readable and compact format so that trade off studies between different runs can be easily performed.

This program is written in FORTRAN and has been implemented on a UNIVAC 1110 under control of EXEC 8 with a central memory requirement of approximately 13K of 36-bit words.

This program was written by Charles M. Nobles and Richard H. Seale of McDonnell-Douglas Corp. for **Johnson Space Center.** *For further information, Circle F on the COSMIC Request Card.*
MSC-16188

Multiple-Compartment Venting

Venting through pipes and orifices, including the effects of heat transfer

A generalized venting program simulates the venting characteristics of multireservoir multiconductor configurations. The reservoirs may be of finite or infinite volume. The infinite-volume reservoirs are characterized by a prescribed pressure, temperature, and crossflow-velocity history. The finite-volume reservoirs may be adiabatic, follow a prescribed temperature history, or follow a prescribed heat-transfer-rate history. The reservoirs may contain the same gas, different gases, or mixtures of nonreacting gases.

Compartment pressure can be predicted readily, provided that the compartment volume, the initial pressure, temperature, and gas composition are known and that the net flow of mass and energy from the compartment can be accurately computed throughout the problem time period. Therefore, the requirement for compartment-pressure history simulation reduces essentially to the development of analytical means for the accurate prediction of mass and energy flow rates between compartments containing various mixtures of gases, connected by pipes and orifices.

The compartments may be interconnected by conductors consisting of pipes and orifices. The pipe conductors may be of constant cross-sectional area or consist of two different-diameter pipes joined at the constriction. The flow in pipes can be treated as adiabatic or isothermal, or it can include the effects of heat transfer due to the difference between the pipe-wall temperature and the gas-stagnation temperature. The computed ideal mass flow rates through orifices are modified by means of experimentally-derived discharge coefficients which account for orifice geometry, pipe bends, and joints. Although pipe-flow crossflow effects are felt to be important, they are not included due to lack of experimental data.

The solution of the transient venting problem is approximated by a first-order quasi-steady-state solution of the reservoir-state properties and conductor-flow equations. That is, at any given time t, steady-state mass and energy flow rates through the conductors are computed with the reservoir conditions held constant. These mass and energy flow rates are then used to compute the reservoir conditions at time $t + dt$.

This program is written in FORTRAN V and has been implemented on a UNIVAC 1108, under control of EXEC 8 with a central memory requirement of approximately 32K 36-bit words.

This program was written by L. K. Donehoo of **Marshall Space Flight Center** *and H. Ikawa, L. P. LeBlanc, and J. A. Sadunas of Rockwell International Corp. For further information, Circle G on the COSMIC Request Card.*
MFS-23581

Steady-State Super/ Hypersonic Inviscid Flow

Three programs for complex vehicle geometries

A package of three programs accurately and efficiently computes the inviscid super/hypersonic flow field about complex vehicle geometries.

A second-order accurate finite-difference scheme is used to integrate the three-dimensional Euler equations in regions of continuous flow, while all shock waves are computed as discontinuities via the Rankine-Hugoniot jump conditions. Blunt-nose entropy layers can be computed in detail. Real-gas effects for equilibrium air are included, using curve fits of Mollier charts. The package can be a very useful tool in the design and analysis of high-speed vehicles, such as supersonic aircraft, hypersonic transports, and reentry spacecraft (shuttle orbiter).

The first of the three programs, STEIN, solves the Euler equations for the flow field. Basic guidelines for the solution are:

- An accurate second-order finite-difference marching technique is used to numerically integrate the governing partial-differential equations;
- Shock waves in the flow field are followed, and the Rankine-Hugoniot conditions are satisfied across them;
- The intersection of two shocks of the same family is computed explicitly;
- Conformal mappings are used to develop a computational grid;

- Body-boundary conditions are satisfied by recasting the equations according to the concept of characteristics;
- The edge of the entropy layer on blunt-nose vehicles is followed from its origin, and the derivatives across the layer are formed, using special techniques;
- Real-gas effects are included when appropriate, by using fits of Mollier charts; and
- Sharp leading-edge wings are computed, using a local two-dimensional solution.

The only limitation to this technique is that the Mach number in the marching direction (nose to tail) must be supersonic at every point in the flow field. The region around the nose of blunt-nosed vehicles must be computed by another technique (see description of BLUNT below); once the flow becomes supersonic, STEIN can proceed with its calculations. STEIN has been used extensively to compute external flow fields and has been found to yield accurate results for a wide variety of vehicle configurations, flying at Mach numbers between 2 and 26 and having angles of attack to $\pm 30°$.

The second program, BLUNT, is used to find flow fields about blunt-nosed portions of the vehicle. BLUNT uses a time-dependent computational technique to asymptotically approach a steady transonic solution. Output from this program can be used by STEIN to define the flow-field points in the initial data surface.

The third program, QUICK, provides the user with a geometry system to model a complex vehicle geometry in a quick straightforward fashion. QUICK consists of a group of initial-defining and logical-checkout routines, which actually set up the mathematical model. A second group of routines is used to interrogate the model for cross-sectional information. QUICK supplies all geometrical information about the vehicle to STEIN.

The programs in this package are written in FORTRAN IV for batch execution and have been implemented on a CDC 6600. The STEIN program has a central memory requirement of approximately 200K octal words.

These programs were written by Frank Marconi, Manuel D. Salas, and Larry S. Yaeger of Grumman Aerospace Corp. for **Langley Research Center.** *For further information, Circle H on the COSMIC Request Card.*
LAR-11891

TRIM-STAB

Aerospace vehicle trim and stability

The program calculates stability and control characteristics of aerospace vehicles, which are usually calculated by either constant-coefficient time-slice linear analysis or by nonlinear simulation. TRIM-STAB performs the calculation of trim and stability using a small perturbation linear analysis technique. The program can analyze vehicles in the flight regimes of:
- Ascent (or boost), in which rocket power is the dominant force
- Entry, in which flight is unpowered and at a high Mach number
- Cruise (or conventional flight), in which aerodynamic forces dominate and jet engine power may be used.

In conceptual form, the program accepts nonlinear aerodynamic characteristics, inertia data, control-system parameters, and flight conditions as input. The program trims the vehicle at the given flight conditions, with trim conditions depending on flight regime. The vehicle is perturbed about the trimmed condition to obtain the linear coefficients to the equations of motion. Next, the linearized equations of motion are constructed in matrix format in the Laplace operator notation. The equations of motion are decoupled into the longitudinal (in plane of symmetry) and lateral (out of plane of symmetry) equations. The degrees-of-freedom included are:
- Three rigid-body translations
- Three rigid-body rotations
- Five symmetrical elastic modes
- Five asymmetrical elastic modes
- Pitch aerodynamic controller
- Pitch-thrust vectoring
- Yaw aerodynamic controller
- Yaw-thrust vectoring
- Roll aerodynamic controller
- Roll-thrust vectoring
- Control laws governing each rigid-body rotational degree-of-freedom
- Ten equations (five longitudinal and five lateral) that can describe point loads
- Four propellant-sloshing equations (two longitudinal and two lateral)
- Thirteen sensor equations (five longitudinal and eight lateral)

Options are provided to limit equations to (a) rigid body only (bare airframe); (b) rigid body plus controllers and control laws; and (c) rigid body, controllers and control laws, elastic modes with auxiliary equations, propellant-sloshing dynamics (ascent only), and sensor equations.

The formed matrix (its size is dependent on the options selected) is expanded into an equivalent, first-order, linear system. The eigenvalues of the equivalent linear matrix that represents the linear system are the roots to the polynomial formed by expanding the determinant of the original matrix. These roots are the stability parameters of the aerospace vehicle. Transfer functions relating the system parameters to a system input are computed as ratios of two polynomials in the Laplace operators. These transfer functions are used to compute: time histories to impulse system inputs, Bode plots, gust response (power spectral density) in the frequency domain, and time-history gust response.

To accommodate program flow, TRIM-STAB is divided into three separate program modules: (1) a driver module, (2) a trim module, and (3) a stability module. The driver module assumes responsibility for overall program control, reading input cards, and setting up all significant storage allocation and default data values. The trim module is set up to fully describe the vehicle in a trim condition in ascent, entry, or cruise mode flight in consideration of the longitudinal and lateral transfer functions. Stability of the vehicle is determined using the stability

(continued on next page)

module, which solves for all desired transfer functions and provides various outputs for analysis.

This program is written in FORTRAN and UNIVAC ASSEMBLER to operate in the batch mode. This program has been implemented on a UNIVAC 1100 Series computer under control of EXEC 8 with a central memory requirement of approximately 60K of 36-bit words.

This program was written by R. E. Barnes and B. J. Kuchta of General Dynamics Corp. for **Johnson Space Center.** *For further information, Circle J on the COSMIC Request Card.*
MSC-14927

Three-Dimensional Supersonic Viscous Flows

Calculations of complete flow around high-speed vehicle

A program for the design of high-speed vehicles determines the complete viscous and inviscid flow around a body of revolution at a given angle of attack when traveling at supersonic speeds. The viscous calculations agree with experimental values for surface and pitot pressures and with surface-heating rates. At high speeds, lee-side flows are important because the local heating is difficult to correlate and because the shed vortices can interact with vehicle components, such as a canopy or a vertical tail.

Lee-side flows are difficult to calculate because thin-boundary-layer theory is not applicable and the concept of matching inviscid and viscous flow is questionable. The parabolic approximation to the compressible Navier-Stokes equations is used to solve for the complete inviscid and viscous regions of flow, including the pressure. The parabolic approximation results from the assumption that the stress derivations in the streamwise direction are small in comparison with derivatives in the normal and circumferential directions. This assumption permits the equation to be solved by an implicit finite-difference marching technique which proceeds downstream from the initial data point, provided the inviscid portion of flow is supersonic. The viscous crossflow separation is also determined as part of the solution. To use this method, it is necessary to first determine an initial data point in a region where the inviscid portion of the flow is supersonic.

Input consists of two parts. Problem description is conveyed by namelist input; initial data are acquired as formatted data. Because of the large amount of run time it can consume, the program includes a restart capability. Output is in printed format and magnetic tape for further processing.

This program is written in update formatted FORTRAN and has been implemented on a CDC 6700 with a central memory requirement of approximately 350K of 60-bit octal words.

This program was written by John V. Rakich of **Ames Research Center.** *For further information, Circle K on the COSMIC Request Card.*
ARC-11087

Aircraft Engine Weight and Dimensions

Estimations made on component basis

A rapid, general-purpose computer program has been written for estimating aircraft engine weight and dimensions. The program estimates engine weights and major dimensions on a component-by-component basis for any engine with components that can be represented within the program. The component-weight data base included in the program reflects selected high-technology engines from supersonic cruise aircraft research studies together with NASA in-house results and some older military supersonic engines. The component correlations are highly simplified and involve a minimum number of parameters. Each component is represented by an individual subroutine using empirical correlations derived from the data base. Refined component definitions or additional components can be easily incorporated.

There are few general-purpose engine-weight computer programs available. One describes a correlation technique for estimating the entire engine weight for turbojets and turbofans based on a few gross parameters such as bypass ratio and overall pressure ratio. These present computer programs are limited to conventional engine types and lack the sensitivity required for design perturbation or tradeoff studies at the component level.

In order to evaluate advanced new engine concepts and associated component tradeoffs, performance and weight estimates are necessary. This new computer program can be applied to a wide variety of engine-cycle concepts provided that appropriate component subroutes are available. The program can be used for preliminary analysis of novel engine concepts, preliminary cycle-selection studies, and component-tradeoff and sensitivity studies.

The program will calculate the weight and dimensions of engines having any combination of the components stored in the data base. The engine components making up a cycle and the interconnections of the components are selected. A cycle program provides the thermodynamic properties of the components. The weight program first computes dimensions of the components, and these dimensions are then used in establishing component-weight relations. Each component is identified in the main program, and the calculation is then directed to the appropriate subroutine. After the calculations for all the components have been completed, the total engine weight is computed by summation.

The results from the program show good agreement with existing relevant engines. The best use of the present program is for design perturbation or cycle-selection studies within a given concept.

This program is written in FORTRAN IV for use on the UNIVAC 1110 series.

This program was written by Leo C. Franciscus of **Lewis Research Center.** *For further information, Circle L on the COSMIC Request Card.*
LEW-12741

Machinery

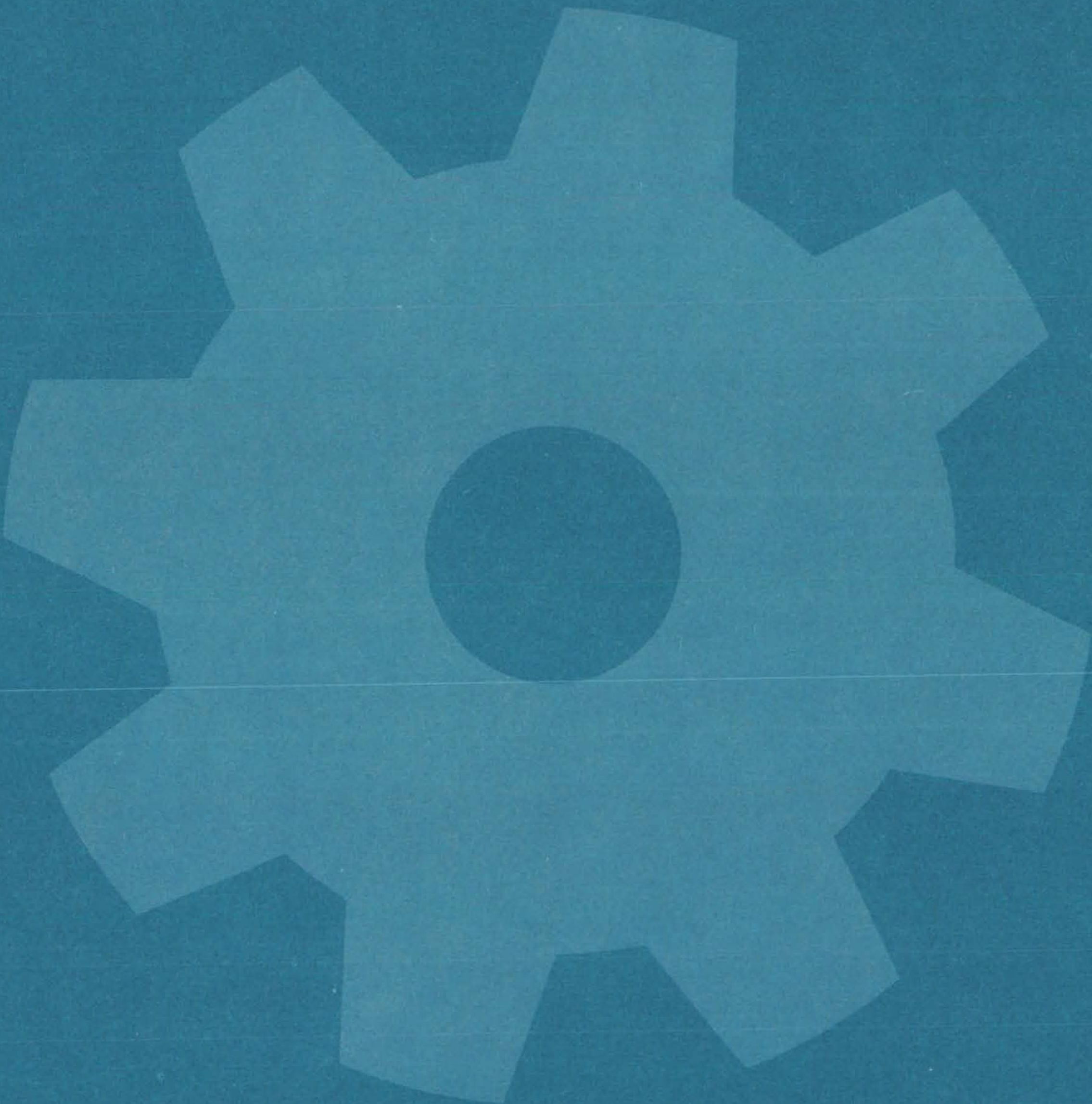

Annular Momentum-Control Device

A rotating ring is used to store momentum in a mechanical system.

Langley Research Center, Hampton, Virginia

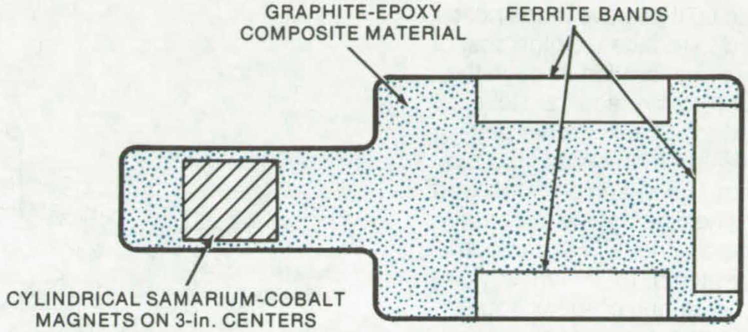

The Momentum-Control Device is a large annular ring 6 ft in diameter. A cross section of the ring, shown above, indicates how a combination of composites and ferroceramic materials are used to achieve an overall effect not possible with conventional materials. In effect, this device is an extremely large dc brushless torque motor.

The annular momentum-control device (AMCD) is a 6-ft (1.8-m) diameter momentum wheel in which momentum is stored in a rotating rim having neither shaft nor spokes. In order to reduce drag, the rotating part (the "rim") is suspended in a magnetic field.

The design of the rim involved consideration of a number of competing requirements:

Structural Requirements

- Strength — The rim had to be made of an extremely strong material because of the high stresses induced by rapid rotation.
- Stiffness — High stiffness was desirable to keep bending-mode frequencies as high as possible to provide the greatest separation between bending and spin frequencies. High stiffness also limits the radial growth at high speeds.
- Damping — Some excitation of bending modes is inevitable; hence, a highly damped material is desirable.
- Density — Since the stress in a rotating rim is proportional to the density of the material, materials with low density are preferred.

Electrical Requirements

- Eddy Currents — The rim must be a nonconductor to eliminate eddy-current losses when the rim passes a magnetic suspension station. All losses result in apparent frictional drag.

Magnetic Requirements

- Permeability — The rim must have regions of high permeability in order to be able to be attracted by the suspension magnets. The permeability must be as circumferentially uniform as possible to reduce losses induced in the support magnets.
- Hysteresis — Hysteresis losses must be as low as possible to reduce drag.
- Drive System — In order for the drive system (motor) to be able to pull on the rim, some sort of circumferential magnetic discontinuity must be provided.

Until fairly recent years, these competing requirements could not have been met. Normal metallic structural materials (aluminum, steel, and the like) could not be used because they are conductive. Normal magnetic materials (such as soft iron) are not only conductive but also have high hysteresis losses. The advent of composite structural materials and ferrite magnetic materials has made the AMCD rim possible.

A laboratory test version of an AMCD rim has been constructed as shown in the figure. The basic structural material is a graphite-epoxy composite with the graphite fibers alined circumferentially. Thus, although the fibers are conductors, they are insulated from one another. In effect, the conducting material is laminated in two directions. The material is extremely strong, has great stiffness, and is somewhat better damped than metals. Moreover, its density is much less than any structural metals.

The magnetic material used for suspension purposes is ferrite, a low-loss ferromagnetic material produced by a sintering process. It is relatively nonconductive, which nearly eliminates eddy-current losses. Moreover, hysteresis losses are very low. Its saturation flux density is not as high as that of iron, but it is satisfactory for this application.

The magnetic discontinuities required by the drive system are provided by cylindrical samarium-cobalt permanent magnets placed at 3-in. intervals in the rim. Such magnets provide sufficient flux for good motor efficiency and are nearly impossible to accidently demagnetize.

This work was done by Joseph Lyman of Cambridge Thermionic Corp. and C. H. Henrikson and F. M. Manders of Ball Brothers Research Corp. for **Langley Research Center.** *Further information may be found in NASA CR-144917 [N76-19457], "Annular Momentum Control Device [AMCD]: Volume I - Laboratory Model Development," a copy of which may be obtained at cost from the North Carolina Science & Technology Research Center [see page A7].*

Inquiries concerning rights for the commercial use of this invention should be addressed to the Patent Counsel, Langley Research Center [see page A8]. Refer to LAR-11914.

Low-Loss Energy Storage Flywheel

Concept for an electromechanical peak-to-average load leveler used in a commercial power grid

Goddard Space Flight Center, Greenbelt, Maryland

Electric utilities have in the past attempted to reduce the high cost of peak power generation through the use of peak-to-average load levelers that use land terrain or other geographic features. In certain parts of the country, geographically inspired levelers lend themselves to energy storage and retrieval: Hydroelectric storage systems, for instance, pump water uphill during off-peak hours where it is stored in a reservoir for later peak-hour use. The method is, of course, limited to locations where geography permits the construction of large reservoirs.

Other storage methods utilizing natural phenomena have been tried, usually with less-than-satisfactory success. One leveling scheme, first tried years ago, used a massive flywheel to convert off-peak electric power to rotating kinetic energy as it was brought to operating speed. Flywheel energy storage permits constant power generation throughout the day/night cycle, thereby eliminating the costly supply/demand power peaks. The flywheel rotor is physically connected to a motor/generator set. Upon peak-load demand, electrical energy is extracted as the flywheel rotor coasts. Rotating flywheel systems, however, have not proved efficient: Energy is dissipated by eddy current (hysteresis) losses, mechanical friction, windage, relatively-poor energy storage per unit weight of the flywheel, and the danger of catastrophic failure in the rotor bearings.

In a modernized concept of a flywheel energy-storage system, energy dissipation is virtually zero. A magnetically-levitated, ironless-armature spokeless rotor is used. It combines the features of homopolar salient poles and a stationary ironless electronically commutated armature. Electronic commutation is a contactless method of sensing rotor position and of controlling current flow in the motor/generator coils to achieve motor (or generator) action. Ironless-armature construction eliminates the core losses due to hysteresis and eddy currents present in a conventional iron armature. The magnetic bearings use field interaction to separate rotating members from stationary members, thus avoiding physical contact and resulting energy loss. Windage losses are overcome by operating the flywheel in a sealed evacuated enclosure.

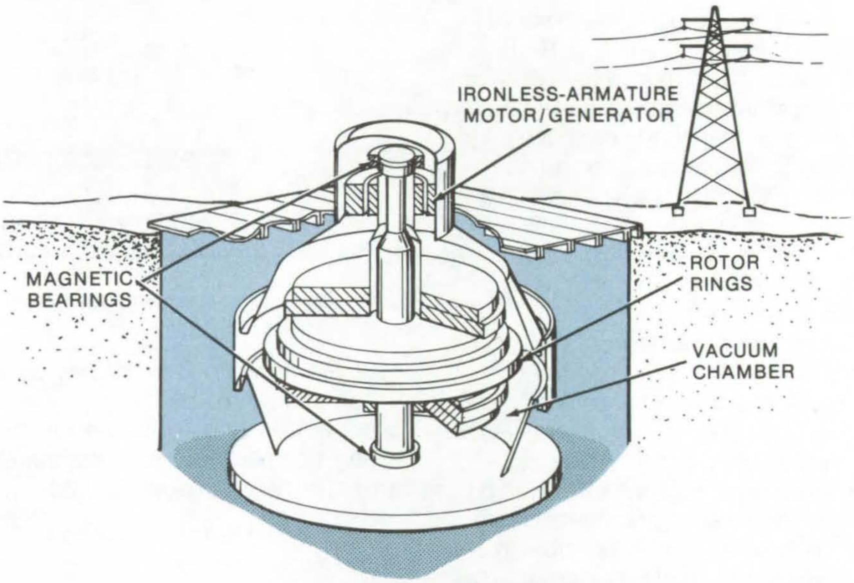

ROTOR NOTES:	
I.D.	14 FT
O.D.	20 FT
HEIGHT	10 FT
WEIGHT	735×10^3 LB
SPEED	1,250 RPM

The **Energy-Storage Flywheel System** is comprised of a motor/generator set, a homopolar flywheel magnetically suspended around the outside of a ring-shaped stator, and an ironless armature mounted to the stator. Potentially located underground, the energy-storage system is housed within a vacuum-tight shroud; internal atmosphere is pumped down to 10^{-3} to 10^{-5} torr to minimize windage loss. The rotor notes indicated are for a proposed 10,000-kWh substation.

To achieve a high specific strength-to-weight density ratio, the rotor is comprised of filamentary, composite (anistropic) material. The inner rim contains a layer of magnetically soft iron shaped to present a series of North/South Pole pairs to the airgap between the stator and the rotor. The poles of one pair are separated from the others by circumferential slots in the iron layer.

As illustrated, an ironless armature, mounted to the stator, extends into the circumferential slot between the poles on the rotor. A permanent magnet in the stator produces a magnetic flux in the airgap between the rotor and stator and through the circumferential slot between the poles. When the storage device operates as a motor, alternating current is supplied to the armature

via electronic commutation. Interaction between the ac in the armature and flux in the circumferential slot produces a force that acts upon the rotor.

In the generator mode, commutation diodes are connected to the proper phases of the armature coil. The flux magnitude passing through the armature is controlled by a field coil located in the stator in shunt with the permanent magnet. It may be ring-shaped samarium cobalt extending along the interior of the ring stator.

To suspend the flywheel rotor without it contacting the stator, permanent magnets are incorporated in the stator for establishing a steady-state magnetic flux. Sets of teeth on the rims face each other to maintain the rotor and stator in axial alinement to create a passive suspension system. Active suspension in the radial direction is provided by a set of electromagnets in shunt with the permanent magnets. Optical sensors distributed along the airgap monitor radial eccentricity. The sensors supply an error signal to the electromagnets which produce a dynamic flux in the airgap and so serve to correct the eccentricity.

This work was done by Harold E. Evans and Philip A. Studer of **Goddard Space Flight Center.** *For further information, Circle 83 on the TSP Request Card.*

This invention is owned by NASA, and a patent application has been filed. Inquiries concerning nonexclusive or exclusive license for its commercial development should be addressed to the Patent Counsel, Goddard Space Flight Center [see page A8]. Refer to GSC-12030.

Closed-Cycle Hydrogen-Fueled Engine

A proposed closed-cycle engine avoids pollution by retaining combustion products.

Caltech/JPL, Pasadena, California

The closed-cycle diesel engine is an internal-combustion powerplant that does not exhaust the byproducts of combustion to the atmosphere, but instead stores them. One possible application is propulsion of undersea warfare vessels, since the diesel does not emit telltale exhaust bubbles. More recently the closed-cycle diesel has been studied for potential use in a pollution-free powerplant using intermittent solar energy.

The proposed powerplant is fueled by a gaseous mixture of hydrogen and oxygen and an inert diluent such as argon. Since the closed-cycle engine can provide high-efficiency energy conversion with zero pollutants (oxides of nitrogen), it may be an environmentally-viable prime mover for a central-station powerplant which is dependent on an intermittent supply such as solar energy.

This version shown in Figure 1 incorporates components to reject waste heat from the thermodynamic cycle, to remove exhaust products from the diluent, to control the amounts of diluent and oxidizer in

(continued on next page)

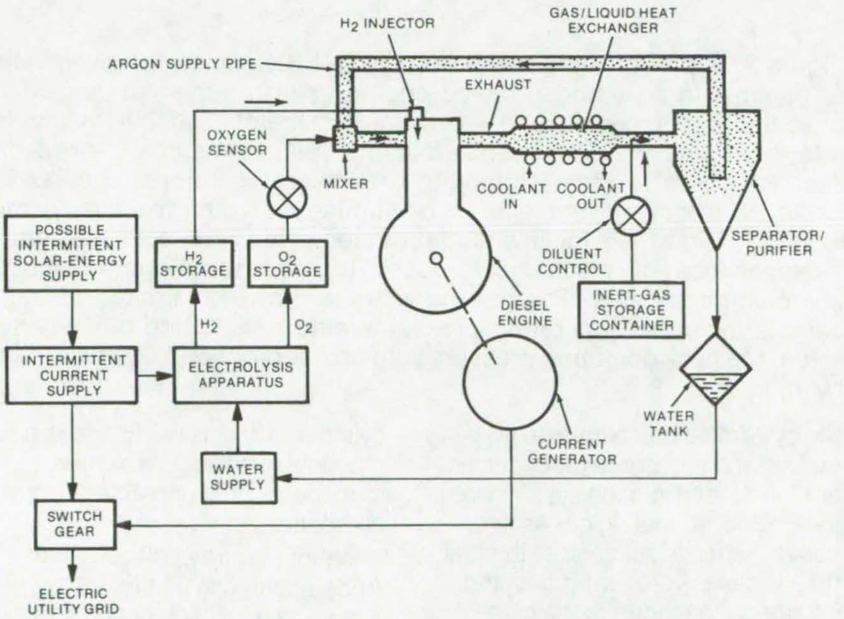

Figure 1. The **Closed-Cycle Hydrogen-Fueled Diesel** stores exhaust byproducts and is therefore termed a "zero emissions" engine. Hydrogen, oxygen, and argon are stored and are used as the fuel, oxidant, and diluent, respectively. Hydrogen is injected into the cylinder approximately at top dead center; oxygen and argon are mixed and also admitted during the intake stroke. During the exhaust stroke the exhaust byproducts are separated into their components; water is stored and recirculated for future use, and other byproducts are filtered and adsorbed.

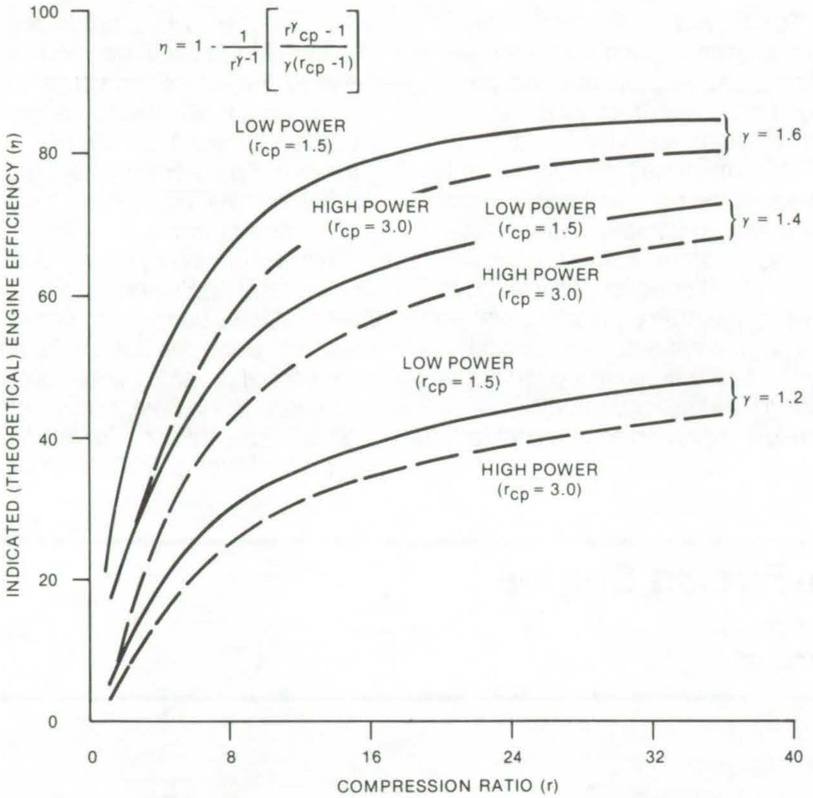

Figure 2. A plot of **Indicated Diesel Cycle Efficiencies** for given values of gamma: In a hydrogen-fueled engine using an inert diluent, if the mole fraction of oxidizer and water vapor are maintained low (by low fuel rate, high pressures, and dense diluent), the gamma of the expanding exhaust gases is high. Complete expansion, therefore, occurs. The brake efficiency of the engine is similarly greater for high-gamma working fluids than for low-gamma fluids. This is due to the relative independence of mechanical losses to load variations in internal combustion engines. The gamma value is, however, limited since, as gamma increases, operating pressures also rise. Citing a 1.6-gamma value, the peak operating pressures are on the order of 3,000 psi (21×10^6 N/m^2).

the system, and to eliminate hydrocarbon and carbonate products that are introduced into the system via the engine lubricating oil. As in a conventional diesel engine, the fuel (in this case hydrogen) is injected into the cylinder during the compression stroke when the piston reaches approximately top dead center. After fuel ignition in the closed-cycle diesel, however, the cylinder exhausts water and residual amounts of hydrogen, oxygen, carbonates, and unreacted hydrocarbons.

A plot (Figure 2) of indicated (theoretical) engine efficiency (η) is shown as a function of compression ratio (r), a ratio of specific heats (γ), and combustion interval (r_{cp}). Each of these factors is coupled to an independent variable in engine design. In this engine, r is 15:1 and r_{cp} is essentially the injection interval.

Exhaust heat is removed in a gas/liquid heat exchanger. After water is removed from the exhaust, the remaining exhaust components are removed with adsorption filters and a catalyst. An oxygen sensor is used to adjust the partial pressure of oxygen in the diluent and to sense the operating pressure in the intake portion of the system to control the makeup of the diluent. Output power is controlled by modulating the mass of hydrogen injected into the cylinder.

To withstand the high pressure and temperatures generated by the combustion process, parts of the engine are fabricated from silicon carbide, silicon nitride, stainless steel, and other high-tensile-strength materials. The pistons are built from silicon nitride to reduce their weight, to limit erosion, and to have a low expansion coefficient. Combustion chambers and cylinder liners are cast stainless-steel alloy, for strength, durability, and low thermal loss. Intake and exhaust ports are coated with carbides for desired low-heat-loss characteristics.

This work was done by Eugene A. Laumann and Rollin K. Reynolds of **Caltech/JPL.** *For further information, Circle 84 on the TSP Request Card.*

This invention is owned by NASA, and a patent application has been filed. Inquiries concerning nonexclusive or exclusive license for its commercial development should be addressed to the Patent Counsel, NASA Resident Legal Office-JPL [see page A8]. Refer to NPO-13763.

Rotating Mobile Launcher

An improved system for
launching a remotely piloted vehicle

Ames Research Center, Moffett Field, California

A proposed apparatus for launching a remotely piloted vehicle (RPV) holds the vehicle on a rotating arm that accelerates until launching speed is reached. Then the RPV and a counterweight at the other end of the arm are released simultaneously to avoid structural damage from unbalanced rotating forces. The arm rotates in a plane that is at an oblique angle with the Earth's surface providing an initial launch path several feet above the ground; yet when the vehicle is at rest it may be serviced at ground level. The support structure may be stationary, or it may be attached to a vehicle as shown in the figure.

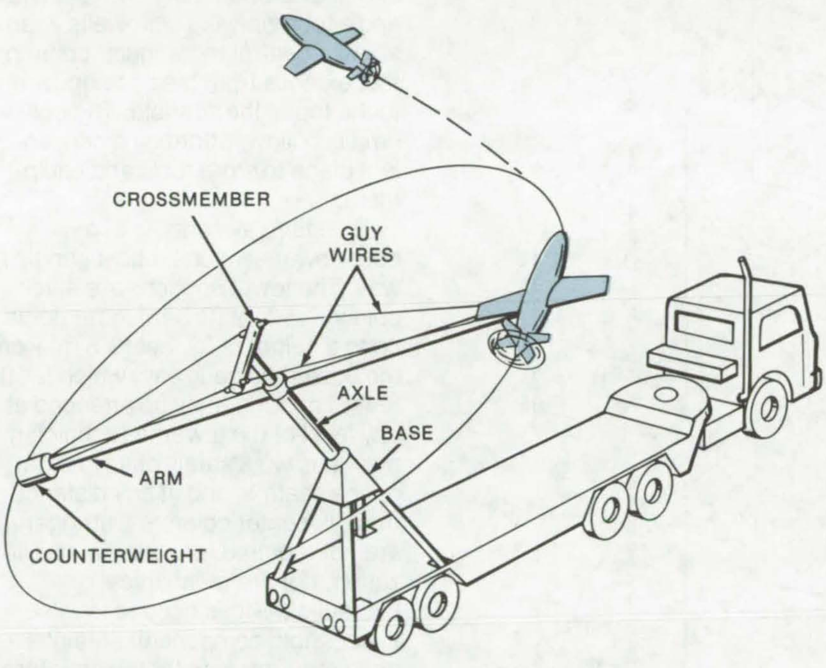

The Mobile Launcher rotates the RPV along the oblique path depicted when the vehicle propulsion system is activated. After the RPV achieves a predetermined velocity, a switch is actuated at the zenith of its path. The RPV and the counterweight are released simultaneously.

The launcher consists of a tripod-like base supporting a stationary axle at one end. The arm is connected to the axle by a rotating bearing. A crossmember is attached to the end of the axle and rotates with respect to it. A pair of guy wires between the crossmember and each end of the arm provides structural rigidity without substantially increasing the mass of the rotating structure.

This work was done by Thomas J. Gregory of ***Ames Research Center.*** *For further information, Circle 85 on the TSP Request Card.*

This invention is owned by NASA, and a patent application has been filed. Inquiries concerning nonexclusive or exclusive license for its commercial development should be addressed to the Patent Counsel, Ames Research Center [see page A8]. Refer to ARC-10979.

Tower-Supported Solar-Energy Collector

A guyed tower extends solar energy collection to three dimensions for efficient space utilization. Placed in the center of a field of heliostats, it supports three receiver/concentrators from crane booms. Open lattice construction reduces wind loading, and the booms can be lowered during heavy winds if necessary to protect the collectors.
(See page 46.)

Adaptive Control for Weld Skate

A modified welding skate with adaptive controls implemented by a digital computer is more stable and more accurate than previous systems. The weld carriage has been made mechanically more stable, and use of digital control instead of analog has reduced welding speed error from about ten percent to one percent.
(See page 142.)

Inexpensive Mass Flowmeter

Fluid flow can be measured with a flowmeter made from off-the-shelf parts plus a "sensor/target" and a combination lever arm and diaphragm. The target is placed in the flow stream and has a known drag coefficient. Its drag is measured by strain gages to determine the flow rate.
(See page 115.)

Mass-Balanced Portable Stairway

Safer scaffold requires no outriggers and less maintenance.

Goddard Space Flight Center, Greenbelt, Maryland

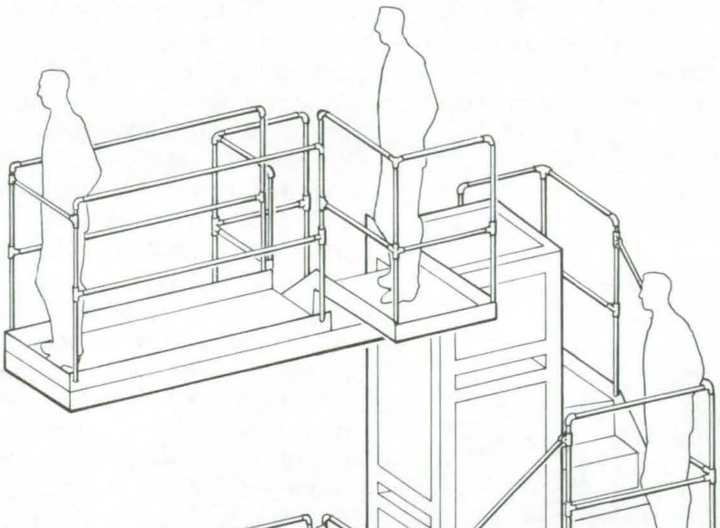

The **Portable Stairway** consists of a base, tower sections, and a gangway which are stacked to the required height and then bolted together for vertical stability. The gangway is vertically-adjustable in 21-inch (54-cm) increments up to the uppermost limit of 32 feet (9.8 m) from the base. The stairway has conventional wheel casters and has been built with an air bearing. The latter version is movable by one person.

A new multilevel upwardly expandable scaffold can accommodate up to four workers and their tools on each level, without danger of collapse or toppling. The stairway and accompanying stair wells wrap about a central rectangular column that extends from the base upward to the top of the scaffold. The column is hollow, affording a convenient place to store tools and equipment.

The stairway consists of a base, tower sections, and a gangway. The tower sections are stackable in 7.5-foot (2.3-m) increments up to a height of 32 feet (9.8 m) from the base. The gangway, which is 10 feet (3 m) long, may be attached at any level of the tower; a technician may thus work safely at any height on the scaffold and at any distance from its center column. Outriggers are not required for stairway stabilization, nor are mechanical or hydraulic devices needed to raise the scaffold components. Maintenance requirements for the structure are thus reduced.

Possible uses for the expandable scaffold include:

- Rudder and propeller maintenance in shipyards;
- Nacelle and engine inspection at airports;
- Ceiling/roof repair at construction sites, and for erecting larger scaffold structures; and
- Cleaning and painting walls and luminaire replacement and maintenance in high-ceiling structures, such as gymnasiums and the like.

This work was done by James J. Kerley, Jr., of **Goddard Space Flight Center.** *For further information, Circle 86 on the TSP Request Card.*

GSC-12172

Hand Fin for Swimming

Paddle mounted on forearm aids propulsion and maneuverability and frees hand for work without interference.

Marshall Space Flight Center, Alabama

The hand fin described here speeds a swimmer's progress over the surface of the water and improves his mobility and quickness of movement under the water, without interfering with the use of his hands when the hands have to be used. The fin is a tapered length of firm rubber or plastic with underhanging loops that fasten to the swimmer's forearm. At the front it has a ring or band to which the user's fingers can cling when he desires to utilize the assistance of the fin. A fin is worn on each arm as shown in the figure.

When the swimmer needs to use his hands for some task, he lets go of the band, and the fin stays in place attached to his forearm until needed again. In the meantime the fin does not affect the use of the hands in any way. When the user is through with his task, he regrasps the band and once again has the aid of the fin in his passage through the water.

The fin should be made of 1/8- to 1/4-inch (3- to 6-mm) thick rubber or plastic. The material should be yielding for safety reasons, but some stiffness is advantageous to prevent excessive flexing.

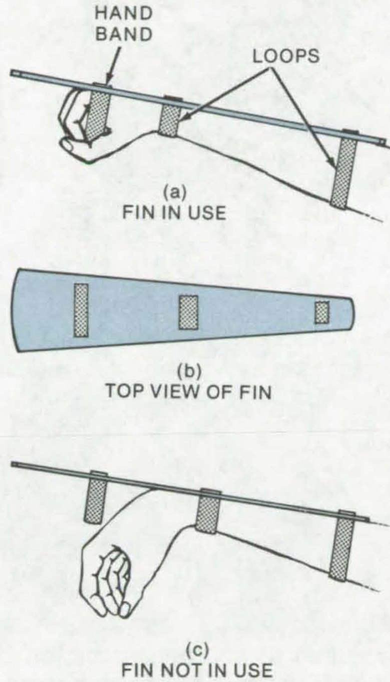

Hand Fin for Swimmers increases speed and improves mobility in underwater maneuvering. Releasing the hand band, as in (c), allows full manual dexterity for grasping, towing, and underwater work.

Swimmers or divers using these fins underwater should keep their hands at their sides and move them in and out in the same way they move their foot flippers. Underwater locomotion is speeded by the use of both the hands and the feet. Use of only the hands allows the diver to rest his legs; or, if his legs are cramped, use of the fins alone enables the diver to continue his progress through the water.

These fins make it possible for a lifeguard to reach a drowning person more rapidly and then considerably ease his task in swimming back to shore with the victim, since he would have only one hand available for paddling. The fins also help in teaching people to swim, giving the trainee much better propulsion and flotation capability.

This work was done by H. L. Martin of **Marshall Space Flight Center.** *No further documentation is available.*
MFS-21632

Sharpening Ball-Nose Mill Cutters

Economical attachment allows faster, more precise grinding.

Langley Research Center, Hampton, Virginia

A new grinding attachment was developed to solve problems that arose in the Experimental Machine Shop at Langley Research Center, when regrinding tip radii of ball-nose end mills made of high-speed steel and cobalt steel, in diameter sizes ranging from 1/2 to 1-1/2 in. (1.3 to 3.8 cm) with shank diameters of 1/2 to 1 in. (1.3 to 2.5 cm). The demand was for single-point end mills and multiflute end mills with straight or spiral flutes. The tools had to meet precise dimensional and geometric tolerances and needed to be reground in quantity.

At that time, no conventional units could sharpen these tools satisfactorily, and a new attachment was developed for a commercially available grinder. In the figure, the new components are shown in the illustration attached to a grinder with an end mill in place.

The attachment is designed so that the centerline of the cutter intersects and is perpendicular to the centerline of the axis through which the cutter will rotate. The toolholder rotates about the centerline of the cutter as it rotates about the vertical axis; it moves in and out on Vee guideways for fast, simple, and accurate settings, using a screw and a direct-reading dial.

A cutting-edge relief angle is incorporated by using the edge of a standard straight grinding wheel and by raising or lowering the axis above

(continued on next page)

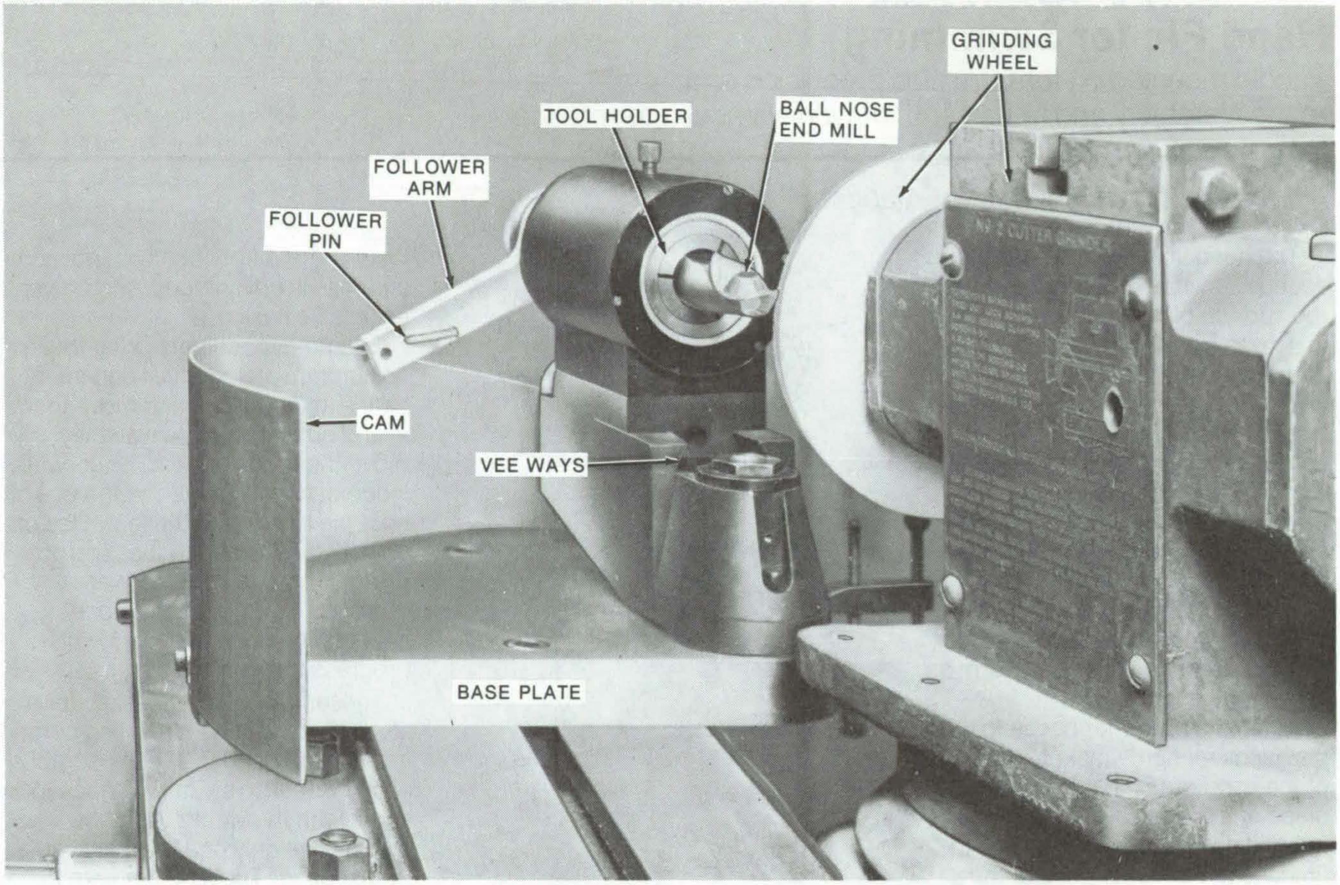

An **Attachment for a Grinding Machine,** used to sharpen precision end mills, increases the accuracy and improves the uniformity and finish of machined parts. The constant relief around the entire profile of the cutting edge will produce a longer tool life. This attachment is relatively an inexpensive tool that will allow ball-nose end mills to be reground with little delay and at lower cost.

or below the center of the cutter by a specified amount. This is a cone-type relief which has uniform clearance around the entire cutting-edge profile. Since the cutters have spiral flutes, it is necessary to rotate the cutter about its centerline. This is done to keep the point on the cutting edge of the mill end at a constant height on the grinding wheel while the toolholder is oscillated through the generating cycle.

To do this a new method was devised. The toolholder has a follower arm connected to it. A pin in the end of the arm rests on a cam. As the holder is oscillated by hand and the pin is held on the cam, it will rotate the cutter the prescribed amount to keep the cutting edge at the same point on the grinding wheel at all times. The cam profile is determined to match each different spiral angle for each size of cutter.

In order to accomplish this, a new feature was incorporated in the unit. It is a leveling device that levels the flutes with respect to the toolholder rotation that generates the ball-nose radius. The follower arm is then connected, and an indicator is placed on the face of the cutting edge at the center. The holder is rotated through the cycle, and the indicator is kept on zero. At small intervals in the cycle, circles are inscribed on the blank cam plate. A smooth line is faired through these circles with a spline and then the cam profile is cut out. All cutters with the same spiral angle can be ground with this cam. The follower arm also has an indexing device built in. After each flute has been ground, the next flute is indexed into position.

This attachment is of rugged construction throughout. The toolholder is mounted in precision ball bearings, and the axis about which it revolves is mounted on taper roller bearings. All of the bearings are preloaded for more rigidity. The extremely high finish and accuracy provided by the reground cutters is largely due to the vibrationless and rigid relation between grinding wheel and cutter.

This work was done by Charles F. Burch of **Langley Research Center.** *For further information, Circle 87 on the TSP Request Card.*

This invention has been patented by NASA [U.S. Patent No. 3,820,286]. Inquiries concerning nonexclusive or exclusive license for its commercial development should be addressed to the Patent Counsel, Langley Research Center [see page A8]. Refer to LAR-10450.

Eliminate Gas-Entrained Dirt from Shaft Seals

Counter pumping and centrifugal force separate debris from fluids.

Lewis Research Center, Cleveland, Ohio

A technique has been developed which excludes gas-entrained dirt from gas-turbine shaft seals. The technique uses a counter-pumping principle in conjunction with a high centrifugal-force field to separate debris entrained in a fluid.

Existing systems for removing particles from seal-pressurizing gas require a swirl chamber. A disadvantage of this method lies in the large pressure drop required to produce a velocity high enough to separate the dirt. The efficiency of the system is reduced because of this pressure drop. An additional disadvantage is that air flow in the separator is greater than the seal leakage, and thus some air is dumped into a low-pressure area.

As shown in the figure, this new technique consists of inscribing a helical groove pattern on a rotating shaft that pumps the seal-pressurizing gas towards the seal. Because of the seal leakage, the seal-pressurizing gas has a flow toward the seal, and the helical groove pattern on the shaft aids this flow and produces a higher pressure on the outlet side of the pump than on the inlet side. The stationary housing (or counter-rotating member) also contains a helical groove pattern that pumps in a direction opposite that of the groove pattern of the shaft.

Gas flow (or fluid flow) with entrained debris entering the shaft grooved area is subjected to high

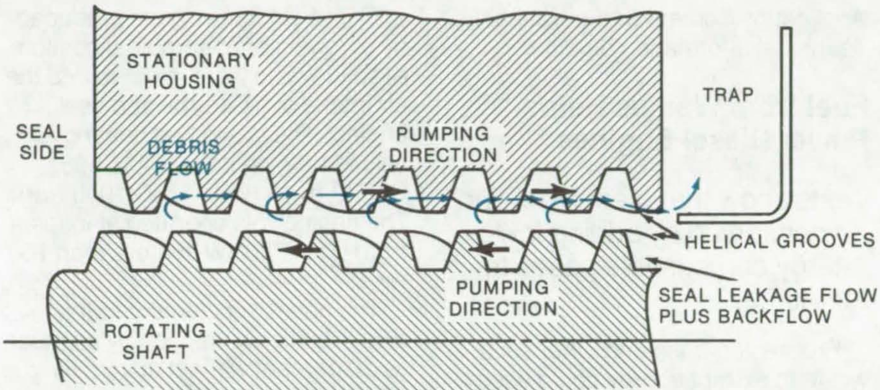

The **Counter-Pumping Dirt Separator** removes debris from a fluid by centrifugal force. Counter-directional grooves on a rotating shaft and a housing cause opposed gas flows along the surfaces fo the halves and cause swirling in the channel. The rotation of the shaft forces entrained particles toward the stationary housing, where the gas flow carries them away from the seal and into a trap.

centrifugal forces due to the swirl motion induced by the groove patterns and rotating of the shaft. Thus debris is centrifuged outward into the outer grooved pattern on the housing. Since the outer grooved pattern has a pumping and gas-flow direction away from the seal, the dirt is pumped away from the seal and can be collected in a suitable debris trap.

A self-acting face seal as described performed successfully in four tests with dust and sand deliberately introduced. It can be used to separate particles entrained in any fluid as long as the particles have greater density than the fluid. In addition, the method can be incorporated as part of the seal envelope and can function without a net fluid pressure drop.

This work was done by Lawrence P. Ludwig of **Lewis Research Center.** *Further information may be found in NASA CR-134739 [N75-19243], "Development of Self-Acting Seals for Helicopter Engines," a copy of which may be obtained at cost from the New England Research Application Center [see page A7].*

This invention is owned by NASA, and a patent application has been filed. Inquiries concerning nonexclusive or exclusive license for its commercial development should be addressed to the Patent Counsel, Lewis Research Center [see page A8]. Refer to LEW-11855.

Books and Reports

These reports, studies, and handbooks are available from NASA as Technical Support Packages (TSP's) when a Request Card number is cited; otherwise they are available from one of NASA's Industrial Application Centers or the National Technical Information Service.

Fuel from Wastes Helps Power Diesel Engines

Tests show that diesel fuel can be conserved by adding low-energy combustible gases to air intake.

Processing trash and other solid waste to extract energy could ease the problems of waste disposal and help meet fuel demands. In such processes, fuel gas can be produced that can either be burned for heat or, perhaps, used in internal-combustion engines. Tests conducted at the Johnson Space Center showed that gas from waste can indeed be used successfully as a fuel supplement for diesel engines.

Gases similar to those produced by pyrolysis or anaerobic digestion of solid waste were injected into the air intake of a Caterpillar diesel engine. The gases had heating values ranging from 164 to 505 Btu/ft^3 (6.1×10^6 to 18.7×10^3 J/m^3). The engine was operated at loads from 60 to 230 kW in more than 100 runs.

The gases supplemented the diesel-fuel consumption by as much as 20 percent without adversely affecting engine performance by precombustion or detonation. In fact, overall fuel efficiency increased slightly for gas plus diesel fuel as compared with diesel fuel alone.

During the tests, the exhaust and other engine temperatures remained essentially constant. No harmful effects on the engine could be found, even when the internal parts of the head were checked for such defects as pitting.

This work was done by Leo G. Monford of **Johnson Space Center.** *Further information may be found in NASA TM-X-58188 [N77-14955], "Performance Characteristics of a Diesel Engine Using Low- and Medium-Energy Gases as a Fuel Supplement [Fumigation]," $3.50, a copy of which may be purchased [prepayment required] from the National Technical Information Service, Springfield, Virginia 22151.*
MFS-16598

Fabrication Technology

Hardware, Techniques, and Processes

Books and Reports

Wetting Agent for Stud Welding

A simple detergent formulation improves aluminum stud welds remarkably.

Marshall Space Flight Center, Alabama

An easily-formulated detergent solution lowers the cost and increases the quality of aluminum stud welds made by capacitor-discharge welding. The detergent, an aromatic polyglycol ether used to clean glassware, is mixed with water and brushed over the weld area. Despite its simplicity, this procedure has remarkable payoffs:

- No bonding of excess metal around the stud,
- Higher welding voltages can be used,
- The arc initiates at a lower voltage,
- Tensile strength and reliability are improved, and
- Final appearance is improved and controlled.

The superiority of this technique can be seen clearly in the photograph. Yet, by eliminating the need for an argon atmosphere around the weld, substantial costs are saved. And, the finished weld is superior to an inert-gas weld — there is no metal flashoff around the stud.

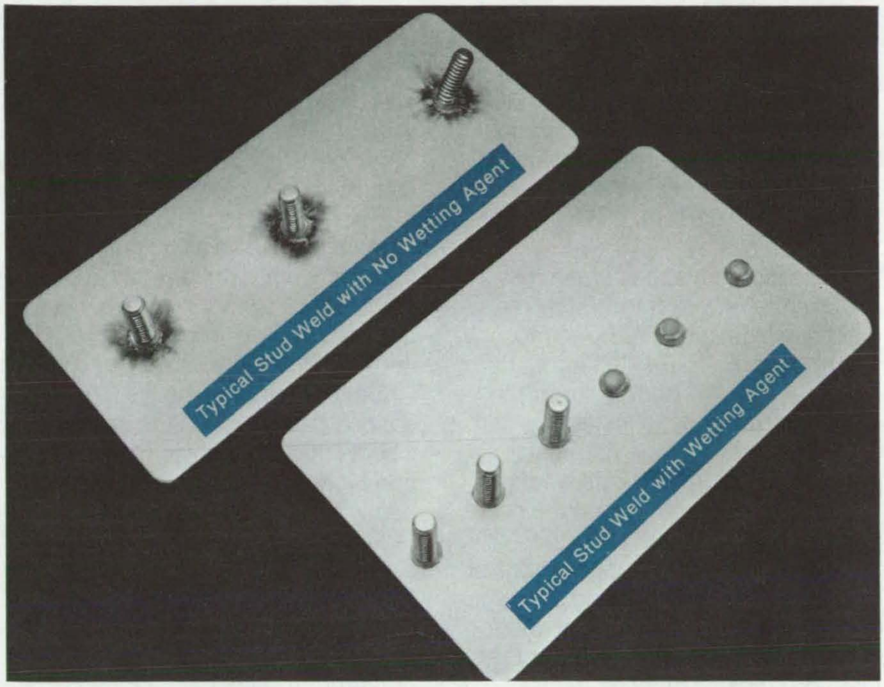

A **Comparison of Welds** shows the improved appearance of the "Super-Stud" welds. Less obvious from the photograph, but equally important, are the improved strength and lower costs, using the new wetting agent.

The wetting agent, nicknamed "Super Stud," is made by diluting a commercial preparation of the poly-glycol ether detergent (available 25 percent by volume in water) with an equal amount of water to give a final detergent concentration of around 10 percent by volume. The mixture is brushed on the weld area and wiped off to remove grease, dirt, and loose oxides that can cause weld impurities. The second step is to brush on an additional coating of the wetting agent, covering the weld area and a surrounding 2-cm radius. The stud is then welded, and the wetting agent will protect the aluminum from oxidation and will cause any excess metal to form small balls that will not adhere to the metal surfaces.

Another advantage of this agent is that it reduces the size of the power supply required — an important consideration with portable equipment. First, the arc-onset voltage is reduced by the removal of oxide impurities during metal preparation; and second, the wetting agent controls and shields the arc, resulting in more efficient use of the arc energy. Without the wetting agent, much of the arc energy is applied to the surface of the baseplate, causing undercut and excessive metal bonding to the plate. With the agent, the stud penetrates cleanly into the baseplate, and no appreciable top-surface bonding occurs. Metallographic examination indicates that in addition to the improved weld penetration, the "Super Stud" protects the eutectic-composition melting of the stud and alloy to increase the tensile strength and reliability of the weld.

"Super Stud" appears to be one of those rare cases where a simple and straightforward process can both reduce costs and improve quality. It is easy to use (the formula is sufficiently viscous for applying to vertical and overhead welds), results in improvements that suggest less expensive and more portable welding equipment, produces a better appearance that can make the process useful for many commercial products, and will allow less-experienced welders to work on a wider range of projects.

This work was done by Clifton L. Green of **Marshall Space Flight Center.** *For further information, Circle 88 on the TSP Request Card.*

Inquiries concerning rights for the commercial use of this invention should be addressed to the Patent Counsel, Marshall Space Flight Center [see page A8]. Refer to MFS-23545.

Adaptive Control for Weld Skate

Modified weld skate maintains constant torch-tip travel rate even with curved work surfaces.

Marshall Space Flight Center, Alabama

By using adaptive control implemented with a digital computer, a modified welding skate is made more stable and about an order of magnitude more accurate than previous systems. The control system represents a significant advance over a similar system developed in the recent past.

Two major advances are incorporated in the new system. First, the weld carriage itself has been modified so that it is more stable mechanically. In the prior system, the torch tip experienced instability whenever the carriage rollers crossed a joint in the skate track. This has been eliminated in the new design.

Second, by going to digital control rather than analog, welding speed error has been reduced from about ten percent down to one percent. In addition, the use of digital techniques allows the use of simpler and less expensive sensors.

Control of the weld skate is based on the solution by computer of general equations that define the geometric relations between a contoured weld-skate track and a contoured workpiece. While the system was designed for gas tungsten arc welding, it can also be adapted to other welding processes, such as gas metal arc, electron beam, laser, submerged arc, and others.

In the new weld skate, the actuator arm, which was directly attached to the wheel trucks in the previous design, has been moved to the center of the skate carriage. This virtually eliminates the weld perturbations caused when the carriage wheels cross a track joint. Relocation of the actuator arm also significantly stabilizes the weld arc by reducing the effects of large variations in the skate-track curvature.

Reliability and accuracy have been increased and costs reduced by replacing the special track-curvature transducer with two commercially-available angular-readout devices. Also, the need for a track-angle sine/cosine analog computer and its electromechanical servomechanism was eliminated, resulting in a more stable and accurate torch-angle servo system. This simplification means fewer parts and improved system reliability.

Finally, the digital computer program used with the new weld skate includes a means to interrogate the computer input and output levels to insure that signals to the weld-skate servosystems do not overstress the mechanical mechanisms. This same scheme further improves the overall accuracy by normalizing extraneous signals.

This work was done by Robert E. Ives and William A. Wall, Jr., of **Marshall Space Flight Center** *and M. Melvin Bruce, Jr., Leslie H. Gard, and Peter P. Pryor, Jr., of SCI Systems. For further information, Circle 89 on the TSP Request Card.*

Inquiries concerning rights for the commercial use of this invention should be addressed to the Patent Counsel, Marshall Space Flight Center [see page A8]. Refer to MFS-23620.

Indirect Resistance Welding

Facilitates fabrication of thin-wall pipe, tanks, and complex shapes

Lewis Research Center, Cleveland, Ohio

Lap joints in thin-wall metal piping, tanks, and structures having unusual or complex shapes can be resistance welded with both the anode and cathode on the same side of the wall. As shown in the figure, in conventional (direct) resistance welding, the anode moves along the joint on one side of the wall while the cathode moves along the joint on the other side of the wall. This may be difficult to achieve when welding long lengths of pipe, tanks, or complex-shaped structures. In such cases, welding can be done more easily by traversing the joint using a hand-held resistance welder with both the anode and the cathode on the same side (indirect resistance welding). A thin-wall pipe for the Space Shuttle has been successfully welded in this way. A 15-in (38-cm) diameter pipe was formed around a mandrel from 0.003-in (0.076-mm) thick Inconel strips with the edges

lapped and then welded by indirect resistance welding.

With this technique, long or continuous length piping and tubing, tanks, and other structures can readily be fabricated from flat sheet stock material.

This work was done by Nelson Ittner and Daniel Laintz of Martin Marietta Corp. for **Lewis Research Center.** *No further documentation is available.*
LEW-12149

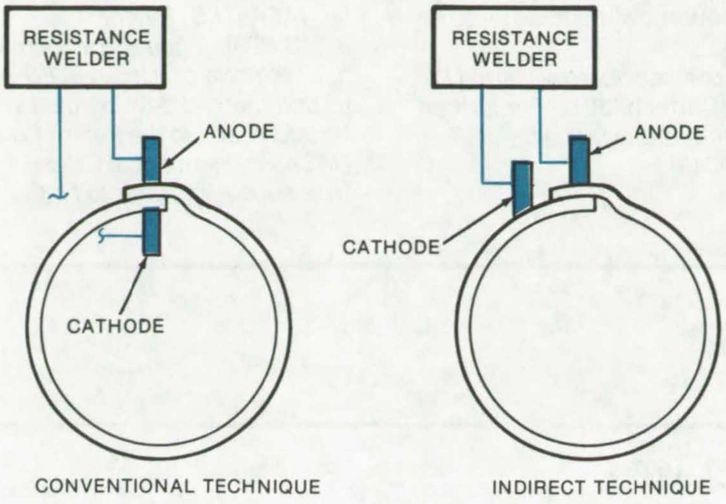

The **Indirect Resistance Welding** technique is shown on the right, as compared to the conventional technique shown on the left. In the indirect method the anode and cathode of the welder are on the same side of the pipe.

Printing Circuits Without a Mask

A proposed technique uses an electronically controlled electrode/nozzle to deposit fine-line metallic patterns.

Caltech/JPL, Pasadena, California

Normally, circuits or other fine-line patterns are plated or etched on substrates by using a mask of the desired pattern. The masking is a major cost contribution in the process and also limits the attainable pattern resolution. Its elimination could greatly advance the state of the art for plating printed-circuit boards and integrated circuit chips.

A new concept for high-resolution fine-line pattern plating is envisioned as a constant-flow stream of plating solution directed from a high-pressure nozzle toward the substrate. The plating solution serves as a positive electrode that can be electronically modulated to create the desired pattern on the substrate, which acts as a negative electrode. An optical scanning device scans a master circuit drawing, and the information is used to modulate the current of the stream (positive) electrode, to produce a plated copy of the drawing. The electrode can also be modulated by digital control from a previously-scanned and recorded control pattern. The thickness of the plated layer is determined by the amount of current supplied and the scan rate.

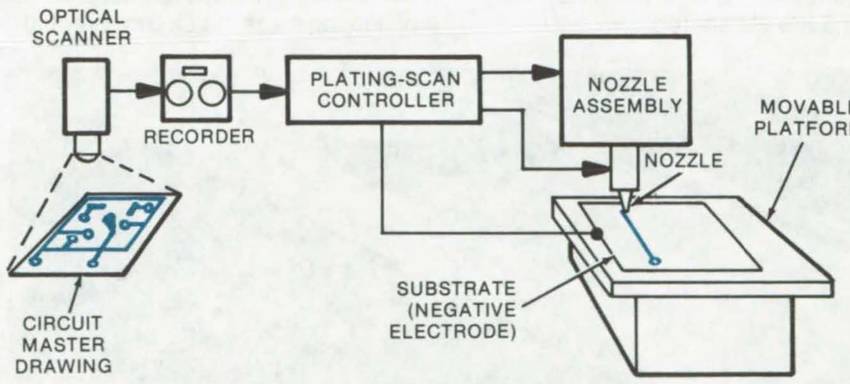

The **Scanning-Nozzle Plating System** includes an optical scanner, a recorder, and a plating scan controller that determines the plating current to the nozzle and the motion of the substrate platform. The nozzle assembly houses the supply of plating solution.

In operation (see figure), the optical scanner (vidicon) first scans the circuit master drawing at a high scan rate. The scan information is transmitted to a recorder, which slows the signals to a rate within the mechanical capabilities of the plating nozzle and the moving platform supporting the substrate. The reduced-rate scanning signals are then sent to a controller that determines the motion of the platform and the amount of current supplied to the nozzle. A nozzle with a very small (1×10^{-3}-mm) orifice sprays the plating solution onto the substrate under high pressure, 500 to 700 psi

(continued on next page)

(3.5×10^6 to 4.9×10^6 N/m^2). This permits fine-line pattern resolution, while continuously cleaning the surface being plated. Although the fluid flow is continuous, actual plating is determined by the plating scan controller. It supplies the appropriate current to the stream electrode in accordance with the master pattern, without the need for masking.

This work was done by Gerald D. Oliver of **Caltech/JPL.** *For further information, Circle 90 on the TSP Request Card.*

This invention has been patented by NASA [U.S. Patent No. 3,810,829]. Inquiries concerning nonexclusive or exclusive license for its commercial development should be addressed to the Patent Counsel, NASA Resident Legal Office-JPL [see page A8]. Refer to NPO-11758.

Shrink Tubing Identifier

A modified typewriter is used to code small-batch lengths of shrink tubing.

Lyndon B. Johnson Space Center, Houston, Texas

An ordinary typewriter platen may be adapted to retain shrink-fit tubing while applying alphanumeric identification. A prior method of identifying shrink tubing is to place it in a heat-operated wire-marking machine. The adapted platen permits less hazardous identification (stamping) of the tubing than was possible when using a heat-operated wire-marking machine, since the initial heating and periodic reheating to between 120° to 177° C (250° to 350° F) between type character changes as required by the wire-marking machine are eliminated.

One version of the new tubing-identification methods, as in Figure 1, uses a multiple-groove platen and a conventional carbon-film ribbon typewriter. Each of the grooves corresponds to a different tubing diameter. The tubing is retained in the grooves (Figure 2) by nylon rods which accommodate corresponding sizes of tubing. After the tubing is cut to size and placed on the nylon rod, it is inserted in the matching platen groove. The platen may be adapted to hold more than one rod of the same size, or more than one rod of varying sizes, as circumferential area around the platen allows. The method works with any platen-bearing typewriter and can be semi-automated by storing the identifying alphanumerics in memory.

Typing errors are corrected by using an ordinary type eraser or denatured alcohol. Typewritten identification is made indelible by applying heat, as during the heat-shrinking process, and is as indelible as that produced when using a heat-transfer machine.

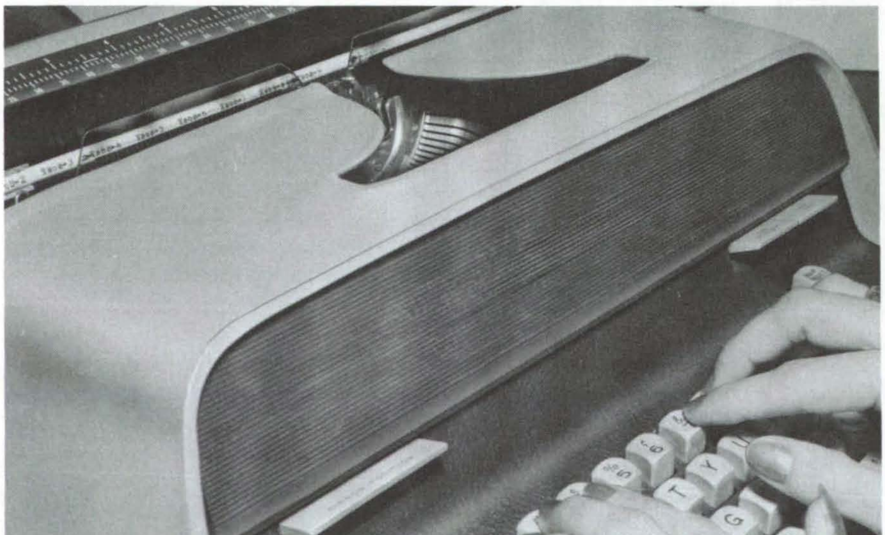

Figure 1. An **Ordinary Typewriter** is modified to transfer alphanumerics to shrink tubing directly. The typewriter platen is grooved to a depth sufficient to hold the tubing. An eraser or denatured alcohol is used to correct mistakes. The method takes the place of a heat-operated wire-marking machine and, besides being less hazardous to operating personnel, is faster.

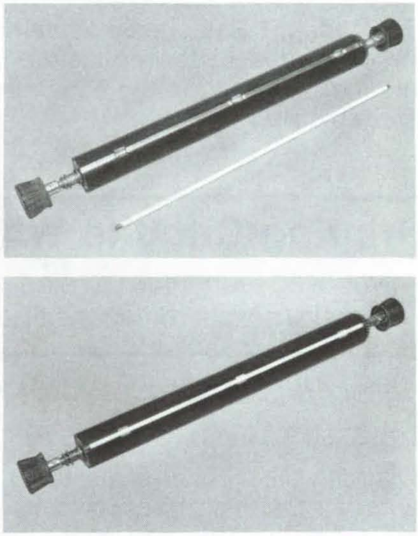

Figure 2. **Tubing To Be Coded** is slipped over a nylon rod (above) and then is inserted into a groove cut into the typewriter platen. Grooves of varying diameter can be cut into the platen (below) for additional sizes of shrink tubing.

This work was done by Roy F. Plummer of Lockheed Electronics Co., Inc., for **Johnson Space Center.** *No further documentation is available.*
MSC-16430

Detecting Wire-Bond Failures

Wire bonds are tested rapidly in a microelectronic assembly.

Marshall Space Flight Center, Alabama

A test procedure detects wire-bond failures in thick-film substrates and thin-film substrates upon which many bonding pads are mounted, such as in hybrid circuits and microelectronic components. Each pair of pads is joined to an identical resistor. The pads and resistors are connected in a series loop, and wires are bonded from one pad to the next, thus shorting the resistors, as shown in the figure. If all bonds are electrically intact, the resistance value measured is almost zero ohms. However, one wire-bond failure results in a measured resistance equal in value to that of one resistor in the circuit.

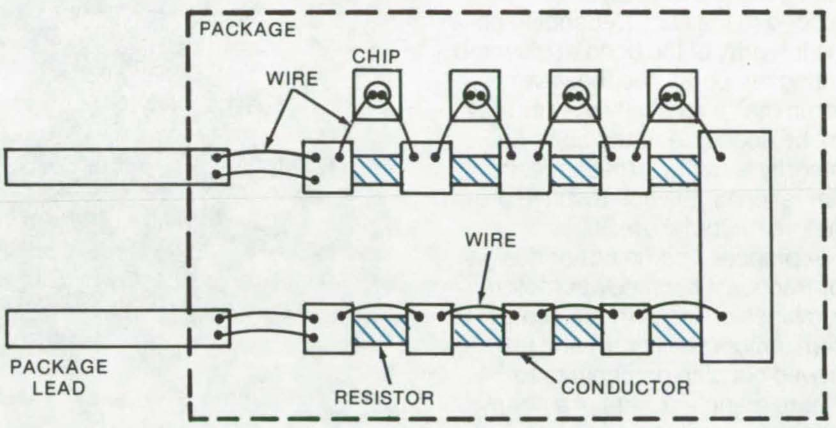

Wire Bonds Are Tested, using a nondestructive method. Series-connected resistors are shorted with wire bonds either from pad-to-pad or from chip-to-pad. Bond failure is detected by noting a stepped increase in resistance. The magnitude of the resistance change is converted into the corresponding number of bond failures.

This test procedure was devised for evaluating the relative failure characteristics of wire-bonding methods (e.g., ultrasonic, thermocompression, gold, aluminum, and the like) in a hermetically sealed package. After all wires are bonded from each pad to the next, the substrate is placed in the package. The ends of the resistor loop are attached to the external package leads. Intermediate points are also connected to external leads; these points help to identify the approximate location of the failed bond. Semiconductor chips are bonded to the device by placing them between the bonding pads. Two wires are bonded to the chip, one per junction.

In one test procedure, the wire-bond pattern configuration consisted of two test patterns. Each measured 1.75 by 0.75 in. (44.45 by 19.05 mm). One configuration was for thin-film circuitry, the other for thick-film circuitry. The thin-film pattern had locations for 1,593 substrate-to-substrate wires and 416 chip-to-substrate wires. Each substrate has a total of 1,801 resistors; 1,593 substrates measure 0.01 in.^{2} (0.25 mm^2) and 208 substrates measure 0.02 in.^{2} (0.51 mm^2). The resistors used had a value of 240±15 Ω.

The thick-film pattern used 760 resistors. Each was jumpered via a single wire. A semiconductor chip can be placed directly on a resistor and then jumpered via two wires. Each resistor measured 0.02 in.^{2} and had a resistance of 190±20 Ω.

This work was done by Angelo Koudounaris of Hughes Aircraft Co. for **Marshall Space Flight Center.** *For further information, Circle 91 on the TSP Request Card.*
MFS-23584

Commutator Assembly Technique

Changes in the contact form factor and bonding procedures enhance reliability of small motors.

Langley Research Center, Hampton, Virginia

Miniature electric motor commutators that are fabricated for high-reliability applications may sometimes be manufactured by procedures with lower-than-average yield rates. In one instance, for example, the 10-carat gold commutator contacts are adhesively bonded to the hub. Depending on the integrity of the bond at elevated curing temperatures, however, commutator reliability may or may not be adequate. If the bond-line integrity is faulty, areas of resin starvation on the hub result in premature motor failure.

A proposed commutator design for fractional horsepower motors combines changes in the contact form factor (see figure) and improved bonding procedures to assure manufacturers of a nearly 100-percent yield rate. A bonding tool that incorporates an elastomeric mold is used to exert uniform pressure to the hub assembly during the adhesive cure cycle. The tool maintains all components in alinement during the elevated-temperature cure cycle while simultaneously permitting the hub to expand as the adhesive cures. The use of the commutator locking bar and the machining sequence needed to turn the commutator assembly down to specified tolerance result in lower internal stresses generated in the hub during the cure cycle. Fractures that normally appear in the hub at this stage of manufacture (and that lower finished-part yield) are thus prevented.

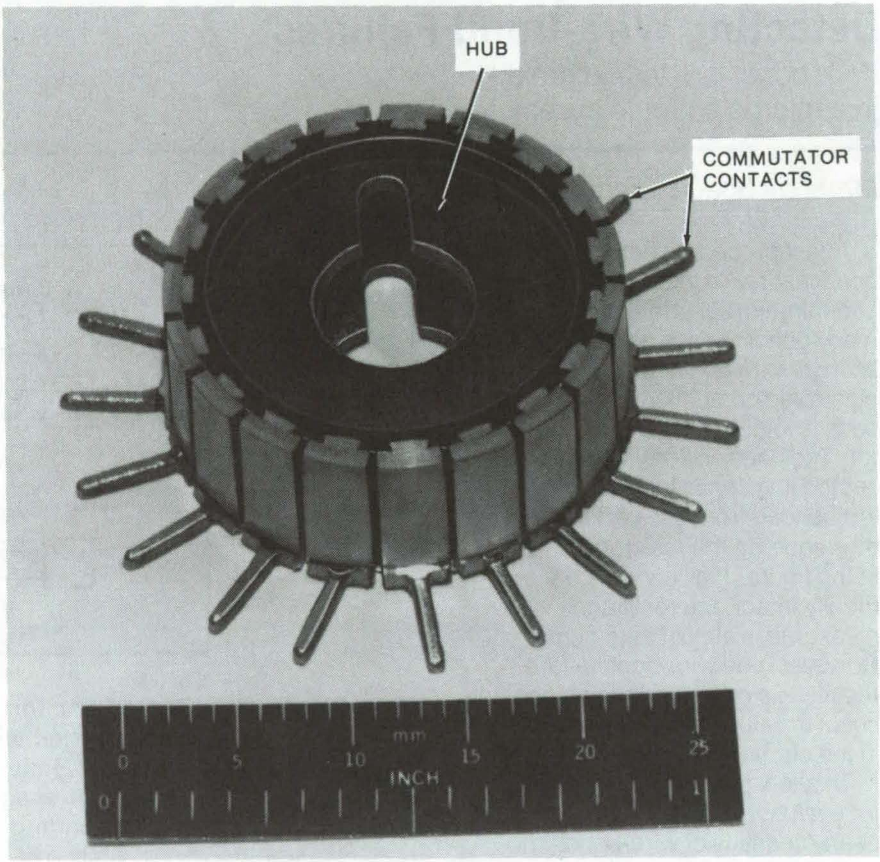

In the new **Commutator Assembly Technique,** the locked-and-bonded hub design (shown) ensures that the motor contacts are mechanically locked to the hub before adhesives are used to bond the hub assembly together. The contacts lock mechanically when positioned in the slotted hub and also provide an adhesive bond line of 0.005 in. (0.013 cm) at all hub interface points.

This work was done by Joseph B. Davenport, Jr., C. Calvin Davis, and G. Michael Jurscaga of **Langley Research Center.** *For further information, Circle 92 on the TSP Request Card.*
LAR-11844

Vibration Improves Single-Crystal Yield

Yield of single GaAs crystals
improved by vibrating scan motor.

Marshall Space Flight Center, Alabama

During the growth of GaAs crystals for research on the effects of growth variables (described in "Growth of GaAs Crystals" MFS-23681 on page 156 of this issue), it was noticed that an apparatus with a damaged and unbalanced scan motor had a better yield of single crystals. This scan motor (see Figure 1), used to move a horizontal heating oven, actually caused an increase in the number of completely single-crystalline crystals when it was damaged.

An analysis showed that the improved yield was statistically significant (see Figure 2). For instance, using two otherwise-identical furnaces, the one with the unbalanced motor produced three single crystals out of four runs; the furnace with the balanced motor produced zero out of six runs.

Vibrations are known to have both harmful and beneficial effects on crystal growth. However, because no thorough and systematic study of vibrational effects is available currently, the reasons for the improved yield had to be hypothesized. After the consideration of several possibilities, the most likely cause was felt to be additional mixing in the liquid ahead of the growth interface.

A controlled, milli-g vibrational force might have introduced a gentle massaging action into the liquid. The longitudinal vibrations (along the axis of the quartz growth tube) could have increased the longitudinal effective liquid mass transfer and reduced the likelihood of longitudinal constitutional supercooling. Transverse vibrations (perpendicular to the tube axis) would increase the transverse, effective liquid mass transfer. Thus the transverse solute-concentration gradients and constitutional supercooling would be reduced. In either case, polycrystalline growth would be suppressed, as was observed.

The experiments were rerun while the entire apparatus was monitored for vibration. Although these experiments were too limited to derive a comprehensive analysis of the effects of vibration, some interesting observations were made:

- The effects of the motor were independent of the particular growth period or furnace used.
- The vibration spectra of the unbalanced motor peaked at milli-g's near 54 Hz.
- Background noises from fans, walking and jumping, and slamming a door were all much weaker than the effects of the scan motor and did not appear to affect crystal growth. A freight train passing within 60 meters did not noticeably affect the background noise spectra. This is particularly interesting, since crystal-growth facilities have been generally placed far from railway tracks, often at great costs.
- All the vibration spectra appeared to be Gaussian. The regularity and periodicity on the waveline autocorrelation curve suggested sinusoidal waveforms.

This work was done by Chou Li of Grumman Aerospace Corp. and D. Nickal of Materials Research Corp. for ***Marshall Space Flight Center.*** *For further information, Circle 93 on the TSP Request Card.*
MFS-23683

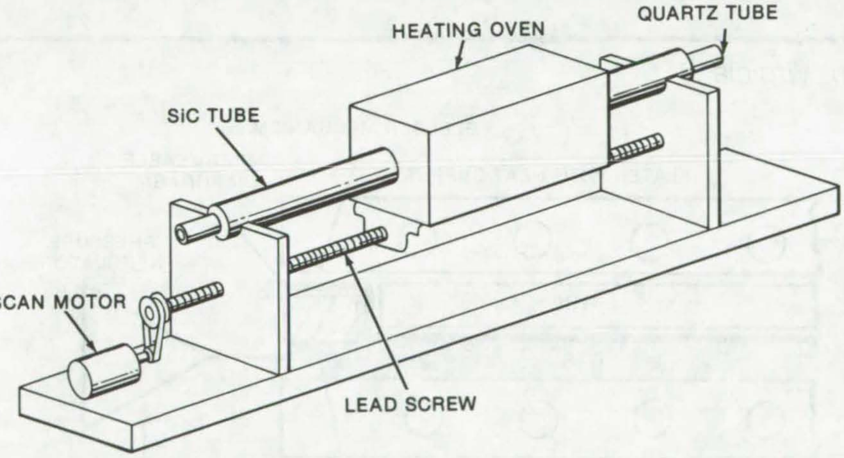

Figure 1. The **Crystal-Growth Furnace** used to fabricate single crystals of GaAs employs a scan motor to move the heating oven. When the motor became unbalanced, its vibrations resulted in an increased yield of single crystals.

MOTOR	FURNACE	GROWTH PERIOD	YIELD
Unbalanced	A	1	3 for 4
Balanced	B	1	0 for 6
Balanced	A	2	0 for 3
Unbalanced	B	2	3 for 3
Unbalanced	A	3	3 for 3
Balanced	B	3	1 for 5

Figure 2. The **GaAs Yield Data** show significant improvement with an unbalanced motor. Two identical furnaces (A and B) were used for three different growth periods. Yield is shown as the number of single crystals obtained for the number of trials.

Microcircuit Photography Technique

Fewer pictures
required for montage

Goddard Space Flight Center, Greenbelt, Maryland

When photographing microcircuits, the aim is to get a print that is both large enough and sharp enough for a person to trace out a signal path. Generally this requires the time-consuming construction of a montage from many smaller photographs.

With a simple change in techniques, engineers at Goddard Space Flight Center have eliminated a lot of the effort required to construct such microphotographs. A montage that formerly required 48 photographs, sized 4 by 5 in. (10 by 13 cm), can be made sharper, using only 12 pictures 8 by 10 in. (20 by 25 cm) in size.

All that is required are two straightforward changes in procedure. First, a flat-field objective lens is used. A conventional non-flat-field lens may appear more suitable, as it offers higher resolution, but only over part of the subject plane. A flat-field plane provides a high level of acuity over the entire plane of the microcircuit.

The second change, equally simple, is the removal of the reflex-viewing box. This box was used because it offered some additional enlargement, but it was found to introduce distortion also. The enlargement can be regained by the proper lens choice.

This work was done by D. Dahms and B. Slaughter of **Goddard Space Flight Center.** *No further documentation is available.*
GSC-12199

Method of Laminating Using a Pneumatic Anvil

Novel laminating method does
not disarrange or crush fibers.

Langley Research Center, Hampton, Virginia

An improved method of laminating a resin-impregnated fiber layup employes a pneumatic anvil. It was developed primarily for nonwoven monofilament material, but it can also be used with broadgoods, felts, and mats. The technique and equipment are a modification to the method of lamination most widely used in research and in industry: a conventional laminating press with solid, matched, opposing mold surfaces. The conventional press offers a wide range of combinations of temperatures, pressures, and layup sizes and shapes; all of these advantages are retained in the new press.

However, with the pneumatic anvil, only one of the opposing mold surfaces in the press is a solid surface; the other consists of gas under pressure. The gas remains distributed uniformly over one side of the layup, forcing the workpiece into intimate contact with the opposing solid mold surface for the entire molding cycle. A simplified illustration of one of the possible configurations of a laminating press employing a pneumatic anvil is shown in the figure.

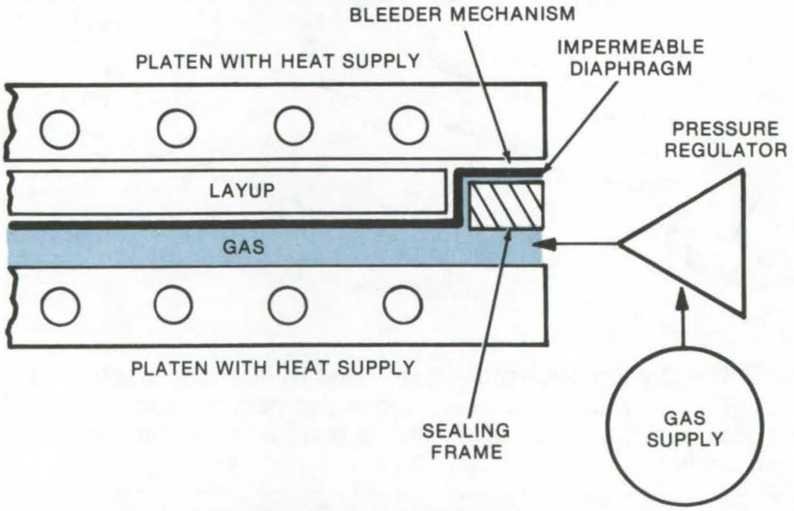

The **Laminating Press With Pneumatic Anvil** replaces one side of the press with gas pressure. This greatly reduces damage and disarrangement of the fibers during layup.

Only one of the press platens is in contact with the workpiece. The pressurized gas is introduced between the other platen and the workpiece. An impermeable diaphragm, such as an elastomer or film, provides the gas seal on the

side of the workpiece. Sealing around the edge of the press frame can be accomplished with elastomeric or metal O-rings, and a bleeder ply or other bleeder mechanism can be used over the layup to allow gases released from the heated resin to escape.

In laminating, the press clamp load is maintained only slightly higher than the gas pressure in order to prevent overloading of the mechanical system.

The primary advantage over the conventional press is that this method does not move, disarrange, or damage fibers during lamination. Lateral movement of the plasticized resin, a problem in conventional laminating procedures, does not occur here, resulting in stable fiber position. Because the gas uniformly distributes pressure over the entire surface of the workpiece, damage from crushing, as occurs from high localized pressure on thickness gradients in conventional press laminating, is eliminated.

This work was done by Wilbur C. Heier of **Langley Research Center.** *No further documentation is available.*
LAR-11850

Rigidified Inflatable Structures

A proposed material could be inflated and then made rigid to hold its shape.

Lyndon B. Johnson Space Center, Houston, Texas

A suggested alternative to conventional inflated structures combines the light weight and ease of implementation of inflatables with the security and permanence of rigid structures. The inflatable would be made from a pretreated material formed to produce the desired shape when blown up. The material would become rigid upon exposure to Sunlight (ultraviolet radiation) or heat. This approach could be used with many current inflatables, such as "bubble" buildings and lifeboats, or could be used to construct equipment that has heretofore been thought unsuitable for inflatables. Some examples are shown in the illustration.

The inflatable would be made from one of a number of currently-available resin/matrix materials (prepreg). The unimpregnated gas-impervious material would be formed in the desired shape, using techniques similar to those for elaborate parade-balloon construction. A two-wall panel approach, as shown in the illustration, would be used.

Next, the inner surfaces of both walls would be coated with a prepreg, chosen for its strength and the method of rigidification, e.g., ultraviolet, thermal, or a gas used for inflation. The treated material is then folded and protected from triggering elements, for shipping.

(continued on next page)

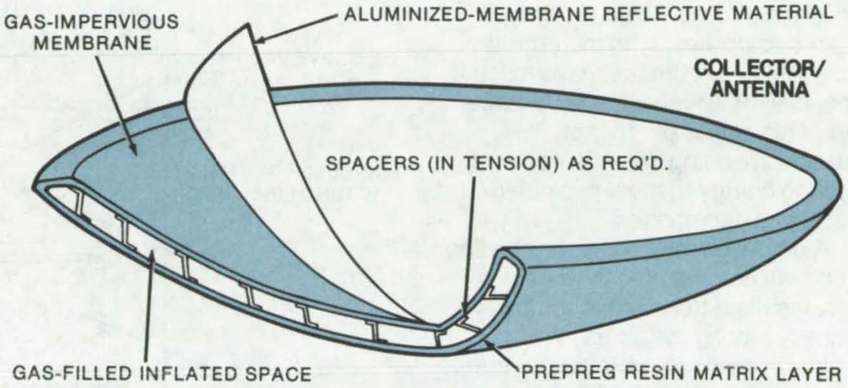

Rigid Inflatables could be constructed from impregnated material that is polymerized by Sunlight, heat, or other means after inflation. The examples above are a few of the applications possible for this technique.

When deployed, the structure is merely inflated under conditions consistent with polymerization requirements. After rigidification, the structure could be made stronger by filling it with a suitable foam.

This work was done by Russell V. Knaus, Jr., of Lockheed Electronics Co. Inc. for **Johnson Space Center.** *No further documentation is available.*
MSC-16069

Rotation Molding of Flywheels

Fiber composites are prestressed for maximum strength at operating speed.

Marshall Space Flight Center, Alabama

At one time, flywheels were regarded as limited to low-energy uses, such as keeping an engine rotating between pulses of energy from the pistons. More recently, fiber composites, with their great strength and lightness, have made it feasible for flywheels to store large amounts of energy. In fact, flywheels are being considered for storing energy to meet peak electrical power demands.

A proposed method for fabricating such large composite flywheels insures that stress is distributed equally among the fibers. When stress is equalized in this way, the storage capacity per kilogram is greatest, and flywheels become even more attractive for high-energy storage.

The fabrication method consists of bonding the fibers to a filler material (usually an epoxy resin) while the flywheel is being rotated at or near its intended operating speed. While rotating but still unbonded, the fibers assume relative positions that insure equally distributed stress. When the bonding material has hardened, it keeps the fibers in these same relative positions. (In the conventional fabrication process, the bonding material — which is necessary to protect and contain the fibers — hardens without rotation and therefore does not allow the fibers to assume their "natural" relative positions during operation. Some fibers are thus understressed while the flywheel is turning, and others are overstressed and prone to failure.)

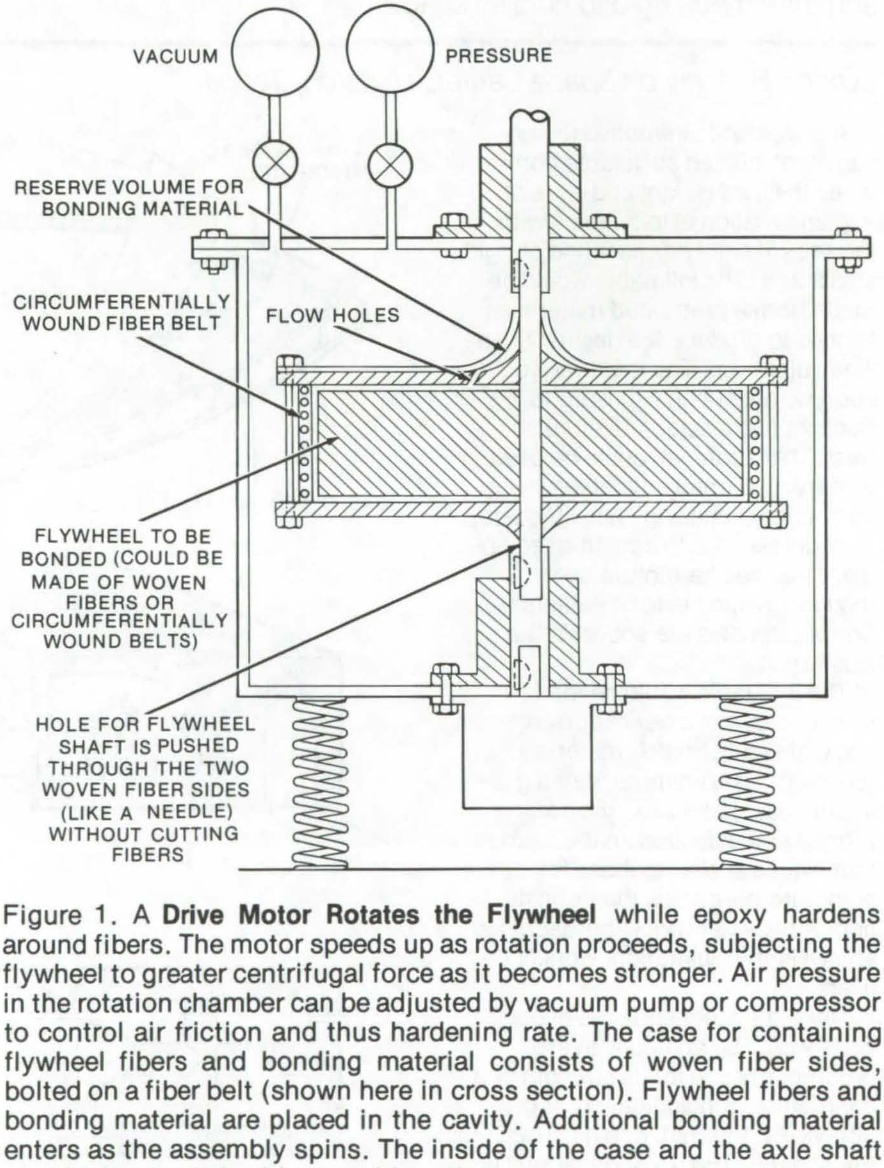

Figure 1. A **Drive Motor Rotates the Flywheel** while epoxy hardens around fibers. The motor speeds up as rotation proceeds, subjecting the flywheel to greater centrifugal force as it becomes stronger. Air pressure in the rotation chamber can be adjusted by vacuum pump or compressor to control air friction and thus hardening rate. The case for containing flywheel fibers and bonding material consists of woven fiber sides, bolted on a fiber belt (shown here in cross section). Flywheel fibers and bonding material are placed in the cavity. Additional bonding material enters as the assembly spins. The inside of the case and the axle shaft should be coated with a mold-parting compound to insure that the molded flywheel can be removed easily.

The proposed fabrication apparatus is shown in Figure 1. A motor rotates a case containing the fibers and the bonding material enters the case from a reservoir. The bonding-material hardening proceeds from the periphery of the wheel where heating from air friction is greatest, toward the interior. The motor speed is gradually increased as the bonding material hardens. If necessary, the apparatus could be operated above or below atmospheric pressure to increase the heating rate, making it possible to program the motor speed to yield the most even stress distribution.

The case that contains the bonding material (see Figure 2) could be made in stages. First, nonstressed fibers could be used for the case. This case could then be used to make a second case by the rotating fabrication process. The second case could be used to make a third, and so forth, each case becoming stronger as the fiber strain at which the bonding material hardens is progressively increased.

This work was done by George M. Weyler, Jr., of **Marshall Space Flight Center.** *For further information, Circle 94 on the TSP Request Card.*

Inquiries concerning rights for the commercial use of this invention should be addressed to the Patent Counsel, Marshall Space Flight Center [see page A8]. Refer to MFS-23674.

Flexible Foam Masking for Parylene Coating

Hybrid-microcircuit masking technique improved to prevent unwanted parylene coating of lead packages.

Marshall Space Flight Center, Alabama

Hybrid microcircuits are frequently coated with a corrosion-protective material such as parylene before a final cover is put on the device. It is necessary, however, that during the coating process, the leads and the lead frame of the package remain totally free of parylene. The conventional masking tape or liquid latex maskant methods result in incomplete masking, lead distortion through excessive handling, spreading of parylene beyond the intended area, and difficulties in removal. To avoid these and other difficulties, a two-part metal fixture can be designed with appropriate foam rubber inserts to protect the leads during coating.

The foam rubber can easily be cut or molded to mate with the pattern to be masked. The resilient foam conforms under the slightest pressure to rough and uneven surfaces, thus completely sealing them from parylene vapors. Mask tooling, shown in the figure, is used to secure and support the parts of the lead package during coating. After coating, the parts can be readily separated by releasing the tooling fasteners.

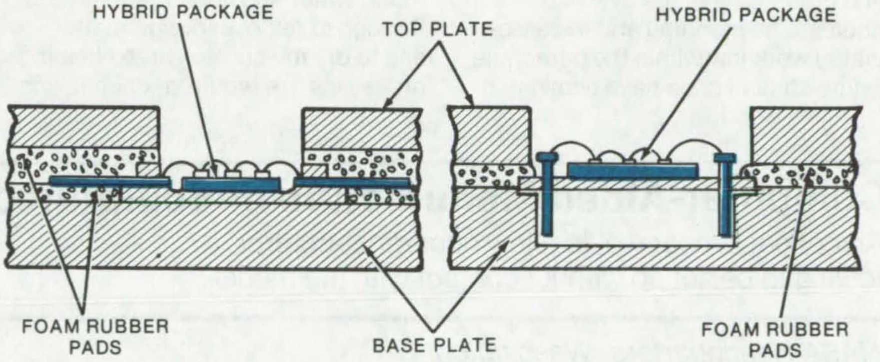

The **Mask Tooling** is shown for a horizontal-lead and a vertical-lead hybrid package. The foam rubber pads will conform to rough or uneven surfaces, yet provides sufficient pressure to hold the part securely.

Since the foam does not adhere to the surfaces, a slight tearing action is all that is required to separate the parylene from the foam rubber at the points where the masked area and the unmasked area meet. The masks can be made to hold individual or multiple devices, and can be adapted to horizontal-lead, vertical-lead, or TO packages.

This work was done by F. W. Oberin of Hughes Aircraft Company, Aerospace Group for **Marshall Space Flight Center.** *For further information, Circle 95 on the TSP Request Card.*
MFS-23129

Monorail for Production Handling of Large Parachutes

Heavy parachutes are transported through work and inspection stations via a monorail system.

John F. Kennedy Space Center, Florida

The problems of handling very heavy, bulky, and large parachutes have led to the development of an overhead monorail conveyor system for chute transport. Each chute measures 50 by 115 ft (160 by 375 m) in diameter and weighs up to 2,000 lb (907 kg) dry and 3,000 lb (1,361 kg) wet, making it difficult to wash, dry, repair, and pack them without the coordinated efforts of several workmen.

The monorail system permits the adaptation of horizontal assembly-line techniques for the refurbishment and processing of the oversize chutes. The monorail and the associated workflow within the parachute refurbishment shop have eliminated the need for vertical drying and washing towers and substantially reduce the manual handling requirements at each of the work stations.

After use, the chutes are received at the shop wound on large reels. Then the chutes are mounted on the monorail, and technicians walk around the chutes and into the canopies to remove debris and untangle and inspect all areas. The parachute is transported to the washer, dryer, repair, and packing areas. Since it is hung on the monorail in a systematic folded arrangement, water and hot air readily pass through to remove foreign matter and to dry the chute. Three cleaning processes are required, each taking about 2 hours, thus making each operation comparable to in-line processing. The dried chutes are further transported via the monorail to tables for inspection and packing. The monorail holds a dry parachute until the table or packing area is cleared of the preceding one.

This work was done by Russell T. Crowell of **Kennedy Space Center.** *For further information, Circle 96 on the TSP Request Card.*
KSC-11042

Inquiries concerning rights for the commercial use of this invention should be addressed to the Patent Counsel, Kennedy Space Center [see page A8]. Refer to KSC-11042.

Computer-Aided Manufacture of Sculptured Objects

An optical sensor would allow numerical-control tooling to be set up without contact with the model.

NASA Headquarters, Washington, D.C.

Using a newly proposed system, the shape and dimensions of delicate or soft objects could be stored in a numerical-control (NC) file without actual contact with the models. An optical profile-measuring system has been proposed as the basis for a tooling technique that would be particularly suitable for art objects; it would also allow industrial parts (such as automobile fenders) to be modeled in a manageable medium, such as clay, and then tooled in metal without preparing an intermediate hard model.

The optical sensor (see "Optical Profilometer," NASA Tech Briefs, Vol. 1, No. 3, pp. 364-365) uses a focused laser (or other light source) to scan the surface of an object. An optical-sensing system is used to determine how far a point on the object is from the laser-beam focus

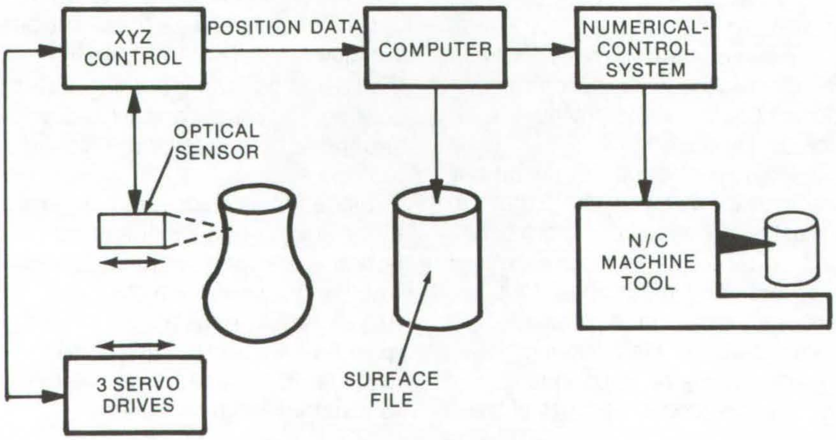

An **Optical NC Tooling System** could be developed by combining a NASA-developed optical profilometer with conventional numerical-control tooling. Because no contact would be required, soft or delicate models could be used, and the useful life of any type of model would be extended.

point. The profilometer is computer controlled to determine characteristics such as surface area, absolute depth, and point-to-point distances. These data could be fed to a modified, but basically standard, numerical-control system.

A possible implementation, as illustrated, would use position servos to control the optical sensor. The sensor data could be fed back to the servos to keep the sensor-to-model distance constant. The data would also be input to a computer to develop a mathematical model of the object surface. The data transformation could be accomplished by using well-established methods, such as B-splines, Coons patches, or other techniques used in existing NC processors. Surface data would then be stored or used immediately to drive a metal-cutting machine tool to produce duplicates or scaled versions of the original model.

As proposed, the system would be limited to models without folds and sharp bends that would create shadows, regardless of how the object is rotated. The object should also be modeled from a material with a uniform reflection (such as most modeling clays) or sprayed with a coating that produces a uniform reflectance.

This work was done by Louis N. Mogavero of **NASA Headquarters.** *For further information on the optical profilometer portion of the system, Circle 97 on the TSP Request Card. HQN-10914*

Heavy-Duty Sandblast Nozzle

Sialon liner resists abrasion, is strong at high temperatures, and costs less.

Caltech/JPL, Pasadena, California

Heavy-duty tungsten carbide or silicon carbide nozzles utilized in industrial sandblasting and similar highly abrasive procedures (paint sprayers, oil drilling, mud drilling) ordinarily have a very limited life. The nozzle liner, by virtue of the application, requies complete replacement about once every 200 hours. By replacing these nozzles with ones made of "sialon" (silicon/aluminum/oxygen/nitrogen), liner wear is lengthened 50 percent in some applications. In addition the replacement cost for a sialon nozzle is only about one-half the cost of a trungsten carbide nozzle.

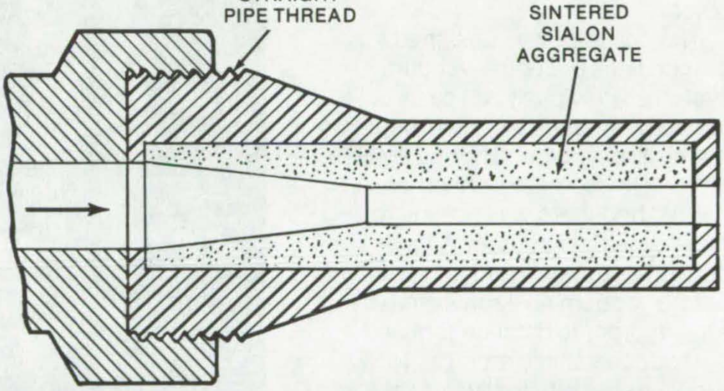

The **Sialon Nozzle,** above, is fabricated by centering a graphite core, shaped as the desired passageway, in a graphite mold. The powdered composite is added, and the assembly is subjected to high temperature and pressure for about 60 minutes. The resulting ceramic solid solution has superior hardness, strength, and resistance to oxidation and abrasion. The casing is added by subsequent injection molding or diecasting.

The sialons are single-phase binary solid solutions of silicon nitride and aluminum oxide or ternary solutions made by including aluminum nitride. The Al_2O_3 may be replaced by Y_2O_3, Cr_2O_3, or a mixture of all three ceramic oxides. Abrasion resistance can be further enhanced by a dispersion of an abrasion-resistant metal carbide such as titanium carbide. The silicon nitride cannot react with the titanium carbide particles to form a silicide, and the resulting ceramic aggregate retains its structural integrity. The solid ceramic solution also retains the crystal structure of the silicon nitride, so that the ceramic has very high abrasion resistance, good strength at high temperatures, and resistance to thermal shock and oxidation. Other oxides can also be added to reduce fabrication temperatures by transient liquid phase sintering.

The sialon nozzles are fabricated by techniques similar to those used in conventional power metallurgy. Typically, the components, in powder form, are sintered in a mold at temperatures around 1,800° C and pressures from 1,000 to 5,000 psi (7×10^6 to 35×10^6 N/m^2).

As shown, the liner is encased in a plastic shell via injection molding; the threads formed at the same time are used to interface the nozzle with a pressurized line. The outer casing could also be fabricated from mild steel. However, the plastic casing is easier to produce, is lighter (and therefore less expensive to ship), and eliminates the need for a separate plastic or rubber washer at the nozzle inlet end.

(continued on next page)

This work was done by Eugene V. Pawlik, Gerald S. Perkins, and Wayne M. Phillips of **Caltech/JPL.** *For further information, Circle 98 on the TSP Request Card.*

This invention is owned by NASA, and a patent application has been filed. Inquiries concerning nonexclusive or exclusive license for its commercial development should be addressed to the Patent Counsel, NASA Resident Legal Office-JPL [see page A8]. Refer to NPO-13823.

Collectors for Vacuum-Cleaning Lines

See-through devices make it easy to retrieve lost parts.

Lyndon B. Johnson Space Center, Houston, Texas

Screws, washers, and other small parts swept up by a vacuum cleaner are collected by a clear plastic filter. The device contains a screen that allows dust and small particles to pass through, but retains larger debris. A friction-held cover opens easily for the removal of collected objects.

The collector was designed for branch lines of central vacuum systems. Previously, all parts collected by vacuum cleaning went into the central system, where they were difficult to separate from other debris, and there was no way to determine their source. A time-consuming search had to be made before vacuuming each assembly area in order to balance tool and part accountability records. Now, it is only necessary to vacuum in the area to find missing items.

The collector should be useful wherever valuable or accountable parts are assembled.

This work was done by Wesley L. Hinze, Peter V. Sauer, Jr., and George W. Williams of Rockwell International Corp. for **Johnson Space Center.** *For further information, Circle 99 on the TSP Request Card.*
MSC-17011

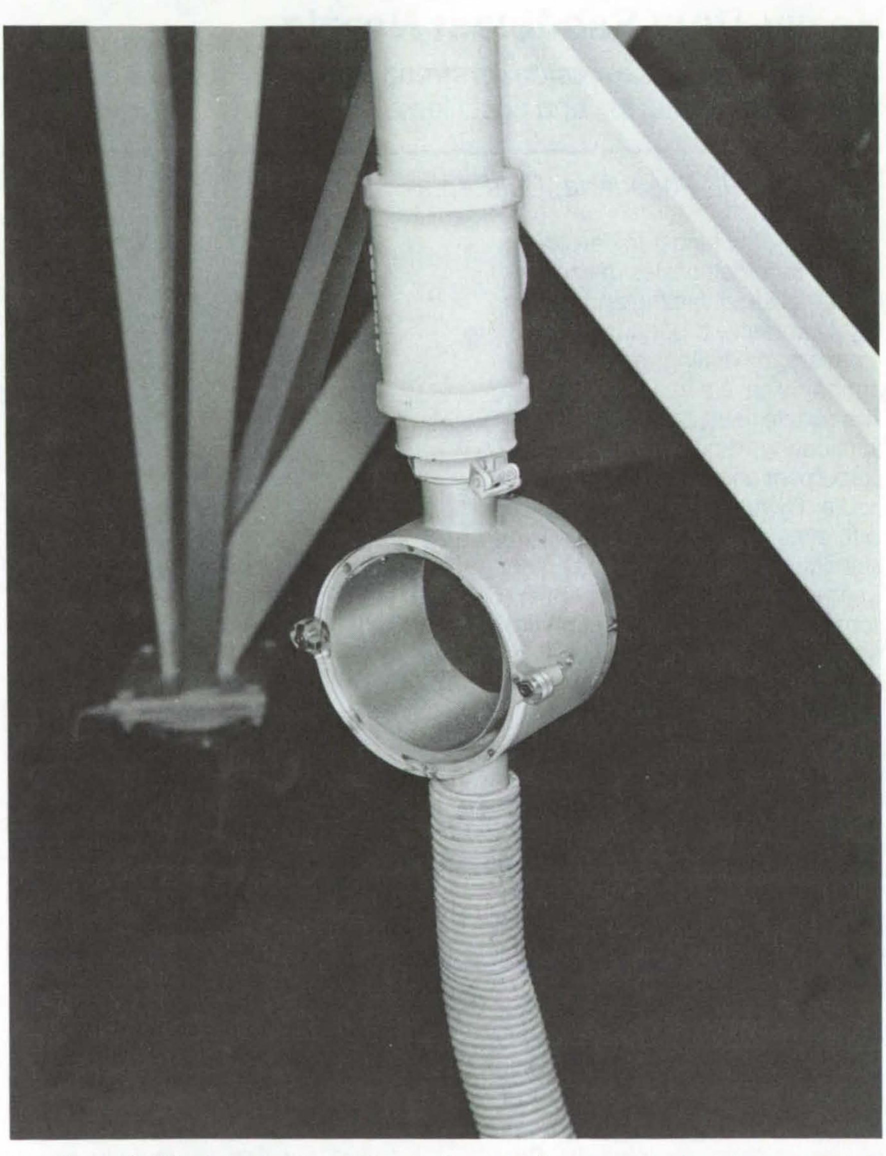

Auxiliary Collector for branches of central vacuum-cleaning systems extracts small parts. Contents of the collector can be seen and removed easily.

Tube-Bending Scale/Protractor

Novel pivot allows direct measurements of bend parameters.

Lyndon B. Johnson Space Center, Houston, Texas

A new combination protractor and scale for measuring tube bends has a novel pivot that allows the tube to remain in contact with the scale arms for all bend angles. It permits rapid and accurate scribing and measurement of mockup fluid lines to obtain production data. Time is saved because it is not necessary to "sight" onto fixed scales, as with other instruments of this type.

The protractor has one stationary scale, and a movable scale that rotates about a pivot located below the scale arm. The pivot bearing is designed so that the zero points of the scales maintain contact for all angular orientations. The tube being measured rests on a ledge surface and is brought into contact with the scale using appropriate spacer bars, as indicated in the figure. In this way, it is possible to read directly the distances between the heel-line intersection and the bend tangency points. The bend angle is read directly from the protractor scale located on the base. The tool can be made to accommodate tubes with reverse bends by removing portions of the sectioned precision scale as necessary.

With the present design, tubes with diameters of up to 1-1/4 in. (3.2 cm) and bend parameter lengths of up to 6 in. (15 cm) may be measured, and similar instruments may be made for larger tubing.

This work was done by Alma U. Millett of Rockwell International Corp. for **Johnson Space Center.** *For further information, Circle 100 on the TSP Request Card.*
MSC-16272

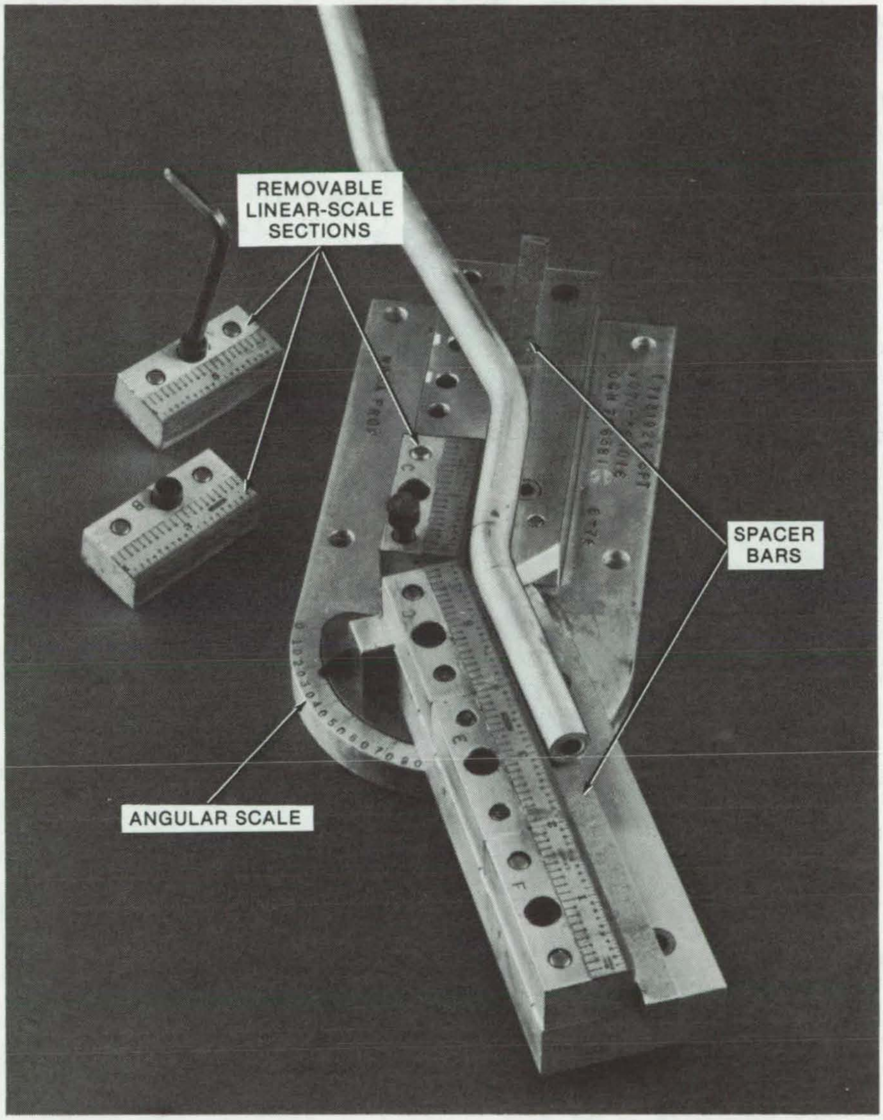

Tube-Bending Scale/Protractor allows the tube to remain in contact with the measuring scales for all bend angles. In the photograph above, scale sections have been removed to measure reverse bends.

Books and Reports

These reports, studies, and handbooks are available from NASA as Technical Support Packages (TSP's) when a Request Card number is cited; otherwise they are available from one of NASA's Industrial Application Centers or the National Technical Information Service.

Growth of GaAs Crystals

A statistically designed experiment allows growth studies with fewer samples.

A study on the effects of melt and growth on solute segregation and crystal quality of GaAs crystal used statistical techniques to reduce sample numbers and experimental costs. It was shown that with only 14 crystals, proper experimental design can be used to achieve results consistent with more detailed experiments.

The experimental design allowed five independent variables, but only four were used:

1. Dopant types — Cr, Si, Te, and Sn;
2. Dopant concentrations — 10^{17}, 5×10^{17}, 10^{18}, and 5×10^{18} atoms/cm^3;
3. Growth rates — 0.10, 0.16, 0.22, and 0.28 in./h; and
4. Temperature gradients — 4°, 6°, 8°, and 10° C/in.

The dependent variables, measured along the crystal axis at 1/2, 1, 1-1/2, and 2 in. from the seeding plane, were:

- Free carrier concentration,
- Hall mobility, and
- Resistivity.

The experimental details are described, and the results of the study are presented in tabular form. In addition, measurements are discussed and compared with other types of studies.

This work was done by Chou Li of Grumman Aerospace Corp. for **Marshall Space Flight Center.** *To learn how to obtain a copy of the report, Circle 101 on the TSP Request Card.*
MFS-23681

Mathematics and Information Sciences

Mathematical Model of Fires

Model allows prediction of effects of different control methods.

Caltech/JPL, Pasadena, California

A synthesis of the available information regarding the constraints on an enclosed fire has been used to develop a mathematical model of five basic constraints. This model allows the future development of a fire to be predicted and can be used to evaluate different control methods at particular stages of the fire.

After ignition, the five constraints considered are:

- Flame-spread rate,
- Fuel-surface limit,
- Airflow limit,
- Quantity of fuel, and
- Original quantity of air.

Initially the rate of energy release is controlled by the flame-spread rate. This is a function of the fire-spread velocity and the fire-front length. A second constraint is the depletion of oxygen supply if ventilation is restricted as in an enclosed area. If all the oxygen in a given volume is burned, the amount of energy released would be 58 kW-min/m^3. Normally, only about one-half of the oxygen is burned, because the flame encounters a lean burning limit.

A third constraint on energy release is reached when the flame has spread to the entire fuel surface. If not constrained by available air, the fire burns at a heat-release rate proportional to the fuel area. Experimental values of heat-release rates for this constraint vary from 50 to 150 kW/m^2 for wood and up to 2,500 kW/m^3 for gasoline.

A fourth constraint is encountered when the combustion becomes ventilation controlled. A heat-release rate has been described as a function of a ventilation parameter and is nearly independent of the characteristics of the fuel. The fifth and final limit on energy release is the total fuel load.

Inspection of the heat release vs. time graph for each constraint allows a prediction of which constraint is controlling the fire at a particular stage. A computer program could be written to help evaluate the effects of different fire-control methods at particular stages of the fire.

This work was done by Clifford D. Coulbert of **Caltech/JPL.** *For further information, Circle 102 on the TSP Request Card.*
NPO-13950

Data Acquisition for Solar and Wind Energy

Versatile automatic system collects data from wind and solar-energy sensors.

Caltech/JPL, Pasadena, California

A "Solar and Microwave Data Acquisition System" (SMDAS) operating at Goldstone, California, collects microwave and solar-energy data. This information is needed for instrumentation programs on atmospheric radio propagation and solar energy. The flexible data system allows changes in the types of data, the number of channels, the location of sensors, and the speed of recording.

A central station is housed in a standard electronics rack, and up to 10 remote stations interface with transducers that sense the data to be recorded. The remote stations are in environmental enclosures that withstand extreme weather conditions. They can be 500 miles (800 km) from the central station or at greater distances with line amplifiers. All power to the remote stations is supplied by the central station.

A remote station is connected to the central station via a cable containing three shielded twisted pairs. It is addressed by a self-clocking 10-bit serial binary word generated by the central station. The remote station senses the addressed channel and generates a 33-bit serial word, which is transmitted to the central station. Several types of data can be accepted by the remote station:

- Analog: up to 160 channels per remote station, in any combination of high- or low-level signals ($\pm$ 10 mV to $\pm$ 10 V full scale) in 8-channel increments each;
- Digital: up to 16 channels of 8-digit 1248 binary-coded decimal (BCD) and up to 4 channels of 8-digit 1224 BCD, making a total of 20 channels per remote station;
- Frequency: up to 10 channels per remote station in any combination of 1 Hz to 1 MHz or 100 Hz to 2 MHz, each range having an input sensitivity of 100 mV rms; and
- Contact Closure: up to 112 per remote station in groups of 8 per address.

The central station has a random-access memory and a flexible data-output format. It automatically or

(continued on next page)

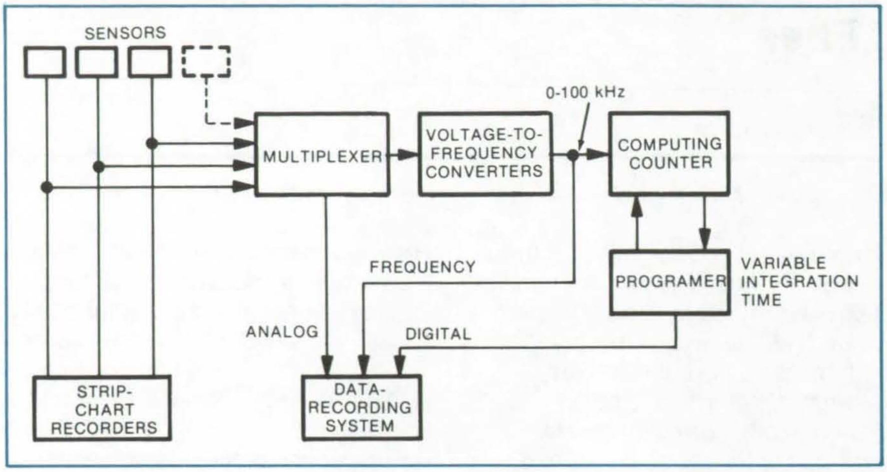

The **SMDAS** includes sensors, such as hemispherical pyranometers, tracking heliometers, and cup anemometers, that produce electrical outputs that may go both to strip-chart recorders and to the system multiplexer. Parameters may be recorded as digital or analog voltages or as frequencies. The voltage-to-frequency converters are used for precise integration.

manually interrogates the remote station, formats the data into 2048 character records, and writes the records on magnetic tape. The magnetic-tape unit allows read-after-write for checking the data as recorded. The scan cycle is adjustable from 1 minute (or less if the total channel capacity is not fully used) to 24 hours.

An independent paper printer allows operators to check the data being recorded on the magnetic tape. An independent visual display of time and any manually selected channel are available in digital form on the central station.

Each record written on the magnetic tape consists of as many data words as there are channels in operation plus header words. The header words include: reference data (selected by thumb wheels on the central station), the number of remote stations in operation, and the time code. Each data word is tagged with the remote-station identification number and channel number.

All input-channel signal conditioning is modularized so that a remote station has minimum configuration without excessive channels. A remote station is expanded to maximum input-channel configuration by the addition of plug-in modules requiring wiring changes. An uninterruptible power source keeps the full system operating during momentary line power failures for at least 10 minutes.

One design objective was to make the errors in data transmission less than the sensor errors. The overall accuracy of the data system is of the order of 0.1 percent compared to ± 2 to 3 percent for typical sensors.

The sensors detect a variety of physical parameters and convert the measurements to electrical signals that appear at the sensor output terminals. Certain key parameters are recorded in analog form on strip-chart recorders for immediate visual checking and comparisons. Some parameters are recorded in digital form, some as a frequency, and the remainder in analog form. The digital recording chain is the most precise, the standard method is the direct analog chain, and the frequency technique is intermediate between the two. The voltage-to-frequency converters are used for precise integration and accuracy in recording. If resistance/capacitance (RC) time constants are used for integration, then components with high stability and high precision must be used.

This work was done by Robert A. Gardner and MacGregor S. Reid of **Caltech/JPL.** *For further information, Circle 29 on the TSP Request Card.*
NPO-13908

Books and Reports

These reports, studies, and handbooks are available from NASA as Technical Support Packages (TSP's) when a Request Card number is cited; otherwise they are available from one of NASA's Industrial Application Centers or the National Technical Information Service.

Liquefied Natural Gas [LNG] Safety

A bibliography for LNG and liquid methane safety

A bibliography has been issued that cites approximately 600 reports concerned with the safety of liquefied natural gas (LNG) and liquid methane. Each citation includes title of the report, author, abstract, source, description of figures, key references, and keywords or subject terms. The bibliography is indexed by key subjects and also by authors.

This bibliography was assembled from a computer search of the NASA Aerospace Safety Data Bank. The results of the search were reviewed and evaluated to ensure that the citations included in the bibliography are relevant items that would be useful to design engineers and safety specialists.

The majority of the citations included were retrieved from the Cryogenics Fluid Safety collection in

the NASA Aerospace Safety Data Bank. Other collections searched included Fire and Explosion Technology and Mechanics of Structural Materials. Citations from the latter two collections relate to the detection of fuel leaks, fighting of aircraft fires with various extinguishing agents, explosions of fuel systems, and fragmentation hazards.

The reports cited contain data helpful with problems associated with LNG and/or methane fires and explosions.

This work was done by Paul M. Ordin of **Lewis Research Center.** *Further information may be found in NASA TM-X-73408 [N77-15208], "Bibliography on Liquefied Natural Gas [LNG] Safety," a copy of which may be obtained at cost from the New England Research Application Center [see page A7].*
LEW-12720

Computer Programs

These programs may be obtained at very reasonable cost from COSMIC, a facility sponsored by NASA to make new programs available to the public. For information on program price, size, and availability, circle the reference letter on the COSMIC Request Card in this issue.

Finite-Element Structural Analysis

Reduction and analysis of data to determine critical loading conditions

The program CRITICAL, aids in the reduction and analysis of finite-element structural-analysis data. It determines the critical loading conditions for critical values of reactions, applied loads, deflections, stresses, internal loads, shear flows, fiber stresses, relative motion between structural points, and so forth. These parameters may have one or more columns of data per node, such that the columns may represent components of forces, deflections, reactions, and so forth. CRITICAL can perform a search on any one column of data or on all columns. It makes the specified search and identifies the load cases that determine the critical values of the selected parameters. CRITICAL can also filter out trivial data and compare the results of one search with the values of a reference load condition. The program could be useful in the structural analysis of any system in which knowledge of the critical loading conditions is required.

The basic finite-element-model data must be input to this program in TRANSPOSE, SEARCH, or CRITICAL format. The TRANSPOSE program is included as part of this package and is described below. Output from the CRITICAL program is in CRITICAL format, such that output data can be reprocessed. The CRITICAL program performs internal checks on many aspects of the input data and prevents waste of computer time on runs containing bad, or nonconsistent, input data. The program is limited to 2,000 distinct load cases. Up to 500 group elements or nodes may be selected during a discrete selection option. Any one column for each node can be selected for determining the most positive and negative values and corresponding load base being identified as critical. The program is also capable of performing a search for the critical positive and negative values for all six columns and can identify the critical loading conditions for each column. The user can specify that the critical search is to find the 1 to 10 most negative and the 1 to 10 most positive values of the variable of interest.

The TRANSPOSE program was developed to reduce data and save the output for subsequent post-processing. By providing the users with options for selecting only certain points (nodes), finite elements, components, loading conditions, data blocks, and specific substructures, the time required to analyze the structure can be greatly reduced. The TRANSPOSE program essentially transposes the finite-element data from one loading condition for all element and node data to the case of one-node-point data for all loading conditions.

Both of these programs are written in FORTRAN IV and have been implemented on an IBM 360-series computer. CRITICAL and TRANSPOSE respectively require approximately 120K 8-bit bytes and 280K 8-bit bytes of central memory. Both are written to be executed in batch mode. Both programs reference a link library that is supplied in load module form as an IEHMOVE unloaded partitioned data set.

This program was written by Tetsuo Furuike and Jack C. Long of Rockwell International Corp. for **Johnson Space Center.** *For further information, Circle M on the COSMIC Request Card.*
MSC-16320

Multivariate-Normality Goodness-of-Fit Tests

Extension of Pearson's chi-square goodness-of-fit test for univariate distributions

The chi-square test of Pearson is often used to determine whether a univariate normal-distribution model adequately describes a sample population so that the statistics of the sample population can be applied to the entire population. This chi-square goodness-of-fit test has been extended to apply to multivariate statistics for application in any field in which data of two or

(continued on next page)

more variables are sampled for statistical purposes.

The basis of the multivariate test is the fact that the exponential of the multivariate normal distribution is distributed as a chi-square variable with degrees of freedom equal to the number of dimensions (variables). The program also provides the Kolmogorov-Smirnov (KS) goodness-of-fit test. This is accomplished by computing the maximum absolute difference between the theoretical multivariate normal distribution and the empirical distribution.

The program is written to handle dimensions two through five, with up to a thousand sets of data. Extensions to higher dimensions could be made with some code modification. These multivariate tests are strictly valid only for independent samples and for multivariate distributions with unimodal marginal distributions. However, the authors believe that the test may still be used subjectively if these restrictions are not met.

Input to the program consists of v sets of N data points, where v is the number of random variables and N is the size of the sample. The output includes the test criteria for the chi-square test and the maximum absolute difference between the theoretical distributions for the KS test. Also included in the output are the theoretical and observed frequencies, degrees of freedom of the tests, a listing of all input data, and all the computed parameters of the multivariate normal distribution including the v means, the v standard deviations, and all the correlation coefficients.

This program is written in FORTRAN for batch execution and has been implemented on a UNIVAC 1100-series computer with a central memory requirement of approximately 28K 36-bit words.

This program was written by Lee W. Falls of **Marshall Space Flight Center** *and Harold L. Crutcher of the U.S. Department of Commerce. For further information, Circle N on the COSMIC Request Card.*
MFS-23523

SUBJECT INDEX

National Aeronautics and
Space Administration

Washington, D.C.
20546

Official Business
Penalty for Private Use, $300

SPECIAL FOURTH CLASS MAIL
BOOK

Postage and Fees Paid
National Aeronautics and
Space Administration
NASA-451

U.S.MAIL

NASA

A new elastomeric foam developed for Ames Research Center is three times as shock absorbent as earlier paddings. Its other special properties make this materi useful for many different products. Shown here, it is used as padding for football helmets; it offers a new lev of protection for players from the Little Leagues to pro teams.